This is to certify that the

dissertation entitled

INVESTIGATION OF ELECTRON SPIN RESONANCE
IN MULTILAYERED CUMN/CU SPIN GLASSES
ABOVE THE FREEZING TEMPERATURE

presented by

Diandra Laia Leslie-Pelecky

has been accepted towards fulfillment
of the requirements for

____Ph.D.____ degree in __Physics__
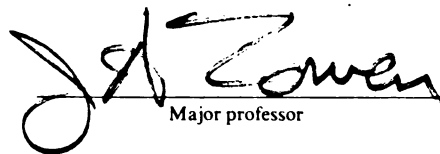
_____
Major professor

Date __09/11/91__

PLACE IN RETURN BOX to remove this checkout from your record.
TO AVOID FINES return on or before date due.

DATE DUE	DATE DUE	DATE DUE

MSU Is An Affirmative Action/Equal Opportunity Institution

c:\circ\datedue.pm3-p.1

INVESTIGATION OF ELECTRON SPIN RESONANCE IN MULTILAYERED
CUMN/CU SPIN GLASSES ABOVE THE FREEZING TEMPERATURE

By

Diandra Laia Leslie-Pelecky

A DISSERTATION

Submitted to
Michigan State University
in partial fulfillment for the requirements
for the degree of

DOCTOR OF PHILOSOPHY

Department of Physics and Astronomy

1991

Interpretat

position, H_o, abov

processes and eve

'ordered' spin gla

$\Delta H(T)$ and $H_x(T)$

glass layer thick

dimensionality ef

$\Delta H(T)$ is

samples having

appropriate for T

of layer thickness

the linewidth itse

trends.

The obser

picture. In the

temperatures sign

ABSTRACT

**INVESTIGATION OF ELECTRON SPIN RESONANCE IN MULTILAYERED
CUMN/CU SPIN GLASSES ABOVE THE FREEZING TEMPERATURE**

By

Diandra Laia Leslie-Pelecky

Interpretation of the Electron Spin Resonance linewidth, ΔH and resonance peak position, H_0, above the freezing temperature, T_f, is difficult due to simultaneous physical processes and even a question as to whether the linewidth is a probe of the long-range 'ordered' spin glass phase, or a measure of short range correlations. We have measured $\Delta H(T)$ and $H_0(T)$ in multilayered $Cu_{1-x}Mn_x$ spin glasses with x = 7% and 11%, and spin glass layer thicknesses, W_{SG}, from 1 nm to 1000 nm at 9 GHz. Finite size and dimensionality effects on T_f have previously been observed in these multilayers.

$\Delta H(T)$ is shown to have the same general form for all layer thicknesses, with samples having $W_{SG} \leq 3$ nm more accurately described by a corresponding form appropriate for $T_f = 0$. Systematic variations in all parameters are seen as a function of layer thickness. The separation of effects due to the depression of T_f and effects on the linewidth itself is necessary in order to correctly understand the physical origin of the trends.

The observed behavior of $\Delta H(T)$ is explained in terms of a correlated cluster picture. In the correlated cluster model, the existence of spin correlations at temperatures significantly above T_f leads to a distribution of cluster sizes and relaxation

times, with the l

clusters become

along with a DM

resonance line.

glasses above T_f

paramagnet phase

of decreasing lay

behavior of the li

phase, in which

temperatures be

temperature of th

times, with the linewidth dominated by configurations with faster relaxation times. As clusters become increasingly correlated, the internal fields generated by the clusters, along with a DM anisotropy field, inhomogeneously broadens the exchange narrowed resonance line. This interpretation suggests that the observation of resonance in spin glasses above T_f is a characteristic of an intermediate phase between the spin glass and paramagnet phases, and not a measurement of the spin glass phase *per se*. The effect of decreasing layer thickness on the formation and growth of clusters, and the resulting behavior of the linewidth is qualitatively discussed. The possibility of a 'Griffiths-like' phase, in which regions of the sample are condensed into the spin glass phase at temperatures between the bulk freezing temperature and the measured freezing temperature of the sample, is considered.

Sor
wav
ener
of ti

"Someday, after we have mastered the winds and the waves, the tides and gravity, we will harness for God the energies of love and then, for the second time in the history of the world, man will have discovered fire."

-Teilhard de Chardin-

This thesis is dedicated to my family:
my mother and father,
my brothers Theodore and Steven,
and most of all,
my husband Richard.

I would like

the initial idea for

the fine points of

members of my co

source of ideas, qu

me advice, inspira

interact with these

I owe a de

Hudson, Stephanie

for doing their job

Life as a

encouragement I r

graduate students I

Loloee, who was a

I would als

his assistance in

International for s

Finally, I c

love of my husba

things.

ACKNOWLEDGEMENTS

TABLE OF CONTENTS

LIST OF TABLES

xi

LIST OF FIGURES

CH

<u>NTRODUCTION:</u>

"Spin
between the
some frozen-i
range order
established. N
a state with a
random direct

This definitio

nature of spin glasse

time explaining why

has gone into under

materials. Most of

phase proper; this

approached from a

development of nar

experiments on the

Measurement of

multilayered samp

transition and the

The organ

introduction to the

necessary to expla

CHAPTER ONE: INTRODUCTION

INTRODUCTION: WHAT IS A SPIN GLASS?

> "Spin Glasses are magnetic systems in which the interactions between the magnetic moments are 'in conflict' with each other, due to some frozen-in structural disorder. Thus no type of conventional long-range order (of ferromagnetic or antiferromagnetic type) can be established. Nevertheless these systems exhibit a 'freezing transition' to a state with a new kind of 'order' in which the spins are aligned in random directions."[1]

This definition, from a review article by Binder and Young, captures the essential nature of spin glasses: although we know a spin glass when we see one, we have a hard time explaining why it *is* a spin glass. Considerable theoretical and experimental effort has gone into understanding the novel properties which appear in such a wide variety of materials. Most of the effort has focused on the behavior of spin glasses in the spin glass phase proper; this thesis investigates the behavior of spin glasses as the transition is approached from above the freezing temperature using Electron Spin Resonance. The development of nanoscale fabrication and characterization techniques has prompted recent experiments on the behavior of the freezing temperature as a function of sample size. Measurement of the Electron Spin Resonance linewidth and position in bulk and multilayered samples has shed additional light on both the nature of the spin glass transition and the characteristics of multilayered spin glasses.

The organization of this thesis is as follows; Chapter One provides an introduction to the experimental properties of spin glasses, and the theoretical concepts necessary to explain these properties. Chapter Two explains the basics of Electron Spin

1

Resonance (ESR), a

glasses, and the exp

fifth chapter is divid

localized moments in

in spin glasses. Havi

with the motivation

detailed in Chapter

conclusions and sug

THE EXPERIMEN

The primary

temperature depen

temperatures below

the cusp as the free

literature as the g

Mydosh[2] in the free

of materials inclu

semiconductors[1,3,4

is shown in Figure

sample has been c

the behavior of the

A measuring field

Resonance (ESR), and Chapters Three and Four outline the major theories of spin

glasses, and the experimental progress in the study of multilayered spin glasses. The

fifth chapter is divided into two sections; the first section outlines the theory of ESR of

localized moments in metals, and the second section summarizes the current state of ESR

in spin glasses. Having laid the necessary conceptual foundation, Chapter Five concludes

with the motivation of the work presented in this thesis. The experimental technique is

detailed in Chapter Six, the data and analysis are presented in Chapter Seven, and

conclusions and suggestions for further experiments are found in Chapter Eight.

THE EXPERIMENTAL SIGNATURES OF SPIN GLASSES

The primary - and most easily observed - signature of a spin glass is a cusp in the

temperature dependent susceptibility, $\chi(T)$, accompanied by hysteretic behavior at

temperatures below the cusp. Throughout this thesis, I will refer to the temperature of

the cusp as the freezing temperature, T_f, although it is also commonly referred to in the

literature as the glass temperature. This cusp was first measured by Cannella and

Mydosh[2] in the frequency dependent susceptibility of AuFe, but is seen in a wide variety

of materials including dilute and concentrated metallic alloys, insulators and magnetic

semiconductors[1,3,4]. A typical plot of $\chi(T)$ for a $Cu_{0.93}Mn_{0.07}$ 1000 nm sputtered film

is shown in Figure 1-1. The solid symbols correspond to measurements made after the

sample has been cooled with no applied magnetic field, and the open symbols represent

the behavior of the susceptibility when the sample is cooled in a magnetic field of 100 G.

A measuring field of 100 G was used for both curves. Above T_f, the behavior is the

185-1: CuMn(7%)

0.20

1000 nm
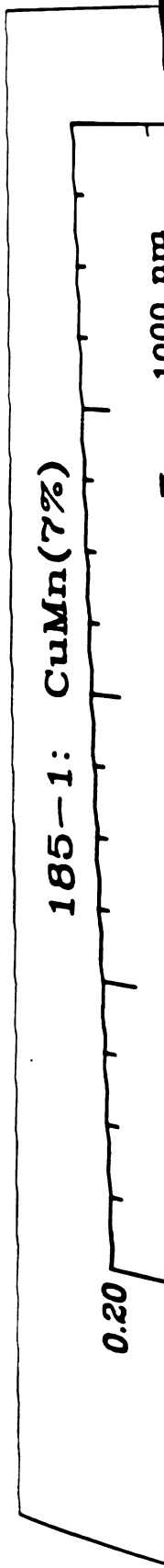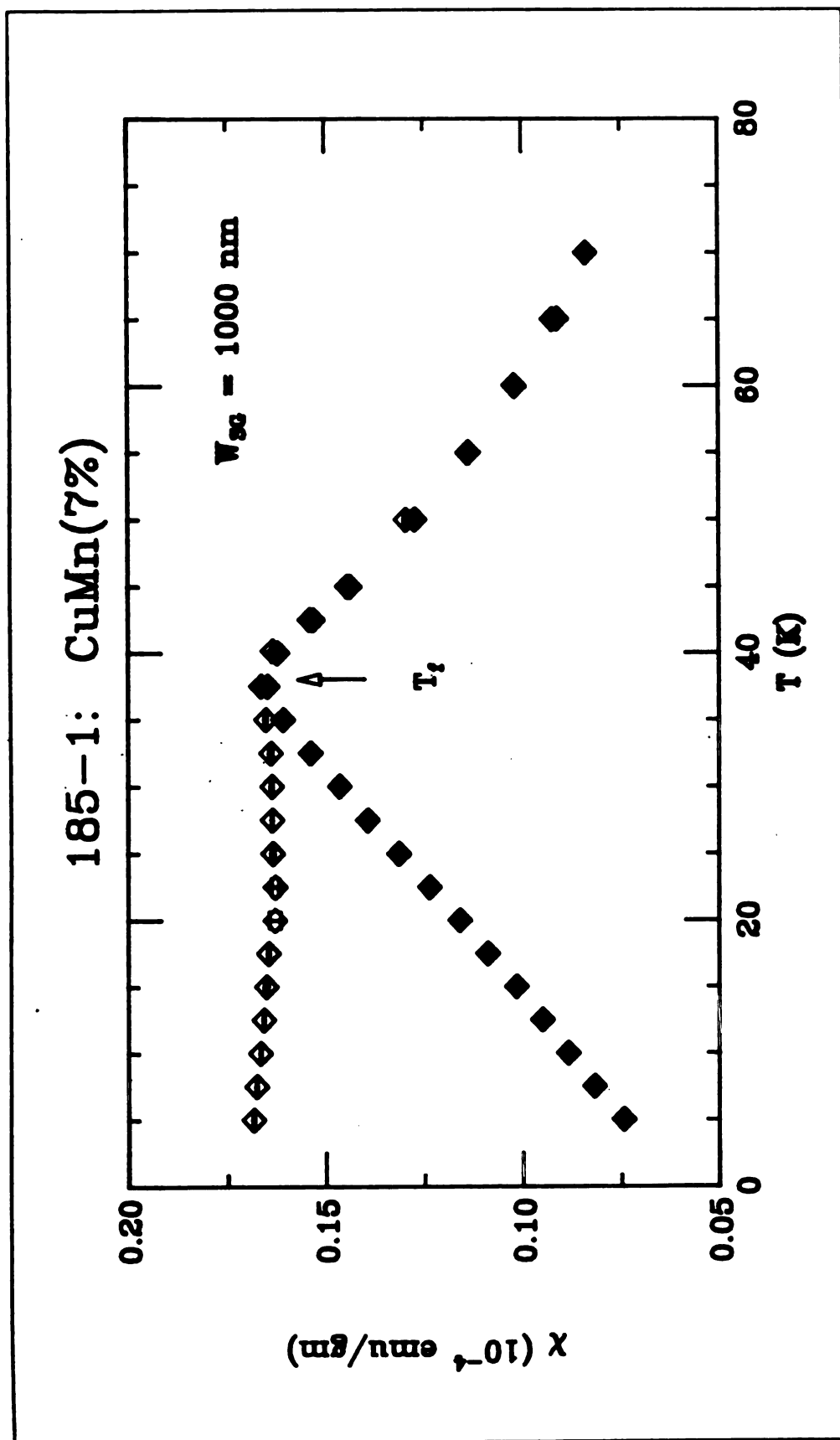
Figure 1-1: *Typical Susceptibility of a 1000 nm $Cu_{0.93}Mn_{0.07}$ Sputtered Film*

same for both th

the cusp, the fiel

toward zero. Th

ferro- and antife

initial assumption

as the onset of re

Mössbauer, nonli

a phase transitio

thermodynamic q

only broad featu

transition occurs.

Specific h

70% of the maxir

exists above the

experiments, thes

as a simple param

scattering[8] in Au

different linewidth

processes of singl

pairs, triples, etc.

of the first, indica

The strong

nonlinear susceptib

same for both the field cooled (FC) and the zero field cooled (ZFC) curves, but below the cusp, the field cooled curve remains roughly constant, while the ZFC curve returns toward zero. The cusp in the susceptibility is reminiscent of the behavior observed in ferro- and antiferro- magnets, which are known to undergo phase transitions, so the initial assumption was that this cusp represented a phase transition. Measurements such as the onset of remanence and irreversibility in the magnetization, and sharp features in Mössbauer, nonlinear susceptibility and anomalous Hall effect experiments also indicate a phase transition at T_f, yet corresponding behavior has not been observed in other thermodynamic quantities. The magnetic specific heat, resistivity and thermopower show only broad features at T_f, leaving open the question of whether or not a true phase transition occurs.

Specific heat measurements[5,6] in CuMn and AuFe show that the entropy is about 70% of the maximum entropy **above** T_f, indicating that some short range magnetic order exists above the transition temperature. Along with thermopower and resistivity[7] experiments, these measurements indicate that a spin glass above T_f can not be treated as a simple paramagnet. Additional evidence for this picture is found in diffuse neutron scattering[8] in AuFe at zero magnetic field, which shows two quasielastic lines with different linewidths. One of these lines is interpreted as corresponding to fast relaxation processes of single spins, while the other line is attributed to the behavior of correlated pairs, triples, etc. As the temperature decreases, the second line grows at the expense of the first, indicating a gradual growth of short range ordering.

The strongest evidence for a true phase transition is the divergence of the nonlinear susceptibility, as first measured in AgMn by Monod and Bouchiat[9] and later

by Levy[10], and Lev

expanded in powers

where χ_{al} is the r

susceptibility could b

a characteristic expor

The extraction of an

temperatures and m

measurements indica

T_f results in a well d

susceptibility have b

Dynamic me

time spectrum is ve

width of the spectru

order at and below T

of 10^{-10} to 10^{-13} secor

are consistent with a

by Levy[10], and Levy and Ogielski[11]. If the temperature dependent susceptibility is expanded in powers of the magnetic field, we find

$$\frac{M}{H} = \chi_0(T) - H^2\chi_{nl}(T) + Order(H^4)$$

1-1

where χ_{nl} is the nonlinear susceptibility. Bouchiat[12] found that the nonlinear susceptibility could be fit to a power law in the reduced temperature (t= $(T-T_f)/T_f$) with a characteristic exponent, γ

$$\chi_{nl}(T) \propto \left[\frac{T-T_f}{T_f}\right]^{-\gamma}$$

1-2

The extraction of an exponent from data appears to depend heavily on the region of temperatures and magnetic fields considered in the scaling analysis. Bouchiat's measurements indicate that restriction of the temperature range to a narrow region around T_f results in a well defined value of $\gamma = 2.2 \pm 0.2$. Alternate analyses of the nonlinear susceptibility have been suggested[13].

Dynamic measurements of the susceptibility have shown[14,1] that the relaxation time spectrum is very broad, even far above T_f. As the temperature is lowered, the width of the spectrum dramatically increases, so that time scales are of macroscopic order at and below T_f. The shortest relaxation times, τ_{min} are thought to be on the order of 10^{-10} to 10^{-13} seconds. The average time scale, τ_{av}, and the minimum time scale, τ_{min}, are consistent with an Arrhenius-type law,

where τ_0 is a propor

thermally activated p

maximum relaxation

the above picture.

Vogel-Fulcher law,

The Vogel-Fulcher

Arrhenius law, but

correspond to the fre

Above T_f, the

critical slowing down

where ν is the critical

critical exponent ($\tau \propto$

If the spin g

susceptibility may rep

$$\tau = \tau_0 \exp\left(\frac{E_{act}}{k_B T}\right) \qquad \text{1-3}$$

where τ_0 is a proportionality constant and E_{act} is an activation energy which measures thermally activated processes involving temperature independent barriers; however, the maximum relaxation time, τ_{max}, does **not** obey an Arrhenius law, and is inconsistent with the above picture. τ_{max} displays a strong temperature variation, and is described by a Vogel-Fulcher law,

$$\tau = \tau_0 \exp\left(\frac{E_{act}}{k_B (T-T_0)}\right) \qquad \text{1-4}$$

The Vogel-Fulcher law describes the frequency dependence of T_f better than the Arrhenius law, but the variable T_0 is generally treated as a parameter and does not correspond to the freezing temperature.

Above T_f, the behavior of the relaxation times may be described in terms of a critical slowing down, with the maximum relaxation time following

$$\tau_{max} = \tau_0 (T - T_f)^{-zv} \qquad \text{1-5}$$

where v is the critical exponent of the correlation length ($\xi \propto t^v$), and z is the dynamical critical exponent ($\tau \propto \xi^{-z}$).

If the spin glass transition is not a true phase transition, the cusp in the susceptibility may represent a 'falling out of equilibrium'. Because the time scales of the

relaxation are macro

probe has a characte

scale longer than t

equilibrium behavior

to increase with decr

is due to non-equilib

the magnitude of the

about the ability of a

field.

Below T_f, the

relaxation time effec

forms depending on

1-1. As this thesis

approaching T_f, expe

reviewed.

THEORETICAL PH

The conflictin

phase and transition c

by the lack of a well-

parameter, a complic

inherent in dealing wi

relaxation are macroscopically long, the system is never completely in equilibrium. Any probe has a characteristic time scale, such that, when the system is relaxing at a time scale longer than that of the measurement, the probe is incapable of measuring equilibrium behavior. Experimentally, the position of the freezing temperature is found to increase with decreasing measuring times, supporting the interpretation that the cusp is due to non-equilibrium effects. The freezing temperature is also found to depend on the magnitude of the magnetic field used in the measurement, which brings up questions about the ability of a system to support spin glass order in the presence of a magnetic field.

Below T_f, the primary experimental spin glass signatures are irreversibility and relaxation time effects. The temperature dependent susceptibility has very different forms depending on whether or not the sample was cooled in a field, as seen in Figure 1-1. As this thesis is mainly concerned with the temperature regime above and approaching T_f, experimental investigations of the spin glass phase *per se* will not be reviewed.

THEORETICAL PROPERTIES

The conflicting experimental evidence surrounding the nature of the spin glass phase and transition complicates theoretical analysis. Calculations are further hampered by the lack of a well-understood Hamiltonian for the system, no obvious choice of order parameter, a complicated and non-periodic ground state, and the analytical difficulties inherent in dealing with random systems.

The free energy surface of a spin glass may be schematically thought of as a multi-valleyed structure, with a large number of local minima, as shown in Figure 1-2a. The free energy surface of a ferromagnet is shown in Figure 1-2b for comparison.
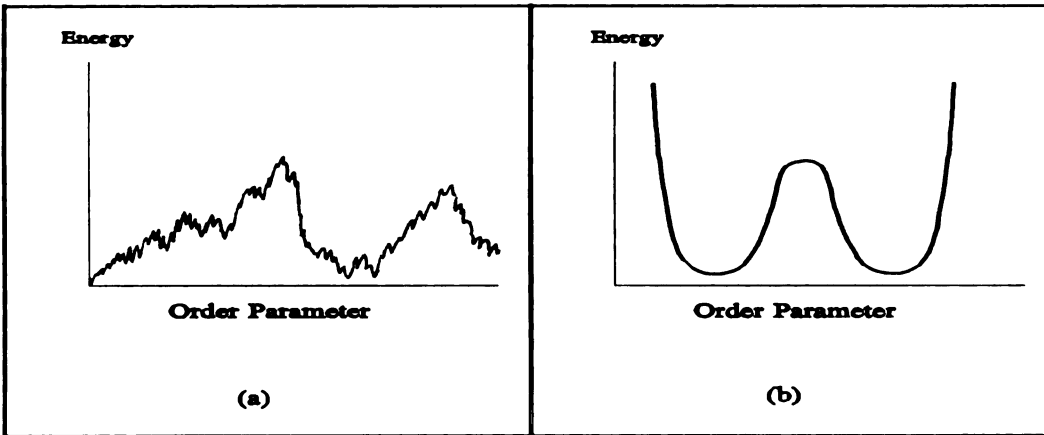
Figure 1-2: *Free energy surfaces for (a) a spin glass and (b) a ferromagnet*

The complicated free energy of a spin glass leads to a large number of states which, although different microscopically, are characterized by the same macroscopic measurable quantities. These degenerate states are separated by free energy barriers which grow as the temperature decreases. The question of whether there is a single (to within field symmetry) ground state, or a large number of ground states is still controversial[15,16]. The answer may in some part be dependent on the vector character (i.e. Ising or Heisenberg)[16,17] and range of magnetic interactions in the material.

A micr

state(s) and th

disorder and fi

introduces a ra

positioning of

Figure 1-3: *A*

Frustrat

constraints. A

Frustration and Disorder

A microscopic spin glass theory which is to explain the nonperiodic ground state(s) and the complicated free energy surface must have two fundamental elements: disorder and frustration. Disorder refers to the lack of periodicity of the spins, which introduces a random element to the interactions. Disorder may be a result of random positioning of magnetic ions on a crystalline lattice or amorphous crystal structure.
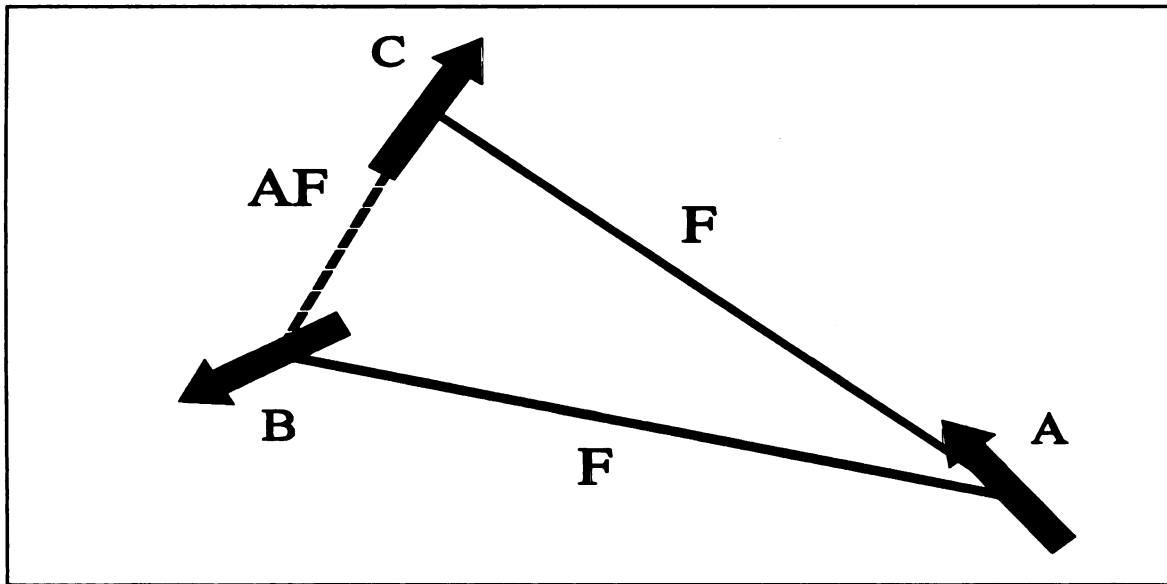
Figure 1-3: *A Frustrated Plaquette of Spins*

Frustration is the inability of a system to simultaneously satisfy all of its ordering constraints. A simple example of a frustrated system is a plaquette of three Ising spins

on the vertices of

between A and C a

B and C is antiferro

their preferred orie

responsible for the r

This combina

can not be removed

both frustration and

real materials. The

from material to mat

in dilute metallic spi

Metallic Spin Glass

Dilute metalli

substituting a small n

the lattice of a host n

and the spins behave

extensively investigat

over which spin glass

on the vertices of an oblique triangle, as shown in Figure 1-3. If the interactions between A and C and between A and B are ferromagnetic, but the interaction between B and C is antiferromagnetic, we can not have a situation in which all three spins are in their preferred orientations. This prevents the onset of long range order and is responsible for the many valleyed free energy.

This combination of frustration and disorder results in a 'serious'[1] disorder which can not be removed by a mathematical transformation. Spin glass theorists agree that both frustration and disorder must be present in any spin glass theory which is to explain real materials. The physical mechanisms responsible for frustration and disorder vary from material to material, so the specific interactions which result in spin glass behavior in dilute metallic spin glasses will be considered next.

Metallic Spin Glasses

Dilute metallic alloys are the canonical spin glasses and are created by randomly substituting a small number of transition metal ions - usually Mn, but sometimes Fe - in the lattice of a host noble metal (Cu, Au, Ag or Pt). The interactions are long-ranged, and the spins behave in a Heisenberg-like manner. Metallic spin glasses have been extensively investigated due to the ease of preparation and the range of concentrations over which spin glass behavior is observed.

The RKKY Interac

The Ruder

explained the long r

conduction electrons

in Cu interact. Hun

orientation of the mo

can be described by

The exchange polari

exclusion principle

wavelength, $\lambda_F = \pi$

polarization of the c

interaction between t

or the trough of the

ferromagnetic and ar

the Mn ions increase

RKKY interaction m

The RKKY Interaction

The Ruderman-Kittel-Kasura-Yosida[18,19,20] (RKKY) interaction originally explained the long range interaction of nuclear spins via hyperfine coupling to a sea of conduction electrons. This interaction can also explain how widely separated Mn atoms in Cu interact. Hund's rules determine the magnitude of the local Mn moment, with the orientation of the moment determined by the exchange interaction, $J(R_{ij})$. The interaction can be described by a Heisenberg Hamiltonian,

$$H = -\sum_{i \neq j} J(R_{ij}) \, \vec{S}_i \cdot \vec{S}_j \qquad \text{1-6}$$

The exchange polarizes the spins of the conduction electrons near the Mn ion. The Pauli exclusion principle causes the conduction electrons to respond with a characteristic wavelength, $\lambda_F = \pi/k_F$, where k_F is the Fermi wavevector. The resulting spin polarization of the conduction electrons is oscillatory and long ranged. The sign of the interaction between the Mn ions depends on whether the second Mn ion is at the crest or the trough of the spin polarization wave created by the first Mn ion, so that both ferromagnetic and antiferromagnetic interactions are present. As the distance between the Mn ions increases, the strength of the interaction decreases. The derivation of the RKKY interaction may be found in a number of texts[21]. The result is

$$J(\boldsymbol{R_{ij}}) = -$$

where λ is the mean

cell, R_{ij} is the distan

host metal. The exp

The RKKY interactio

mean free path effec

$$J(\boldsymbol{I}$$

Figure 1-4 sh

moments (R_{ij}). The

the RKKY interactio

resulting in frustratio

In theory, we

would yield a simpl

Morgownik and My

an attempt to corro

glasses. They founc

as to increase the pr

PtMn. Their analysi

$$J(R_{ij}) = -\left(\frac{J_{\it eff}^2}{\mu}\right)\left(\frac{\left(\frac{k_F a_o}{2}\right)^6}{\pi^3}\right)\left[\frac{\sin(2k_F R_{ij})-2k_F R_{ij}\cos(2k_F R_{ij})}{(2k_F R_{ij})^4}\right]e^{-\frac{R_{ij}}{\lambda}} \qquad 1\text{-}7$$

where λ is the mean free path of the conduction electrons, a_o^3 is the volume of the unit cell, R_{ij} is the distance between Mn ions i and j, and k_F is the Fermi wave vector of the host metal. The exponential term accounts for the finite mean free path of the electron. The RKKY interaction is frequently written in terms of the asymptotic limit, neglecting mean free path effects

$$J(R_{ij}) = J_o\left(\frac{\cos(2k_F R_{ij} + \phi_o)}{(k_F R_{ij})^3}\right) \qquad R_{ij} \rightarrow \infty \qquad 1\text{-}8$$

Figure 1-4 shows the RKKY interaction as a function of the distance between the moments (R_{ij}). The random placement of the ions provides disorder and the presence of the RKKY interaction is responsible for both ferro- and antiferro- magnetic interactions, resulting in frustration.

In theory, we expect an equal number of positive and negative interactions, which would yield a simple Curie Law paramagnetic susceptibility in the region above T_f. Morgownik and Mydosh[22] carefully investigated the high temperature susceptibility in an attempt to corroborate the expression for the RKKY interaction in metallic spin glasses. They found that deviations from ideal random mixing occurred in such a way as to increase the probability of ferromagnetic interactions in CuMn, AuMn, AuFe and PtMn. Their analysis showed that even small deviations from random mixing make big

differences i

antiferromagr

J	
	—

Figure 1-4:

The Mn-Mn

sites by Mn,

Many

glasses from

sublinear dep

calculation in

differences in the interactions. In CuMn, the Mn nearest neighbor interaction is antiferromagnetic, while the next nearest neighbor interaction is ferromagnetic.
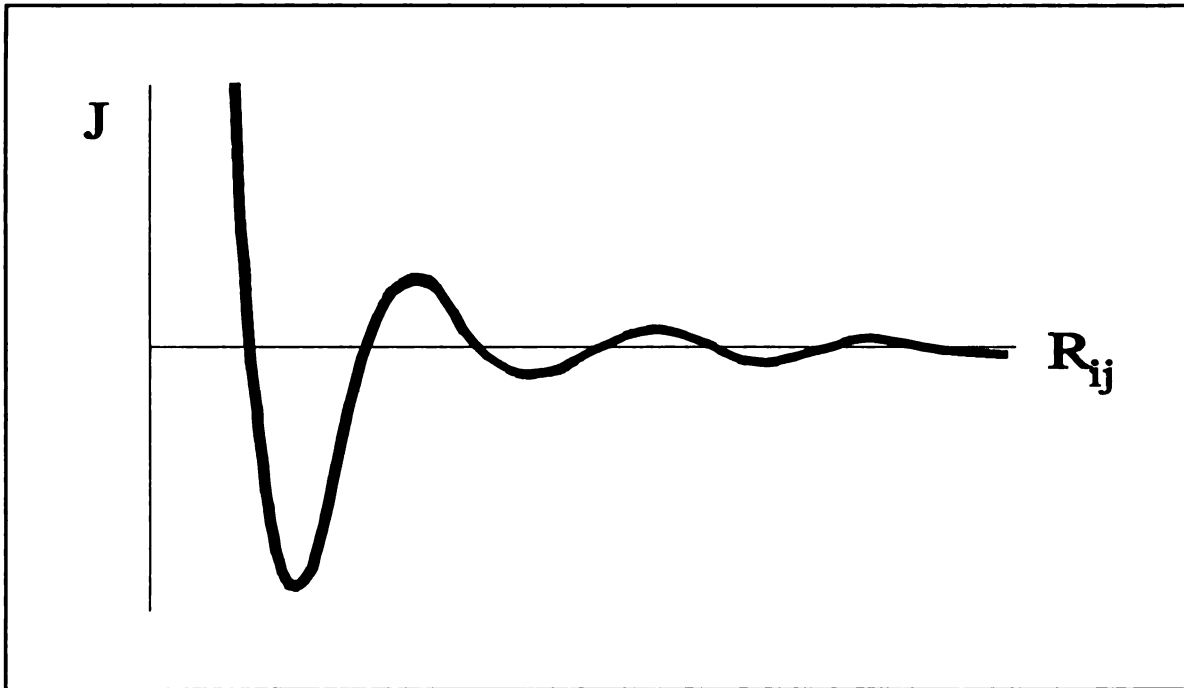
Figure 1-4: *The RKKY interaction as a function of distance between atoms*

The Mn-Mn distance[23] is maximized by preferential occupation of next nearest neighbor sites by Mn, so that the predominant interactions are ferromagnetic.

Many theoretical calculations attempt to predict the behavior of T_f in metallic spin glasses from the form of the RKKY interaction, and especially to explain the observed sublinear dependence of T_f on concentration. Larsen[24] has presented a mean field calculation in which the freezing temperature is given by

where the square ro

over neighbor spins

using a quenched u:

greater than the ave

ion. Levy and Z

corrections to the 1.

by a factor of more

be six times more in

more important tha

asymptotic form of

than 6 nm in CuMn

there will always be

corrections to the 1.

Anisotropy

Anisotropies

constraints on the in

systems, which theo

dimensions, exhibit

$$kT_f \sim \sum_j \sqrt{\sum_{i \neq j} [J(r_{ij})]^2}$$
<div align="right">1-9</div>

where the square root represents the local energy scale of spin j (with the sum running over neighbor spins). Larsen has derived a sublinear dependence of T_f on concentration using a quenched uniform model in which only those moments which are at a distance greater than the average nearest neighbor distance are included in the sum for a given ion. Levy and Zhang[25,26] have demonstrated that failure to include preasymptotic corrections to the $1/R^3$ behavior overestimates T_f by a factor of two for $Cu_{0.99}Mn_{0.01}$, and by a factor of more than three for $Cu_{0.95}Mn_{0.05}$. They find preasymptotic corrections to be six times more important than mean free path effects in $Cu_{0.94}Mn_{0.06}$ and eight times more important than mean free path effects for $Ag_{0.94}Mn_{0.06}$. This means that the asymptotic form of the RKKY interaction can not be applied to pairs separated by less than 6 nm in CuMn and 3.5 nm in AgMn[10, 158] In concentrations larger than 100 ppm, there will always be neighbors within this limit, demonstrating the importance of the corrections to the $1/R^3$ behavior.

Anisotropy

Anisotropies increase the frustration in a system by placing additional ordering constraints on the individual spins. Some authors[27] contend that nominally Heisenberg systems, which theoretically are not expected to exhibit a phase transition in three dimensions, exhibit phase transitions only because of the presence of anisotropy.

Computer simulat

anisotropy is not fur

question.

Although dip

of these anisotropies

most significant an

(DM) anisotropy,

scattering from a th

is a strong spin orb

is at the origin, anc

$$H$$

Because of the c

anisotropy is unic

the exchange coef

below T_f, where

Computer simulations[28] and experimental measurements[29] offer evidence that anisotropy is not fundamental to the ordering phenomenon. This remains an unresolved question.

Although dipolar anisotropies are present in metallic spin glasses, the magnitudes of these anisotropies are too small to be responsible for ordering in CuMn or AuFe. The most significant anisotropy in metallic spin glasses is the Dzyaloshinskii-Moriya[30,31] (DM) anisotropy, which described the interaction between two spins via spin-orbit scattering from a third atom. This anisotropy is especially pronounced if the third atom is a strong spin orbit scatterer (i.e. Pd, Fe, or Co impurities in CuMn). If the impurity is at the origin, and the two spins are at R_1 and R_2, the DM anisotropy has the form

$$H_{DM} = \left(-J_{DM}\right) \frac{\sin[k_F(R_1 + R_2 + (R_2 - R_1))] + \phi_{DM}}{[1 + ck_F(R_1 + R_2 + (R_2 - R_1))]}$$

$$\times \frac{(\vec{R}_1 \cdot \vec{R}_2)(\vec{R}_1 \times \vec{R}_2) \cdot (\vec{S}_1 \times \vec{S}_2)}{R_1^3 R_2^3 (R_1 - R_2) k_F^3} \qquad \text{1-10}$$

Because of the coupling of the spin cross product to the spatial cross product, this anisotropy is unidirectional. Typically, J_{DM} is approximately 1/10 of the magnitude of the exchange coefficient of the RKKY interaction. The DM anisotropy is most important below T_f, where the anisotropy acts to maintain the frozen direction of the spins.

SUMMARY

In this (

briefly reviewe

transition has b

true equilibrium

properties - has

spin glasses hav

metallic spin gl

SUMMARY

In this Chapter, some of the experimental properties of spin glasses have been briefly reviewed. Experimental evidence for and against the existence of a true phase transition has been discussed, and an alternative explanation - that a failure to achieve true equilibrium during the course of the measurement is responsible for the observed properties - has been suggested. The theoretical concepts necessary to a discussion of spin glasses have been introduced, with particular attention paid to the properties of metallic spin glasses.

INTRODUCT

Chapter

general theory

points is discus

where these b

complicated sp

BASIC THEO

As an ic

S. Each spin h

where the μ_b is

CHAPTER TWO

INTRODUCTION TO ESR

INTRODUCTION

Chapter Two focuses on the basic theory of Electron Spin Resonance (ESR). The general theory of ESR in non-interacting and interacting spin systems far from critical points is discussed. The material in this chapter provides a foundation for Chapter Five, where these basic formulas will be modified to describe ESR in the much more complicated spin glass system.

BASIC THEORY OF ESR

As an idealized case, consider a system of spins, each with angular momentum S. Each spin has a moment, μ, given by,

$$\vec{\mu} = -g\ \mu_B \vec{S} \qquad\qquad 2\text{-}1$$

where the μ_B is the Bohr magneton,

$$\mu_B = \frac{e\hbar}{2mc} \qquad\qquad 2\text{-}2$$

and g is the

positive. and

defined as

When

The occupatio

statistical mecl

of frequency h

microwave en

Classical Equ

We car

and moment

governed by tl

and g is the 'g factor'. The charge of the electron, e, will always be taken to be positive, and the minus sign accounted for explicitly. The gyromagnetic ratio, γ, is defined as

$$\gamma = \frac{g\mu_B}{\hbar} \qquad\qquad 2\text{-}3$$

When a magnetic field is applied, (2S+1) Zeeman levels result for each spin. The occupation of these levels by an ensemble of spins is described by the appropriate statistical mechanics, and results in a net magnetic moment. An applied microwave field of frequency hν induces transitions between Zeeman levels. Resonance occurs when the microwave energy is equal to the energy difference between two Zeeman levels.

$$h\nu = g\mu_B H \qquad\qquad 2\text{-}4$$

Classical Equations of Motion

We can treat the spin as a charged, classical 'top' with angular momentum $\hbar S$, and moment $\mu = -\gamma\hbar S$. The motion of the charged top in a magnetic field will be governed by the classical equation

$$\left(\frac{d\vec{\mu}}{dt}\right) = \gamma \vec{H} \times \vec{\mu} \qquad\qquad 2\text{-}5$$

Wher

the moment a

Larmor prece

Altho

calculation le

where the Ha

to

which is the s

the microwav

the same resu

the microwav

effects.

In exp

H_1, at right a

the properly r

When **H** is a constant vector ($\mathbf{H_o} = H_o\mathbf{k}$), the resulting motion is precession of the moment at a fixed angle with respect to $\mathbf{H_o}$, with frequency $\omega_o = \gamma H_o$. This is called Larmor precession, and the frequency ω_o is the Larmor frequency.

Although the above description is entirely classical, a quantum mechanical calculation leads to the same results. We start from the Heisenberg equation of motion,

$$i\hbar\frac{d}{dt}\mu_{op} = [\mu_{op}, H] \qquad \text{2-6}$$

where the Hamiltonian is the Zeeman interaction. Calculation of the commutator leads to

$$\frac{d}{dt}<\vec{\mu}_{op}> = \gamma\vec{H} \times <\vec{\mu}_{op}> \qquad \text{2-7}$$

which is the same as Equation 2-5. The details of extending the quantum case to include the microwave field may be found in a number of references[32,33,34]. As we obtain the same results classically as quantum mechanically - even in treating the presence of the microwave field - the more intuitive classical picture can be used in discussing these effects.

In experiments, we apply a static field, $\mathbf{H_o}$, and a smaller, time dependent field, $\mathbf{H_1}$, at right angles to the applied field. The time dependent field is usually written as the properly rotating part of an oscillating field,

The counter-rotati

Equation 2-8 is any

and may be neglec

We can tran

at rest. This refer

equation of motion

where the prime de

frame, and

In this refere

The motion of the

frequency of the alte

$$\vec{H}_1 = H_1\cos(\omega t)\,\hat{i} + H_1\sin(\omega t)\,\hat{j} \qquad\qquad \text{2-8}$$

The counter-rotating part of this field is obtained by letting $\omega \rightarrow -\omega$. If the field of Equation 2-8 is anywhere near resonance, the counter-rotating part is far from resonance and may be neglected. The presence of H_1 modifies Equation 2-5

$$\frac{d\vec{\mu}}{dt} = -\vec{\mu} \times \gamma\left(\vec{H}_\bullet + \vec{H}_1(t)\right) \qquad\qquad \text{2-9}$$

We can transform this equation to a reference frame in which both H_1 and H_0 are at rest. This reference frame rotates about the z direction with frequency ωk. The equation of motion in the rotating frame is

$$\left(\frac{\partial\vec{\mu}}{\partial t}\right)' = -\vec{\mu} \times \gamma\,\vec{H}_{eff} \qquad\qquad \text{2-10}$$

where the prime denotes the derivative taken with respect to quantities in the rotating frame, and

$$\vec{H}_{eff} = \hat{k}\left(H_o - \frac{\omega}{\gamma}\right) + H_1\,\hat{i} \qquad\qquad \text{2-11}$$

In this reference frame, the moment precesses about H_{eff} in a cone of fixed angle. The motion of the moment is periodic, with frequency γH_{eff}. At resonance, the frequency of the alternating field is equal to the Larmor frequency; equivalently, we see
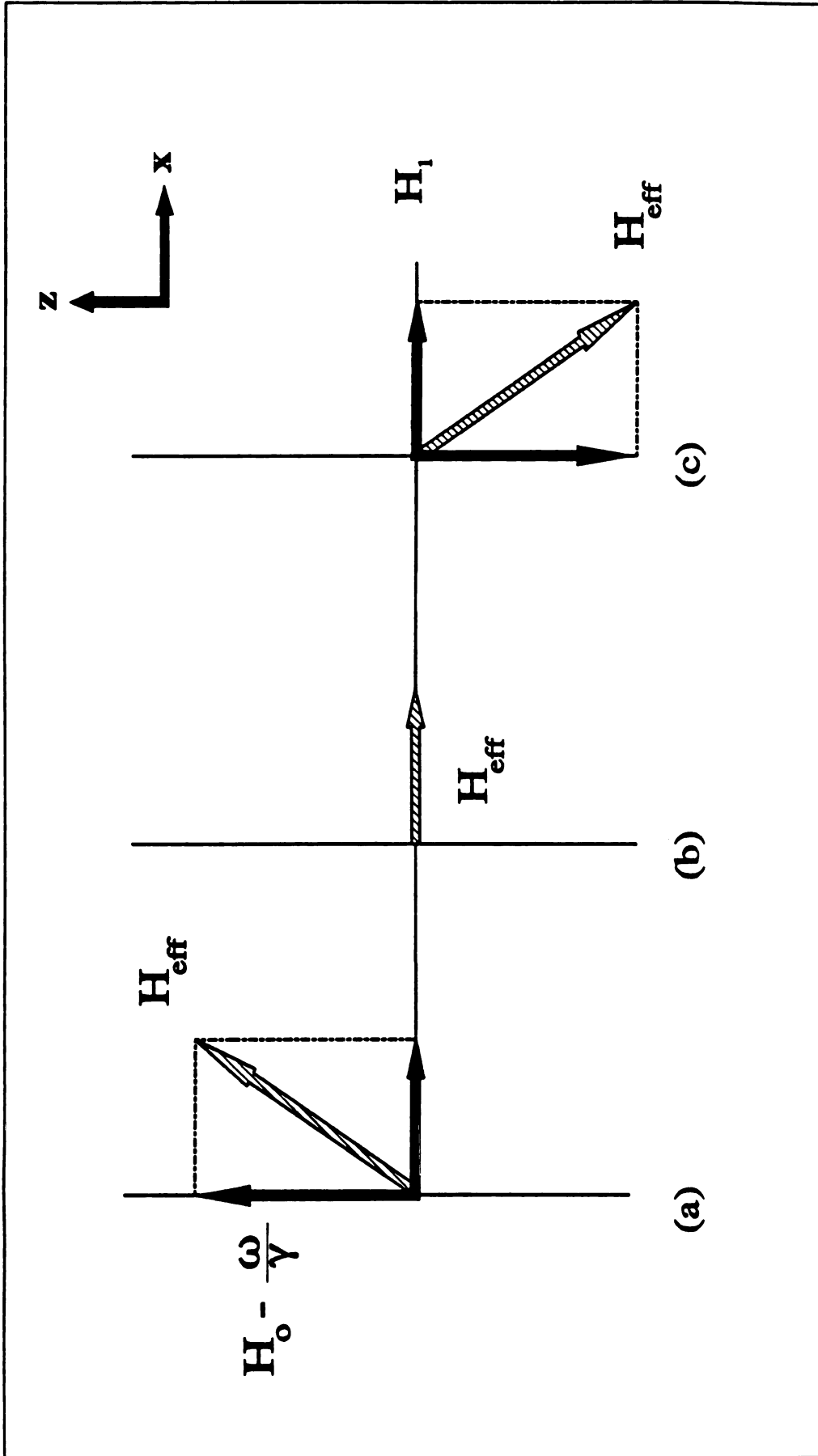
Figure 2-1: *Position of the effective magnetic field (a) above, (b) at, and (c) below resonance as viewed in the rotating reference frame*

that this implies th

rotating reference f

z component, as s

H_{eff} is negative, as

when $H_{\text{eff}} = H_1$, a

arrow. H_1 is alon

In a quantu

quantum levels. T

from an energy sta

energy correspond

Bloch Equations

Up to this p

being transferred o

would have a reso

making transitions b

with some net abso

spins, or to the latt

finite resonance lir

phenomenologically

Bloch posited

relax exponentially

that this implies that $H_{eff} = H_1$. Figures 2-1 a,b, and c illustrate the behavior in the rotating reference frame. If H_o is above resonance (greater than ω/γ), H_{eff} has a positive z component, as shown in Figure 2-1a. If H_o is below resonance, the z component of H_{eff} is negative, as shown in Figure 2-1c. Figure 2-1b shows the system at resonance, when $H_{eff} = H_1$, and $(H_o-\omega/\gamma)$ is zero. In all three figures, H_{eff} is shown by the shaded arrow. H_1 is along the x-axis and $H_0 - \omega/\gamma$-is in the x direction.

In a quantum description, a spin flip corresponds to a transition between two quantum levels. The absorption of energy from the microwaves enables the spin to flip from an energy state corresponding to being aligned with the field to a state with a higher energy corresponding to a position antialigned with the field.

Bloch Equations

Up to this point, we have considered the spins as perfect oscillators, with energy being transferred only between the spins and the magnetic fields. This ideal system would have a resonance line with no width. In a real system, spins are constantly making transitions both from lower energy states to higher energy states, and back again, with some net absorption. In order to de-excite, a spin must transfer energy to other spins, or to the lattice. Both processes take a finite amount of time, which results in a finite resonance linewidth. Felix Bloch[35] introduced the idea of relaxation times phenomenologically into the equations of motion to account for these processes.

Bloch posited that the magnetization, if pushed out of equilibrium, will tend to relax exponentially to its thermal equilibrium value, M_o. The z component of M grows

as individual mor

moments to give u

relaxation time, T

Interactions

applied field. For

locally, so that e

magnetization is re

components, and i

The Bloch

rotating reference

The details

The spin-lattice rel

and the rotating fi

susceptibility will

phase with the rota

absorptive behavio

metals, the comple

as individual moments making up M flip to relax M_z toward M_o, which requires the moments to give up energy to the lattice. This process is characterized by the spin-lattice relaxation time, T_1.

Interactions between spins can destroy the magnetization perpendicular to the applied field. For example, the dipolar interaction can randomly modify the value of H_{eff} locally, so that each spin precesses at a slightly different rate. The perpendicular magnetization is relaxed by destroying the coherence in the individual perpendicular spin components, and is characterized by the spin-spin relaxation time, T_2.

The Bloch Equations, which describe the motion of interacting spins are (in the rotating reference frame):

$$\frac{dM_z}{dt} = -\gamma \left(\vec{M} \times \vec{H}_{eff} \right)_z + \frac{M_o - M_z}{T_1} \qquad \text{2-12a}$$

$$\frac{dM_{x,y}}{dt} = -\gamma \left(\vec{M} \times \vec{H}_{eff} \right)_{x,y} + \frac{M_{x,y}}{T_2} \qquad \text{2-12b}$$

The details of the solution to the Bloch equations can be found in Appendix A. The spin-lattice relaxation time is usually much longer than the spin-spin relaxation time, and the rotating field, H_1 is taken to be much smaller than the applied field, H_0. The susceptibility will be complex, as the magnetization has components both in and out of phase with the rotating field. The imaginary part of the susceptibility (χ'') describes the absorptive behavior of the sample, while the real part (χ') describes the dispersion. In metals, the complex surface impedance results in the absorbed power being proportional

to a mixture of th

is

The functi

derivatives are sh

assumption of exp

and these lineshap

linewidth, ΔH, is

is proportional to

EXPERIMENTA

The simple

microwaves down

microwave guides,

and converted into

transmitted), and is

absorbed by the sam

to a mixture of the real and imaginary parts. The susceptibility from the Bloch equations is

$$\chi' = \frac{1}{2}\chi_o(\omega_o T_2)\left(\frac{(\omega_o - \omega)\ T_2}{1 + (\omega - \omega_o)^2\ T_2^2}\right) \qquad \text{2-13}$$

$$\chi'' = \frac{1}{2}\chi_o(\omega_o T_2)\left(\frac{1}{1 + (\omega - \omega_o)^2\ T_2^2}\right) \qquad \text{2-14}$$

The functions which result from the solution of the Bloch equations and their derivatives are shown in Figure 2-3a and b; they are Lorentzian and result from the assumption of exponential relaxation. Other types of lines are observed experimentally, and these lineshapes may be derived by assuming other forms of the relaxation. The linewidth, ΔH, is usually measured as the peak-to-peak value of the first derivative, and is proportional to the inverse of the relaxation time, T_2.

EXPERIMENTAL DETECTION OF THE RESONANCE

The simplest experimental set up consists of a microwave source, which sends microwaves down a transmission line and into a resonance cavity. Using various microwave guides, the reflected (or transmitted) microwave energy is sent to a detector and converted into a current. This current is proportional to the power reflected (or transmitted), and is smaller than the incident power (P_i) by an amount equal to the power absorbed by the sample (P_a). As the magnetic field is swept, (P_i-P_a) vs. field is plotted,

Power Absorbed (Arb. Units)

dP/dH (Arb. Units)

Figure 2-2: *(a) Absor*
derivatives
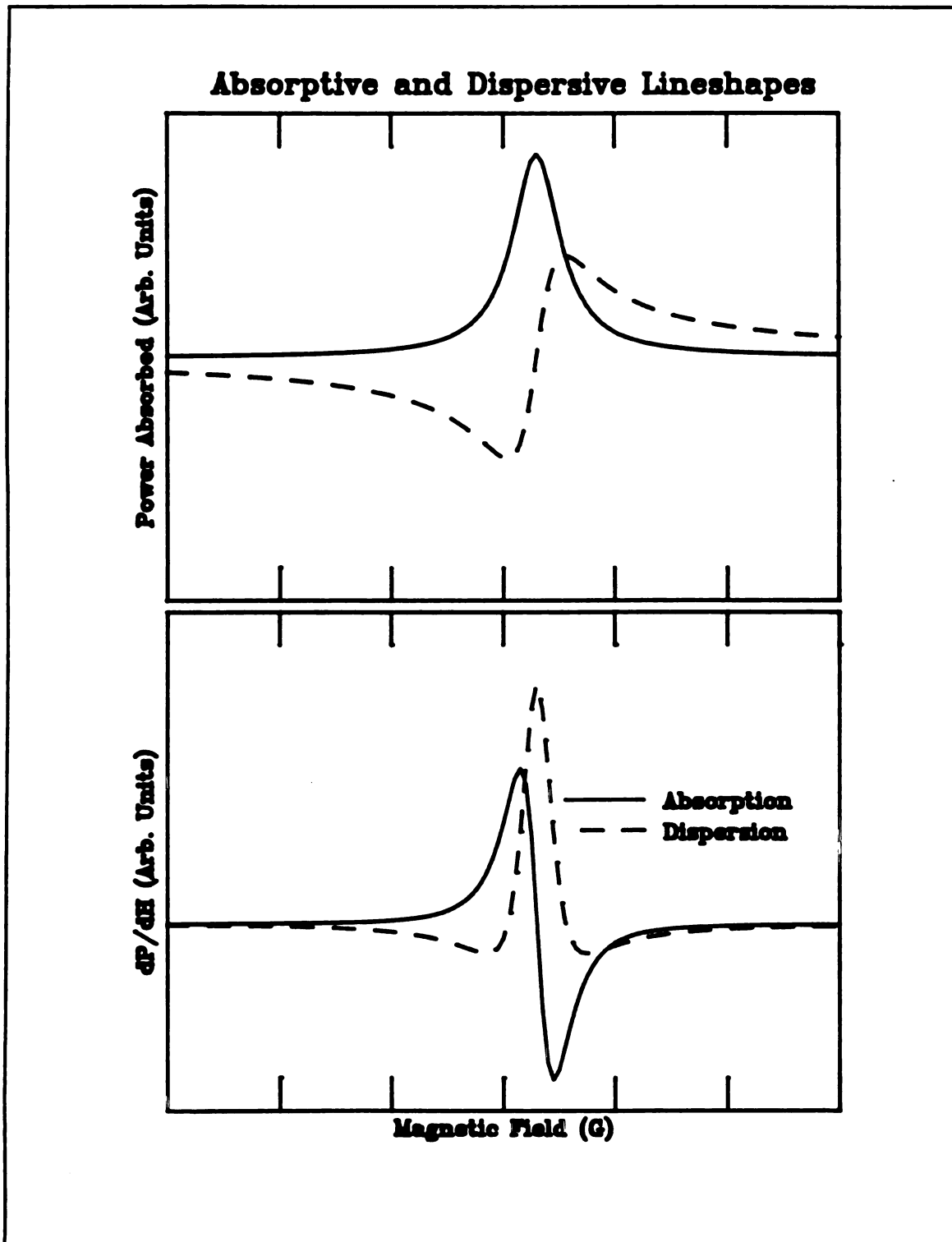
Figure 2-2: *(a) Absorptive and dispersive parts of the Lorentzian lineshape and (b) their derivatives*

and can the

interest (w

order to im

description.

The

motion of a

and spin-lat

Equations.

spins. A pr

given.

and can then be analyzed to extract parameters which relate to physical quantities of interest (which will be explained in Chapter 5). This basic set up can be modified in order to improve the detection of the signal, but the essentials are all present in this brief description.

SUMMARY

The basic elements of electron spin resonance have been presented in terms of the motion of a classical moment in a field. Relaxation times, which result from spin-spin and spin-lattice interactions have been phenomenologically considered within the Bloch Equations. Chapter Five will extend this simple model to the case of strongly interacting spins. A preliminary description of the experimental detection of the resonance has been given.

Spin

procedural

be included.

questions ab

schools of

Edwards-Ar

hierarchical

low lying ev

the droplet t

arising from

In or

or not the sp

the formalis

chapter brief

down' near a

on developir

the hierarchi

CHAPTER THREE

SPIN GLASS THEORIES

INTRODUCTION

Spin glasses pose a challenging problem for theorists. In addition to the procedural complications inherent in treating disordered systems, frustration must also be included. In addition, the wide variety of materials displaying spin glass behavior and questions about ergodicity and measuring time must be considered. There are two major schools of spin glass theory; the first developed from the mean field theory of the Edwards-Anderson and Sherrington-Kirkpatrick models, and is referred to as the hierarchical or mean field model. The second is a scaling theory which expresses the low lying excitations of a spin glass in terms of critical exponents, and is referred to as the droplet theory. This section will summarize the development of and important results arising from these two schools of thought.

In order to understand spin glass theory, and especially the question of whether or not the spin glass ordering is a true phase transition, the idea of phase transitions and the formalism used in their description must be understood. The first section of this chapter briefly reviews phase transitions and scaling formalism. The concept of 'slowing down' near a critical point will also be reviewed. The second part of this chapter focuses on developing a conceptual understanding of the two major spin glass theories. While the hierarchical model is mathematically rigorous, the upper critical dimension - the

lowest dim

to real syste

predictions

experiment

A w

identifying

Electron S

glass phase

theories di

experiment

droplet mo

Resonance

PHASE TR

Deta

references[36]

discontinuity

the divergen

heat in ferr

point, which

A ph

so that the t

lowest dimension at which mean field exponents are valid - is 6, which makes application to real systems questionable. While less theoretically rigorous, the droplet theory makes predictions which distinguish between two and three dimensions and can be experimentally tested.

A word of caution: most of the theoretical effort to this point has focused on identifying the nature of the spin glass transition and of the resulting phase. The Electron Spin Resonance experiments discussed in this thesis investigate how the spin glass phase is approached from above the transition temperature. A lot of spin glass theories dismiss this regime as being 'paramagnetic' and do not address the experimentally observed ordering effects above T_f discussed in Chapter One. Neither the droplet model nor the hierarchical model has specifically addressed Electron Spin Resonance experiments.

PHASE TRANSITIONS AND FINITE SIZE EFFECTS

Details of the study of phase transformations may be found in many references[36,37]. Mathematically, a phase transition is indicated by a singularity or discontinuity in some derivative of the free energy. Experimentally, this is indicated by the divergence of some measurable quantity (i.e. the magnetic susceptibility and specific heat in ferromagnets). The point at which the transition occurs is called the critical point, which separates the two phases.

A phase transition corresponds to the spontaneous breaking of some symmetry, so that the two phases must be described by two different functions which can not be

analytica

symmetr

order pa

above t

thermod

the order

non-zero

will be s

F

which a

approach

spatial reg

themselve

give rise

discussed

Th

approache

a critical e

as the cr

asymptotic

accompany

analytically continued across the critical point. In the ferromagnet example, a rotational symmetry exists above the Curie temperature, and is broken when the spins align. The order parameter, is (generally) a thermodynamically measurable quantity which is zero above the critical point and non-zero below and is introduced to describe the thermodynamics of the phase with the broken symmetry. In the ferromagnet example, the order parameter is the magnetization, which is zero in the paramagnetic phase and non-zero in the ferromagnetic phase. Anticipating future results, the order parameter will be symbolized by q.

Fluctuations measure the range of correlation functions; i.e., the distance over which a disturbance - like a spin wave - 'remembers' its initial state. As the system approaches a phase transition, fluctuations in the order parameters extend over large spatial regions and persist for very long times. Mathematically, the fluctuations manifest themselves as singularities. The time dependent properties of the critical fluctuations give rise to the dynamics via the fluctuation - dissipation theorem, which will be discussed later in the context of ESR theory.

The divergent behavior of a thermodynamic quantity as the critical point is approached is described by scaling, and the nature of the singularity is characterized by a critical exponent. The mathematical definition indicates that the behavior of a function as the critical point is approached is given in terms of a limit, so that f(x) is asymptotically proportional to x^λ. This asymptotic limit may not exist, but the accompanying formalism has been shown to describe experiment very well. We say that

where Δx

Crit

variety of r

they belong

related to t

or the corr

Table 3-1 s

Critical Sl

As t

to reach the

process is b

thermodyna

fluctuations

are always e

with other e

$$f(x) \sim (\Delta x)^\lambda \quad \rightarrow \quad \lim_{\Delta x \rightarrow \infty} \left[\frac{\ln f(x)}{\ln (\Delta x)} \right] = \lambda \qquad \text{3-1}$$

where $\Delta x \sim (x-x_c)$ and x_c is the critical point.

Critical exponents have proven to be exceptionally useful. In many cases, a large variety of materials can be characterized by the same set of exponents, so we say that they belong to the same universality class. Many of the thermodynamic quantities are related to the reduced temperature, t, which is defined by

$$t = \left| \frac{T - T_c}{T_c} \right| \qquad \text{3-2}$$

or the correlation length, ξ, which measures the range of a pair correlation function. Table 3-1 summarizes and defines some of the common critical exponents.

Critical Slowing Down

As the critical point is approached, a system will take increasingly longer times to reach the equilibrium state due to the presence of fluctuations. The description of this process is based on the thermodynamics of irreversible processes, and is called the thermodynamic or conventional theory of critical slowing down[38]. Physically, critical fluctuations of various sizes (with the average size being equal to the correlation length) are always excited. These excitations can then split up into smaller excitations, merge with other excitations, or dissipate into random heat, etc, with the available dissipation

Syn
c
$\hat{\beta}$
$\hat{\gamma}$
ν
$\hat{\delta}$
z

Table 3-1: Summary of Critical Exponents

Symbol	Characterizes	Definition
α	Specific Heat	$C_V \sim t^{\alpha}$
β	Order Parameter	$q \sim t^{\beta}$
γ	Susceptibility	$\chi \sim t^{\gamma}$
ν	Correlation Length	$\xi \sim t^{\nu}$
δ	Equation of State	$H \sim M^{\delta}$ (t=0)
z	Relaxation Time	$\tau \sim \xi^{z}$

paths deter

used to de

approach t

characteris

where z is

critical poi

of an orde

measureme

relaxation t

Note that th

spin glasses

exponent.

paths determining the relaxation time of the system. Critical slowing down has been used to describe the behavior of ordered ferromagnets and antiferromagnets as they approach their ordering temperatures[39,40]. Dynamic critical scaling predicts that the characteristic relaxation time of a system, τ, goes like

$$\tau \sim \left(\frac{T-T_f}{T_f} \right)^{-z\nu} \qquad \text{3-3}$$

where z is the dynamic exponent, and ν is the correlation length exponent. As the critical point is approached, the relaxation time will become infinite, indicating the onset of an ordered state. Care must be taken in relating this equation to experiments, as measurements usually measure an average relaxation time, and not a characteristic relaxation time. The average relaxation time is related to an average exponent, z_{av}, by

$$\tau_{av} \propto \left(\frac{T-T_f}{T_f} \right)^{-z_{av}\nu} \qquad \text{3-4}$$

Note that the scaling laws are written in terms of the characteristic relaxation time. For spin glasses, Ogielski[41] has shown that $z_{av} = z - \beta/\nu$ where β is the order parameter exponent.

A

therefore,

peak, and

volume c

are allow

An exam

3-1. The

line show

T

in the in

We can a

occur (in

rounding

Finite Size Effects on Critical Exponents

A phase transition can occur only when the thermodynamic limit ($N \rightarrow \infty$) is taken; therefore, a finite system will display a rounded cusp with a finite height, instead of a peak, and the position of the cusp will be displaced from the position of the infinite volume case. The simplest example is that of a system in which all dimensions but one are allowed to become infinite. The size of the finite dimension will be denoted by L. An example of the behavior due to the finite size on the specific heat is shown in Figure 3-1. The dashed line shows the specific heat in the infinite volume limit, and the solid line shows the results for a finite system.

The difference between the position of the peak in the finite case and the position in the infinite case is measured by ϵ, the fractional shift.

$$\epsilon(N) = \frac{T_c - T_m(N)}{T_c} \qquad \text{3-5}$$

We can also define a temperature, T^*, at which the first deviations from the infinite limit occur (indicated by the arrow in Figure 3-1), so that we may further define a fractional rounding, $\delta(N)$, where

$$\delta(N) = \frac{T^*(N) - T_m(N)}{T_c} \qquad \text{3-6}$$

Figure 3-1:

The

the interacti

ground state

energy is th

neighbors at

where N^x i

dimensionali
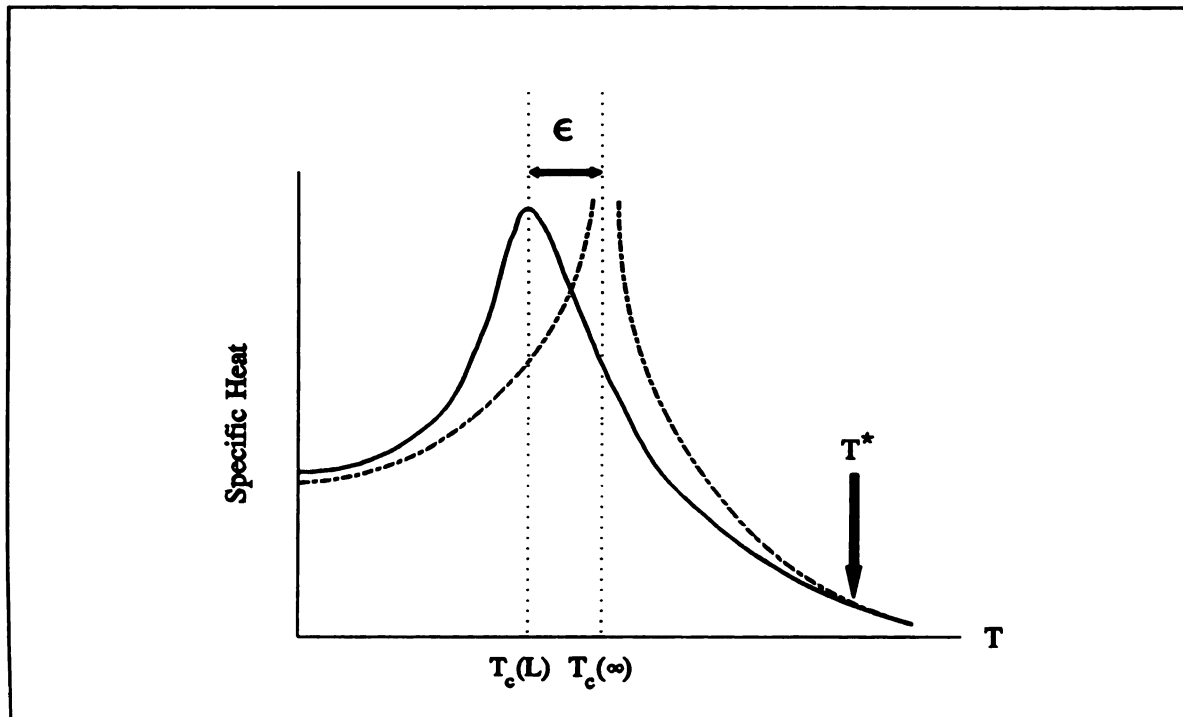
Figure 3-1: *An example illustrating finite size effects on the specific heat*

The magnitude of the critical temperature is a measure of the overall strength of the interactions. In a naive mean field picture, $k_B T_c$ is directly proportional to the total ground state energy. As an example, for a finite nearest neighbor Ising model, the total energy is that of the infinite system minus lost coupling energy due to the lack of neighbors at the surface.

$$Nk_B T_c \propto E(N) \approx dJN - JN^x \qquad \text{3-7}$$

where N^x is the number of boundary spins, J is the exchange, and d is the dimensionality. The shift will obey

$$\varepsilon \sim L^{-\lambda} \qquad\qquad\qquad \text{3-8}$$

where λ is called the shift exponent. The correlation length, ξ, which is a measure of the range of the correlation function, diverges with the reduced temperature as

$$\xi(T) \approx t^{-\nu} \qquad\qquad\qquad \text{3-9}$$

When the correlation length for a finite sample approaches sample size, finite size effects should be observed. λ and ν are (in general, but not always[37]) related by

$$\lambda = \frac{1}{\nu} \qquad\qquad\qquad \text{3-10}$$

MEAN FIELD THEORY

The Edwards-Anderson Model

The Edwards-Anderson (EA) model[42], was the first to apply standard mean field theory to the spin glass problem. This model considers classical spins placed on the vertices of a cubic lattice, with only nearest neighbor interactions. An equal likelihood of ferromagnetic and antiferromagnetic interactions is assumed, with the interaction strengths given by a Gaussian distribution. This model successfully predicts a cusp in

the sus

experim

S

which th

Edwards

written

so that t

Use of t

T

spin at t

In using

replica la

the susceptibility, but also predicts a cusp in the specific heat, which is not experimentally observed.

Solving the mean field problem for spin glasses requires a quenched average, in which the log of the free energy instead of the free energy itself must be averaged. Edwards and Anderson used the 'replica trick', in which the partition function, Z, is written

$$Z^n \sim 1 + n \ln Z \qquad\qquad \textbf{3-11}$$

so that the quenched average, denoted by an overbar, can be written

$$\overline{\ln Z} = \lim_{n \to 0} \left(\frac{\overline{Z^n} - 1}{n} \right) \qquad\qquad \textbf{3-12}$$

Use of the replica trick allows the calculation of the quenched average.

The EA order parameter is the spin correlation function q_{EA}, which correlates a spin at time t_1 to its value at some later time, t_2;

$$q_{EA} = < \vec{S}_i(t_1) \cdot \vec{S}_i(t_2) > \qquad\qquad \textbf{3-13}$$

In using the replica trick, n copies of the original system have been introduced. In replica language, q_{EA} can be interpreted as the correlation between a single spin, in two

different rep

definition of

where q_{EA} de

The Sherring

Sherrin

range case, in

to evaluate the

thermodynamic

disorder, the re

EA model, the

indices identify

parameters shou

replica symmetr

defined by

different replicas. If the Greek indices α and β represent two replicas, an alternate definition of q is:

$$q_{EA} = <\vec{S}_i^\alpha \cdot \vec{S}_i^\beta> \qquad \alpha \neq \beta \qquad \qquad \text{3-14}$$

where q_{EA} defined this way is called the overlap.

The Sherrington-Kirkpatrick Solution

Sherrington and Kirkpatrick (SK)[43,44] extended the EA model to the infinite range case, in which interactions are allowed between all spins. The replica trick is used to evaluate the quenched average, which allows calculation of the free energy and thermodynamically measurable quantities. In the evaluation of the average over the disorder, the replicas become correlated. Instead of one mean field parameter, as in the EA model, the SK model introduces two parameters - $q_{\alpha\beta}$ and m_α, where the greek indices identify replicas. SK assumed that all replicas must be equal, so that these parameters should display no dependence on the replica index. This assumption, called replica symmetry, takes $q_{\alpha\beta} = q$ ($\forall$ $\alpha\beta$) and $m_\alpha = m$ ($\forall$ α). These parameters are defined by

$$m_i = < \sum_i <S_i>>_d = \frac{1}{N}\sum_i m_i \qquad \qquad \text{3-15}$$

where th

thermal a

resulting

T

T

does not

free ener

$S(T=0)$

analytic

of a mea

$$q = <\frac{1}{N} \sum_i <S_i>^2>_d = \frac{1}{N} \sum_i m_i^2 \qquad \text{3-16}$$

where this q is the same as the Edwards-Anderson order parameter, $<>$ indicates an thermal average, and $<>_d$ indicates an average over disorder. The different phases resulting from this solution are summarized in Table 3-2.

Table 3-2: Phases Resulting From the Sherrington-Kirkpatrick Analysis

q	m	Phase
0	0	Paramagnet
$\neq 0$	0	Spin Glass
$\neq 0$	$\neq 0$	Ferromagnet

There are some difficulties with this solution. For $T \leq T_f$, the spin glass phase does not represent a minimum of the free energy - the paramagnetic phase has a lower free energy. Even more troubling, at low temperatures, the entropy is negative, with $S(T=0) = -0.16$. Theorists have questioned the use of the replica trick, the order of the analytic continuation of the replica trick and the thermodynamic limit, and the validity of a mean field approach in general. Thouless, Anderson and Palmer (TAP)[45] showed

that, at high

trick, but ob

among other

assumption o

broken led to

Replica Sym

The re

detailed, and

conceptual sp

sources[4].

Imagi

the horizonta

zeros. Meas

the product o

is the number

In the

into blocks, s

that, at high temperatures, the same solution can be obtained without using the replica trick, but obtained different results below T_f. This led de Almeida and Thouless[46], among others, to the conclusion that the problem with the SK solution was the assumption of replica symmetry. The crucial realization that replica symmetry must be broken led to the current conceptual picture described by the hierarchical model.

Replica Symmetry Breaking

The replica symmetry breaking (RSB) solution of the mean field problem is rather detailed, and only a brief outline will be given for the purpose of establishing a conceptual spin glass picture. Excellent reviews of the details are available in other sources[47].

Imagine that the $q_{\alpha\beta}$ can be arranged in a matrix, with the α index running along the horizontal and the β index along the vertical. The diagonals of this matrix will be zeros. Measurable quantities will be related to the trace of this matrix, and the trace of the product of this matrix with other matrices. α and β both run from 0 to n, where n is the number of replicas and eventually must be taken to 0 to recover the free energy.

In the first iteration of symmetry breaking[48], Parisi suggested dividing the matrix into blocks, so that the diagonal blocks form one set, and the off diagonals form another.

Element

blocks a

Parisi th

diagonal

shown in

M

temperatur

Elements in the diagonal blocks are given the value q_1, and those in the off-diagonal blocks are given the value q_0, as illustrated below:

$$
\left[
\begin{array}{cccc|cccc}
0 & q_1 & q_1 & q_1 & q_0 & q_0 & q_0 & q_0 \\
q_1 & 0 & q_1 & q_1 & q_0 & q_0 & q_0 & q_0 \\
q_1 & q_1 & 0 & q_1 & q_0 & q_0 & q_0 & q_0 \\
q_1 & q_1 & q_1 & 0 & q_0 & q_0 & q_0 & q_0 \\
\hline
q_0 & q_0 & q_0 & q_0 & 0 & q_1 & q_1 & q_1 \\
q_0 & q_0 & q_0 & q_0 & q_1 & 0 & q_1 & q_1 \\
q_0 & q_0 & q_0 & q_0 & q_1 & q_1 & 0 & q_1 \\
q_0 & q_0 & q_0 & q_0 & q_1 & q_1 & q_1 & 0
\end{array}
\right]
\qquad \text{3-17}
$$

Parisi then suggests[49] that this procedure be repeated to infinite order. Each time, the diagonal matrices further are subdivided, so that, on the second iteration, the matrix shown in Equation 3-17 becomes

$$
\left[
\begin{array}{cc|cc|cccc}
0 & q_2 & q_1 & q_1 & q_0 & q_0 & q_0 & q_0 \\
q_2 & 0 & q_1 & q_1 & q_0 & q_0 & q_0 & q_0 \\
\hline
q_1 & q_1 & 0 & q_2 & q_0 & q_0 & q_0 & q_0 \\
q_1 & q_1 & q_2 & 0 & q_0 & q_0 & q_0 & q_0 \\
\hline
q_0 & q_0 & q_0 & q_0 & 0 & q_2 & q_1 & q_1 \\
q_0 & q_0 & q_0 & q_0 & q_2 & 0 & q_1 & q_1 \\
q_0 & q_0 & q_0 & q_0 & q_1 & q_1 & 0 & q_2 \\
q_0 & q_0 & q_0 & q_0 & q_1 & q_1 & q_2 & 0
\end{array}
\right]
\qquad \text{3-18}
$$

Monte Carlo simulations[44] of spin glasses predict an internal energy at zero temperature of $U(0) = -0.76 \pm 0.01$. The replica symmetric solution of the SK model

results i

gives S

$U(0) =$

rapidly.

The free

to this c

energy 1

Ultrame

N

organiza

three sta

This is t

isosceles

any valu

of states

further c

than sor

times. i

organiza

results in $S(0) = -0.16$, $U(0) = -0.798$. The first iteration of replica symmetry breaking

gives $S(0) = -0.01$, and $U(0) = -0.765$, and the second iteration gives $S(0) = -0.03$ and

$U(0) = -0.7636$, indicating that the replica symmetry breaking solution converges

rapidly. In the limit of infinite iterations, the order parameter, $q_{\alpha\beta}$ becomes a function.

The free energy then becomes a functional of $q(x)$, and can be maximized with respect

to this continuous variable. Various approximations can be made to calculate the free

energy for different temperature and field regimes.

Ultrametricity

Mezard, *et. al.*[50], and Mezard and Virasoro[51] related the hierarchical

organization of states to the calculation of statistical quantities. They find that, given any

three states, at least two pair of them will have the same overlap with probability one.

This is the characteristic of an ultrametric space: any three points in space will form an

isosceles triangle, with the two equal angles larger than or equal to the third one. For

any value of q, the states are organized into non-overlapping clusters, such that any pair

of states inside the cluster has an overlap greater than q. Each of these clusters can be

further decomposed into smaller clusters which group together states with overlap greater

than some q', where $q' > q$. This procedure can be repeated an infinite number of

times, indicating that the set of pure states obeys a hierarchical ordering. The

organization of hierarchical space is schematically pictured in Figure 3-2

Figure 3-

In

state as a

vertices

correspor

at a give

contained

Th

The high

overlap.

exists a p

magnetiza
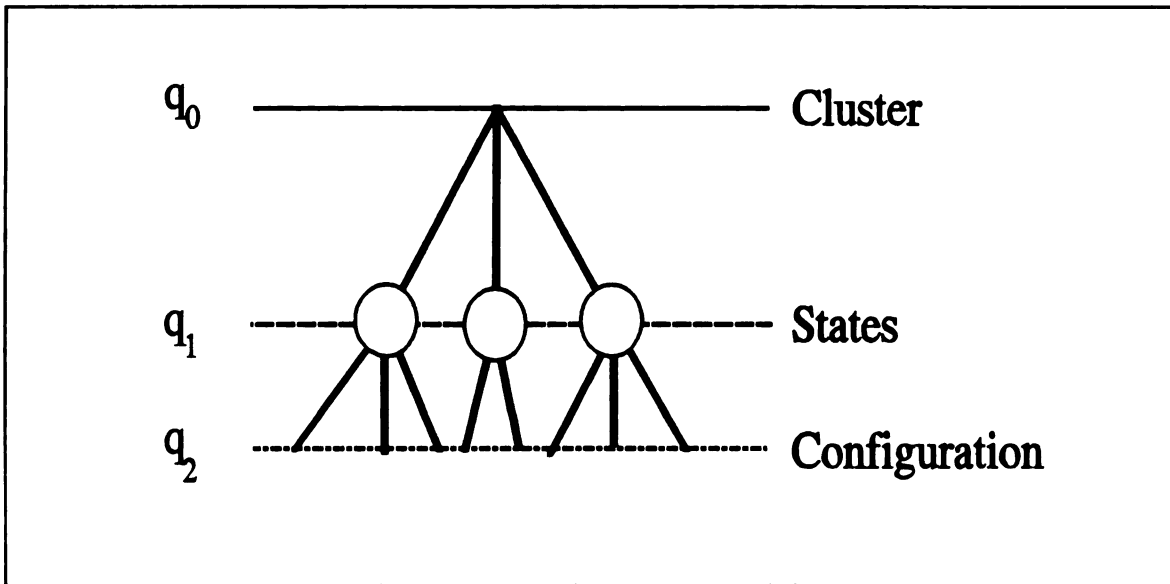
Figure 3-2: *Topology of ultrametric states*

In this figure, the highest level will correspond to a cluster. If we define a pure state as a state which cannot be broken down into a combination of other states, the three vertices shown correspond to pure states, with $q_1 = q_{EA}$. q_2 will be equal to 1 and correspond to different configurations within a pure state. To calculate the magnetization at a given site, an average is taken over a large representative set of configurations contained in the cluster.

The overlap between two states depends only on their closest common ancestor. The higher up you have to go on the tree to find a common ancestor, the smaller the overlap. All the pure states with a common ancestor share a common property; there exists a partition of the N sites into disjoint macroscopic cells such that the average magnetization of each of these states in every cell is the same, within some given

resoluti

taking a

(and the

field.

AT and

T

hierarchi

experime

a magnet

W

describe

Thouless

the Ising

Above th

energy of

free energ

valleys is

resolution. This has enabled the development of a rather complicated procedure for taking averages using the hierarchical tree for the purpose of computing the free energy (and thermodynamic quantities calculable from the free energy) at any temperature and field.

AT and GT Lines

The mean field picture has stimulated some exotic calculations based on the hierarchical structure of states, but has also resulted in some more conventional and experimentally testable predictions. The question of what happens to a spin glass when a magnetic field is applied has been addressed by both theoreticians and experimentalists.

Within mean field theory, two lines in the magnetic field - temperature plane describe the effect of the field on the spin glass transition temperature. De Almeida and Thouless[46] (AT) predicted that the dependence of the freezing temperature on field, for the Ising mean field model, would be described by

$$H_{AT}(T) \propto \left(\frac{T_f - T}{T_f} \right)^{-\frac{3}{2}}$$

3-19

Above this line, the free energy is smooth with a single valley as found in the free energy of a paramagnet, while below this line, the free energy becomes the complicated free energy surface of a spin glass. The time the system takes to transit between any two valleys is macroscopic, so we see irreversible behavior associated with the onset of this

state. The A

the paramagn

For H

the componer

Gabay and T

should occur

The longitudir

claimed that tl

replica symmc

part to experin

freezing of the

be thought of

irreversible be

irreversibility

existence of a (

transverse degr

crossover from

fields. This has

mean field theor

state. The AT line marks the transition between the reversible behavior associated with the paramagnetic phase and the irreversible behavior due to the spin glass phase.

For Heisenberg spins, the presence of a field selects a preferred direction, so that the components of the spin longitudinal and transverse to the field will freeze differently. Gabay and Toulouse[52] (GT) predicted that the freezing of the transverse components should occur at the GT line, which is defined by

$$H_{GT}(T) \propto \left(\frac{T_f - T}{T_f} \right)^{-\frac{1}{2}} \qquad \text{3-20}$$

The longitudinal components will freeze at the AT line. Gabay and Toulouse originally claimed that the region between the GT and AT lines represented the region where the replica symmetric solution is correct, but this has been shown to be incorrect[53], due in part to experimental indications that the longitudinal components will be affected by the freezing of the transverse components. For Heisenberg spin glasses, the GT line may be thought of as the line marking the transition from reversible behavior to weakly irreversible behavior, and the AT line as indicating the transition from weak irreversibility to strong irreversibility. Little experimental evidence exists for the existence of a GT line in real materials. Anisotropy which couples the longitudinal and transverse degrees of freedom (like the DM) has been predicted to be responsible for a crossover from Ising-like behavior in low fields to Heisenberg-like behavior in high fields. This has been experimentally observed by Fert and Levy[54] and predicted within mean field theory by Kotliar and Sompolinsky[55].

Dynamic

hierarchical app

below T_f, and w

introduces dyna

The SK

artificially introd

were used in the

the autocorrelati

down with a dec

Sompolin

equations for the

which favors th

calculation esche

equation of moti

which is the resp

spin fluctuations

of the system is p

with the results f

field spin glasses.

Dynamics Within the Mean Field Model

Dynamics in the mean field model can be broken into two approaches. The hierarchical approach uses the mathematics of ultrametricity to predict the dynamics below T_f, and will shed no light on the present investigation. The second approach introduces dynamics into the SK model and can be used above T_f, as well as below.

The SK model has no natural intrinsic dynamics, so the dynamics must be artificially introduced, usually within an equation of motion approach. Glauber dynamics were used in the SK paper to predict that the susceptibility should diverge as t^1, and that the autocorrelation function ($C(t) = \,<S(t)\,S(t+\tau)>$) should experience critical slowing down with a decay rate proportional to t^{-2}.

Sompolinsky and Zippelius[56] used a self consistent formulation of the Langevin equations for the relaxation of soft spin (S is a continuous variable in a symmetric well which favors the values ± 1) fluctuations in the Edwards-Anderson model. Their calculation eschews the use of replicas, relying on linear response theory to generate an equation of motion for the spin variable in terms of a propagator (Green's Function), which is the response function of the spins to the field. Above T_f, the low frequency spin fluctuations will be characterized by a generalized damping function. The relaxation of the system is predicted to diverge at a rate t^1. Their results above T_f are in agreement with the results from the SK model and calculations on generalized short-ranged mean field spin glasses. The relaxation time may be found from

where C(t) is

where P(τ') is

Using

Use of the m

diverges with

z varies from

Heisenberg sp

field along th

summarized in

Experin

remanent mag

focus on coolin

to some final m

increases rapid

glass is 'caugh

the states have

$$\tau = \frac{1}{1 - C} \int_0^\infty [C(t) - C]\, dt \qquad\qquad 3\text{-}21$$

where C(t) is the spin spin correlation function. The average relaxation time is given by

$$\tau_{ave} = \int_0^\infty P(\tau')\, \tau'\, d\tau' \qquad\qquad 3\text{-}22$$

where $P(\tau')$ is a probability distribution of relaxation times.

Using dynamical scaling at zero field, Sommers and Fischer[57] predict $z\nu = 2$. Use of the mean field value of $\nu = 0.5$ predicts $z = 4$. The average relaxation time diverges with $z_{av}\nu = 1$, predicting that $z_{av} = 2$. When a field is applied, the exponent z varies from 4 at H = 0, T = T_f to 5.0 as H goes to infinity and T to 0. In a Heisenberg spin glass, Fischer[58] finds that z keeps its universal value of 4 in non-zero field along the entire GT line. Dynamic critical exponents for spin glasses are summarized in Appendix B.

Experimentally, the hierarchical picture has been used to predict the decay of remanent magnetization and ageing phenomena below T_f. Most of these experiments focus on cooling the system through the freezing temperature in a constant magnetic field to some final measurement temperature. As the cooling takes place, the number of states increases rapidly as a result of the formation of the multivalleyed free energy; the spin glass is 'caught' in a large number of metastable states. The number and properties of the states have been calculated within the hierarchical model. Various phenomena can

be examined by

before making t

after the measu

predicts that fiel

it takes for the s

field. As the

temperature, ne

change the mea

are concerned

hierarchical mc

THE DROPL

The d

Moore[61,62]. F

making predic

behavior. Fis

assumes that t

the nature of c

not the param

singularity in

energy and en

T, but since tl

be examined by varying the magnitude of the cooling field, the amount of time elapsed before making the measurement, the length of time the cooling field is allowed to persist after the measurement temperature has been reached, etc. The hierarchical model predicts that field cooling decreases the barrier heights between states, so that the time it takes for the system to change from one state to another should depend on the applied field. As the amount of corrugation in the free energy increases with decreasing temperature, new metastable energy minima are constantly appearing, which should change the measurable quantities of the system. The experiments presented in this thesis are concerned with the regime above and nearing T_f, so the predictions of the hierarchical model below T_f will not be further considered.

THE DROPLET MODEL

The droplet model was first proposed by McMillan[59,60], and Bray and Moore[61,62]. Fisher and Huse[63,64,65] (FH) have formalized and extended this model, making predictions which differentiate between two dimensional and three dimensional behavior. Fisher[66] has noted that, contrary to conventional dynamic scaling, where one assumes that the relaxation time of a system with fluctuations on scale L goes like L^z, the nature of disordered systems implies that the natural log of relevant parameters and not the parameters themselves are the proper scaling variables. In ordered systems, the singularity in the free energy which causes a critical point is due to competition between energy and entropy. The contribution of entropy to the free energy is on the order of T, but since the characteristic scale of the free energy is also of order T, there will in

effect be no

behavior of

energy with

have region

is very wide

factor, the di

The F

placed Ising

represent the

describe the n

presented is of

coherent colle

group of spins

excitations will

short spatial ex

behavior, will

spins.   The t

thermodynamic

The FH

ferromagnet, θ is

and FH argue tha

effect be no barriers, and no activated behavior. Barriers will exist in systems where the behavior of the free energy is caused by competition between two different types of energy with at least one energy being random. Since every quantity on the scale L will have region to region fluctuations due to randomness, the distribution of barrier heights is very wide. If the time for surmounting a barrier is proportional to the Boltzmann factor, the distribution of barrier heights should result in activated scaling.

The Fisher-Huse model starts with an Edwards-Anderson lattice of randomly placed Ising spins with short range interactions. In the same way that spin waves represent the low energy excitations for ferromagnets, FH developed an ansatz to describe the nature of the low lying excitations in spin glasses. The conceptual picture presented is of a collection of non-overlapping droplets. A droplet is a minimum energy coherent collection of spins with one phase, separated by a domain wall from another group of spins which differ by a universal spin flip. The majority of the low energy excitations will be high frequency excitations involving small groups of spins, and having short spatial extent. The low frequency excitations, which will dominate the long time behavior, will involve the coherent flipping of a droplet containing a large number of spins. The thermodynamic properties of the system are determined by how thermodynamic quantities scale with droplet size.

The FH Ansatz is that the free energy of a droplet of size L scales as L^{θ}. For a ferromagnet, θ is equal to d-1, but in a spin glass, frustration will reduce the exponent, and FH argue that

The distributio

median. and s

If θ <

some length s

will prevent sp

and the param.

which allows u

If θ is

activated at lov

will always be

will dominate

length scales g

Relaxat

barriers. The l

to scale like L

proportional to

system, τ, will

$$\theta \leq \frac{d-1}{2} \qquad\qquad 3\text{-}23$$

The distribution of droplet free energies will have a width which is comparable to its median, and scales like $L^{-\theta}$.

If $\theta < 0$, large, low energy excitations at T = 0 will be numerous, so that, on some length scale, there will be a large density of quasi-independent excitations which will prevent spin glass ordering. In this regime, the transition temperature must be zero, and the paramagnetic correlation length, ξ_+, is given by

$$\xi_+ \sim \left(\frac{1}{T}\right)^{\frac{1}{|\theta|}} \qquad\qquad 3\text{-}24$$

which allows us to identify $\nu = (1/\theta)$.

If θ is positive, then very few of the large scale droplets will be thermally activated at low temperatures. The distribution of droplet widths is very broad, so there will always be some droplets which will be active at any temperature, and these droplets will dominate the equilibrium measurements. Low lying excitations will occur on all length scales greater than the correlation length.

Relaxation of the low lying excitations is hindered by the presence of energy barriers. The height of barriers to relaxation of a droplet of length scale L are assumed to scale like L^ψ, for $L \leq \xi$ and where d-1 $\geq \psi \geq \theta$. The relaxation of these modes is proportional to the Boltzmann factor. The characteristic relaxation time of the whole system, τ, will be due to those droplets at scale ξ; at scales greater than ξ, the effects

of entropy redu

The relaxation

be found in a 2

for $T > T_f$, an

The Behavior o

The Fish

glass systems w

relaxation time

than the correlat

the measurement

of the cusp being

Decreasin

behavior. For te

of entropy reduce the barriers, and the regions of size ξ will flip roughly independently. The relaxation time of the full system (assuming a zero transition temperature as would be found in a 2D system) satisfies;

$$\ln \tau \sim \frac{1}{T^{1+\psi_2 \nu_2}} \qquad \text{3-25}$$

for $T > T_f$, and where subscripts on the exponents denote their dimensionality.

The Behavior of Thin Films Within the Droplet Model

The Fisher-Huse theory has been modified[63] for application to multilayered spin glass systems with spin glass layer thicknesses W_{SG}. On time scales shorter than the relaxation time of the system, only fluctuations of the system on length scales shorter than the correlation length will be measured. A cusp in the susceptibility results when the measurement time, t_m, becomes shorter than the equilibration time, with the position of the cusp being given by

$$\frac{T_f(t_m)}{T_c} \sim \left(\frac{W_{SG}^{(\psi_3 + \psi_2 \nu_2 \theta_3)}}{\ln t_m} \right)^{-(1 + \nu_2 \psi_2)} \qquad \text{3-26}$$

Decreasing W_{SG} results in a crossover between two and three dimensional behavior. For temperatures far below T_f, the relaxation time at scale ξ is

which results i

time.

This prediction

W_{SG} larger thar

Near T_t,

finite size scalin

where z_3 is the

critical scaling

W_{SG} and the tru

less than the m

correlation lengt

by

$$\ln \tau \sim \frac{W_{SG}^{(\Psi_3 + v_2 \Psi_2 \theta_3)}}{T^{(1 + \Psi_2 v_2)}}$$ 3-27

which results in a measured freezing temperature which depends on the measurement time,

$$\frac{T_f(t_m)}{T_g} \sim \left[\frac{W^{\Psi_3 + \Psi_2 v_2 \theta_3}}{\ln(t_m)} \right]^{\frac{1}{1 + v_2 \Psi_2}}$$ 3-28

This prediction assumes thin layers, $T_f(W_{SG})$ much less than the bulk value $T_f(\infty)$, and W_{SG} larger than the average separation between Mn impurities.

Near T_f, the relaxation time of the film will be governed by conventional dynamic finite size scaling,

$$\tau \sim W_{SG}^{z_3}$$ 3-29

where z_3 is the three dimensional dynamic critical exponent. (In the case that dynamic critical scaling doesn't apply, we can simply write $\tau(W_{SG},T_g)$ as a general function of W_{SG} and the true freezing temperature, T_g). The relaxation time of the system must be less than the measuring time, or the system will fall out of equilibrium before the correlation length reaches the size of the film. The relaxation time of the system is given by

or

In the

by

which introduce

The Effect of N

For thre

predicted; the

occurs when th

symmetry about

third phase is w

expected to exis

In the Fi

freezing transiti

$$\ln(\tau \, t^{\nu_3 x_3}) \sim (t^{\nu_3} W_{SG})^{\psi_3 + \nu_2 \psi_2 \theta_3} \qquad \text{3-30a}$$

or

$$\tau \sim t^{-\nu_3 x_3} \exp\left[t^{\nu_3(\psi_2 + \theta_3 \nu_2 \psi_2)} W_{SG}^{(\psi_2 + \theta_3 \nu_2 \psi_2)} \right] \qquad \text{3-30b}$$

In the critical region, the shift of the freezing temperature from T_g will be given by

$$\frac{T_g - T_f(t_m)}{T_g} \sim W_{sg}^{-\frac{1}{\nu_3}} \left[\ln\left(\frac{t_m}{W_{sg}^{\nu_3}} \right) \right]^{[(\psi_3 + \nu_2 \psi_2 \theta_3)\nu_3]^{-1}} \qquad \text{3-31}$$

which introduces logarithmic corrections to the measurement of ν_3.

The Effect of Magnetic Fields

For three dimensional droplet models in an applied field, three phases are predicted; the first is a paramagnetic phase, as for the Ising case. The second phase occurs when the symmetry in the direction of the field is broken, but the rotational symmetry about the field still exists, in analogy to the GT line in mean field theory. The third phase is when symmetry is broken in all directions. Only two ground states are expected to exist.

In the Fisher-Huse model, the presence of a small applied field will suppress the freezing transition. The relaxation times will grow, but not diverge, as T_f is approached.

The broad dist

temperature $T_f($

time scales long

is predicted to 1

which is only w

enough. The lc

In magnetic fie

$(J \sim k_B T_g)$, the

appreciable hyst

THE GRIFFIT

Griffiths'

nonanalytic func

temperature of t

that of the pure

macroscopic reg

represent averag

The broad distribution of relaxation times will result in freezing characterized by a temperature $T_f(H, t_m)$, below which the majority of the relaxation phenomena occur on time scales longer than the measuring time. For small fields, the freezing temperature is predicted to be

$$\frac{T_g - T_f(H, t_m)}{T_g} \sim H^{\frac{2}{\gamma + \beta}} \left(\ln(\omega \tau_0) \right)^{\frac{d-2\theta}{\psi(\gamma + \beta)}} \qquad 3\text{-}32$$

which is only weakly dependent on the measuring time if the measuring time is small enough. The logarithmic factor is a correction to the de Almeida-Thouless prediction. In magnetic fields where the Zeeman energy is comparable to the exchange energy $(J \sim k_B T_g)$, the collective aspects of spin glass freezing should not be seen, and appreciable hysteretic phenomena will occur only at very low temperatures.

THE GRIFFITHS PHASE

Griffiths[67] showed that the free energy of a dilute Ising ferromagnet is a nonanalytic function of the external magnetic field for all temperatures below the critical temperature of the corresponding non-dilute system. When the temperature is between that of the pure system and the ordering temperature of the dilute system, there exist macroscopic regions of the sample which are ordered. Static measurements, which represent average quantities, are incapable of detecting these regions.

ph

ordering

thus dom

ground st

infrequen

the size c

is the tem

dilute ma

In

a nonexp

ferromag

and for a

R

phase in

correlatio

temperatu

perturbati

Physically, large 'rare' regions which are characteristic of systems with higher ordering temperatures will relax more slowly than the average of the system, and will thus dominate the long time dynamics. These large clusters will lock into one of two ground states (related by a global spin reversal) and will flip into the opposite state infrequently. Regions of a particular size will dominate on a particular time scale, with the size of the dominant regions increasing with time. The Griffiths temperature, T_G, is the temperature of the corresponding non-dilute phase, which is higher than that of the dilute magnet; $T_c \leq T_G$.

In the Griffiths phase ($T_c < T < T_G$), relaxation of these clusters will result in a nonexponential form for the spin autocorrelation function, $C(t)$. For a random Ising ferromagnet[68];

$$C(t) \sim \exp[-A(\ln t)^{\frac{d}{d-1}}]$$

3-33

and for a random Heisenberg ferromagnet[69]

$$C(t) \sim \exp(-Bt^{\frac{1}{2}})$$

3-34

Randeria, Sethna and Palmer[70] have considered the possibility of a Griffiths phase in spin glasses. In a d-dimensional short range Ising spin glass, they find the correlation function to be bounded below by the expression in Equation 3-34 in some temperature range above the spin glass transition. The bound disappears to all orders in perturbations about high temperature and dimensions, which is perhaps why there is no

evidence

Figure 3-

T

Figure 3-

Th

real syste

swamped

support t

paramagn

Th

simulation

evidence for this phase in mean field theory. They suggest the phase diagram shown in Figure 3-3.
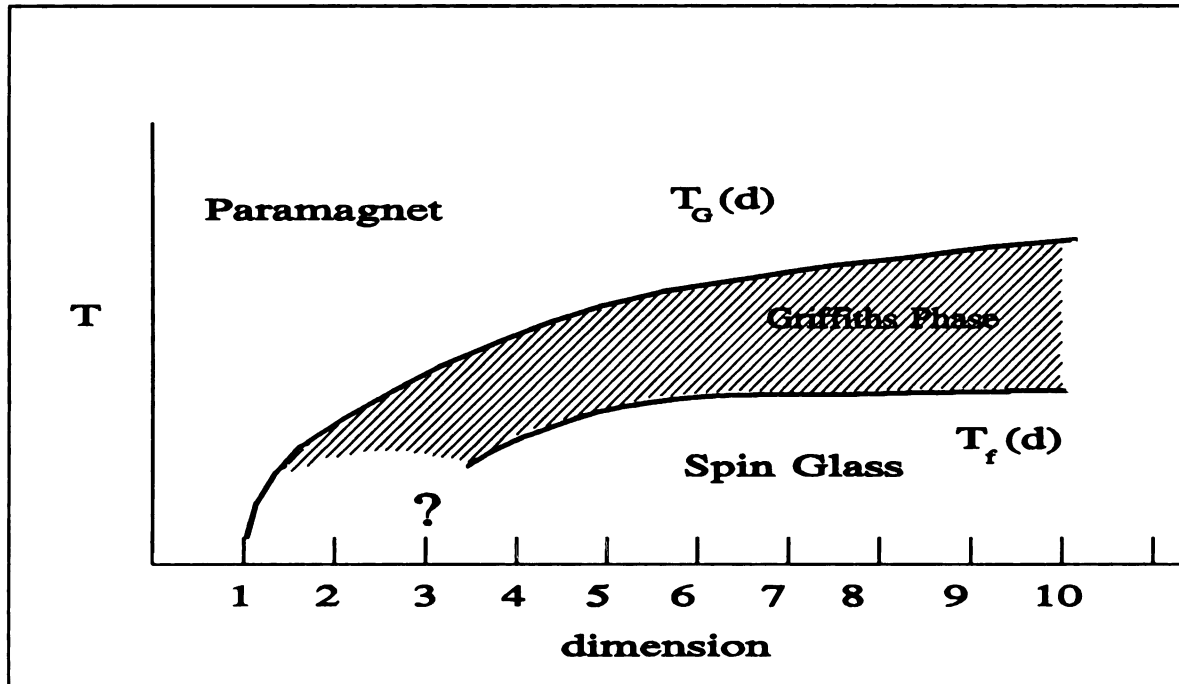
Figure 3-3: *Temperature - dimension phase diagram for Ising spin glasses (after Ref 70)*

The authors emphasize that the lower bound is strictly for an ideal system; in a real system, sample inhomogeneities would enhance clustering, and the bound would be swamped. The experimental observations of ordering above T_f described in Chapter One support the existence of an intermediate phase between the spin glass ordering and paramagnetic phases.

Theoretical existence of this phase is found in Ogielski's[41, 163] Monte Carlo simulations of the dynamic behavior of short range three dimensional Ising spin glasses

in a m

nonran

As the

1.5 T,.

relaxat

regime

of thes

seen as

simula:

SUMN

of spir

dimens:

upper c

differen

extensiv

magneti

of the fr

next cha

15,000 C

in a magnetic field. Three distinct regimes are noted; Above the Curie point of the nonrandom ferromagnetic Ising model, (T_c = 3.8 T_f), paramagnetic behavior is observed. As the temperature is lowered, a different type of behavior is seen between 3.8 T_f and 1.5 T_f, in which short range correlations cause a change in the form of the decay of the relaxation functions. The spin-glass correlation length and the correlation times in this regime are very small compared to those in the spin glass phase, as is the rate of increase of these quantities with decreasing temperature. From 1.5 T_f to T_f, critical behavior is seen as the spin glass phase is approached. Ogielski finds $z_{av}\nu$ = 7.2 ± 0.1 from these simulations.

SUMMARY

The hierarchical/mean field and droplet models present two very different pictures of spin glasses. The biggest difference between them for our purposes is the dimensionality of the models. The hierarchical model is a mean field model with an upper critical dimension of 6. The droplet model considers experimentally measurable differences between two and three dimensional behavior. The droplet model has been extensively used in previous analyses of multilayered spin glasses.

The other major difference between the models is the effect of an applied magnetic field. Within mean field theory, the AT and GT lines predict the dependence of the freezing temperature on magnetic field. Experimentalists, as we shall see in the next chapter, have claimed measurement of the AT/GT line(s) in fields of up to 15,000 G. The droplet picture predicts a similar dependence of the observed T_f (to

within

measur

Fisher-

transiti

have r

The fo

T_f is v

'param

region

of the

experi

of the

under

behav

approa

within a logarithmic dependence on measuring time), but with the caveat that this measurement represents a falling out of equilibrium and not a phase transition. In the Fisher-Huse formalism, the presence of any finite magnetic field will prevent a spin glass transition.

The novelty of the spin glass phase and questions about the nature of the transition have resulted in a lack of theoretical investigation of the temperature region above T_f. The formation of clusters and the onset of short range order at temperatures far above T_f is well documented experimentally and indicates that labeling this region as simply 'paramagnetic' is incorrect. The idea of a 'Griffiths phase', in which macroscopic regions of a sample become correlated at temperatures above the ordering temperature of the sample as a whole, has been suggested to explain the behavior in this regime. No experimental evidence of a Griffiths phase in spin glasses has been reported.

This brief foray into spin glass theory may appear to have shown only that neither of these theories will be of any use in explaining results above T_f. A conceptual understanding of these pictures is important in that any theory developed to explain the behavior above T_f must be consistent with one of these interpretations as T_f is approached.

glasse

of bc

transi

frequ

of mt

be co

summ

multi

dimer

occur

RKK\

and S

sampl

size e

CHAPTER FOUR

REVIEW OF PREVIOUS STUDIES OF

MULTILAYERED SPIN GLASSES

INTRODUCTION

This chapter summarizes the current understanding of multilayered metallic spin glasses. Extensive measurements of T_f in multilayers and subsequent analysis in terms of both finite size and dimensionality effects are reviewed, and the picture of the transition from three to two dimensions is established. The importance of measuring frequency and field will be investigated for relevancy to the ESR study. Measurements of multilayered semiconducting spin glasses and a two dimensional Ising spin glass will be compared with results from metallic multilayers. The final section of this chapter will summarize the current understanding of finite size and dimensionality effects in multilayered metallic spin glasses.

An important question in the study of spin glasses is the value of the lower critical dimension (LCD). The LCD is the dimension below which a phase transition can only occur at zero temperature. Computer simulations[28] indicate that the LCD for long range RKKY spin glasses should be between two and three. Advances in thin film fabrication and SQUID technology have made possible the creation and measurement of spin glass samples on a nanometer scale. In long range ordered magnets, like ferromagnets, finite size effects are not evident until sample size is on the order of monolayers, due in part

58

to the

system

much

the di

ideal

too s

multi

nonr

glass

<u>MU</u>

expe

and

are

rang

perc

30 n

were

times

to the strength of the spin-spin interactions, and the non-random nature of the spin system. In spin glasses, the complex interactions cause observable finite size effects at much larger layer thicknesses. Further reduction of the size of the sample can reduce the dimensionality of the material. These properties make thin film spin glass structures ideal for investigation of the LCD and finite size/dimensionality effects.

As the spin glass thickness decreases, the corresponding magnetic signal becomes too small to measure with standard susceptometers. This necessitates the fabrication of multilayers - structures which separate the spin glass layers with buffer layers of nonmagnetic material of sufficient thickness to prevent coupling between different spin glass layers.

MULTILAYERED METALLIC SPIN GLASSES

Kenning, et. al.,[71,72] fabricated the first multilayered CuMn structures to experimentally determine the lower critical dimension (LCD). Details of the fabrication and characterization of these samples will be given in Chapter 6, as the same techniques are used in this thesis. Samples were fabricated with spin glass layer thicknesses, W_{SG}, ranging from 1000 nm to 2 nm, with Mn concentrations of 4, 7, 14 and 21 atomic percent. Interlayers of Cu and Si were studied, with experimental results indicating that 30 nm of Cu and 7 nm of Si are sufficient to prevent interlayer coupling. Measurements were made in a SQUID susceptometer in magnetic fields of 100 - 200 G and measuring times of 300-400 seconds. The freezing temperature from these quasi-static

mea

sus

Fin

the

the

T/V

whe

enti

valic

conc

a va

are (

Base

the r

≥ 2

other

be th

measurements is extracted from the position of the cusp in the temperature dependent susceptibility.

Finite Size and Dimensionality Effects on T_f

Both finite size and dimensionality effects have been observed in the behavior of the freezing temperature as a function of layer thickness. Finite size scaling predicts that the freezing temperature of a sample with spin glass layer thickness W_{SG} (represented by $T_f(W_{SG})$) is given by

$$\frac{T_f(\infty) - T_f(W_{SG})}{T_f(\infty)} \sim W_{SG}^{-\lambda} \qquad \text{4-1}$$

where λ is the inverse of the correlation length exponent, ν. Although data over the entire range of layer thicknesses can be fit to Equation 4-1, finite size scaling should be valid only in a small region about the bulk value of T_f. Fitting the data from all concentrations to a single exponent results in a value of $\lambda = 0.7 \pm 0.05$, which implies a value of $\nu = 1.4 \pm 0.1$. By plotting log $[T_f(W_{SG})/T_f(\infty)]$ vs. log$[W_{SG}]$, two regimes are observed, separated at about 20 nm. (Figure 7-4 shows an example of such a plot.) Based on this observation, and the frequency dependent data which will be discussed in the next section, Kenning, et. al. chose to use finite size scaling for samples with W_{SG} $\geq$ 20 nm, resulting in a value of $\nu = 1.1 \pm 0.3$. This value can be compared with other measurements of ν shown in Appendix B. If the correlation length is defined to be the sample thickness at which size effects are first noticeable, Kenning, et. al. find

$\xi =$

conc

larg

in t

alrea

rour

a tru

prec

3-3]

whe

dime

An e

revis

Huse

in A

struct

$\xi = 100$ nm. The normalized plot of $T_f(W_{SG})/T_f(\infty)$ vs. layer thickness shows that concentrations from 4 at.% to 14 at.% all exhibit the same behavior, indicating that larger concentrations do not display markedly increased ferromagnetic interactions.

One prediction of finite size scaling - a rounding of the divergence - is not seen in these samples. Sputtered samples may be sufficiently strained so that the cusp is already broadened beyond the point where rounding might be seen. Alternatively, the rounding may not be observed because the feature in the susceptibility is a cusp and not a true divergence.

Below the 20 nm length scale, the data can be analyzed using the Fisher-Huse prediction for the freezing temperature for small layer thicknesses as given by Equation 3-31. We can write this as

$$\frac{T_f(W_{SG})}{T_f(\infty)} \sim W_{SG}^a \qquad\qquad 4\text{-}2$$

where $a = (\psi_3 + \psi_2 \nu_2 \theta_3)/(1 + \nu_2 \psi_2)$ and the subscripts on the exponents indicate dimensionality. Fitting to $2 \leq W_{SG} \leq 20$ nm, a value of $a = 0.5 \pm 0.1$ is obtained. An extension of this study to thinner samples and including data for AgMn[73] finds a revised value of $a = 0.8$, which is in agreement with the requirement from the Fisher-Huse theory that $a \leq \psi \leq 2$. Stubi, et. al.[74] have shown that similar behavior is seen in AgMn/Ag, AgMn/Cu and CuMn/Ag as is seen in CuMn/Cu, suggesting that these structures belong to the same universality class.

tempe

times

depen

static

times

susce_j

with t

a criti

like

where

equilit

that th

Frequency Dependence of the Freezing Temperature

At high temperatures, spin glass susceptibilities obey a Curie law. At some temperature (as high as 5 T_f[22]), deviations from this behavior appear as the relaxation times begin to increase. Below this temperature, the susceptibility is frequency dependent, and the magnetization exhibits irreversibility and waiting time effects. The 'static' or equilibrium susceptibility still follows the Curie law, but longer and longer times are needed to experimentally measure this behavior. The ability to measure the susceptibility over a wide range of frequencies provides a powerful means of comparison with theory. We have seen in Chapter 3 that standard phase transition dynamics predict a critical slowing down of the relaxation times, so that the maximum relaxation time goes like

$$\tau_{max} = \tau_0 \left(\frac{T_f - T_g}{T_g} \right)^{-zv} \qquad 4\text{-}3$$

where T_f is the freezing temperature measured at frequency $\omega = 1/\tau_{max}$, and T_g is the equilibrium freezing temperature. The Fisher-Huse thermally activated dynamics predicts that the frequency dependence of the freezing temperature should behave like

$$\ln\left(\frac{\tau_m}{\tau_0} \right) \sim \frac{(T_f - T_g)^{-\psi v}}{T_f} \qquad 4\text{-}4$$

In t

Freq

seco

Univ

of 1

cusp

the

of th

typi

mea

1.40

Ising

whic

1000

secor

$zv =$

of th

In the case of two dimensional behavior, Equation 4-4 is modified by setting $T_g = 0$.

Frequency dependent susceptibility measurements with measuring times from 10^{-4} to 10^4

seconds have been made on multilayered CuMn/Cu samples by the group at Uppsala

University[75]. Zero-Field Cooled (ZFC) measurements were made at measuring fields

of 10 G. As the observation time decreases, (increasing frequency), the location of the

cusp moves towards higher temperatures and broadens in all layer thicknesses; however,

the magnitude of these effects in thick ($W_{SG} = 1000$ nm) samples are only about 20%

of the those seen in the thin ($W_{SG} = 3$ nm) sample. The frequency dependence can be

typified by the quantity k;

$$k = \frac{1}{T_f} \frac{dT_f}{d(\log_{10} t)}$$

4-5

For the 1000 nm film, k has a value of 1/200 at $t = 1$ s, in agreement with

measurements of bulk (not sputtered) CuMn films. In the 3 nm film, k was found to be

1/40. This is in qualitative agreement with Monte Carlo simulations on 2D short-range

Ising spin glasses[76] which found k to be approximately 1/20, and 3D simulations[77],

which predict a value of k = 1/60.

If the dynamic behavior of the films is analyzed in terms of Equation 4-3, the

1000 nm film is fit with $z\nu = 9 \pm 1$, and $T_g = 66 \pm 0.2$ K, where τ_0 is $10^{-13(\pm 1)}$

seconds. Fitting the 3 nm data to this expression, however, results in a value of

$z\nu = 19$, which suggests that standard critical slowing down is not a good description

of the dynamics of thin spin glass layers.

Fitting the data from the 3 nm sample to Equation 4-4 with a zero T_g results in a value of $\psi\nu = 1.6 \pm 0.2$, with $\tau_0 = 10^{-13(\pm 1)}$ seconds. The value of $1+\psi\nu$ is in rough agreement with the value of 2 found from Monte Carlo simulations[75,76]. The data may also be fit to Equation 4-4 with a finite transition temperature. For $0 < T_g < 10$ K, $\psi\nu$ is between 1.1 and 1.6.

These measurements have been extended to samples with W_{SG} from 2 nm to 1000 nm. For $W_{SG} \leq 4$ nm, fitting to the activated dynamics with zero freezing temperature yields a consistent value of $\psi\nu = 1.6 \pm 0.1$. If this fit is continued to thicker samples, the exponent grows anomalously. Samples with $W_{SG} \leq 50$ nm can be fit to Equation 4-4 with the same exponent of $\psi\nu = 1.6 \pm 0.1$. These measurements have been important in confirming the change in the dimensional character of multilayered spin glasses as the spin glass layer thickness is reduced.

Other Measurements on Multilayered Spin Glasses

Gavrin, et. al.[78], have investigated sputtered multilayers of $Cu_{0.92}Mn_{0.08}/Al_2O_3$. The choice of Al_2O_3 as the interlayer material is designed to eliminate concerns about interfacial alloying, transmission of the RKKY interaction across layers, and to simplify characterization. W_{SG} ranged from 4 nm to 125 nm, with the Al_2O_3 layer having a constant thickness of 7.5 nm. Sample composition was confirmed by microscopy and x-ray analysis.

The values of T_f from susceptibility measurements were fit to Equation 4-1, with an exponent of $\lambda = 0.64 \pm 0.07$ ($\nu = 1.6$) describing the data for all thicknesses. DC

measurer

from low

vs. thick

8.8 nm)

suscepti

for all s

values c

made b

at high

sample.

extracte

differer

measur

suscept

measur

Finite

impuri

varying

an and

measurements of nonlinear susceptibility, in which the linear susceptibility is extrapolated from low field measurements, show distinct differences in the scaling behavior for thin vs. thick samples. The crossover exponent, δ, is found to be about 7 in thin (6 nm and 8.8 nm) samples, and 4.4 in the bulk. The value of ν obtained from the nonlinear susceptibility measurements is 3.4 in thin samples, and 1.6 in the bulk film. $\beta \approx 0.9$ for all samples. The value of η is 0.5 in thin samples and 0.11 in thick samples. These values can be compared to values in Appendix B.

Measurement of the nonlinear susceptibility in CuMn/Cu multilayers has been made by the Uppsala group[79] using an ac technique at low fields, and a dc technique at high fields. The measurements were made on a 2 nm $Cu_{0.87}Mn_{0.13}$/Cu sputtered sample, and critical exponents different from those of Gavrin,*et. al.* were reported. The extracted exponents were: $\gamma = 9.3, \nu = 4.5, \beta = 0$ and $\eta = 0$, some of which are quite different from those found by Gavrin, *et. al.* Our experience with dc nonlinear measurements has indicated that the extrapolative determination of the linear susceptibility is not straightforward, and we would expect the more sensitive ac measurements of the Uppsala group to be more accurate.

Finite Size Effects in Metallic Films

The anomalous Hall effect, which is a measure of the magnetization of the impurity spins, has been studied in flash evaporated $Au_{0.99}Fe_{0.01}$ and $Au_{0.95}Fe_{0.05}$ films varying from 40 nm to 4 nm[80,81]. The strong spin-orbit coupling in AuFe results in an anomalous component in the Hall resistivity when an external magnetic field is

appl

resi

appl

decr

the

$r =$

less

Effe

to H

Exp

has

expo

field

obse

Ag

not c

temp

from

applied. T_f is determined from the maximum in the temperature dependent Hall resistivity. The Hall measurements are made by zero field cooling the sample, then applying a measuring field between 100 G and 500 G. As the sample thickness decreases, the freezing temperature decreases, with larger measuring fields broadening the cusp. The freezing temperatures are fit to Equation 4-1 ,with an exponent of $\nu = 1.6 \pm 0.4$. A deviation from finite size scaling was seen in films with thicknesses less than 10 nm, but was not analyzed in terms of possible dimensionality effects.

Effect of Magnetic Field on T_f in Metallic Multilayers

Arguments have been made for a DM anisotropy induced crossover from Ising to Heisenberg-like behavior in bulk spin glasses as the magnetic field strength is changed. Experimental measurement of the nonlinear susceptibility[82] in bulk AgMn and CuMn has been analyzed using anisotropy as a scaling parameter. Two sets of critical exponents result, one of which is ascribed to 'Ising like' behavior and results from low field measurements, and the other of which is labeled 'Heisenberg' behavior and is observed in high fields. Torque measurements made by Campbell, *et. al.*[83] on $Ag_{0.074}Mn_{0.026}$ indicate that, for fields between 1 kG and 20 kG, the value of $T_f(H)$ does not change by more than 10%. Similar results are cited for CuMn.

Kenning, *et. al.*[84] have studied the effect of magnetic field on the freezing temperature in $Cu_{0.93}Mn_{0.07}/Cu$ multilayers with W_{SG} from 2 nm to 1000 nm in fields from 2 G to 15000 G. The behavior in low field is described[85] by

and

wh

He

W_s

exp

dep

in

to

<u>M(</u>

$x =$

M_0

1.8

str

a va

$$T_f(H) = T_f(0)\left[1 - \left(\frac{n+2}{4}\right)^{\frac{1}{3}}\left(\frac{g\mu_B H}{k_B T_f(0)}\right)^{\frac{2}{3}}\right] \qquad 4\text{-}6$$

and high field behavior by

$$T_f(H) = \tilde{T}_f(0)\left[1 - \left(\frac{(n+2)(n+1)}{8}\right)^{\frac{1}{3}}\left(\frac{g\mu_B H}{k_B \tilde{T}_f(0)}\right)^{\frac{2}{3}}\right] \qquad 4\text{-}7$$

where, in both expressions, $n = S(S+1)$, and $T_f(0)$ and $\tilde{T}_f(0)$ are the Ising and Heisenberg zero field freezing temperatures. Kenning, *et. al.* find the behavior for all W_{SG} to be qualitatively described by these equations, although the prefactor of the Ising expression differs from the experimental measurement by an order of magnitude. The depression of T_f is more pronounced in the Ising regime (from 2 G to about 500 G) than in the Heisenberg regime (above 500 G). No dimensionality or finite size corrections to this behavior are noted, and the crossover field appears to be the same for all W_{SG}.

MULTILAYERED SEMICONDUCTING SPIN GLASSES

Awschalom, *et. al.*[86] studied the dilute magnetic semiconductor $Cd_{1-x}Mn_xTe$, with $x = 0.069$ to 0.20. Multilayered structures with CdTe interlayers were grown by Molecular Beam Epitaxy (MBE) with spin glass layer thicknesses from 8.6 nm to 1.8 nm. X-ray diffraction and low temperature photoluminescence confirmed the layered structure and concentration. The ac magnetic susceptibility was measured at 97 Hz and a variety of temperatures. Contrary to the effects seen in metallic multilayers, decreasing

W,

te

sa

in

a

in

pa

m

to

a

cc

cc

a

e

ir

b

p

W_{SG} resulted in a broadening of the susceptibility peak, but no shift to lower temperatures. The observation of rounding may be due to the low strain in MBE grown samples, which may explain why this phenomena is not seen in sputtered films.

The interactions in CdMnTe are short ranged, with the nearest neighbor interaction 5 times that of the next nearest neighbor exchange. This means that there are a number of isolated single spins and also small clusters of spins which preferentially interact with each other and not with surrounding spins. At low temperatures, the paramagnetic clusters result in a 1/T divergence of the susceptibility. The rounded maximum indicates the onset of short range spin glass ordering, and the broadness is due to the blocking of the establishment of long range order. This is interpreted as proof that a 2D structure is incapable of supporting spin glass order.

Hysteretic effects were seen in the thinnest samples with the highest concentration, with the warming susceptibility having a greater magnitude than the cooling measurements. The hysteretic effects are due to the trapping of the system in a metastable state; when the system is cooling, the establishment of short range order creates preferential states. As the temperature continues to decrease, the energy barriers increase, and the system is trapped. In the lowest concentration (x= 0.07), a 1/T behavior is seen for all thicknesses, which indicates that when the system consists primarily of small isolated clusters of spins, dimensionality is unimportant.

TV

gla

of

bro

Th

ap

Ag

tho

TH

IN

of

20

mea

exp

activ

temp

TWO-DIMENSIONAL SPIN GLASSES

Dekker, *et. al.*[87] have investigated the behavior of the two dimensional Ising spin glass $Rb_2Cu_{1-x}Co_xF_4$, with x = 0.22. AC susceptibility measurements over 15 decades of time show frequency dependent behavior beginning as high as 2 T_f, with an extremely broad distribution of relaxation times. Fits to Equation 4-3 result in a value of $z\nu$ = 15. The activated dynamics of Fisher-Huse given by equation 4-4 with T_g = 0, as appropriate to a true two dimensional system, find $\psi\nu$ = 2.2 $\pm$ 0.2 and τ_0 = (2$\pm$1) x 10^{-13}. Use of the same equation with a finite T_g resulted in a worse fit. Ageing phenomena seen in this material[88] are found to be qualitatively different than those seen in 3D.

THE CURRENT PICTURE OF DIMENSIONALITY AND FINITE SIZE EFFECTS IN MULTILAYERED SPIN GLASSES

Based on the static and the dynamic measurements, we have the following picture of dimensionality crossover and finite size effects in multilayered spin glasses. For 20 nm $\leq W_{SG} \leq$ 1000 nm, deviations from bulk behavior in the static and dynamic measurement of T_f can be analyzed in terms of finite size effects. The correlation length exponent, ν, has a value of 1.1 $\pm$ 0.3 when fit to samples in this thickness regime.

For thin samples, the behavior of the freezing temperature is described by the activated scaling of Fisher-Huse, as given by Equation 4-4 and its zero freezing temperature modification. Frequency dependent susceptibility measurements over 8

decades in ti

for two dime

find a crosso

The fr

decrease wi

demonstrate

decades in time show that $T_g = 0$ for $W_{SG} \leq 5$ nm, and provide convincing arguments for two dimensional behavior. In the intermediate regime (5 nm $\leq W_{SG} \leq 20$ nm), we find a crossover behavior described by Equation 4-4 with a finite T_g.

The freezing temperature is observed to increase with increasing frequency, and decrease with increasing magnetic field; the former effect has been shown to demonstrate dimensionality dependence, while the latter has not.

This c

ESR given in

summarizes t

ordered mate

of ferro- and

manner to s

magnets is c

ailored to E

Five conclu

General B

In

both of w

linear in t

CHAPTER FIVE

ESR IN SPIN GLASSES

INTRODUCTION

This chapter is divided into three parts: the first part extends the basic theory of ESR given in Chapter 2 to the ESR of magnetic moments in metals. The second part summarizes the experimental situation of ESR in spin glasses and other magnetically ordered materials. Of special interest are results of linewidth and peak position studies of ferro- and antiferro- magnets, as many of these materials behave in an analogous manner to spin glasses. The ESR of one and two dimensional ferro- and antiferro-magnets is discussed. The third section looks at theoretical explanations specifically tailored to ESR in spin glasses. Having provided the necessary background, Chapter Five concludes with the motivation and goals of this experiment.

General Behavior

In spin glasses, the linewidth as a function of temperature, $\Delta H(T)$, has two trends, both of which are also seen in other materials. At high temperatures, the linewidth is linear in temperature and described by

a p

The

<u>ESP</u>

to lc

whic

ferro

$$[\Delta H(T)]^{linear} = A + BT \qquad\qquad \textbf{5-1a}$$

As the freezing temperature is approached from above, the linewidth diverges as a power law in the reduced temperature, t, with a characteristic exponent, κ

$$[\Delta H(T)]^{\alpha} = C\left(\frac{T-T_f}{T_f}\right)^{-\kappa} \qquad\qquad \textbf{5-1b}$$

The standard equation used in the analysis of ESR data above T_f is therefore

$$\Delta H(T) = A + BT + C\left(\frac{T-T_f}{T_f}\right)^{-\kappa} \qquad\qquad \textbf{5-2}$$

ESR IN SPIN GLASSES: THEORY

This section begins with a theoretical explanation of the linear behavior common to localized moments in metallic hosts, and is followed by a summary of the approaches which have been used to explain the behavior near the ordering temperature in ferromagnets, antiferromagnets, and spin glasses.

state

the e

rang

reson

linew

state

prov

was

impu

obser

$g =$

the r

ident

antife

the cor

ESR of Localized Moments in Metallic Hosts

The major applications of ESR in metals are; 1) determination of spectroscopic states of ions in various hosts, 2) determination of relaxation times, 3) information about the exchange interaction between localized moments, and 4) studying long and short range magnetic order. The two measurable quantities we will be interested in are the resonance peak position, H_0 (related to the inverse of the effective g value) and the linewidth, ΔH. Measurement of the g value provides information about the spectroscopic state of the ion and the energy scale of the resonance, and measurement of the linewidth provides information about relaxation phenomena.

The first experimental report of the ESR of localized moments in metallic hosts was made by Owen, *et. al.*[89] in 1956 in $M_{0.99}Mn_{0.01}$, where M is Cu, Ag or Mg. Mn^{2+} impurities in non-metallic hosts show six separate resonance lines. Owen, *et. al.* observed a much wider single line, with no fine or hyperfine structure, centered around g = 2. As the temperature was reduced, the linewidth broadened, and the position of the resonance peak shifted to lower fields. At the time, spin glasses had not been identified as such, and the divergent behavior was explained in terms of antiferromagnetic interactions.

ESR Equations for Transition Ion-Metal Systems

In the ESR of transition ions in metals, two spin components must be considered; the conduction electrons, which are denoted here by a subscript 'e', and the ions, denoted

by

app

to b

ave

maj

whe

and

where

by the subscript 'i'. Consider first an assembly of conduction electrons and ions in the approximation of immediate relaxation and far from any critical point. Taking all ions to be equivalent (and all electrons to be equivalent), a simple relation exists between the average magnetization and the effective field, so that we can write the static magnetization of the ions and of the conduction electrons per ion (or per electron) as

$$\vec{M}_i \equiv \chi_i \vec{H}_0 = \chi_i^0 (\vec{H}_0 + \Lambda \vec{M}_e) \qquad \text{5-3a}$$

$$\vec{M}_e \equiv \chi_e \vec{H}_0 = \chi_e^0 (\vec{H}_0 + \Lambda \vec{M}_i) \qquad \text{5-3b}$$

where Λ is the molecular field coefficient, given by

$$\Lambda = \frac{2 \left(\sum_{(ij)} J(R_{ij}) \right)}{g_i \, g_e \, \mu_B^2} \qquad \text{5-4}$$

and the susceptibilities of the ions and electrons are given by

$$\chi_i^o = (g_i \mu_B)^2 \frac{S(S+1)}{3kT} \qquad \text{5-5a}$$

$$\chi_e^0 = \frac{1}{2} (g_e \mu_B)^2 \rho(E_F) \qquad \text{5-5b}$$

where $\rho(E_F)$ is the density of states at the Fermi surface.

Re

by

ele

wit

mer

spir

resp

rela

quic

Ove

can

whei

T_e an

Relaxation Rates

The relaxation processes in the ESR of localized moments in metals are governed by the presence of three distinct components; the lattice, the ions and the conduction electrons. In Chapter Two, we considered only one type of spin which could interact with other spins of its own type and with the lattice. In the ESR of transition ions in metals, there are four relaxation processes. The conduction electrons and the localized spins can each relax to the lattice, with characteristic relaxation times T_{eL}, and T_{iL} respectively. In addition, the conduction electrons and the localized moments can cross-relax (with times T_{ei} and T_{ie}). T_{ie}, the Korringa relaxation time, is a measure of how quickly the spins of the localized moments relax to the conduction electrons. T_{ei}, the Overhauser rate is a measure of the reverse process. The Korringa and Overhauser rates can be calculated by using a rate equation approach.

$$\frac{1}{T_{ie}} = \frac{4\pi}{\hbar}(\rho J)^2 kT \qquad \textbf{5-6a}$$

$$\frac{1}{T_{ei}} = \frac{8}{3\hbar}\pi c S(S+1)\rho J^2 \qquad \textbf{5-6b}$$

where J is the exchange coefficient and c is the concentration of magnetic ions.

Figure 5-1 schematically illustrates the relaxation paths available to these systems. T_{ie} and T_{ei} are the relaxation times between the ion and the conduction electrons, and T_{eL}

and T_{iL} are the relaxation times between the spins and the lattice. T_{iL} is very long compared to the other times.
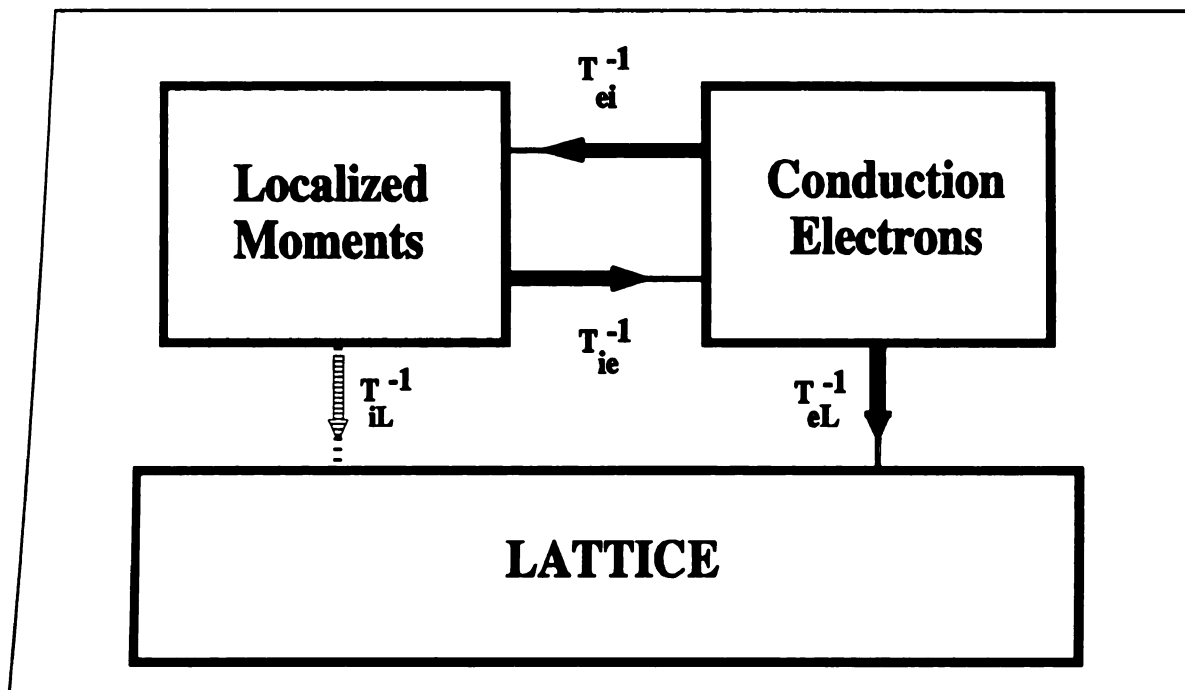
Figure 5-1: *Available relaxation paths for transition ion-metal systems*

We can identify three regimes: in the first two regimes, we can treat the electrons as if they were in static thermal equilibrium. If the electrons relax rapidly to the lattice (isothermal approximation), the linewidth is determined by the ion-electron relaxation rate, $1/T_{ie}$. In the adiabatic regime, the electron magnetization doesn't respond rapidly enough to follow the rf field, so that the resonance width is determined by the relative values of T_{iL} and T_{ie}. In these two regions, we can replace the conduction

electron spin and number operators by their expectation values. This leaves us with an equation of motion for the ionic magnetization.

$$\frac{d\vec{M_i}}{dt} = g_i \mu_B \vec{M_i} \times (\vec{H} + \Lambda \vec{M_e}) = g_i \mu_B (1 + \Lambda \chi_e) \vec{M_i} \times \vec{H} \qquad \text{5-7}$$

which introduces an effective g factor,

$$g = g_i(1 + \Lambda \chi_e) = g_i(1 + \Lambda \chi_e^0 + \Lambda^2 \chi_e^0 \chi_i) \qquad \text{5-8}$$

The first two terms are temperature and concentration independent, while the last is proportional to concentration and inversely proportional to temperature. The g-shift due to the second term is called the Knight shift and is observed for many metals with Eu^{2+}, Gd^{3+}, and non-S state ions. In the adiabatic regime, both the first and second order (in Λ) g-shifts are seen, while in the isothermal regime, the second order shift is not observed. The linewidth is given by

$$\Delta H \sim \frac{1}{T_{eff}} = \frac{1}{T_{iL}} + \frac{1}{T_{ie}} \left[1 - \frac{\theta}{T} \right] \equiv A + BT \qquad \text{5-9}$$

where A is the linewidth at T = 0, called the residual linewidth, and B is the thermal broadening coefficient. In theory, $1/T_{iL}$ is the residual (T = 0) linewidth, although in practice, there may be other contributions to this quantity. The presence of the ($1-\theta/T$) term is due to assumption of a Curie-Weiss behavior of the susceptibility. Note that this expression results in a concentration independent value for B. If we cannot treat the

electrons

cannot tra

of the shi

Ph

maintain

directly to

relaxation

of spins to

to the latt

can trans

between

to the loc

become

bottlene

In gene

will be

the el

electrons as being in thermal equilibrium, then T_{eL} becomes important. If the electrons cannot transfer energy to the lattice fast enough, the system is 'bottlenecked', and neither of the shifts in equation 5-8 are observed.

Physically, we can explain the bottleneck as follows: the impurity spins want to maintain equilibrium with the lattice, and there are two routes to do this; relaxation directly to the lattice, and relaxation via the conduction electrons. We expect that the relaxation of the spins directly to the lattice would be slow compared to the relaxation of spins to the conduction electrons. If the conduction electrons can transfer their energy to the lattice fast enough, the linewidth will be dominated by how fast the localized spins can transfer energy to the conduction electrons ($1/T_{ic}$). If the relative relaxation rates between the spin systems are such that the conduction electrons can transfer energy back to the localized moments faster than they can transfer energy to the lattice, energy can become trapped between the conduction electrons and the moments, which results in a bottleneck. The linewidth will be due to both sets of spins, as they are locked together. In general, a bottlenecked system will not display a g-shift, so that the observed g value will be close to that of the conduction electrons.

Hasegawa[90] modified the Bloch equations to include the cross relaxation between the elements in the system, resulting in the Bloch-Hasegawa equations.

$$\frac{d\vec{M}_i}{dt} = g_i \mu_B \vec{M}_i \times (\vec{H} + \Lambda \vec{M}_e) - \left(\frac{1}{T_{ie}} + \frac{1}{T_{iL}}\right) \delta \vec{M}_i + \frac{g_i}{g_e} \frac{1}{T_{ei}} \delta \vec{M}_e \qquad 5\text{-}10a$$

Va[...]

isothermal [...]

large, we [...]

$T_L \approx T_{cL}$ [...]

may be w[...]

where

and

$(\chi$ [...]

the e[...]

$$\frac{d\vec{M_e}}{dt} = g_e \mu_B \vec{M_e} \times (\vec{H} + \Lambda \vec{M_i}) - \left(\frac{1}{T_{ei}} + \frac{1}{T_{eL}}\right)\delta \vec{M_e} + \frac{g_e}{g_i}\frac{1}{T_{ie}}\delta \vec{M_i} \qquad \text{5-10b}$$

Various approximations are made to solve this system of equations. In the isothermal regime, $(1/T_{eL})$ is very large and the electrons relax quickly. If (g_i/g_e) is very large, we recover the adiabatic regime. In the strongly bottlenecked limit, $g_i \approx g_e$ and $T_{iL} \approx T_{eL}$, with the rates of relaxation to the lattice both small, the equation of motion may be written

$$\frac{d(\vec{M_e} + \vec{M_i})}{dt} \approx g\mu_B(\vec{M_e} + \vec{M_i}) \times \vec{H} - \frac{1}{T}\delta(\vec{M_e} + \vec{M_i}) \qquad \text{5-11}$$

where

$$g = \left[\frac{g_e \chi_e + g_i \chi_i}{\chi_e \chi_i}\right] \qquad \text{5-12}$$

and

$$\frac{1}{T_{eff}} = \left[\frac{\frac{1}{T_{eL}}\chi_e^0 + \frac{1}{T_{iL}}\chi_s^0}{\chi_e + \chi_i}\right] \qquad \text{5-13}$$

In general, the host susceptibility is much smaller than that of the magnetic ions $(\chi_i^0 > \chi_e^0)$, the ion g factor is equal to the effective electron g-factor, and we find that the effective relaxation rate (and hence the linewidth) goes like

where B is

to Equatio

but is diff

g value, ir

systems, s

In

account fc

fine struc

Residua

interna

althou

we ca

$$\frac{1}{T} \approx \frac{1}{T_{iL}} + \frac{\chi_e^0}{\chi_i^0}\frac{1}{T_{eL}} = \frac{1}{T_{iL}} + \frac{T_{ei}}{T_{eL}}\left(\frac{1}{T_{ie}}\right) \equiv A + BT \qquad 5\text{-}14$$

where B is inversely proportional to the concentration of magnetic ions. This is similar to Equation 5-9, which describes the behavior in the adiabatic and isothermal regimes, but is different in that the bottlenecked expression is concentration dependent. The g value, indicated by the position of the resonance peak, should be constant. In real systems, some combination of bottlenecked and isothermal/adiabatic behavior is expected.

In more detailed calculations, the Bloch-Hasegawa equations can be modified to account for the motion of the conduction electrons throughout the sample, hyperfine, and fine structure splitting.

Residual Width and Thermal Broadening

The nonzero value of the residual width at low concentrations is attributed to local internal field effects (such as the presence of anisotropy) and not to relaxation effects, although these effects are included in the ion-lattice relaxation rate. From Equation 5-14, we can write the residual width in field units as

and the th

where b_K

Ev

properties

Although

no addit

frequenc

part of

aligned

broade

there

affec

is fc

hun

beca

$$A = \frac{\hbar}{8 \, \mu_B \, T_{iL}}$$ 5-15a

and the thermal broadening coefficient may be written

$$BT = \frac{T_{el}}{T_{eL}} b_K T$$ 5-15b

where $b_K = (1/T_{ic})/T$ is the unbottlenecked Korringa rate given by Equation 5-6a.

Experimental studies[91] correlate the residual width to local strains and structural properties. Barnes[91] suggests that the behavior is due to internal field distributions. Although the RKKY interaction commutes with the total magnetization and should cause no additional linewidth, the part of the RKKY interaction transverse to the field is frequency dependent. This suggests that, if the appropriate limits hold, the transverse part of the RKKY interaction cannot follow the rf field. The spins are locked into an aligned configuration, producing an internal field, which results in inhomogeneous broadening. For S-ion states, random strains should have a fairly negligible effect, since there is almost no angular momentum in the ground state. Dipole-dipole broadening may affect the residual width, but this quantity is small in the Mn alloys.

For AgMn with concentrations on the order of a thousand ppm, the residual width is found to decrease with increasing concentration for concentrations higher than a few hundred ppm. Concentration and frequency dependence has not been tested in detail, because magnetic ordering phenomena obscure the linear behavior. When a third

impurity (S

residual wic

In g

explained th

where B is

which can '

the value o

The Effec

Li

mechanis

chapter.

Inhomc

throug

slightl

merge

states.

homog

impurity (Si or Al) is added to CuMn (Mn concentration on the order of 0.1%), the residual width is roughly proportional to the concentration of the additional impurity.

In general, the residual width would be expected to be positive. Stewart[92] explained that A is related to the "true" residual width, A_0, via

$$A = A_0 - B\,\theta \qquad\qquad 5\text{-}16$$

where B is the same thermal broadening coefficient, and θ is the Weiss temperature, which can be measured from high temperature susceptibility measurements. If $\theta > 0$, the value of A measured by ESR experiments will be negative.

The Effect of Magnetic Ordering on Linewidth

Line broadening or narrowing is the result of interactions between spins. Specific mechanisms for the spin glass problem will be discussed in the last section of this chapter. Linewidths may be broadened homogeneously, or inhomogeneously. Inhomogeneous broadening is a result of the existence of different Larmor frequencies throughout the sample. In effect, each of the spins sees a different field, and has a slightly different resonance frequency. This results in a distribution of individual lines merged into one overall line or envelope, but with no change in the lifetimes of the states. Inhomogeneous broadening may be due to experimental artifacts, such as poor homogeneity of the magnetic fields across the sample, or unresolved fine or hyperfine

structure.

or irregula

The

change the

due to: 1) c

with the

5) motiona

interaction

dipolar in

In

local fiel

on the d

resonanc

the inter

greater

distant

increa

lines

inter

grea

large

structure. The linewidth may also be inhomogeneously broadened due to inhomogeneity or irregularities in the sample.

The width of a homogeneously broadened line is entirely due to processes which change the lifetime of the states between which the transition takes place. This may be due to; 1) dipolar interaction between like spins, 2) spin-lattice interaction, 3) interactions with the radiation field, 4) diffusion of excitations throughout the sample, or 5) motionally narrowing fluctuations in the local field, such those due to as exchange interactions. Two of these interactions will be important to the problem at hand: the dipolar interaction, and the phenomenon of exchange narrowing.

In the case of dipole-dipole interaction between spins of different types, random local fields are set up at each spin site. The interaction between a pair of spins depends on the distance between them and their orientations. The dipolar field displaces the resonance line from that of a single ion by an amount which depends on the strength of the interaction. The greater the number of pairs with a given interaction strength, the greater the net intensity of the interaction and the further the shift. As we look at more distant ions, the interaction will diminish in size as the separation between the spins increases, but there are more spins with which to pair at larger distances. The resonance lines which are displaced a small amount from their single ion position are due to strong interactions with a small number of other spins, and so the intensity of these lines is greater. Lines which are displaced by a large amount are a result of interaction with a larger number of spins at a greater distances, and will be less intense. The line profile

should then reflect the distribution of the dipolar fields, with a width on the order of $\mu_B r_o^{-3}$.

If the interaction is between like spins, the field is homogeneously broadened. The precessing components of one magnetic dipole set up an oscillatory field at another dipole, which (because all the spins have the same Larmor frequency) is at the precise frequency to cause resonance transitions, and vice-versa. These transitions are equivalent to the exchange of quanta between the spins, and gives an additional broadening which is homogeneous in nature, as the lifetime of the individual ion in a given quantum state is shortened.

The other important mechanism is the exchange interaction, which we can think about simply by considering a two level-two spin system. For antiferromagnets, the antiparallel state is lowest in energy; however, the one up, one down state ($|\uparrow\downarrow\rangle$) is not an eigenstate of the exchange Hamiltonian. The eigenstate is a linear combination of $|\uparrow\downarrow\rangle$ with $|\downarrow\uparrow\rangle$, which results in the system oscillating between the two states at the exchange frequency, $J/\hbar$. When the exchange energy is large compared to other energies, the orientation of the spins is being changed at a rate of order $J/\hbar$, which causes a fluctuation in the local dipolar field at a similar rate. The fluctuations cause the dipolar broadening to be less effective. This phenomena results is a line which is narrowed near the center and broadened at the wings, and is called exchange narrowing.

wher

functi

force.

functi

respon

spin-sp

a damp

Lineshape, Correlation Functions and the Relaxation Rate

The formalism used to describe the behavior of ESR lines in the presence of spin-spin interactions near a critical point has been developed by Kubo, Mori, Kawasaki and Tomita[93,94,95,96,97]. We are interested in the linear response of a system (the spins) to a perturbation (the magnetic field).

The fluctuation-dissipation theorem links a spectral density function with a time correlation function; alternatively, it may be thought of as describing the relationship between the response of a driven system and the correlations in its equilibrium fluctuations.

$$J(\omega) = \int_{-\infty}^{\infty} <\bar{A}(t)B(0)> \; e^{i\omega t} \; dt \qquad\qquad 5\text{-}17$$

where J is the spectral density distribution, and $<A(t)\,B(0)>$ is a time correlation function which measures the fluctuations of the system in response to the applied driving force. In the case of ESR, the spectral density distribution is the power absorbed as a function of frequency (or field) - which is the lineshape and will be denoted by $I(\omega)$. The response function will be the correlation function of the random forces which result from spin-spin interactions.

The Bloch equations with an rf field are the same as the equation of motion for a damped oscillator. The oscillator has natural frequency ω_0, which is modified by the

driving force in a random way, with this randomness broadening the lineshape. The frequency of the oscillator may be written

$$\omega(t) = \omega_0 + \omega_1(t) \qquad \qquad \text{5-18}$$

where $\omega_1(t)$ represents the random fluctuations in frequency, with a time average of zero. In the ESR experiment, $\omega(t) = \gamma H(t)$, where $H(t)$ contains the static and rotating rf fields. The equation of motion of the magnetization is

$$\frac{dM_x}{dt} = i\,\omega(t)M_x \qquad \qquad \text{5-19}$$

We are interested in an ensemble average of M_x. Assuming that we can replace the time averages with ensemble averages, we can integrate Equation 5-19.

$$<M_x(t)> \ = \ M_x(0)\ e^{-i\omega_0 t} < \exp(i\int_0^t \omega_1(t')\ dt')> \qquad \qquad \text{5-20}$$

$\phi(t)$, the relaxation function of the oscillator, is

$$\phi(t) = \exp\left(i\int_0^t \omega_1(t')\ dt'\right) \qquad \qquad \text{5-21}$$

so that we can write

$$< M_x(t) \, M_x(0)^* > \; = \; | \, M_x(0) \, |^2 \, e^{-i\omega_0 t} \, \phi(t) \qquad\qquad \text{5-22}$$

which links the expectation of the magnetization to the relaxation function. By the fluctuation-dissipation theorem, Equation 5-17, we can write the resonance absorption spectrum, $I(\omega-\omega_0)$ as

$$I(\omega - \omega_0) \; = \; \frac{1}{2\pi} \int\limits_{-\infty}^{\infty} e^{-i(\omega - \omega_0)t} \phi(t) \, dt \qquad\qquad \text{5-23}$$

where this expression has been normalized to 1. This equation represents an absorption centered at ω_0 which is broadened by the random modulation ω_1. We can define two characteristic parameters of the broadening; The amplitude of modulation, Δ, is given by the average of the square of the modulation process, $<\omega_1^2>$. Using the central limit theorem, we can write the modulation in terms of a Gaussian,

$$\Delta^2 \; = \; \int\limits_{-\infty}^{\infty} (\omega - \omega_0)^2 \, I(\omega - \omega_0) \, d\omega \qquad\qquad \text{5-24}$$

The correlation time, τ_c, is defined

$$\tau_c \; = \; \int\limits_{0}^{\infty} \psi(t) \, dt \qquad\qquad \text{5-25}$$

where the correlation function of the modulation, $\psi(t)$, is given by

$$\psi(t) = \frac{1}{\Delta^2} \langle \omega_1(t)\, \omega_1(t+\tau) \rangle \qquad\qquad \text{5-26}$$

ψ(t) measures how much the modulation at time $t+\tau$ is influenced by the value of the modulation at some earlier time t; if ψ(t) is 0, there is no correlation. τ_c corresponds to the time after which the correlation function is reduced to less than one half the initial value -- this tells us how fast the effects of the perturbation vanish after the perturbation is removed.

If τ_c is large compared with $1/\Delta$ (slow modulation), the intensity distribution will directly reflect the distribution of the modulation. The width of the lineshape will be about Δ. If τ_c is small (fast modulation), a disturbance will not last for a significant time, so that fluctuations are smoothed out, and the resonance line will be sharper around the center. In the limit $\Delta\tau_c \to 0$, the line will be Lorentzian, and the half-width will be on the order of $\Delta^2\tau_c$ (which is less than the corresponding linewidth for the Gaussian). $T > \tau_c$ for most times, so the Lorentzian behavior will be most significant near t = 0, and the line will be Gaussian in the wings.

In the ESR spectra of magnetic solids, the slow dipolar interactions broaden the lines, resulting in a Gaussian shape, while the exchange interactions - if large enough - narrow the line. The speeds of the respective modulations are about 10^8 - 10^9 Hz for the dipolar interaction, and an order of magnitude faster for the exchange interaction, so that the exchange narrowing condition is fulfilled in most cases.

In the limit of rapid exchange modulation;

$$\left\langle \exp\left[i\int_0^t \omega_1(t')\,dt' \right] \right\rangle \sim \exp\left[-\int_0^t (t-\tau)\left\langle \omega_1(\tau)\,\omega_1(0) \right\rangle d\tau \right] \qquad \text{5-27}$$

and the Kubo-Tomita formula results:

$$\phi(t) \propto \exp\left[-\int_0^t <\omega_1(\tau)\,\omega_1(0)>\,d\tau \right] \qquad \text{5-28}$$

We recognize the brackets as being proportional to the correlation function of the modulation. In this limit, the relaxation function decays exponentially; $\phi(t) \sim \exp(-t/\Gamma)$, where Γ is a complex value related to the linewidth and lineshift. Including all of the constants,

$$\Gamma = \frac{1}{\chi} \int_0^\infty \exp^{-i\omega_0\tau} <\omega_1(\tau)\,\omega_1(0)>\,d\tau \qquad \text{5-29}$$

where χ is the static susceptibility. The linewidth is given by the real part of Γ, and $1/\omega_0$ times the imaginary part gives the shift in the resonance position. This equation may also be derived from a Green's function solution of the equation of motion, where Γ is the self energy. In general, Equation 5-29 will apply if

$$\left\langle \omega_1(\tau)\,\omega_1(0) \right\rangle = \frac{\left\langle [H'(\tau),M_+(0)]\,[M_-(0),H'(0)] \right\rangle}{<M_+(0)M_-(0)>} \qquad \text{5-30}$$

where H′ is a perturbation Hamiltonian, and the time dependence of the perturbation Hamiltonian is accounted for by an interaction representation approach. The important point about this equation is not its complexity, but rather that it contains a four spin correlation function, as does the relaxation function of the modulation.

In exchange narrowed dipolar broadening, the strength of the exchange is greater than the dipolar strength, so we can treat the Hamiltonian, H, as the unperturbed Hamiltonian, $H_{Zeeman} + H_{Exchange}$, plus a perturbation $H′ = H_{Dipolar}$. We can redefine the relaxation function to remove the faster Zeeman and exchange frequencies, and focus on the slower dipolar effect. Evaluating the correlation function for the dipolar case,

$$\psi(t) = \frac{1}{\hbar^2} \sum_M \sum_{ijkl} F_{ij}^M F_{kl}^{-M} S_{ijkl}^M(\tau)$$

5-31

where M is the change in the total Zeeman quantum number ($M = 0, \pm 1$, or ± 2), the $F_{ij}^{(M)}$ the angular dependence from the dipolar functions, and the $S_{ijkl}^M(\tau)$ is a four spin time correlation function.

$$S_{ijkl}^M = \langle S_{i\alpha}(\tau) S_{j\beta}(\tau) S_{k\gamma}(0) S_{l\delta}(0) \rangle$$

5-32

where the greek indices are z, + or -, and the i,j,k,l label the spin sites. This function measures the probability that, at time τ, the spin value on site i is α, and the spin value on site j is β, given that the spins on sites k and l had values δ and γ at time = 0. This four spin correlation function must be decoupled in order to find expressions which can be compared with the experimental measurements. Given the number of combinations

of spins which must be considered, this is not a simple calculation, and usually must be tailored to the system in question. In cases away from the critical point, the four-spin correlation function can be decoupled into products of two spin or one spin correlation functions. This is the starting point of the analysis which will be used in the latter part of this chapter.

Dimensionality Effects on ESR Linewidth and Lineshape

The magnetic dimensionality of a sample is not necessarily the same as the spatial dimensionality. Magnetic dimensionality will depend on the lattice structure, but also on the strengths and the ranges of the interactions. The characteristic time for decay of the spin correlation function, ψ, in three dimensions, is proportional to $\hbar/J$. Propagation of disturbances in one dimension is much more difficult than in three dimensions, as there are fewer relaxation pathways available. In lower dimensions, long time behavior of the relaxation function will be dominant. Experimentally, the decay of $\psi(t)$ is determined to be Gaussian for short times, but diffusive (approximately $t^{-d/2}$) for long times. The dimensionality dependence is a result of the diffusive nature of the motion of the disturbances.

The expression for the characteristic time contains an integral over the correlation function, with the correlation function diverging like $t^{1/2}$ for 1D and like $\ln(t)$ in 2D. One of the experimentally observed effects is a significantly different lineshape, which falls somewhere between Gaussian and Lorentzian. The shape of one dimensional lines is close to Lorentzian in the center, but decreases more rapidly. The slow decay of the

correlation in a one dimensional system does not allow the system to reach the fast exchange regime typical of Lorentzian lines, but leaves the system in an intermediate state. Short time phenomena are generally dependent on the number of nearest neighbors coupled by the interaction, while the long time phenomena are most dependent on the availability of paths for the disturbance. The one dimensional lineshape is predicted to be the Fourier transform of $\exp(-t^{3/2})$, and the angular and temperature dependences should also be different from that of the three dimensional prediction.

Observation of the different lineshapes and angular dependence of lower dimensionality materials is not straightforward. The differences are much greater in one dimensional materials than in two, with most two dimensional materials having a lineshape indistinguishable from a Lorentzian. The appearance of a Lorentzian lineshape in one and two dimensional materials is due to the fact that only a very weak interchain or interplanar coupling is needed to create paths for propagation of a disturbance, thus simulating three dimensional behavior[98]. The same reasons are responsible for the onset of divergent behavior seen in one and two dimensional materials which should not support magnetic order. In many cases, the deviations from Lorentzian behavior are so small that they can only be seen in single-crystal precision experiments specifically geared to sensitive observation of the lineshape.

EXPERIMENTAL RESULTS

This section focuses on the experimental investigation of spin glasses in the regime above and approaching T_f, and presents the two models used to understand these

results. The same general behavior of the linewidth and shift is seen in a wide variety of spin glasses; we will see that many ferro- and antiferro- magnets share the same characteristics as spin glasses. Representative data from long range ordered magnets, as well as data from low dimensional magnets will be reviewed for its pertinence to the present problem.

Metallic Spin Glasses

<u>CuMn</u>

The first ESR investigations of spin glasses were performed by Owen[89], and Griffiths[99] on CuMn. The anomalous behavior of the linewidth and shift were discussed in the beginning of this chapter.

Salamon and Hermann[100] found the same behavior - a divergent linewidth and a shift of the resonance to lower fields - in $Cu_{0.75}Mn_{0.25}$, attributing the divergence of the linewidth to the critical nature of the dynamics of the spin glass phase in support of a phase transition at T_f. Critical slowing down of the relaxation time as T_f is approached lessens the effectiveness of the exchange narrowing of the dipolar broadening causes the linewidth to diverge, as is also seen in insulating antiferromagnets[101].

Starting from the Equation 5-29, the random forces are roughly approximated by writing $<\omega_1(t),\omega_1(0)> = \omega_d^2$, the dipolar frequency, for times between 0 and τ_c[102]. The relaxation rate and the fractional g-shift are given by

$$\frac{1}{T} = \frac{\omega_d^2 \tau_e}{\chi} \qquad\qquad \frac{\Delta g}{g} = \frac{1}{2\chi} \omega_d^2 \tau_e^2 \qquad\qquad \text{5-33}$$

or, relating these quantities to the linewidth and resonance shift in field units;

$$\Delta H = \frac{\hbar}{g\mu_B} \omega_d^2 \tau_e \qquad\qquad (H - H_0) = \frac{\hbar}{g\mu_B} \omega \, \omega_d^2 \tau_e \qquad\qquad \text{5-34}$$

where χ is the static susceptibility, ω_d is the dipolar frequency $= g^2\mu_B^2/\hbar v$ and v is the volume per spin. τ_e is the characteristic spin-spin relaxation time, and is equal to the inverse of the exchange frequency, ω_e. The expression for the line shift in Equation 5-34 is a low frequency approximation. We can combine the equations in 5-33 to find an expression for the relaxation rate in terms of the shift and the linewidth.

$$\frac{1}{\tau_e} = \left(\frac{g}{\Delta g}\right)\frac{2}{T} \qquad\qquad \text{5-35}$$

By plotting the relaxation rate as a function of temperature, Salamon showed that the effective relaxation rate goes like the t^{-1}. A more detailed analysis of data for $Cu_{0.97}Mn_{0.03}$[103] found the same behavior with exponent -1.3. This is compared to a mean-field calculation of Kinzel and Fischer[104], which predicts that the relaxation rate should diverge as t^{-2}. The fit of the relaxation rate did not take the contribution from the linear behavior at high temperatures into account, which may have influenced the value obtained for the exponent. Deviations from the power law behavior are seen near T_f.

Both the shift and the excess width are related to the four spin correlation function, so we can derive a relationship between them.

$$(\Delta H)^{\alpha} \sim \left[\frac{H_o - H(g=2)}{H(g=2)}\right]^{\Xi} \qquad \text{5-36}$$

where H(g=2) is the value of the resonance peak position corresponding to a g-value of 2, and Ξ is predicted to be twice the exponent governing the linewidth divergence. Experimentally, this relationship is difficult to test, because of the small temperature range over which both H_o significantly differs from the high temperature value and the power law behavior still holds.

AgMn

Most of the ESR work in metallic spin glasses above T_f has been performed on $Ag_{1-x}Mn_x$, in part due to the lack of chemical clustering and the ease of sample preparation. Mozurkewich, et. al.[105] proposed that the dominant mechanism for broadening in metallic spin glasses is the DM anisotropy and not the dipolar interaction. To test this theory, a spin orbit scatterer, Sb, at a concentration y (in at.%) was added to some of the AgMn samples, so that the study considered $Ag_{1-x}Mn_xSb_y$ with x from .026 to .10 and y from 0.06 to 0.57. Measurements were made over a frequency range from 1 to 9 GHz. These measurements and the subsequent analysis have the most relevance to our experiment, so they will be reported in more detail.

$\Delta H(T)$ in both the AgMn and the AgMnSb samples exhibited the behavior characterized by Equation 5-2, with the parameters obtained from fitting shown in Table 5-1. The residual width, A, increases linearly with y and decreases linearly with x. The thermal broadening, B, increases linearly with increasing Sb concentration, with the rate of increase largest in the smaller Mn concentrations. This behavior is due to the lessening of the bottleneck due to the introduction of another relaxation path.

The divergence strength, C, increases linearly with increasing Sb concentration, with the strong dependence on Sb concentration precluding dipole-dipole interaction as the major source of line breadth near T_f. Calculations using a DM anisotropy[106] as the primary broadening mechanism predict a linear dependence of the excess linewidth on both x and y. The linear dependence on y is observed, but a weaker than linear dependence on x is seen, which is attributed to the same effects responsible for the sublinear dependence of T_f on x. The possibility of chemical clustering at the higher concentrations is also noted.

The values of the exponent κ all lie between 1.2 and 1.8, with the values for the undoped AgMn being roughly concentration independent and ranging from 1.2 to 1.4. The addition of Sb tends to increase the exponent from 1.3 at small concentrations to 1.8

Table 5-1: Parameters describing the dependence of $\Delta H(T)$ on Mn and Sb concentration in $Ag_{1-x}Mn_xSb_y$ from Mozurkewich, et. al.[105].

x(at%)	y(at.%)	$T_f(K)$	A(G)	B(G/K)	C(G)	κ
2.6	-	10.18	-8	2.48	21	1.4
2.6	0.06	9.98	-7	2.75	24	1.3
2.6	0.17	9.79	3	3.15	24	1.6
2.6	0.22	9.65	4	3.29	30	1.5
2.6	0.46	9.10	16	4.35	43	1.8
2.6	0.57	8.67	32	4.60	48	1.8
5.8	-	19.28	-43	2.53	34	1.2
7.8	-	24.56	-70	2.67	37	1.4
10.3	-	31.43	-105	2.68	40	1.4

at the largest concentrations. This is attributed to depression of the range dependence

of the exchange coupling by the spin orbit scatterers. Departure from power law

behavior is observed as the freezing temperature is approached, with the departure

occurring at higher reduced temperatures for higher frequencies and lower

concentrations.

At high temperatures, the resonance peak position is found at g $\approx$ 2. As T$\rightarrow$T$_f$,

the line shifts to lower fields, with the shift being much stronger for lower frequencies

than for higher ones. The shift cannot be properly described as a pure g-value shift, nor

as a simple, frequency independent internal field. The magnitude of the low frequency

shift is insensitive to Mn concentration (at any given reduced temperature), but shifts

more strongly with increasing Sb concentration. The behavior of the shift with Sb

concentration is correlated to the behavior of the linewidth with Sb concentration,

indicating that they arise from the same mechanism. From equation 5-34, at low

frequencies, the resonance peak position should diverge as the reduced temperature to

a power twice that of the linewidth divergence. As already mentioned, this is

experimentally difficult to verify, because the resonance peak position is different from

the high temperature value only over a small temperature region before the line becomes

too broad to accurately measure. The strong Sb dependence of the data reported by

Mozurkewich,*et. al.*, indicates that the dominant linewidth mechanism is an exchange

narrowed anisotropy, and not the previously predicted exchange narrowed dipolar

broadening.

Wu, *et. al.* [107] have measured frequency dependence of the linewidth and shift

in Ag$_{1-x}$Mn$_x$ (x=2.6 at.%) at frequencies from 1 and 10 GHz. The critical part of the

spin-spin relaxation rate is calculated using the DM anisotropy instead of the dipolar interaction as the broadening mechanism. Critical scaling in both field and frequency are (separately) applied, and critical exponents extracted. For frequency scaling, the linewidth is written

$$(\Delta H)^{ex} = C t^{-x} G(\omega\tau) \qquad where \quad \tau = \tau_0 t^{-\nu z} \qquad 5\text{-}37$$

and νz is found to be 2.5 $\pm$ 0.3. Field scaling results in an expression for the excess linewidth

$$(\Delta H)^{ex} = C t^{-x} G(H\tau) \qquad where \quad \tau = \tau_0 t^{\frac{\beta+\gamma}{2}} \qquad 5\text{-}38$$

which yields a value of $(\beta + \gamma)/2 = 2.5 \pm 0.3$. The crossover exponent, $\phi = \beta + \gamma = 5.0 \pm 0.5$. These values can be compared with other measured and theoretically calculated values shown in Appendix B.

An interesting sidenote to this analysis is that one freezing temperature is used in the scaling for all frequencies, which the authors claim determines a unique (to about 10%) T_f, good for all fields and frequencies. In this field regime, the Gabay-Toulouse line predicts a constant value of T_f, so Wu, et.al. interpret T_f as the GT transition temperature.

Baberschke, et. al.[108] and Mahdjour, et. al.[109] noted that the magnetization, and not the temperature is the variable occurring in the Bloch-Hasegawa equations, and plotted the linewidth as a function of susceptibility, where the susceptibility is measured

at a magnetic field equal to the resonance peak position. As T_f is approached, the magnetization becomes highly nonlinear, departing from its usual Curie-Weiss temperature dependence. This departure is larger for larger applied magnetic field (corresponding to larger ESR frequencies), which they cite as the reason why 'frequency dependence' is observed. By plotting $\Delta H(T)$ vs. χ, all frequency dependence is removed, which indicates that this is a field and not a time window effect. The excess part of the linewidth can be analyzed in terms of a power law in χ_s/H^2, where χ_s is the nonlinear susceptibility, and the scaling holds for all frequencies and for reduced temperatures down to T_f. A similar analysis has been applied to $(LaGd)Al_2$[110,111].

Other Spin Glasses

Eu$_x$Sr$_{1-x}$S

Eu$_x$Sr$_{1-x}$S is a Heisenberg system, with cubic NaCl structure. The compound can, depending on concentration, be paramagnetic, ferromagnetic, or a spin glass. The nearest neighbor interaction is ferromagnetic, and the next nearest neighbor is antiferromagnetic, with long range magnetic dipolar interactions the sole source of broadening. The non-metallic nature of this system precludes the bottlenecked behavior; the linewidth is temperature independent until magnetic correlations start to cause broadening[112]. The same type of frequency dependence (a weakening of the divergence with increasing frequency) is observed[113]. Dynamic scaling has been used to explain the frequency dependence of the linewidth[114].

Concentrated Metallic Spin Glasses

In concentrated metallic spin glasses, direct exchange, and not the long range RKKY interaction dominates. Hou, *et. al.*[115,116] analyzed this behavior in $Fe_8Ni_{72}P_{20}$, and $Fe_{10}Ni_{70}P_{20}$, finding that these materials behaved similarly to the materials mentioned above.

Park, *et. al.*[117,118], studied amorphous $Fe_xNi_{80-x}P_{14}B_6$ and sputtered $Mn_{48}B_{52}$ films. Contrary to results found in dilute metallic spin glasses, the linewidth does not diverge strongly. As T_f is approached, the linewidth becomes very broad, but remains measurable through the freezing temperature. As the temperature is lowered below T_f, the linewidth decreases and finally disappears. The divergent behavior above T_f is fit to a phenomenological expression,

$$(\Delta H)^\alpha = C \left(\frac{T}{T_0}\right)^n \exp\left(-\frac{T}{T_0}\right)$$

5-39

where n is either 1 or 0. Frequency effects similar to those seen in the other spin glasses are seen, but there appears to be a 'resonant frequency', for which the rise in linewidth is faster than either higher or lower frequencies. This resonant frequency is about 3 GHz for the Fe compound, and 4 GHz for the Mn compound. In contrast to the dilute metallic spin glasses, the ESR linewidth shows no history dependence on the cooling field for fields up to at least 17 kG. In the Fe series, increasing the iron concentration decreases the strength of the divergence and increases the breadth of the minimum in

$\Delta H(T)$. Bhagat, *et. al.* [119] have shown that Equation 5-39 can be used to fit data from both concentrated and dilute metallic spin glasses.

GdAl

Malozemoff and Jamet[120] studied amorphous $Gd_{0.37}Al_{0.63}$ films sputtered onto Kapton. The linewidth is fit to a power law with exponent between 1.5 and 2. Frequency dependent measurements reveal a flattening of the divergence with increasing frequency. Exchange narrowing is predicted to account for the linewidth at temperatures above T_f; near the freezing transition, where a departure from the power law behavior is observed, a local field model based on the presence of ferromagnetic clusters is suggested.

Misc. Spin Glasses

Fiorani, *et. al.*[121], found divergent behavior in the insulating spinel solid solution $CdIn_{2-x}Cr_xS_4$ for x between 0.6 and 1.7. The spin glass mechanism is preferential occupation of the octahedral sites of the spinel structure by the Cr, which gives rise to F and AF bonds. As with the concentrated metallic spin glasses, the linewidth measurements are insensitive to the magnetic field in which the sample was cooled. The broadening of the linewidth and the shift in the resonance peak position are attributed to random internal fields. The value of the linewidth saturates near T_f, then decreases, with an accompanying deviation from a Lorentzian shape well above T_f. In

the region near T_f, the lineshape is Gaussian in the center and very narrowed in the wings. Similar results have been seen in $Cu_{2x}Cr_{2x}Sn_{2-2x}S_4$[122].

Aronson, Salamon and Hauser[123] studied the concentrated amorphous spin glass MnSi, in which the spin relaxation is dominated by random anisotropic fields, with linewidth and shift results identical to the concentrated metallic spin glasses.

Koche, *et. al.*[124] studied the divergence of the linewidth in pseudobrookite ($Fe_2 TiO_5$) in a percolation context, modeling the sample as one 'infinite' cluster of spins coexisting with smaller finite clusters. The low energy excitations of the infinite cluster are treated as spin waves, with the finite clusters providing relaxation channels. The DM interaction links the finite clusters and the infinite cluster. The linewidth can be satisfactorily fit to an exponential form,

$$(\Delta H)^{ex} = A \exp\left(-\frac{T}{T_f}\right)$$ 5-40

Ferromagnets, Antiferromagnets and Low Dimensionality

The divergence of the ESR linewidth is noted for many -- but not all -- ferromagnets and antiferromagnets. Taylor and Coles[125] identified a series of intermetallic compounds, including both ferromagnetic and antiferromagnetic materials, which display the same temperature dependence of the linewidth and the resonance peak position as seen in the spin glasses. The materials are atomically well ordered, and include dilute alloys like $GdZn_{17}$, as well as compounds like $GdAl_2$ and Pd_2Eu.

Measurements were made on powdered samples at 9 GHz. At high temperatures, these materials follow an A+BT behavior, and at some temperature, denoted by T_b, deviation from the linear behavior in the form of an diverging linewidth is noted.

In the ferromagnetic compounds, T_b is between 1.2 and 1.5 T_c, for all compounds except Cu_6Gd, which broadens at about $6T_c$. In the antiferromagnets, broadening is also seen at 1.5 - 2 T_c in most compounds, with the exception of: Cu_4Gd ($2T_c$), $EuAl_4$($4T_c$), $GdZn_{12}$ ($5T_c$), and Gd_2Zn_{17}($10T_c$). The high temperatures at which broadening occurs is related to the presence of short range order. The short range order is induced by anisotropy in the exchange interaction; large enough anisotropies can effectively reduce the dimensionality of the material.

$Zn_{13}Mn$ has a highly anisotropic crystal structure; along the c axis, Mn atoms are 5.1 Å apart, with only a single Zn atom between them. Adjacent chains of Mn atoms are separated by at least 6.6 Å, with several Zn atoms in between the Mn. Susceptibility measurements indicate that chains of Mn along the c axis order first, at a temperature of about 120 K. This intrachain ordering is 'quasi one dimensional' and therefore weak, but strong enough to sustain short range order. Full 3-d ordering is not seen until about 23 K[126]. ESR measurements show that the g value of the material is equal to 2 at high temperature, begins to increase at 120 K, and reaches a value of 3 at 4 K. The broadening at temperatures far above T_c is linked to the onset of the quasi-1-dimensional (or short range) order. One possible source for a large amount of short range order occurs when the RKKY interaction favors spin ordering which cannot be maintained due to the strict periodicity of the lattice. This frustration would result in a fairly extended

temperature range over which the free energy would be minimized by the existence of short range order.

In the short range ordered regime, Kawasaki[94] used the formalism outlined in the first part of this chapter and calculated that the linewidths in antiferromagnets could be described by

$$\Delta H(T) \propto (T-T_N)^{-|P|} \qquad \qquad \text{5-41}$$

with an exponent of $P = 5/3$. Experimental values of P range from 0.5 to 1.6, depending on the material. Seehra and Castner[127] measured $\Delta H(T)$ for MnF_2, a uniaxial antiferromagnet, and found $P = 1.17$. Burgiel, et. al.[128] found the same behavior, but with exponent 3/8. Zimmerman, et. al.[129] measured $P = 0.58$ in the antiferromagnet $CuCl_2 \cdot 2H_2O$. Measurements of MnO and MnS[130,131], found $P = 3/4$ for both materials.

Seehra[132] measured the frequency dependence of the excess linewidth in MnF_2 near the critical temperature. The frequency dependence starts at a reduced temperature of about 0.15, with higher frequencies producing narrower linewidths. Frequency dependence is also noted in MnS[131]. All of the measurements of P cited above, except Seehra and Caster's were performed at 35 GHz, which may explain the low values of the exponents.

As in spin glasses, anisotropy appears to play a very important role in the presence of a divergence. Although the linewidth of MnF_2 - a strongly anisotropic antiferromagnet - diverges, the cubic antiferromagnets $RbMnF_3$, $KMnF_3$, and KMn:

MgF_3 show a slight narrowing as T_N is approached from above. The role of anisotropy in the divergent nature of the ESR linewidth was theoretically investigated in antiferromagnets by Huber[101], and Seehra[133], in much the same manner as Mozurkewich, *et. al.*[105] did with AgMn. These theories will be discussed in the last section of this chapter.

ESR in 1 and 2 Dimensional Materials

Because of the importance of long time relaxation behavior in 1 and 2 dimensional systems, the dependence of linewidth on temperature should be different. In one dimension, for exchange narrowed dipolar broadening, the expression corresponding to Equation 5-34 is

$$\frac{1}{T} \sim (\omega_d^2)^{2/3} (\tau_e)^{1/3} \qquad \text{5-42}$$

In the canonical linear chain antiferromagnets TMMC $((CH_3)_4NMnCl_3)$[134], and $CsMnCl_3 2H_2O$[135], the same divergent behavior of the linewidth is observed; however, the line broadening begins at much higher temperatures than the resonance shift and the ordering behavior is dependent on the direction of the sample with respect to the field. As the temperature decreases, short range order begins to grow, so that small clusters are formed. These clusters randomly provide local fields, which results in a shift of the resonance line. Although a one dimensional compound can not support order, the small

clusters are ordered enough to approximate the behavior seen in the three dimensional ordered compounds.

Other ESR experiments with TMMC have substituted diamagnetic or paramagnetic impurities, which tend to block or slow down the rate of spin correlations. Linear chain ferromagnets, such as CHAC [$(C_6H_{11}NH_3)CuCl_3$] and CHAB [$(C_6H_{11}NH_3)CuBr_3$] also display the g-shift seen in the antiferromagnets; the linewidth results were not reported[136]. The lineshift move towards higher fields for the hard axes, and towards lower fields for the easy axis.

In magnetically 2-D manganese bromide and manganese chloride salts, $\Delta H(T)$ also obeys a straight line at high temperatures (due to coupling of the spin system and the phonon system through the DM anisotropy, and a divergent part which follows Equation 5-2[137]. The exponent is observed to have a value on the order of 2, and a different angular dependence of the linewidth than three dimensional compounds.

Richards and Salamon[138] studied the behavior of the two dimensional antiferromagnet K_2MnF_4. The problem is treated within the theory of two dimensional exchange narrowed dipolar interactions, and the linewidth may be calculated by assuming a Gaussian form for the short time behavior of the relaxation function, and a diffusive behavior for long times. Qualitatively, the calculated linewidths predict the same temperature dependence as that observed. The numerical agreement is not ideal, but given that the theory has no adjustable parameters, these results are very good evidence that the exchange narrowed dipolar broadened formalism can distinguish two dimensional behavior from three dimensional behavior.

The antiferromagnet $K_2Mn_cMg_{1-c}F_4$ displays crossover behavior from one to two dimensions, depending on the Mn concentration. As the Mn sites are diluted with Mg, the paths for spin diffusion becomes blocked, resulting in one dimensional behavior indicated by a change in the lineshape. The crossover to one dimension can be determined within the context of a percolation problem. As the amount of Mn increases, the lineshape becomes increasingly Lorentzian although, even at $c=1$, the line is significantly non-Lorentzian. The behavior of $\Delta H(T)$ is dependent on the angle between the normal to the 2D plane and the applied field, with the dependence being more pronounced for lower concentrations. Although the data was not fit to a theoretical form, the raw data seems to indicate that the exponent takes on one value for all of the samples obeying two dimensional behavior, and gradually increases as the Mg concentration increases.

Walsh, *et. al.* [139] found the same behavior in $Rb_2Mn_cMg_{1-c}F_4$, a dilute two dimensional antiferromagnet which is closely related to the 2D Ising spin glass $Rb_2Cu_{1-x}Co_xF_4$. These effects were explained in the context of percolation theory, which predicts that the linewidth will diverge like $T^{-4.5}$ in the 2D case. The data do show a divergence in the samples which are two dimensional, and a much weaker divergence in the 'one dimensional' samples, but the predicted power law behavior is not observed.

THEORIES OF ESR IN SPIN GLASSES

Now that we have looked at the general theory of ESR in localized metallic moments, and data from spin glasses, ferromagnets and antiferromagnets, we turn to the

specific theories which have been advanced to explain the behavior of the ESR linewidth in spin glasses. There are two general approaches. The first theory can be characterized as a mean field approach, which uses the Mori-Kawasaki treatment of ESR near critical points. The second approach is a cluster model in which the dominant processes above T_f are the formation of regions of correlated spins. These two theories have a subtle, but very important difference. The mean field theory assumes that the behavior of the ESR linewidth is a divergence associated with the phase transition into the spin glass phase. The correlated cluster model implies that, at temperatures above T_b, but below T_f, the behavior of the ESR linewidth in spin glasses is actually a measure of a paramagnetic phenomena.

Mean Field ESR Theory

Huber studied the behavior of the linewidth near critical points in ferromagnets[140], antiferromagnets[101], and AgMn[141] using the Mori-Kawasaki treatment. The Hamiltonian is taken to include the RKKY exchange interaction and the DM anisotropy is the broadening mechanism. The Random Phase Approximation used to decouple the four-spin correlation function emphasizes two spin correlation functions, which is analogous to considering that single spin flip events are most important. In ferromagnets, the linewidth is predicted to diverge as $\chi^{-3/4}$. In antiferromagnets (specifically MnF_2), dipolar anisotropy is introduced, with the linewidth is predicted to diverge as $(T/\chi)\xi^{5/2}$. Using the relationships between the susceptibility and the correlation length, and between the correlation length and the reduced temperature, he

finds that the linewidth should diverge like $(T-T_N)^{-\kappa}$, where κ is between 1.2 and 1.6. This lower limit is determined by using the mean field relationship between ξ and t, and the upper limit by using the experimentally measured relationship $\xi = (T-T_N)^{-2/3}$. The accuracy of both expressions decreases as the temperature gets farther from T_N. Critical slowing down is suggested as the reason for the divergence. The predictions are valid in the temperature range from T_N to 2 T_N. Theoretical predictions of the angular dependence of the linewidth within the framework of this theory have been experimentally verified[133].

The broadening of the linewidth as a function of temperature and the eventual departure from the predicted power law behavior can be qualitatively considered as follows: When the exchange energy is much larger than the anisotropy and Zeeman energies, the usual picture of exchange narrowing applies. As the Neel temperature is approached, the mean free path of an excitation increases due to increasing correlations between the spins. Cluster formation decreases the frequency of the exchange modulation, resulting in broadening. At some temperature, the modulation frequency becomes comparable to the anisotropy frequency or the Larmor frequency, and the exchange narrowing picture fails. Below the temperature where the exchange frequency is on the same order as the Larmor frequency, the measuring frequency becomes important, so that increasing measuring frequency results in a deviation from power law behavior at a higher reduced temperature.

Based on the measurements of Mozurkewich, *et. al.*[105], Levy, Morgan-Pond and Raghavan[106] used the Mori-Kawasaki/Kubo-Tomita formalism with a DM anisotropy as

v

r

li

re

T

be

to

a

te

th

i

t

the broadening mechanism. Configurational averages over the random distributions of the exchange, DM and dipolar couplings must be made for application to spin glasses.

The four spin correlation function is expanded by expressing it in the basis in which the RKKY interaction is diagonal. The decoupling is exact for an infinite range model, but emphasizes single spin flips as being the most important contributions to the line. A mean field expression for the two spin correlation functions is assumed for the resulting decoupled expression. The assumptions cause the model to break down near T_f. Morgan-Pond[142] estimates that the corrections to the mean field approximations become important below $t = 1/4$ in AgMn.

Both the divergence of the linewidth and the shift of the resonance peak position to lower fields are predicted from this theory, but these quantities are not presented in a closed analytic form. Their quantitative predictions for $\Delta H(T)$ as a function of temperature agree remarkably well with the low frequency data, especially considering that no adjustable parameters are used. Higher frequency data does not match as well in the region where it differs from the low frequency data, due to the approximations used in the decoupling procedure. This analysis has been successfully applied to EuSrS[143,144]; it is simpler in this case because the only broadening mechanism is the dipolar interaction. Agreement with low frequency experiment has been extraordinary, considering that there are no adjustable parameters.

The Correlated Cluster Model

Experimental evidence indicates that correlations begin at temperatures far above T_f. Barnes[145] adapted and extended the Bloch-Hasewaga treatment of ESR of localized moments in metals to treat spin glasses. At high temperatures, correlations between spins can be neglected, and the behavior of the linewidth is explained by the Bloch-Hasegawa equations. As T_f is approached, correlations will become increasingly important as pair, triples, etc. form. Clusters will form when the correlation between the spins in the cluster exceeds some critical value of J. The Boltzmann factor weighting causes these clusters to essentially drop out of the thermodynamics of the system.

We now have a four component system consisting of the lattice, the conduction electrons, correlated clusters, and the uncorrelated ions. A schematic picture of the system is shown in Figure 5-2.

This results in the introduction of a myriad of additional relaxation times. T_{ce} and T_{ec} represent the relaxation time of a spin in a correlated cluster to a free spin and vice-versa. We now have three Bloch-Hasegawa equations; one for the conduction electrons, one for the correlated clusters, and one for the uncorrelated ions.

We have to consider the conditions under which the correlated spins and the uncorrelated spins will have a common resonance. The solution for the case of common resonance requires that an appreciable number of correlated spins are present, which is satisfied in a temperature regime with an upper limit of a few times T_f. The same range also applies to the bottlenecked case.
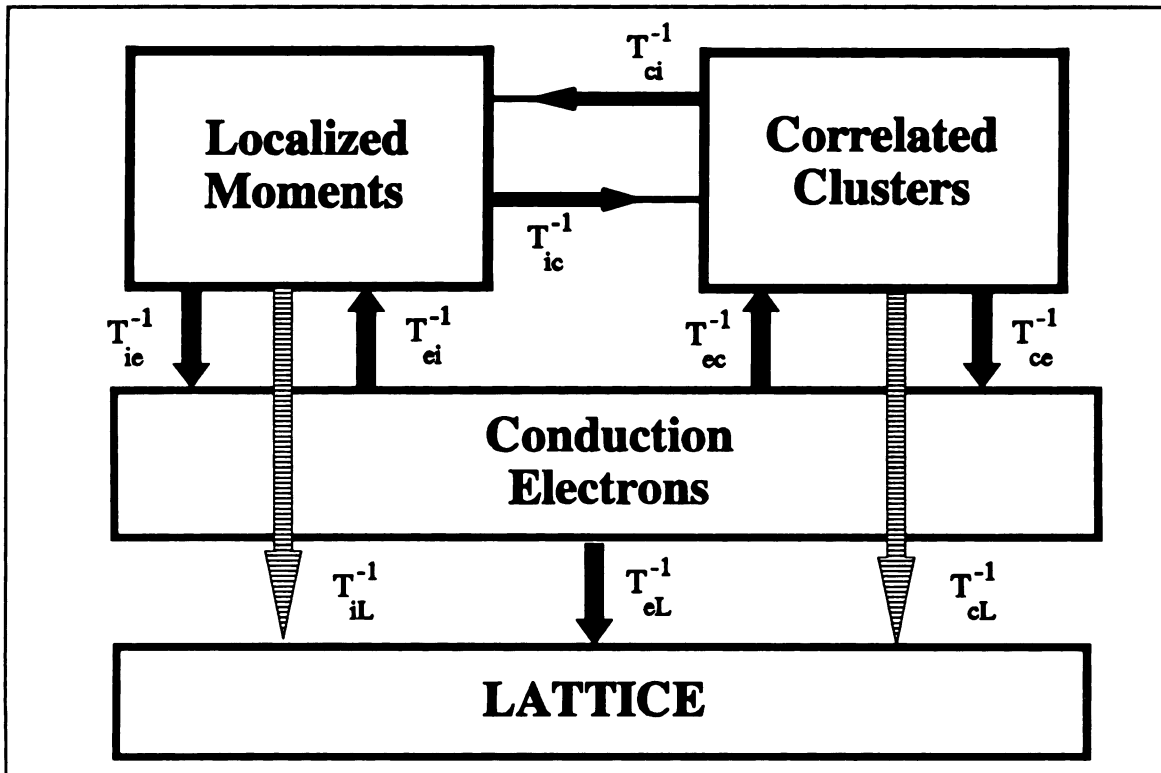
Figure 5-2: *Allowed relaxation paths for the correlated cluster model*

In Barnes' original picture, clusters are either ferromagnetic or antiferromagnetic. If a pair is antiferromagnetically correlated, there is no net magnetization, so the only effect on the Bloch-Hasegawa equations is a decrease in the concentration of free spins. If the pair is ferromagnetically coupled, Barnes' calculation shows that the Korringa rate $(1/T_{ce})$ decreases by a factor of two, but the Overhauser rate $(1/T_{ec})$ increases by a factor of four, which favors bottlenecking.

For both bottlenecked and non-bottlenecked systems, the same high temperature linear behavior is observed. As the temperature decreases, clusters become more

important. The thermal broadening and the residual width are found to be dependent on the degree of short range correlation. As T_f is approached, Barnes cites experimental evidence of the importance of the DM anisotropy and assumes an EA phase transition to obtain the divergent behavior. Two broadening mechanisms are present; the internal fields due to the clusters, and a random-effective field due to the DM interaction. The anisotropy can be accounted for in an effective moment to lattice relaxation time, T_{iL}. The broadening fields will be narrowed by cross relaxation between the clusters and the free ions. In particular, the residual width will be proportional to $1/T_{iL}$, where (using Equation 5-34),

$$\frac{1}{T_{iL}} \sim <(\omega_a)^2> \tau_i \qquad \qquad \text{5-43}$$

where τ_i is the mean relaxation time of the local moments and ωa is the anisotropy frequency. This implies that the ESR linewidth is due to the contribution from the local moments, and not the spins contained in correlated clusters. If an Edwards-Anderson type phase transition is assumed, $\tau_i \sim t^1$, and

$$\Delta H(T) \sim \frac{1}{T_{iL}} \sim <(\omega_a)^2> \tau_i^0 \left(\frac{T_f - T}{T_f} \right)^{-1} \qquad \qquad \text{5-44}$$

Barnes[91] notes that, since there is little reason to expect measurements to yield mean field values, the exponent should be used as a parameter. In particular, if the correlation length goes like $t^{-\nu}$, and the critical relaxation time goes like the correlation length to an

exponent, ζ, we would predict a divergence which goes like $t^{-\nu\zeta}$. For antiferromagnets, the relaxation time goes like $\xi^{-3/2}$, so the exponent governing the divergence of the linewidth (κ) would be equal to $-3/2\nu$.

Barnes offers a conceptual explanation for the frequency dependence of the ESR linewidth in the bottlenecked system Y:Gd[146], which is an antiferromagnet at higher concentrations, and a spin glass at lower concentrations. The homogeneous relaxation processes continue all the way down to $T=0$, so that broadening as the ordering temperature is approached must be inhomogeneous in nature. The highly correlated clusters generate an internal field distribution with a small average value, which results in inhomogeneous broadening. If a system is strongly enough bottlenecked, the narrowing effect due to cross relaxation will overcome the inhomogeneous broadening. The strength of the bottleneck is proportional to the root mean square of the Knight shift (which scales with frequency) and the Korringa rate, so that the bottleneck is more effective at higher frequencies and explains the deviations from power law behavior as a function of frequency.

Comparison of the Models

Although these two models predict the same behavior of the linewidth, their foundations are very different, with the mean field theory attributing the ESR linewidth divergence and lineshift to spin glass phenomena, and the droplet model attributing these effects to paramagnetic (uncorrelated) spins. Both models agree that anisotropy is a significant broadening mechanism in spin glasses, especially near T_f.

The mean field approach does not present a functional form for the divergence, so there is no obvious relation between κ and other exponents. Other calculations have been performed by Bruinsma[147] who determined $\kappa = \nu z$ by averaging the DM interaction in a scaling context, and by Henley[147] who decoupled the four-spin correlation functions and found $\kappa = \nu z - 2\beta$.

SUMMARY

The theoretical treatment of the ESR of localized moments in metals indicates that the linear behavior, $\Delta H(T) = A + BT$ is due to the temperature dependence of competing relaxation rates. The correlation function formalism which predicts the linewidth and lineshape in the case of strongly interacting spins has been outlined, with general comments on how the cooperative behavior of the spins can narrow or broaden the resonance line. Qualitative differences between ESR in low dimensional materials and in three dimensions have been noted.

Experimentally, we have seen that the divergent behavior of the ESR linewidth, along with the accompanying line shift, has been observed in one and two dimensional antiferromagnets and ferromagnets. Anisotropy appears to be the dominant mechanism for the behavior of the linewidth near T_f, both in spin glasses and in other magnets. The set of ferro- and antiferro- magnets which display this divergence are all anisotropic, with the low dimensional materials being the limiting case of strong anisotropy. In lower dimensional magnets, data taken with the field along the easy axis exhibits the standard shift of the resonance field to lower fields; data taken with the fields along a hard axis

shifts to high fields. Measurement of the linewidth and shift at higher frequencies results in a departure from the power law behavior for $\Delta H(T)$ at higher reduced temperatures than measurements at lower frequencies. This frequency dependent has been seen in both antiferromagnets and spin glasses.

Interpretation of ESR in spin glasses above T_f has been primarily phenomenological, in terms of Equation 5-2, due to the lack of specific theories (with the exception of the AgMn analysis of Levy, Morgan-Pond and Raghavan which is valid only for low frequencies) addressing this temperature regime. Two theories have been presented. The first theory assumes that the divergent nature of the ESR linewidth is due to critical slowing down near a phase transition. The second theory attributes the linewidth to inhomogeneous broadening due to the formation of internal local fields of correlated clusters, with cluster formation beginning at a few times T_f. This second theory is compatible with the existence of an intermediate phase between the paramagnetic and the spin glass phase.

ESR investigation of thin film ferro- and antiferro- magnets have primarily focused on behavior below the ordering temperature, so there has not been an extensive investigation of ESR in multilayered magnets to which we could compare our spin glass measurements.

MOTIVATION FOR THE EXPERIMENT DESCRIBED IN THIS THESIS

Now that the intricacies of spin glasses have been explained, the principles behind the ESR experiment and theory have been discussed, and the literature pertinent to ESR

in spin glasses has been reviewed, a statement of the motivation of the work presented in this thesis is in order. As we have seen, spin glass properties are a function of dimensionality, measuring time and magnetic field. The previous studies of multilayered metallic spin glasses have primarily been of three types; 'DC' susceptibility measurements made at 100 G and measuring times on the order of 300 seconds, 2) susceptibility measurements from 10^{-4} seconds to 10^4 seconds at a fields of 10 G, and 3) field dependent susceptibility measurements from 2 G to 15000 G at measuring times of 300 seconds. This group of experiments covers a small region of frequency-field space, as shown in Figure 5-3. All of these experiments probe the behavior of one quantity - the freezing temperature - as layer thickness is reduced. The observed effects have been analyzed in terms of finite size scaling and dimensionality effects.

ESR experiments at 9 GHz have a measurement time of 10^{-10} s, and require magnetic fields from 1 to 6 kG. This represents a very different time regime than probed by susceptibility measurements and investigates the behavior of a quantity (the ESR linewidth and shift) different from the freezing temperature. We would like to answer the following questions:

1) Does the expression (Equation 5-2) used to describe the ESR linewidth in bulk samples apply for all layer thicknesses, or is an alternate expression needed to describe the behavior of the very thin (2D) samples?

2) If the exponent κ is a critical exponent, will it take on two different values in the different dimensional regimes?

3) Are there substantial changes in the lineshape as a function of layer thickness

hich might be indicative of 2D behavior and therefore provide additional evidence of the

change in dimensionality in these multilayers?
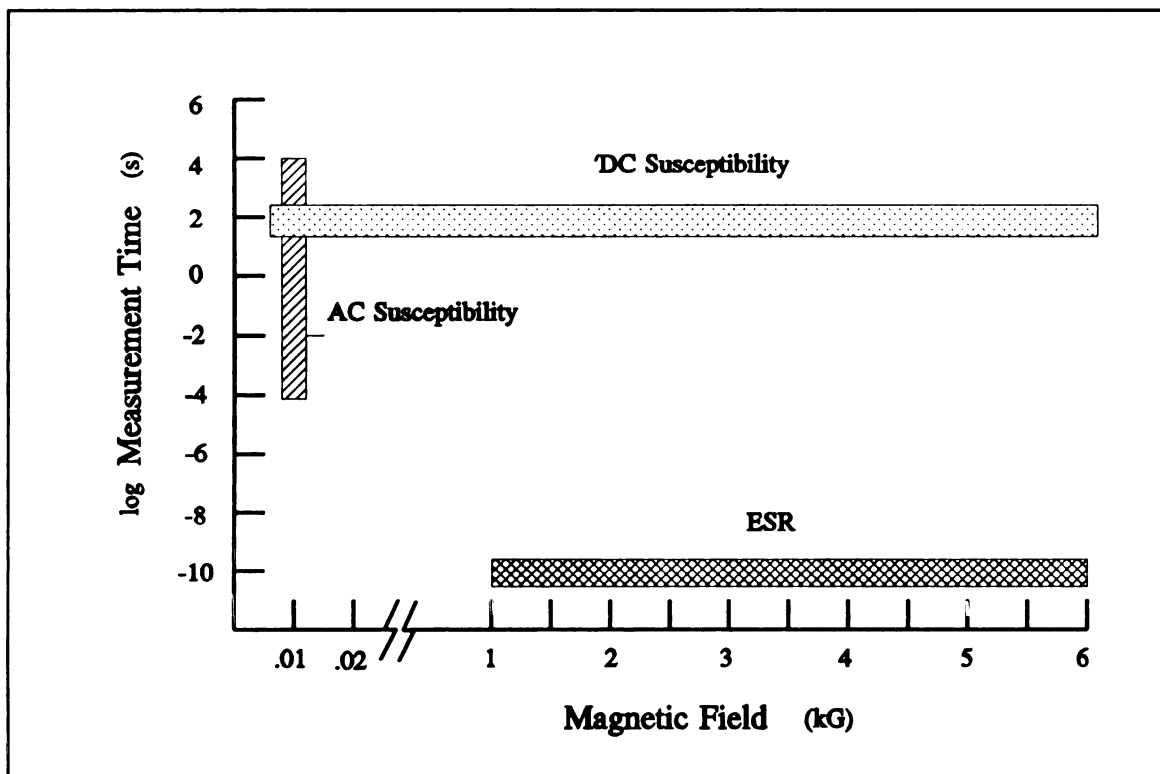
Figure 5-3: *Measurement regimes of techniques used in the investigation of metallic multilayers in the time-magnetic field plane*

4) Does the lineshift behave in the same manner for all W_{SG}? If the shift and the

divergence of the linewidth arise from the same mechanism, we expect this to be true.

If they arise from a different mechanism, one of the mechanisms may be more or less affected by the changing sample size.

5) Is the observed departure from power law behavior as T_f is approached dependent on W_{SG}? The mechanism for this departure in bulk materials is not clear.

6) Substantial evidence exists for the onset of correlations above T_f in spin glasses; these correlations have a broader spectrum of relaxation times than a paramagnet, but nowhere near the extended time scales of the spin glass phase. Long time probes like the DC susceptibility - and even the AC susceptibility - would be insensitive to these phenomena. If there is indeed a 'Griffiths phase' in spin glasses, the time scale of the correlations would observable only to high frequency probes like μSR, neutron scattering and ESR.

7) Most importantly, can the results of this study shed any light on the question of whether the mean field or the correlated cluster model is the most accurate description of ESR in spin glasses?

In summary, this study is designed to test the behavior of spin glasses in the temperature regime above T_f, in a field-frequency regime quite different from that of the susceptibility experiments. We hope to extend our knowledge about ESR in spin glasses to metallic multilayers, and hopefully to shed some light on the general behavior of spin glasses on the approach to T_f.

CHAPTER SIX

EXPERIMENTAL METHODS

INTRODUCTION

This section details the experimental techniques used in this study and is divided into three parts. The first part describes the fabrication of the target and the sputtering of the samples. This is followed by a discussion of characterization techniques used to determine the quality of the samples, and is primarily a summary of work done by the MSU spin glass group. The third section details the experimental techniques used in sample preparation and data taking for the Electron Spin Resonance (ESR) experiment.

Sample Naming Convention

The samples sputtered are multilayers of the form W_{SG} nm of spin glass and W_{IL} nm of interlayer material, with N bilayers. The standard way of referring to these samples is $W_{SG}/W_{IL}/N$, with all thicknesses given in nanometers. As discussed in Chapter 4, W_{IL} = 30 nm for copper and 7 nm for silicon.

SAMPLE FABRICATION

To have enough spins in a sample for a measurable signal, multilayers were fabricated with W_{SG} nm of the spin glass interlayered with a suitable amount of non-magnetic material which prevents magnetic interactions between spin glass layers. The original study[71,72] investigated the effects of using both silicon and copper as the interlayer materials. Samples with copper interlayers were chosen for the ESR experiment because a) most of the measurements done on multilayered spin glasses at the time focused on copper interlayers b) the silicon interlayered samples are not as close to ideal multilayers as the copper interlayered samples and c) the copper interlayers should not produce an independent ESR signal.

Target Production

The CuMn targets were alloyed in an RF induction furnace from 99.9999% pure copper and 99.99% pure Mn purchased from Aesar, Inc. A cylindrical graphite boat of radius 6.5 cm and depth 2 cm was painted with boron nitride to prevent contact between the boat and the target. Two coats of boron nitride were applied, with each coat allowed to dry overnight. Prior to alloying, the constituents were etched in nitric acid, rinsed in de-ionized water and then in alcohol, and weighed. The Mn, which was etched immediately before alloying to prevent oxidation, was placed at the bottom of the boat and covered with the copper. The crucible and metals were immediately placed in a quartz vacuum chamber encircled by the RF coils. The chamber is evacuated to a

pressure of approximately 10^{-6} torr, flushed three times, and then backfilled with a 90% Argon/10% Hydrogen mixture. The Argon provides an inert atmosphere, while the hydrogen helps remove oxygen which may outgas as the metals are heated.

The temperature of the boat was measured using an optical pyrometer. Because of the difference in the melting points of the two metals ($T_m^{Cu} = 1083$ °C, $T_m^{Mn} = 1244$ °C), the Mn is placed in the bottom of the boat, and covered with copper so that the Mn is in contact with the heating graphite boat. The temperature is slowly increased by increasing the current through the rf coils. As the temperature rises, the copper melts and surrounds the Mn. As the temperature is increased, the Mn begins to dissolve. At or near 1244 °C, the molten mixture begins to swirl in the boat. The alloy is held at this temperature for approximately five minutes to encourage mixing. The current is gradually decreased, and the sample is allowed to cool. A crust, probably made up of contaminants and MnO, forms on the top of the liquid as the mixture cools. The target is removed from the vacuum compartment after reaching room temperature and turned on a lathe to a final radius of 5.7 cm and a thickness of approximately 1.25 cm.

The concentration of the target is determined by comparing susceptibility measurements of the freezing temperature to known values of T_f as a function of Mn concentration. In general, a small (1 or 2 percent) excess of Mn is necessary in alloying the target. We believe the loss of Mn in the alloying process is due to oxidation and failure to alloy homogeneously, resulting in a larger concentration of Mn and MnO on the surface which is then machined away.

Prior to being placed in the sputtering chamber, the target is washed with alcohol. The target is presputtered for a few minutes prior to sample deposition to remove surface impurities acquired during the machining process. The Cu target used for the interlayers was purchased commercially from Varian, Inc.

Sputtering Apparatus

In sputtering, the surface atoms of a target (CuMn or Cu) are emitted as a result of bombardment by energetic particles (Ar^+ ions in this case). The sputtering chamber is a stainless steel cylinder of radius 23 cm and height 48 cm. Four DC sputtering sources are available, but we used only two targets at a time in the fabrication of these samples. The sputtering sources are mounted so that target particles are sputtered upward. A Substrate Positioning and Measurement Apparatus (SPAMA) is suspended from the top of the tank at a height of about 10 cm from the targets. The motion of the plate is controlled by a computer programmed stepper motor. The SPAMA holds up to sixteen substrates, grouped in eight pairs of two. In earlier sample runs, two of each sample configuration were simultaneously sputtered, with the midpoint between the two samples centered over the sputtering source. Concerns about the angular distribution of the sputtered ions changed this procedure to making samples one at a time, with each sample centered over the source. Each removable part of the sputtering chamber is etched in an acid solution to remove any metal left from the last sputtering run, then rinsed with acetone and alcohol. Rubber or cloth gloves were worn at all times when

working inside the chamber, or with parts placed inside the chamber to reduce contaminants which might degrade the vacuum.

Silicon (preferably 100, but also 110, or 111 orientation) was chosen as the substrate material due to its smooth surface and ease of cleaving. After having been cut into 1/2" x 1/2" squares, the substrates are cleaned in an ultrasonic cleaner first in acetone and then in alcohol. In earlier runs, the substrates had been cleaned with Alconox before the acetone and alcohol, but we were advised that this procedure scratches the surface of the silicon, and this step was removed. The substrates are mounted in the SPAMA and placed in the sputtering chamber. A capillary fed LN_2 substrate cooler, which can cool the substrates to or below room temperature, was installed to minimize diffusion during sputtering. Thermocouples attached to opposing sides of the SPAMA are used to determine the temperature during the sputtering process.

Once the chamber is loaded and closed, it is pumped down by a roughing pump followed by a cryopump. The chamber is baked for 24 hours to allow outgassing, resulting in a base pressure of $\leq 2 \times 10^{-8}$ Torr. Ultra-pure Argon gas is passed through a cold trap and a gas purifier before backfilling the chamber to a pressure of 2.5×10^{-3} Torr.

Argon atoms are ionized by accelerating electrons from a hot filament through the gas flowing across the target. By holding the target at a negative potential, the positive Ar ions are accelerated toward the target. The sputtering parameters are experimentally determined so that the resulting CuMn layers are homogenous and preferential sputtering of one component of the alloy over the other is avoided. Both Cu and CuMn are sputtered at currents from 0.6 A to 0.7 A and voltages of about 400 V (which means an

incoming Ar ion energy of approximately 400 eV). Quartz crystal Film Thickness Monitors (FTMs) were used to measure the deposition rate of both sources before sputtering. Typical sputtering rates are 1.1-1.6 nm/s for both the Cu and the CuMn targets.

In sputtering from alloys, one type of atom may be preferentially emitted from the target. The transition temperatures of 500 nm films and target shavings showed no more than $\pm$ 1 K difference, which indicates that the degree of preferential sputtering in CuMn is small or non-existent.

The sputtering process is inherently random, which we believe contributes to achieving a uniform distribution of Mn atoms; however chemical clustering, especially at higher concentrations, is a possibility. We have minimized both this problem, and the problem of diffusion at interfaces by keeping the substrates cooled to room temperature or less during the sputtering process. The effect of cooling on multilayer quality has been demonstrated to be especially significant in CuMn/Si[74]. The detailed analysis of the freezing temperature in these multilayers has shown scaling behavior to hold for samples with concentrations up to 14%, indicating that increased ferromagnetic interactions in larger concentrations are not likely.

CHARACTERIZATION

An ideal multilayer structure has crystalline layers and perfect periodicity (meaning flat, abrupt interfaces between layers with no intermixing). Although the multilayers produced by sputtering are not ideal, the studies cited in Chapter Four have

shown that the quality of the samples is sufficient for the observation of numerous interesting spin glass properties. Because knowledge of how closely these samples approximate ideal multilayers is fundamental to further studies, many characterization techniques were used to determine the integrity of the multilayers. The initial investigations have provided a consistent picture of the quality of the sputtered multilayers, so one or two of these techniques are now used as routine checks. In the CuMn/Cu samples, the primary techniques used were profilometer measurements, x-rays, and susceptometry. Although investigation into the detailed structure of sputtered multilayers continues, the sample production process should be regarded as consistent and well-established. This section outlines the methods which have been used to establish the quality of the samples and summarizes the conclusions of the spin glass group to date.

The step most conducive to intermixing of the layers is the actual sputtering process. Ag-Cu multilayers, which were made because Ag and Cu are immiscible, indicate that even with 0.8 nm/0.8 nm samples, the sputtering process must be good enough to keep the two metals from spreading more than two atomic layers (.4-.5 nm). The total spreading of the host materials is .8-1 nm for a given layer.

Diffusion of the Mn into the buffer layer is the most likely source of significant deviations from ideal layering. Diffusion of Mn in Cu in defect free material at room temperature and even at temperatures comparable to those reached during the sputtering process is fairly negligible. The sputtered materials, however, are highly polycrystalline, resulting in grain boundaries and other defects at a concentration of about 1%. If these defects were all vacancies, then Mn diffusion into the bulk might be a problem.

Some susceptibility measurements indicate that subtle changes in the magnitude and qualitative characteristics of $\chi(T)$ occur over short (days or weeks) time frames after sputtering, but no change in the value of T_f is observed and these measurements are highly preliminary. Measurements of samples on time scales of a few months to more than two years after sputtering show no perceptible changes in either x-ray measurements or the value of T_f.

As a further test of the possibility of diffusion, samples were sputtered with the substrates held at different temperatures ranging from ambient to below room temperature. No significant changes in the values of T_f were observed.

X-Ray Studies

X-ray diffraction uses Bragg reflection, in which periodic structures in the sample scatter an incident x-ray beam of wavelength λ at an angle θ.

$$\sin(\theta) = \frac{l\lambda}{2a} \qquad \qquad 6\text{-}1$$

where l denotes the order of the reflection and a measures the periodicity of the sample. Measurements are taken at large angles (LAXD) and at small angles (SAXD). In a single crystal, measurement of the angle of a reflection peak allows calculation of the spacing between the crystal planes. The individual lattice parameters of the layers are periodic only within the layers, so the real periodicity is in the bilayer spacing, d

(d = W_{SG} + W_{II}). The lattice parameters for the spin glass and interlayers are a_{SG} and

a_{Cu}, with n_{SG} and n_{Cu} denoting the numbers of atoms in each bilayer, so that

$$d = n_{SG} a_{SG} + n_{Cu} a_{Cu} \qquad\qquad 6\text{-}2$$

In the limit of thick layers, several Bragg peaks corresponding to the bilayer

thickness will occur in the region where the Bragg reflections would have been seen for

the individual layer thicknesses, resulting in strong main peaks at these angles,

surrounded by satellite peaks. In the limit of thin layers, the two peaks corresponding

to the individual layer thicknesses coalesce into one main peak at an average lattice

spacing.

Satellites are a result of periodic variations in electron density and lattice

parameters. By modeling these variations according to a square wave or sine wave

profile, a theoretical prediction of the position and intensities of the x-ray peaks can be

calculated, using the layer thicknesses as the parameters.

In CuMn/Cu, no SAXD satellites are found. LAXD satellites are seen, but are

weak for concentrations of Mn < 7 at.%. The lack of the SAXD satellites is not

surprising, because the electron densities are very similar in CuMn and Cu. In addition,

30 nm of copper are needed to decouple the spin glass layers. This means that the value

of d is at least 32 nm which, according to Equation 6-1, means that 2θ = 0.25 degrees.

Experimentally, the direct x-ray beam obscures detection at this angle. The similarity

of the electron densities diminishes the intensity of the satellites, so that the first order

l=0 satellite intensity is 0.000006 of the main peak. In order to test the layering in the

CuMn/Cu system, samples were made with thinner values of both the copper and the spin glass layers. Measurements performed on these samples showed weak SAXD peaks, and we believe these measurements to be representative of the CuMn/Cu series. Calculated values of the bilayer thickness in CuMn/Cu from LAXD measurements are less than 10% different from the value indicated by the deposition rates measured by the film thickness monitors.

The crystallite dimensions can be estimated from the widths of the LAXD lines, using

$$S = \frac{K\lambda}{\beta\cos(\theta)} \qquad\qquad 6\text{-}3$$

where S is the crystallite size, K is a constant on the order of unity, λ is the x-ray wavelength, θ is the Bragg angle, and β is the width of the peak in radians. In CuMn/Cu, the LAXD reflections were from the <111> planes, indicating strong crystallite orientation. Measured crystallite sizes for CuMn(7%)/Cu[148] are 44 nm for W_{SG} = 2 nm, 43 nm for W_{SG} = 3 nm, and 37 nm for W_{SG} = 5 nm.

Microscopy

Kenning[148] performed transmission electron and field emission scanning transmission electron microscopy on a number of samples. The samples were coated in epoxy and microtomed; if they were still too thick, they were ion milled. Direct TEM imaging confirms the layered structures and polycrystalline nature of the material.

Energy Dispersive X-Ray analysis (EDX), which detects changes in chemical composition, was used by scanning across the sample in the direction of layer growth. Studies in CuMn(21%)/Cu again confirm the layered structure of the materials down to the beam resolution of about 10 nm.

Resistivity

The resistivity of the samples was measured using a Van de Pauw[149] technique. The results were compared with the predictions of three models: 1) a perfectly layered model, in which interfaces do not contribute to the resistivity, 2) a Fuchs model, in which diffuse scattering occurs at the interfaces[150], and 3) a uniform model in which the Mn is assumed to have diffused uniformly throughout the sample. The diffuse scattering model, in which an electron is scattered at the interface such that it loses knowledge of its initial direction, is expected to be closest to the experimental situation and this is confirmed by the resistivity measurements. The measured resistivities lie between the values predicted by models 1 and 2, consistent with the assumption of layered materials. Profilometer measurements of the total sample thickness were also made to check for any gross inconsistencies.

To summarize the structural characterization: We believe our CuMn/Cu samples to be polycrystalline, with 111 texture along the axis perpendicular to the layers (i.e. along the growth direction.) The layer spreading in these structures is probably not more than 0.5 nm.

SQUID Measurements

Measurement of the susceptibility as function of temperature, $\chi(T)$, is the primary way of determining the freezing temperature. A typical $\chi(T)$ was shown in Figure 1-1 for a sputtered CuMn film. The susceptibility measurements are made in a MPMS (Quantum Designs) computer controlled SQUID, with a temperature range of 2 K to 400 K, and in magnetic fields up to 55000 G. Prior to measurement, the magnet is soft quenched (brought to zero by alternating between consecutively decreasing positive and negative magnetic fields) in order to eliminate any remanent fields which may affect the zero field cooled susceptibility. The measurement protocol is as follows: after soft quenching, the sample is brought to a temperature sufficiently above T_f, and is lowered to 5 K in zero field. A measuring field of 100 G is applied, and measurements are made as the temperature is stepped back to about 100 K. The sample is then returned to 5 K in the 100 G field. Field cooled measurements have been made in both directions - with the temperature starting out low and increasing, and from higher temperatures down. No changes in the value of T_f are found, but a technical glitch in the SQUID requires us to make measurements from low temperature to high. The freezing temperature is extracted by visual inspection.

ELECTRON SPIN RESONANCE (ESR) TECHNIQUES

Figure 6-1 shows a block diagram of the Varian 4500 ESR system. The microwave source is a klystron driven bridge which operates at 9.3 GHz with a power

output of about 1 mW. The bridge is connected to a standard 3 cm microwave resonant cavity which operates in the TE 110 mode. At the sample resonance, the resonant frequency of the cavity will change, which changes the coupling of the klystron to the cavity. A sinewave modulation technique which compares the returning signal with a reference signal is used to keep the klystron locked on the cavity resonance. This procedure is called Automatic Frequency Control, or AFC.

The reflected ESR signal is detected using field modulation, in which a 10 kHz ac magnetic field is superposed on the larger applied field via Helmholtz coils mounted on either side of the resonant cavity. The resulting signal is proportional to the first derivative of the power absorbed by the sample and is sent to the Y axis of the xy recorder. A Fieldial field sweep allows us to sweep the applied magnetic field, H_1, by varying the amount of current sent to the magnet. The applied field is measured by a Hall probe gaussmeter, and the output of the gaussmeter is fed to the X axis of the xy recorder. The result is a plot of the first derivative of the power absorbed by the sample as a function of magnetic field. This data is fed from the plotter through some electronics and an A/D converter into a PC (not shown on the block diagram) for analysis.

An Oxford ESR-9000 liquid Helium flow cryostat (not shown in Figure 6-1) is used to control the temperature from 300 K to 4 K. A Au-Fe/constantan thermocouple is mounted directly underneath the sample region to detect the temperature. The temperature is regulated by controlling the power supplied to two resistive heaters in the cryostat, which allows us to maintain the temperature at a stability of $\pm$ 1 K for long periods of time.
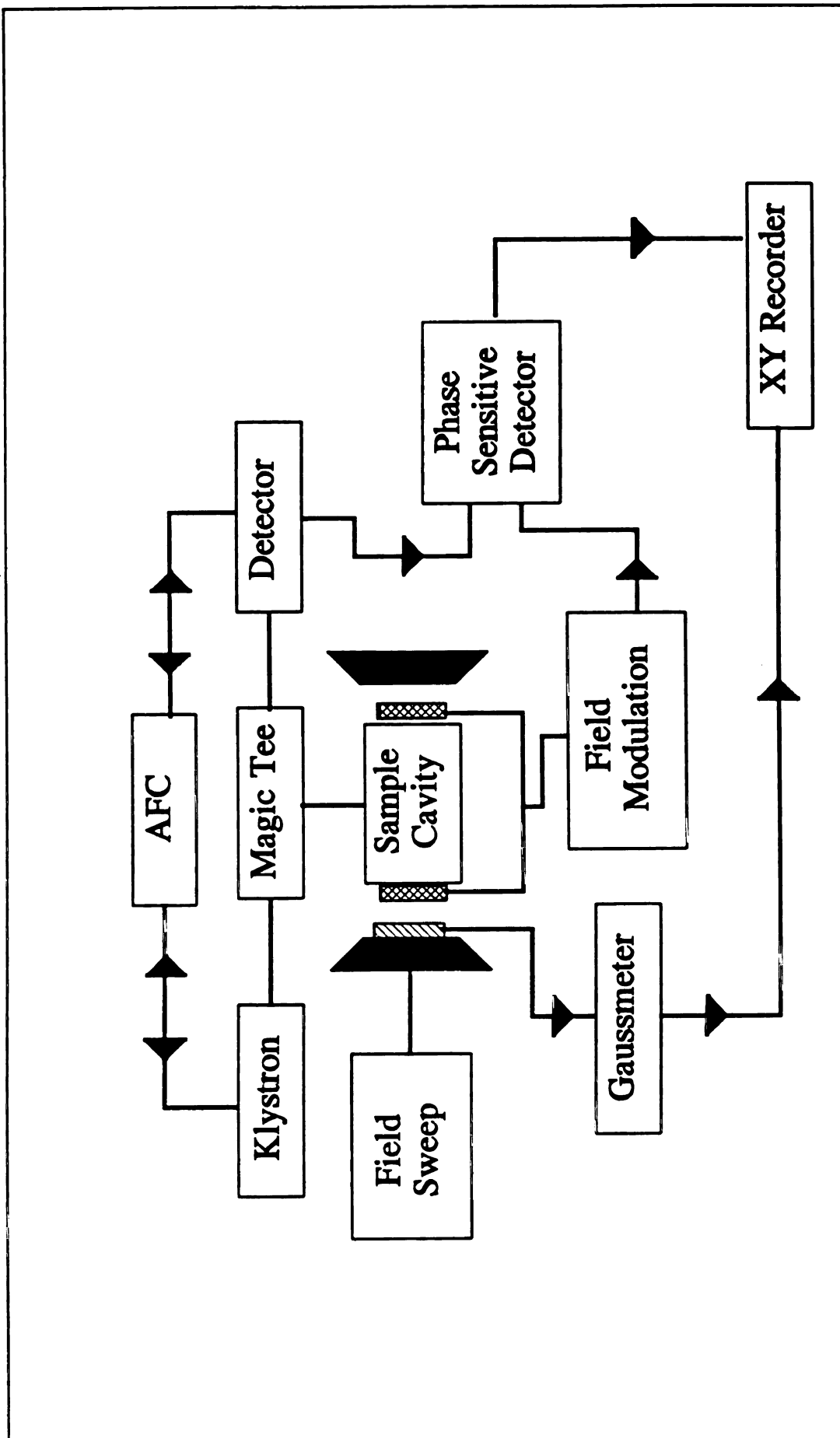
Figure 6-1: *Block diagram of the ESR system*

ESR Sample Preparation

A stainless steel razor blade washed in acetone is used to carefully peel the samples from the silicon substrates. Due to the overall thinness of the sample, this was not straightforward. Wetting the samples with acetone periodically during the separation helped in film removal. In most cases, the films could not be pulled off in one piece.

After separation, the films are mounted on flattened spectroscopic quality 4 mm quartz rods using Apiezon 'N' grease. Prior to mounting, the rods are cleaned in Hexaflouric acid, acetone and hexanes, and checked in the ESR for contamination. The total area of the mounted sample was approximately 4 mm by 1.1 cm. The sample rods are placed in the cavity so that the plane of the layers in the film is parallel to the applied magnetic field.

Skin Depth Effect

One problem associated with ESR experiments in these multilayers is a result of the attenuation of microwaves in metals. The microwaves are exponentially attenuated as the depth of penetration into the sample increases. In metals, the skin depth, δ (in units of meters), is given by

$$ I = I_0\, e^{-\frac{x}{\delta}} \quad \text{where} \quad \delta = \sqrt{\frac{2}{\omega \sigma \mu_o}} \qquad \text{6-4} $$

where ω is equal to $2\pi\nu$, (ν in Hz), σ is in inverse Ω-m, and μ is in Ω-m-s (note that 1 Ω-m-s = 1 N/A^2). At five skin depths, only 1 percent of the initial electric field remains, and only 0.01 percent of the incident power.

The original investigations into the effect of the skin depth on ESR in metals were pursued by Dyson[151], who developed a theoretical expression for the lineshape, and by Feher and Kip[152], who experimentally confirmed the predictions. Dyson realized that diffusion of conduction electrons in and out of the skin depth would alter the ESR lineshape, as only the skin depth was (effectively) 'seen' by the resonance experiment. Dyson showed that the diffusion of electrons in metals throughout the skin depth changed the shape and the intensity of the resonance line, resulting in a first derivative having a positive lobe three times bigger than the corresponding negative lobe. Dyson derived the following formula for the power absorbed by a metallic sample of thickness θ

$$P(H) = \left(\frac{c}{4\pi}\right)^2 H_1^2 \ Re\left[\frac{2}{\sigma\theta}\left(F + \frac{1}{2}\pi\nu\chi a^2 T_2 GF^2\right)\right] \qquad \textbf{6-5}$$

where

$$F = u \ \tan(u) \qquad u = \frac{\theta}{2\delta}(1+\imath) \qquad \textbf{6-6}$$

$$G = \frac{1}{(w^2 + u^2)^2}\left[2u^2\frac{\cot w}{w} + (w^2 - 3u^2)\frac{\cot u}{u} + (w^2 - u^2) \ csc^2(u)\right] \qquad \textbf{6-7}$$

$$w = \frac{1}{2} a (\xi + \iota\eta) \qquad\qquad a = \frac{\theta}{\delta} \sqrt{\frac{T_D}{T_2}} \qquad\qquad 6\text{-}8$$

$$\xi = sgn(x) [(1 + x^2)^{\frac{1}{2}} - 1]^{\frac{1}{2}} \qquad \eta = sgn(x) [(1 + x^2)^{\frac{1}{2}} + 1]^{\frac{1}{2}} \qquad 6\text{-}9$$

$$x = \frac{2\mu_B T_2}{\hbar} (H_o - H) \qquad\qquad 6\text{-}10$$

δ is the skin depth, T_D is the time it takes an electron to diffuse through a skin depth, and T_2 is the electron spin-spin relaxation time. The linewidth itself does not change, but the shape and the intensity of the line do.

For layered samples, we can define an effective skin depth by summing the attenuation in each layer. This does not take the complex effects of reflection and/or refraction at the interfaces into account, but this detail is unimportant for the purposes of this experiment. We do, however, have to consider the differences in the conductivities of the CuMn and the Cu, as pure Cu, with its higher conductivity, will more effectively attenuate the microwaves. The 30 nm thickness of copper required to decouple the spin glass layers is the limiting factor on the skin depth. The resistivity of sputtered Cu films is measured to be 2 ± 1 $\mu\Omega$-cm. The resistivity of $Cu_{1-x}Mn_x$ is about 8 $\mu\Omega$-cm for x = 0.04, and ranges to 41.43 $\mu\Omega$-cm for x=0.14, where all measurements cited were made at room temperature. The effective skin depths thus

range from 2100 nm for a multilayer with $W_{SG} = 1000$ nm to 754 nm for multilayer with $W_{SG} = 1$ nm (for x = 11%).

When the time it takes an electron to traverse the sample is less that the time it takes the electron to diffuse through the skin depth, the Dysonian lineshape reduces to a Lorentzian. Dyson cites an upper limit to this approximation when the sample is less than four times the skin depth, while Feher and Kip claim that the limit will experimentally apply when the sample is 'less than' the skin depth.

In our experience, we find that Lorentzian lines result if the sample thickness is no more than 3/4 of the skin depth. This limit on the number of spins presents some difficulty in acquiring data at high temperatures, as the signal to noise is poor in samples with small W_{SG}; however, we find this constraint preferable to the complications inherent in analyzing the Dysonian lineshape. The average sample thickness ranges from 1000 nm (for spin glass films which have no copper layer) to 500 nm.

We investigated a number of options which might reduce the constraints placed on the experiment by the skin depth problem. From Equation 6-4, we see that we can only change the conductivity of the sample or the frequency at which the measurements are made. Increasing the Mn concentration increases the resistivity of the spin glass layers, but the limiting factor is the requisite 30 nm of copper, so that no significant advantage is gained by small increases in Mn concentration. Above 16%, clustering and other factors begin to become important, so increasing the skin depth via an overall increase in resistivity is not possible.

We sputtered buffer layers of 1000-2000 nm of copper onto the silicon substrates prior to fabricating the samples in an attempt to increase the total sample thickness. The

very thick layer of copper would block out the microwaves entirely on one side of the sample, so that we would still have a Lorentzian lineshape due to the microwaves incident on the other side of the sample. Data taken on these samples appeared to depend on the thickness of the buffer layer, and concerns that we might block out spin glass behavior led us to abandon this idea.

Measurements made at the Wisconsin College of Medicine Electron Spin Resonance Center (WCOMESRC) on $Cu_{0.96}Mn_{0.04}/Cu$ samples at 1, 2, 4 and 9 GHz show that samples which are Dysonian at 9 GHz are Lorentzian when measured at lower frequencies. This confirms that the observed lineshapes are in fact due to the skin depth effect and not a spin glass property. In standard resonant cavity ESR, the cavity size increases as frequency decreases, which results in decreased sensitivity. A loop-gap resonator system, like the ones employed by WCOMESRC, requires the same amount of sample for 1 GHz as for 9 GHz measurements, with comparable sensitivity. Further measurements at WCOMESRC were not pursued due to a lack of adequate temperature control, but we have shown that the loop-gap system would be an ideal experimental apparatus for measuring the ESR of multilayered spin glasses at low frequencies.

Background Signal

Samples are sputtered directly onto silicon squares, and then separated from the substrates for measurement. The silicon wafers we buy are generally surplus wafers, the dopant and concentration of which varies according to what the vendor has available. Our study has shown that some of the dopant either diffuses into the sample, or adheres

to the back of the sample, resulting in a background to the ESR line. We believe that this signal is due to magnetoresistive effects of the silicon dopants on the cavity resonance. The magnitude of the background varies from sample to sample and, as detailed records of which substrates were used for which run were not kept, it is difficult to make any further correlations between substrate dopant and the extent of the background. The background is significant only in samples with small W_{SG}, as the signal from the spin glass in thicker layers is much larger than the background. In some cases, background was seen on one ESR sample, but not on another ESR sample taken from the same silicon square, indicating that this may be a result of how the sample is removed from the substrate. The use of acetone in the removal was shown to have no effect on the presence or lack of a background signal.

Figure 6-2 shows the background, as observed at $T = 300$ K in a $Cu_{0.89}Mn_{0.11}/Cu$ 3/30/20 sample. At this temperature, the spin glass signal is much weaker than the background, so the signal seen here is primarily due to the background. The spin glass signal can be seen as a very small feature centered at about 3300 G. Below 2000 G, the background has a negative curvature and is nonlinear; over the rest of the field range, the background is linear with a positive slope, allowing us to subtract it during the fitting process.

Measurement Protocol

The data presented for a given sample was all taken during the course of a single data run to avoid small changes due to sample position and orientation in the cavity,
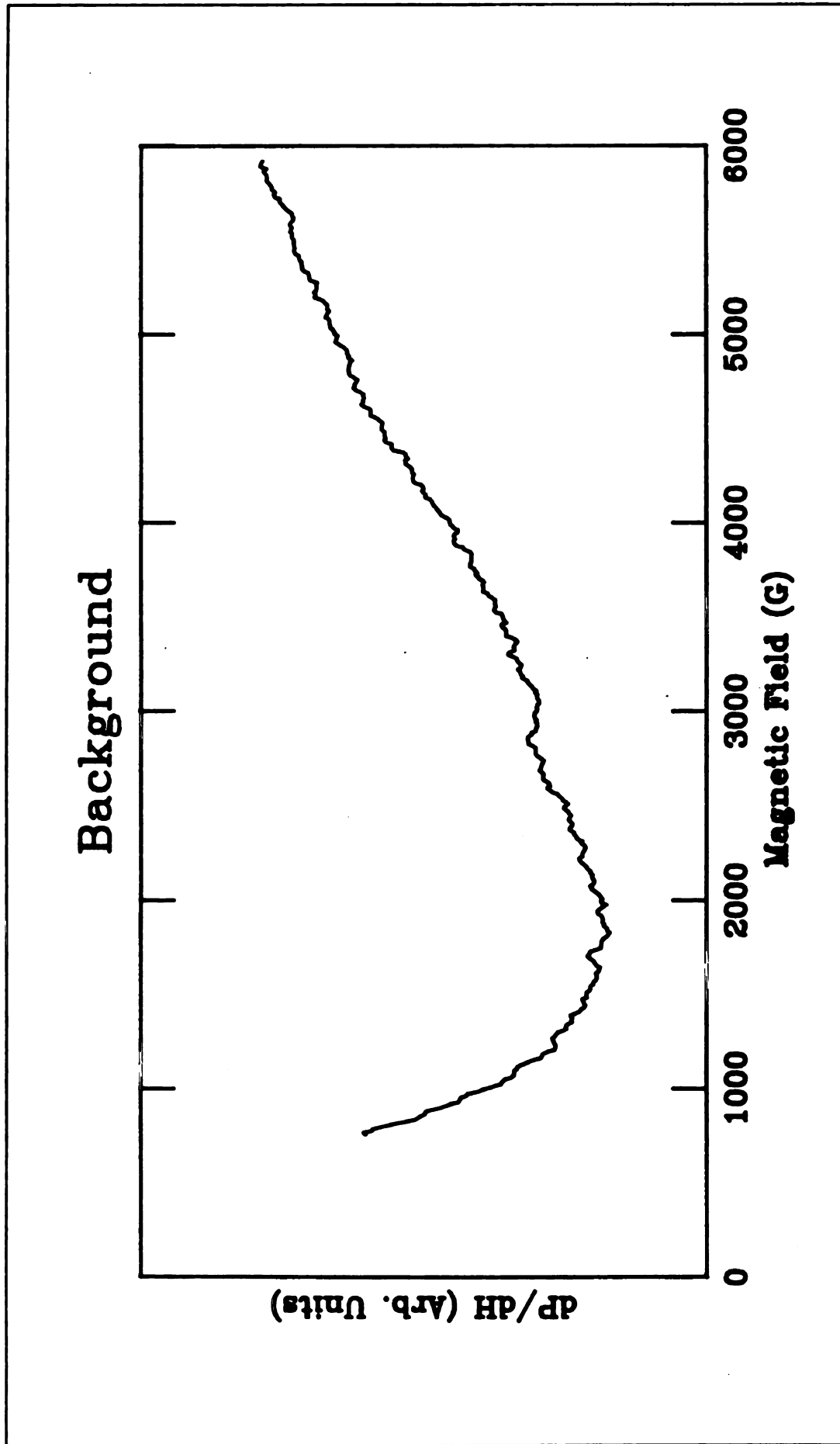
Figure 6-2: *Background due to dopants from the silicon wafers*

thermal cycling effects, and more significantly, hysteretic effects. Data is taken starting at room temperature, with the field turned completely to zero while the sample is being cooled to the next temperature. A residual field of about 20-30 G exists during the cooling; however, the measurement fields are much larger than this field, and we expect the residual field to have no effect on the data. The temperature increments are dependent on the behavior of the line; at high temperature, data is taken every 10 K. As the rounding of the $\Delta H(T)$ line begins, data is taken every 5 K. In the regime of the divergent behavior, $\Delta H(T)$ has such a large slope that small temperature changes result in very large changes in the linewidth, so that data must be taken every 2.5 K. Data points are taken until the line becomes too broad to measure, or too weak to observe.

In cooling from T_1 to the next temperature to be measured, T_2, the temperature is not allowed to fall below T_2 to avoid hysteretic effects. Hysteretic behavior has been routinely observed in these samples, but has not been investigated in any systematic manner. As an example, consider a measurement at temperature T_1 ($T_1 > T_f$) which results in a linewidth ΔH_1. The sample is cooled to temperature T_2, where T_2 is also above T_f. After waiting some time at T_2, the sample is returned to T_1 and the linewidth is remeasured. The resulting value will be smaller than ΔH_1. As time goes on, with the system sitting at T_1, repeated measurements of the linewidth will result in increasing values of ΔH, until the original value is returned.

SUMMARY

This Chapter has detailed the fabrication and characterization of the multilayers used in the Electron Spin Resonance experiments. Based on the sum of the investigations performed on these samples, we claim that the CuMn/Cu multilayers are polycrystalline in nature, with the value of W_{SG} modified by less than 0.5 nm due to diffusion of Mn into the copper layers.

The ESR system has been described, and two problems - the skin depth effect and the background - have been discussed. The skin depth problem limits the total thickness of our samples to less than about 3/4 of the skin depth, so that the average sample thickness is 600-1000 nm. A background, which is due to the magnetoresistive behavior of impurities which are transferred from the substrate to the ESR sample, is linear in the field range of 2000 G to 6000 G, enabling us to fit it with little difficulty. The measurement protocol has been summarized, and the routine observation of hysteretic behavior noted.

CHAPTER SEVEN

DATA AND ANALYSIS

"It appears that the quantitative analysis of such ESR measurements (above T_f) is a complicated problem"[1]

SUMMARY OF SAMPLES ANALYZED

Data was taken on three complete sputtering runs, with some additional measurements made on other samples. The concentration regime over which data can be taken across a wide range of temperatures and layer thicknesses is small, due to the skin effect and background problems discussed in the last chapter. For lower concentrations, the ESR line is undetectable at high temperatures, even in the thickest samples. In samples with concentrations greater than 16%, the lines becomes extremely broad, making reliable extraction of a linewidth and position difficult.

Tables 7-1 through 7-4 detail the configurations of the samples studied. All of the samples studied were either single layer films, or had Cu interlayers of 30 nm, so the samples will be referred to solely by the spin glass layer thickness, making note of any exceptions. Tables 7-1 through 7-4 may be consulted for additional information.

Table 7-1: Configurations of Run 243 - $Cu_{0.89}Mn_{0.11}$

Run 243 - $Cu_{0.89}Mn_{0.11}$				
Sample	W_{SG}(nm)	W_{Cu}(nm)	N	T_f (K)
243-12	500	30	3	47.5
243-11	100	30	5	47.5
243-8	50	30	6	45.0
243-7	30	30	17	42.5
243-6	10	30	17	35.0
243-4	7	30	18	31.0
243-2	3	30	18	20.5
243-1	1	30	18	10.0

Table 7-2: Configurations of Run 185 - $Cu_{0.93}Mn_{0.07}$

Run 185 - $Cu_{0.93}Mn_{0.07}$				
Sample	W_{SG}(nm)	W_{Cu} (nm)	N	T_f (K)
185-1	1000	-	1	38.0
185-5	100	30	5	38.0
185-2	50	30	6	36.0
185-4	30	30	15	35.0
185-3	7	30	16	25.0
185-10	5	30	16	23.5
185-6	3	30	17	17.5

Table 7-3: Configurations of Run 245 - $Cu_{0.93}Mn_{0.07}$

Run 245 - $Cu_{0.93}Mn_{0.07}$				
Sample	W_{SG} (nm)	W_{Cu} (nm)	N	T_f (K)
245-1	30	30	15	33.0
245-3	10	30	17	27.0
245-4	9	30	17	26.0
245-6	7	30	18	23.5
245-7	6	30	18	22.0
245-8	5	30	18	21.0
245-12	3	30	18	16.5

Table 7-4: Configurations of Additional Samples Run

Other Samples Analyzed					
Sample	x	W_{SG} (nm)	W_{Cu} (nm)	N	T_f (K)
265-2	16	500	30	3	67.5
220-15	7	500	-	1	39.0
220-16	7	500	1	1	39.0
85-4	4	500	-	1	24.0

ANALYSIS OF THE FREEZING TEMPERATURE

Figures 7-1 through 7-3 show the freezing temperatures as a function of the log of the spin glass layer thickness for runs 243, 185 and 245 respectively. This behavior can be fit to the finite size scaling form

$$\epsilon = \frac{T_f(\infty) - T_f(W_{SG})}{T_f(\infty)} \sim W_{SG}^{-\lambda} \qquad \text{7-1}$$

where $T_f(\infty)$ is the bulk freezing temperature. The value of λ is obtained by the slope of a linear regression of $\log(\epsilon)$ vs $\log(W_{SG})$. The fits are limited to samples with $W_{SG} \geq 30$ nm, although data down to 9 nm had to be included in order to use the linear regression program in fitting the 245 run. The correlation length exponent, ν, is $1/\lambda$. The fit values are summarized in Table 7-5.

Table 7-5: Parameters from Finite Size Scaling Fits of T_f

Sputter Run Number	Smallest W_{SG}	λ	ν
243	10 nm	0.98 ± 0.10	1.02 ± 0.10
185	7 nm	0.79 ± 0.08	1.27 ± 0.12
245	9 nm	0.78 ± 0.06	1.28 ± 0.10
All 7%	10 nm	0.80 ± 0.08	1.25 ± 0.13
All samples	10 nm	0.78 ± 0.08	1.28 ± 0.13
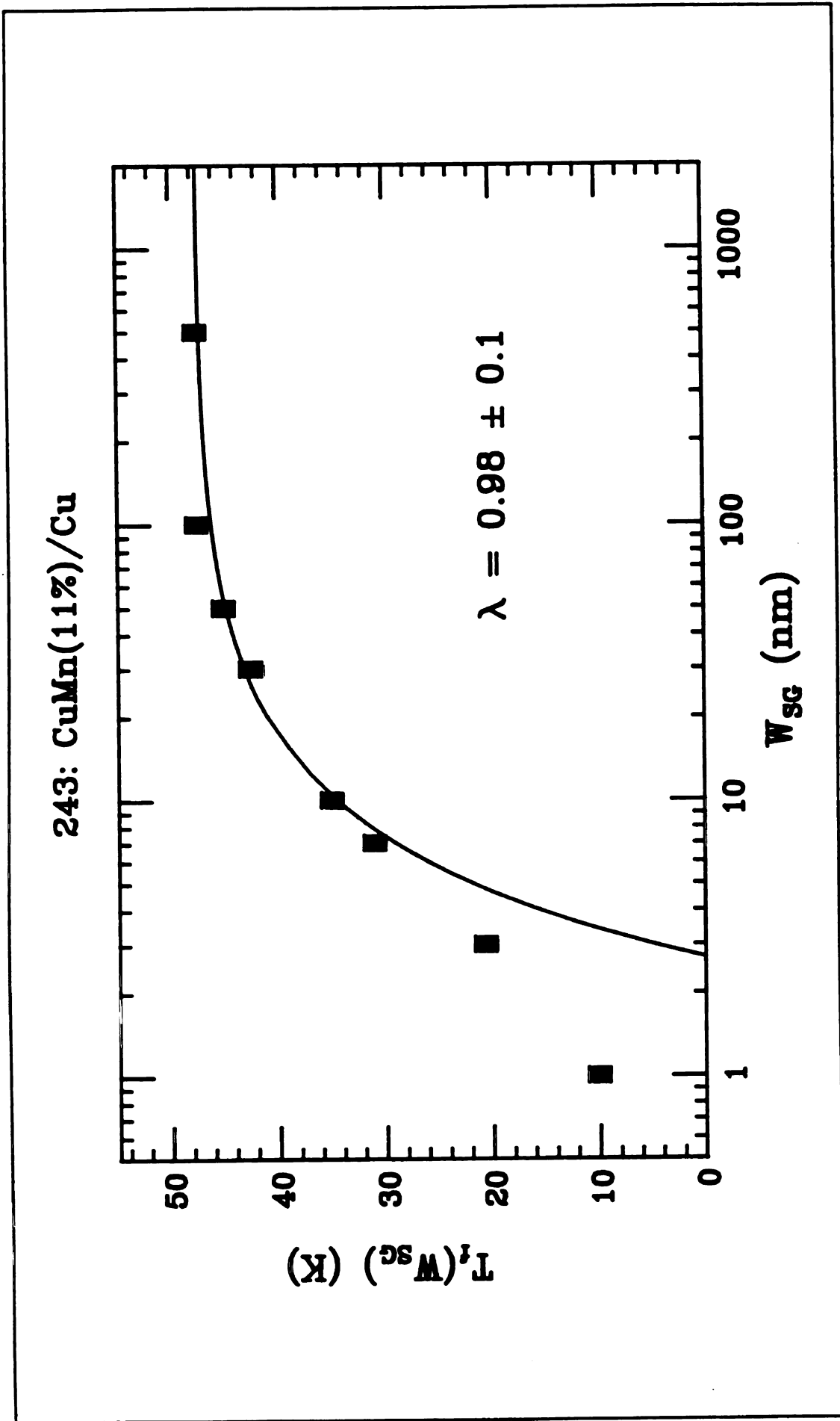
Figure 7-1: *Depression of $T_f(W_{SG})$ as a function of W_{SG} for Run 243 - $Cu_{0.89}Mn_{0.11}$*
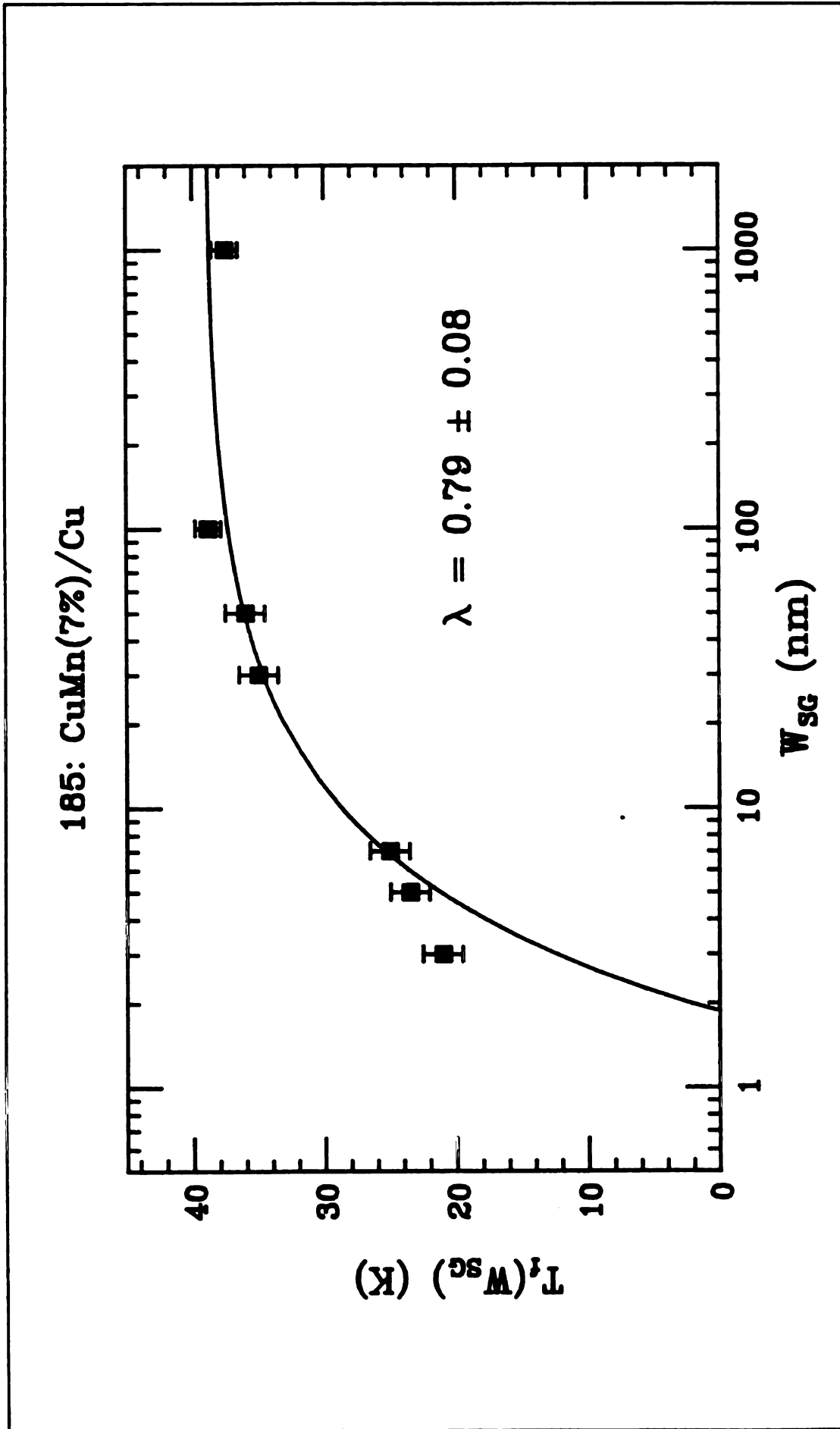
Figure 7-2: *Depression of $T_f(W_{SG})$ as a function of W_{SG} for Run 185 - $Cu_{0.93}Mn_{0.07}$*
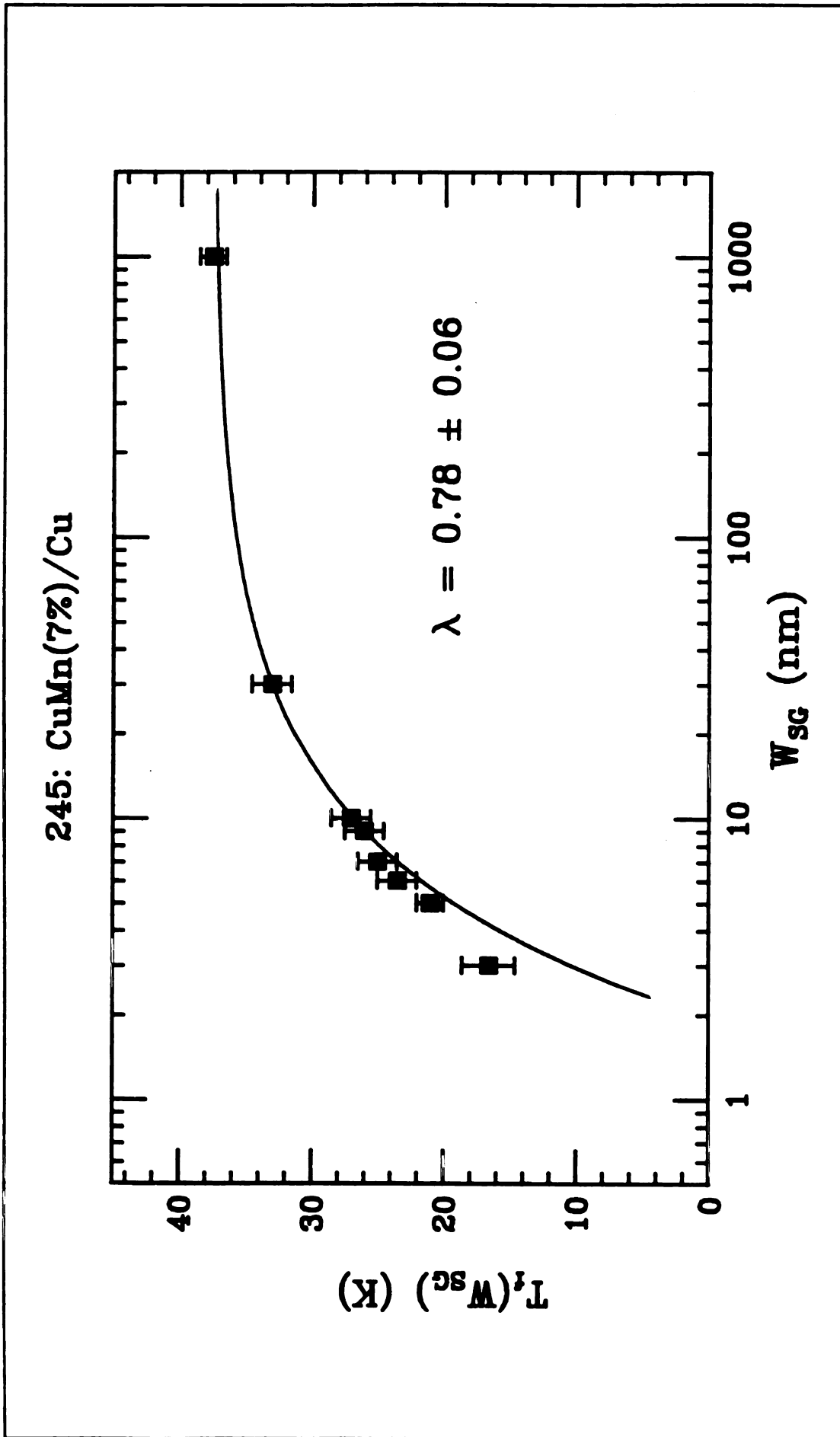
Figure 7-3: *Depression of $T_f(W_{SG})$ as a function of W_{SG} for Run 245 - $Cu_{0.93}Mn_{0.07}$*
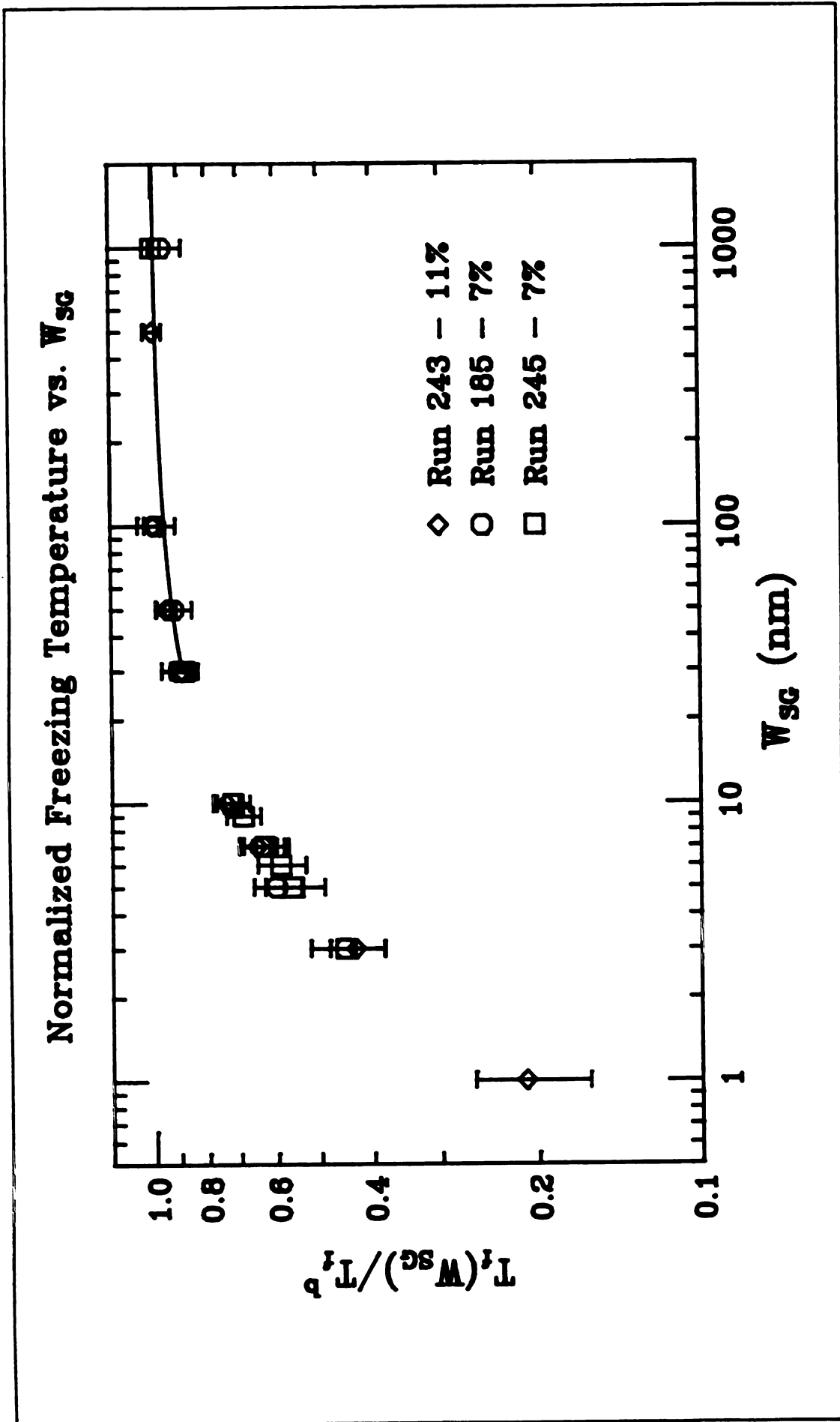
Figure 7-4: $T_f(W_{SG})/T_f(\infty)$ as a function of W_{SG} for all concentrations

Figure 7-4 shows a normalized plot of $\log(T_f(W_{SG})/T_f(\infty))$ vs $\log(W_{SG})$ for all samples. The solid line indicates the prediction of Equation 7-1 for the value of $\nu = 1.25 \pm 0.13$ found by fitting all concentrations. This value, along with the general trends represented by this analysis, are in agreement with those determined by all of the past work on CuMn/Cu multilayers, indicating that these samples are of the same quality as those described in Chapter Six.

LINEWIDTH ANALYSIS

As explained in Chapter 2 and Appendix A, the resonance line detected by the ESR spectrometer in metals is proportional to a mixture of the real and imaginary parts of the susceptibility. The Lorentzian dispersion and absorption signals are given by

$$\chi' = \frac{x}{1 + x^2} \qquad \chi'' = \frac{1}{1 + x^2} \qquad \text{7-2}$$

where

$$x = \frac{H - H_o}{\frac{\sqrt{3}}{2}\Delta H} \qquad \text{7-3}$$

The first derivative resonance lines captured by the computer are fit to $\alpha_1 \chi' + \alpha_2 \chi''$, with the ratio of α_2/α_1 held constant for each run. For the 185 data run, $\alpha_2/\alpha_1 = 9.0$, while for all other runs, $\alpha_2/\alpha_1 = 7.0$. The linewidth is relatively

insensitive to small changes in the value of α_2/α_1, while the resonance peak position may change by as much as 20-30 G when α_2/α_1 is changed by 1.

Figure 7-5 compares the lineshapes at 100 K for the smallest (1 nm) and the largest (500 nm) W_{SG} from the 243 ($Cu_{0.89}Mn_{0.11}$) run, along with the calculated fits. The individual dots are the discrete values accumulated via the A/D converter, and the thin line is the fit. The linewidth of the 500 nm sample is 373 $\pm$ 10 G, and the resonance position, H_0, is 3294 $\pm$ 10 G. The corresponding parameters for the 1 nm sample are ΔH = 360 $\pm$ 14 G, and H_0 = 3315 $\pm$ 12 G. In fitting the 1 nm sample, only the portion of the data taken in fields greater than 2000 G was used in order to avoid effects from the nonlinear part of the background. These lineshapes are representative of all data taken.

Figure 7-6 illustrates the contributions from the real and imaginary parts of the susceptibility and the background for a 500 nm $Cu_{0.89}Mn_{0.11}$ multilayer. The solid line is the total curve, the dotted line is the contribution from the $\alpha_2\chi''$ term, the dashed line is the contribution from the $\alpha_1\chi'$ term, and the dot-dashed line is the linear background contribution. Observed lineshapes are Lorentzian for all layer thicknesses. Small changes in the character of the lineshape near T_f are seen; the shape tends to distort from pure Lorentzian, and the peak height decreases.

157
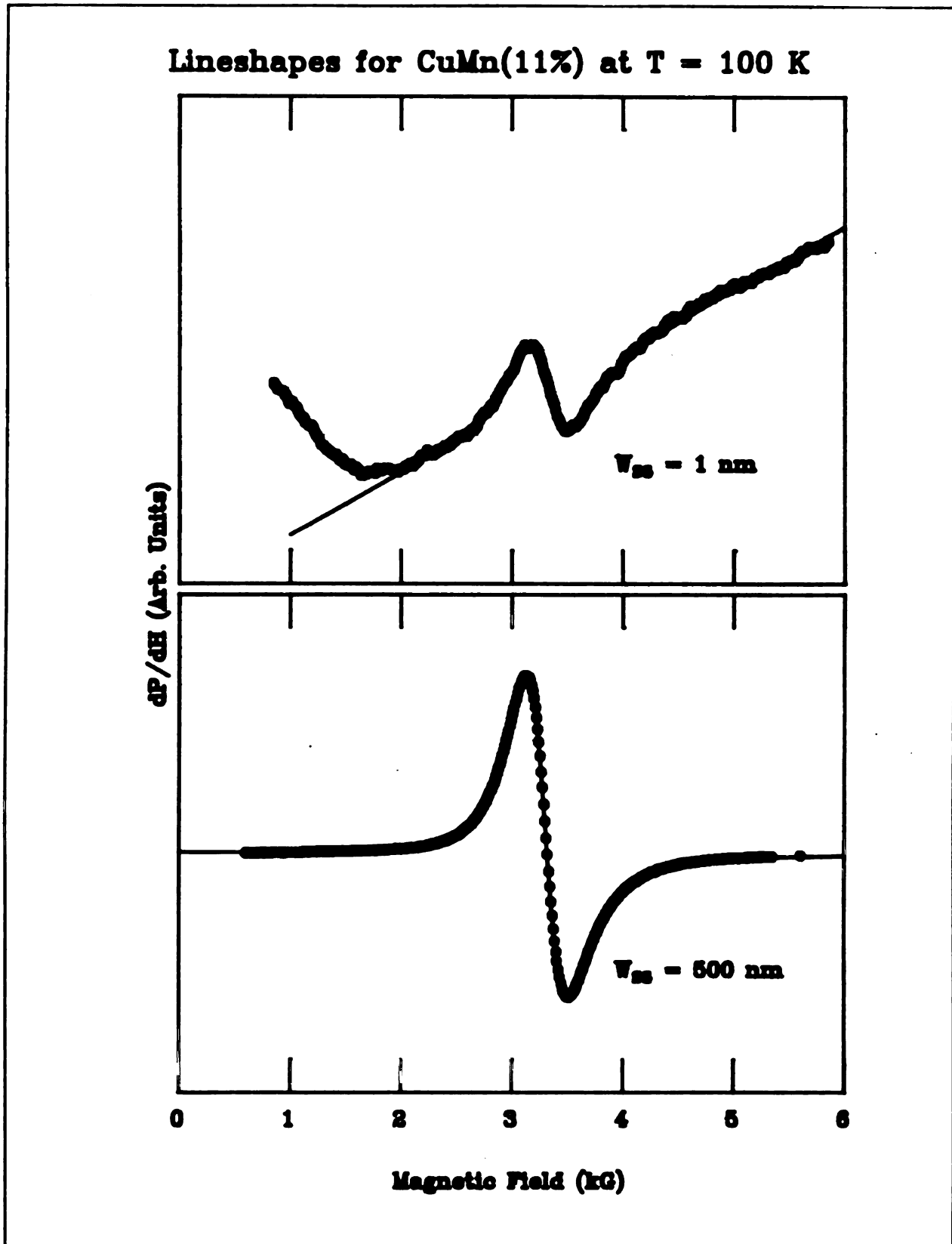
Figure 7-5: *Representative lineshapes for a) a 1 nm $Cu_{0.89}Mn_{0.11}$ and b) a 500 nm $CuMn_{0.89}Mn_{0.11}$ sample*
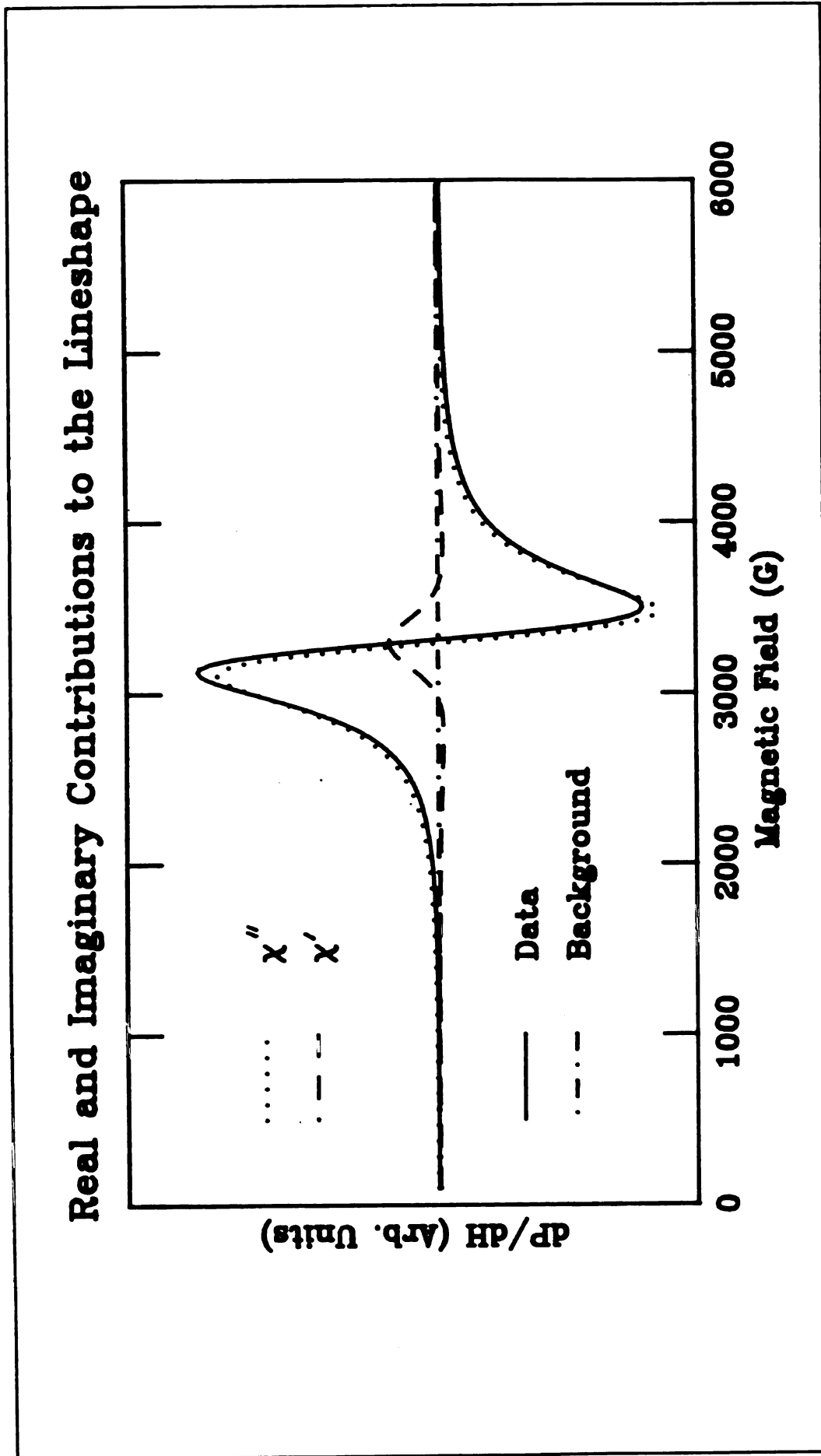
Figure 7-6: *Contributions from the real and imaginary parts of the susceptibility and the background in fitting a Cu$_{0.89}$Mn$_{0.11}$ 500 nm sample*

Fitting Protocol

The standard expression used in the analysis of the ESR linewidth is

$$\Delta H(T) = A + BT + C \left(\frac{T - T_f(W_{SG})}{T_f(W_{SG})} \right)^{-\kappa} \qquad \text{7-4}$$

Fitting to equation 7-4 can be somewhat complicated, depending on the temperature range of the data to be fit. A standard nonlinear least squares computer fit was used. We found that systematic errors and spurious divergences were avoided if the value of κ was fixed and the other three parameters allowed to vary. κ was then incremented, and the fit repeated, with the value of κ resulting in a minimum reduced chi-squared selected as the best fit. All values for T_f are subject to an accuracy of ± 1 K. The fits are noticeably worsened if the value of T_f is changed by more than a few percent.

Departure from the Power Law Behavior Near T_f

Departure from the power law behavior near T_f has been observed in bulk metallic spin glasses, with the departure occurring at higher reduced temperatures for higher frequencies. This reduces the range of temperatures over which Equation 7-4 can be fit. To determine where this departure begins, the fit was repeated, removing the lowest temperature data point each iteration. At some temperature, continued removal

of points ceased to change the parameters or improve the reduced chi-squared value. The temperature at which this insensitivity to continued removal of points occurs (denoted T^*) is the minimum temperature used for the fit. The reduced temperature corresponding to T^* is denoted t^* ($t^* = (T^*-T_f)/T_f$).

Concentration Dependence

Figure 7-7 shows the concentration dependence of $\Delta H(T)$ for four bulk ($W_{SG} = 500$ or 1000 nm) $Cu_{1-x}Mn_x$ samples ($x = 0.04, 0.07, 0.11$ and 0.16) and illustrates the point made in the introduction regarding the concentration range over which data can be taken for this experiment. For the 4% sample, data could not be acquired above 200 K in a 500 nm film due to thermal effects. The data acquired on the bulk samples is the strongest data as a result of the constraints on the total sample thickness due to the skin depth effect, so this data indicates (as has been experimentally confirmed) that our chances of acquiring meaningful data in samples with smaller W_{SG} are not good. The data for the 16% sample shows extremely broad lines, with $\Delta H(T)$ having a minimum value of about 900 G. Fitting lines this broad is difficult, as contributions from negative fields must be included in the fit to accurately represent the lineshape. Also, the line becomes too broad to fit in the spectrometer range at temperatures above 2 T_f, which limits fitting in the critical area near T_f. Table 7-6 shows the values obtained by fitting $\Delta H(T)$ for bulk samples (500 nm or 1000 nm) at four different concentrations.

Table 7-6: Concentration Dependence of $\Delta H(T)$ *in Bulk Spin Glasses*

c (%)	T_f (K)	A (G)	B (G/K)	C (G)	κ
4	24.0	34 $\pm$ 15	2.65 $\pm$ 0.15	107 $\pm$ 14	1.5
7	37.5	-132 $\pm$ 32	2.94 $\pm$ 0.04	248 $\pm$ 33	1.5
11	47.5	-245 $\pm$ 13	3.36 $\pm$ 0.01	328 $\pm$ 13	1.5
16	67.5	-184 $\pm$ 37	4.47 $\pm$ 0.20	672 $\pm$ 25	1.5

All concentrations can be fit by Equation 7-4 with an exponent of $\kappa = 1.5 \pm 0.1$. We see that, with the exception of the 16% sample, the residual linewidth, A, monotonically decreases with increasing concentration, while the thermal broadening coefficient, B, monotonically increases with increasing concentration. The divergence strength, C, also monotonically increases. The results for all parameters are in general agreement with the findings of Mozurkewich, *et. al.*[105] in AgMn. (See Table 5-1 for Mozurkewich's results). The residual width and the thermal broadening - with the exception of data from the 16% sample - depend linearly on Mn concentration. The failure of the 16% sample to follow this trend may be due to chemical clustering, or inaccurate extraction of the linewidth in this run due to the very broad resonance lines. The residual width decreases at a slope of 40 G/at.%, reaching a value of 0 at about 5 at.%. This can be compared to Mozurkewich, *et. al.*'s slope of 13 G/at.% and

162
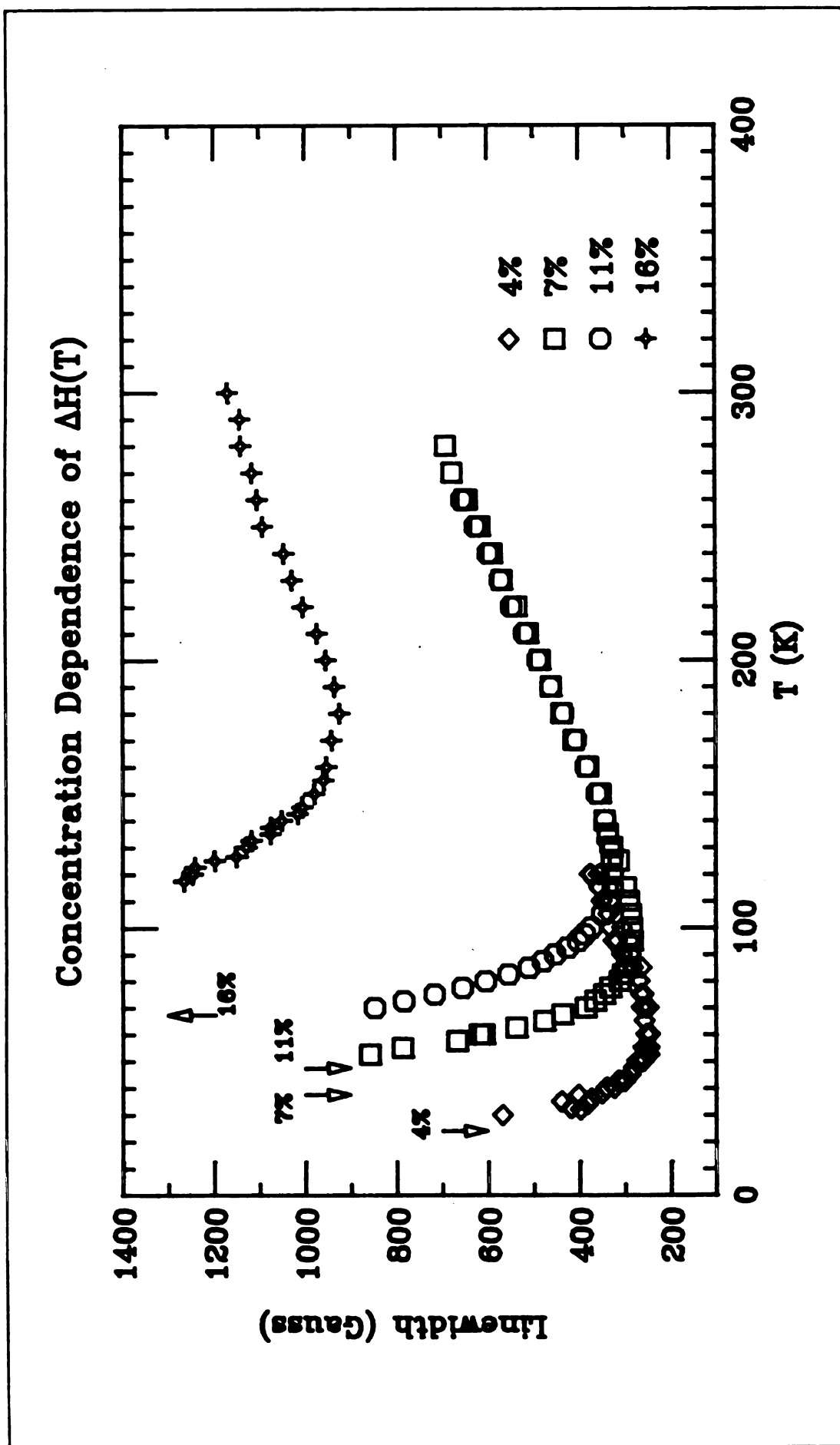
Figure 7-7: *Dependence of ΔH(T) on concentration for bulk samples*

zero intercept at 2 at.%. The thermal broadening coefficient in our CuMn samples increases at a rate of .1 G/K-at%, compared to 0.04 G/K at.%. in AgMn. The divergence strength, C, is predicted[106] to depend linearly on Mn concentration, but a sublinear dependence has been observed by Mozurkewich,*et. al.* If the 16% data is ignored, we also see a sublinear dependence in C. This may be attributable to the same effects as are responsible for a sublinear dependence of T_f on concentration, such as the importance of preasymptotic RKKY corrections. Figures 7-8 through 7-10 plot the magnitudes of the parameters as a function of concentration. The straight lines in Figures 7-8 and 7-9 represent fits to the linear behavior.

The position and value of the minimum linewidth also change monotonically with concentration, as shown in Table 7-7 and Figure 7-10. The temperature at which the linewidth has its minimum value is defined to be T_{min}, and the minimum linewidth is ΔH_{min}. T_{min} can be fit to a power law in c; we find that $T_{min} \sim c^{(.74)}$.

Table 7-7: Concentration Dependence of the Positions and Values of the Minimum Linewidth for $Cu_{0.89}Mn_{0.11}$

c (at.%)	T_{min} (K)	ΔH_{min} (G)
4	60.0	245
7	97.5	282
11	115.0	325
16	180.0	923
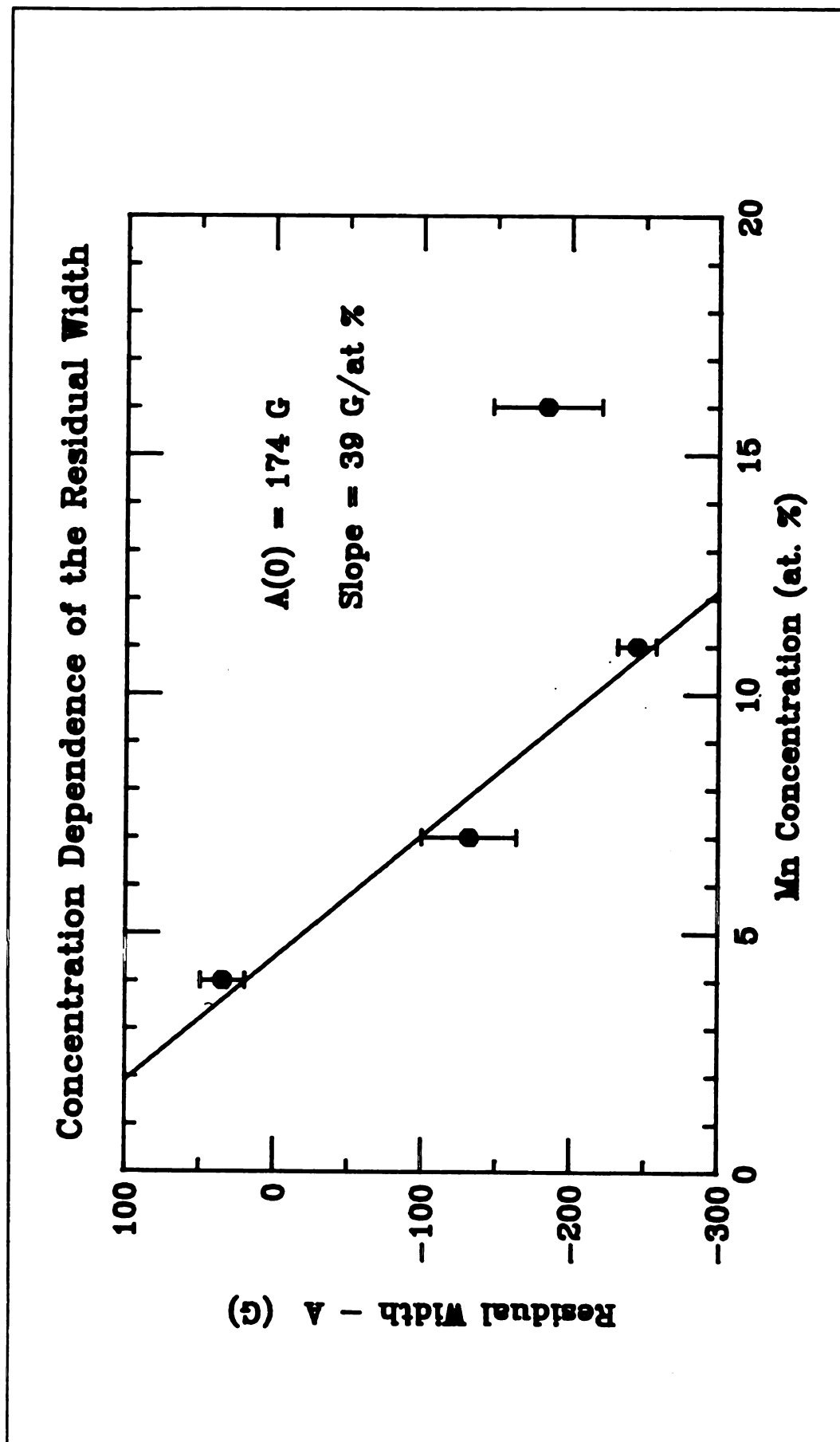
Figure 7-8: *Dependence of the Residual Width, A, on Mn Concentration*

Concentration Dependence of the Thermal Broadening

B(0) = 2.24 G/K
Slope = .10 G/K-at %

Mn Concentration (at. %)

Thermal Broadening — B (G/K)
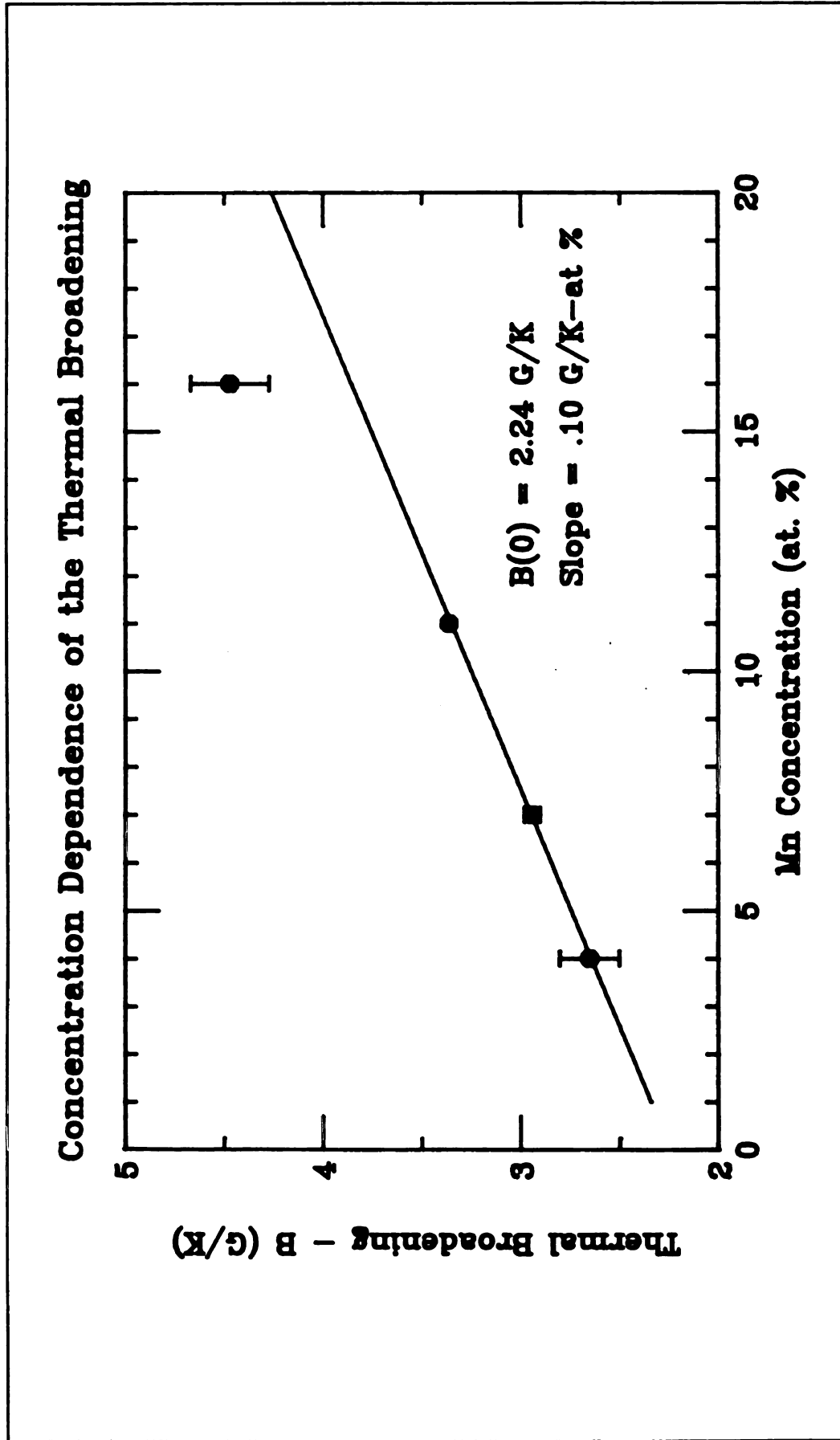
Figure 7-9: *Dependence of the Thermal Broadening, B, on Mn Concentration*
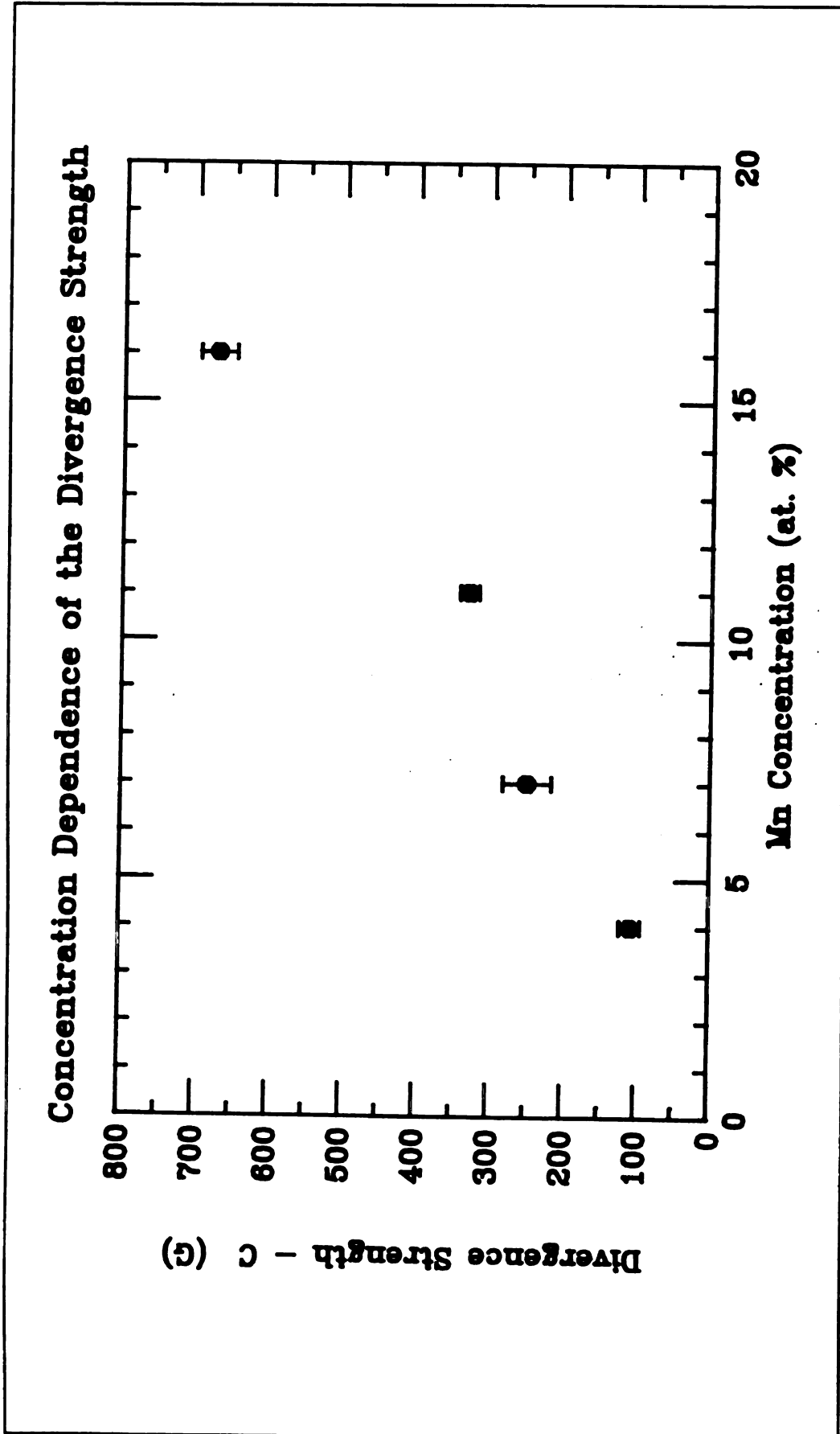
Figure 7-10: *Dependence of the Divergence Strength, C, on Mn Concentration*
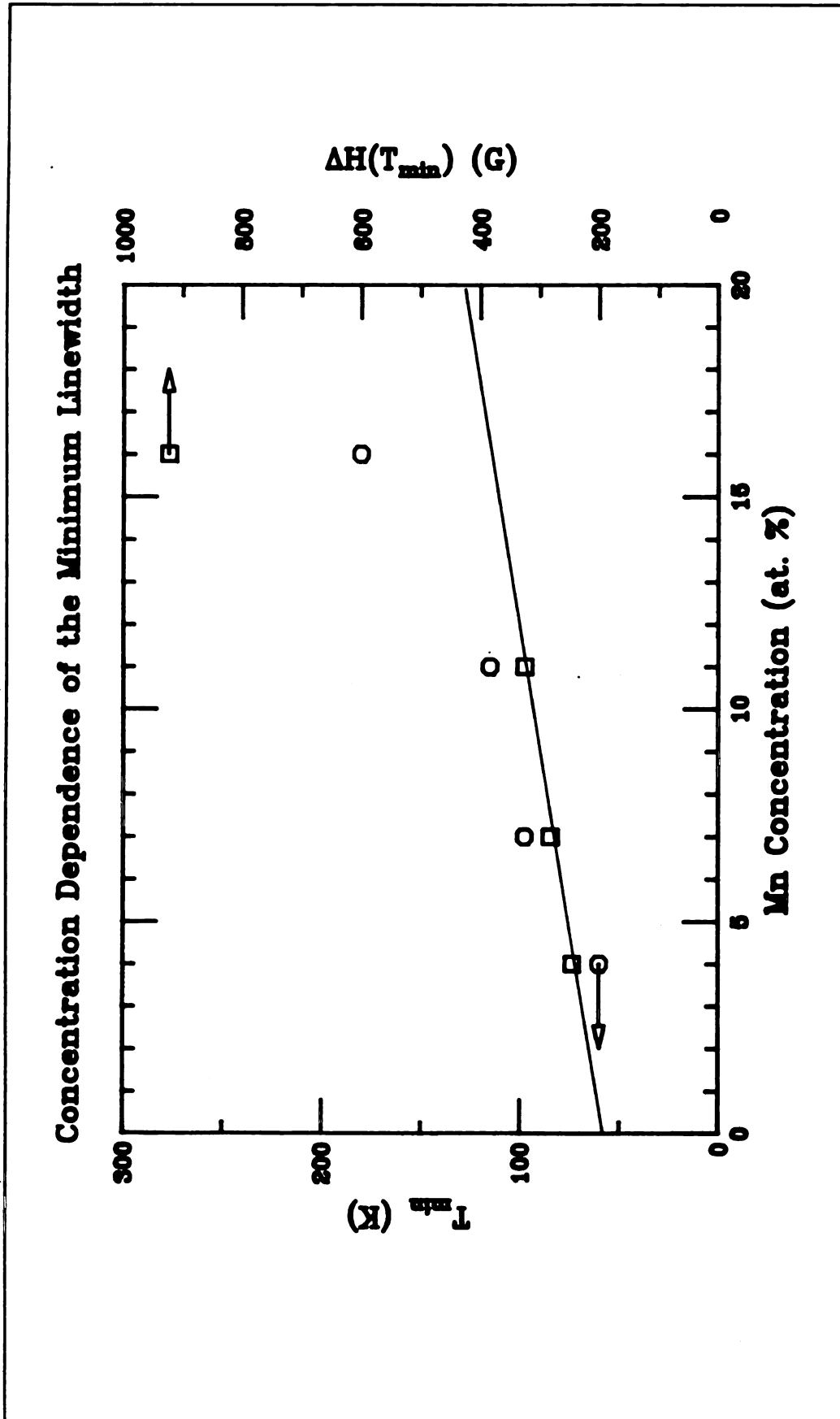
Figure 7-11: *Concentration Dependence of the Position and Value of the Minimum Linewidth in Bulk Samples*

The temperature at which $\Delta H(T)$ departs from power law behavior is tabulated in Table 7-8. We see that lower concentrations obey a power law to lower reduced temperatures than do higher concentrations.

Table 7-8: Dependence of t^* on concentration

c (at. %)	t^*
4	.46
7	.63
11	.64
16	.96

LAYER THICKNESS DEPENDENCE

Figures 7-12 through 7-19 show $\Delta H(T)$ and $H_0(T)$ for the 243 run, Figures 7-20 through 7-26 correspond to the same data for the 185 sample, and Figures 7-27 through 7-33 illustrate the behavior of the 245 sample. In all figures, the lower graph shows $\Delta H(T)$ and the upper plot shows $H_0(T)$. The error bars are less that the size of the
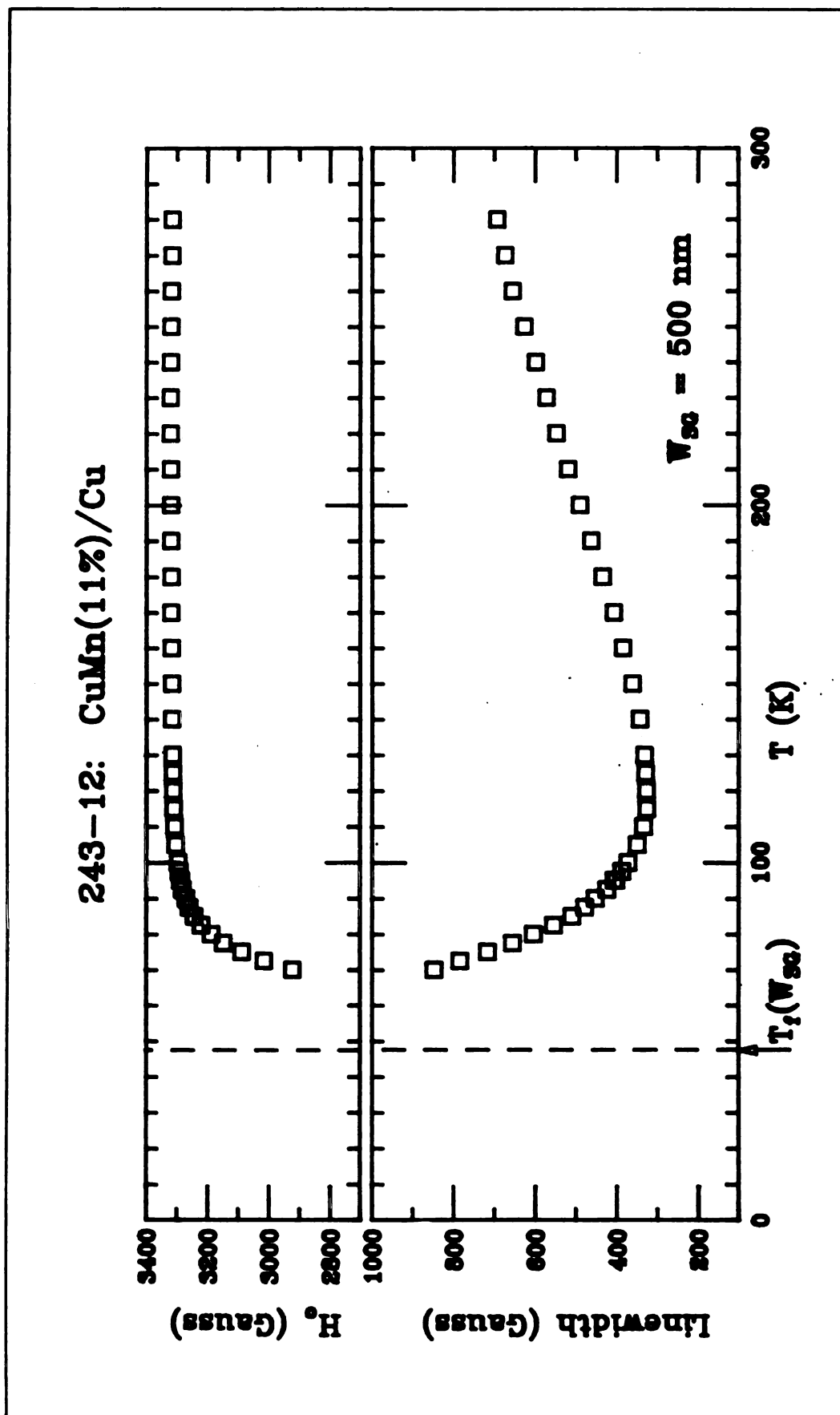
Figure 7-12: $\Delta H(T)$ and $H_0(T)$ for Sample 243-12 - $Cu_{0.89}Mn_{0.11}$ - 1000 nm
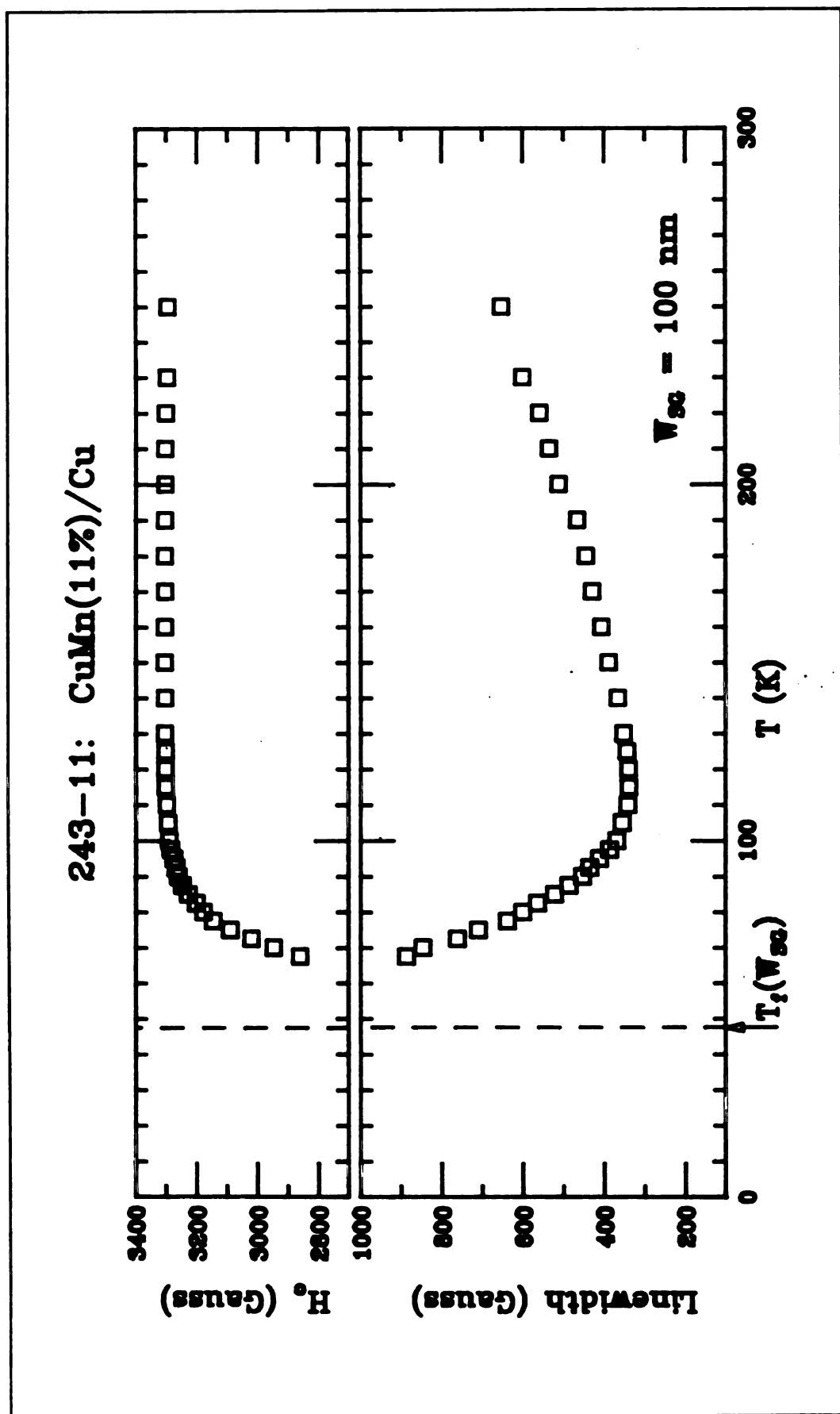
Figure 7-13: $\Delta H(T)$ and $H_0(T)$ for Sample 243-11 - $Cu_{0.89}Mn_{0.11}$ - 500 nm

243–8: CuMn(11%)/Cu

$W_{sc} = 50$ nm

H_o (Gauss)

Linewidth (Gauss)

$T_f(W_{sc})$

T (K)
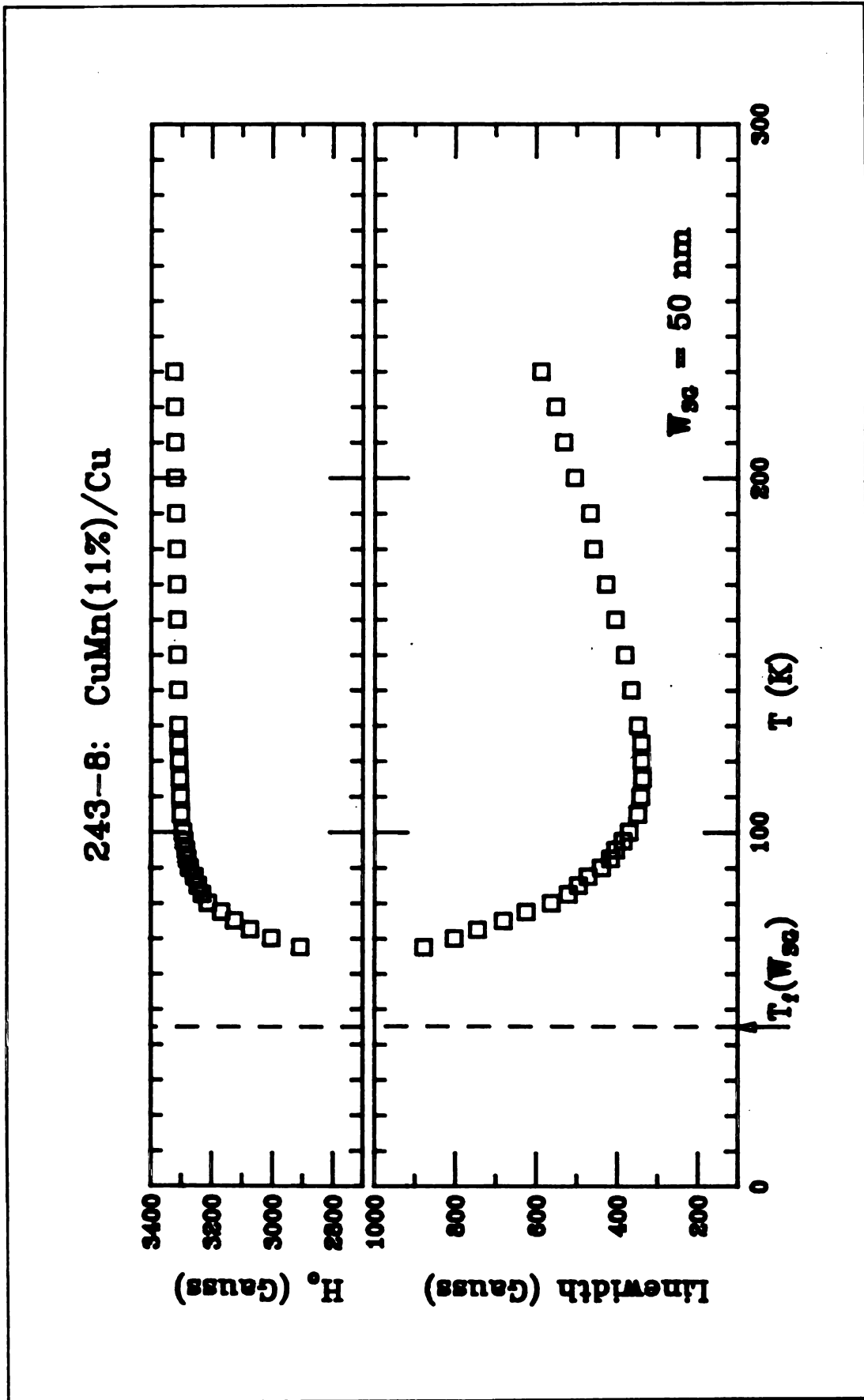
Figure 7-14: $\Delta H(T)$ and $H_o(T)$ for Sample 243-8 - $Cu_{0.89}Mn_{0.11}$ - 50 nm
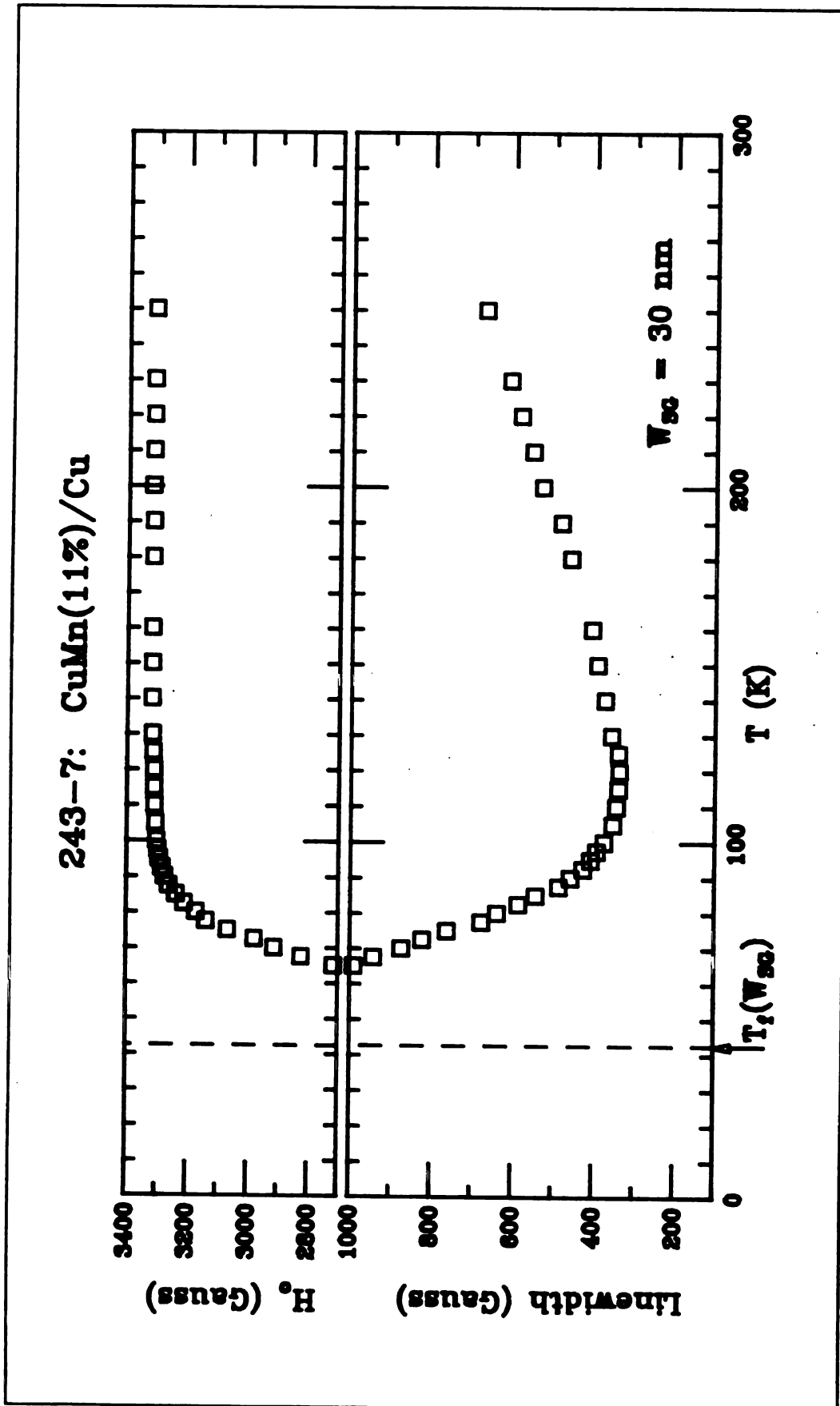
Figure 7-15: $\Delta H(T)$ and $H_0(T)$ for Sample 243-7 - $Cu_{0.89}Mn_{0.11}$ - 30 nm
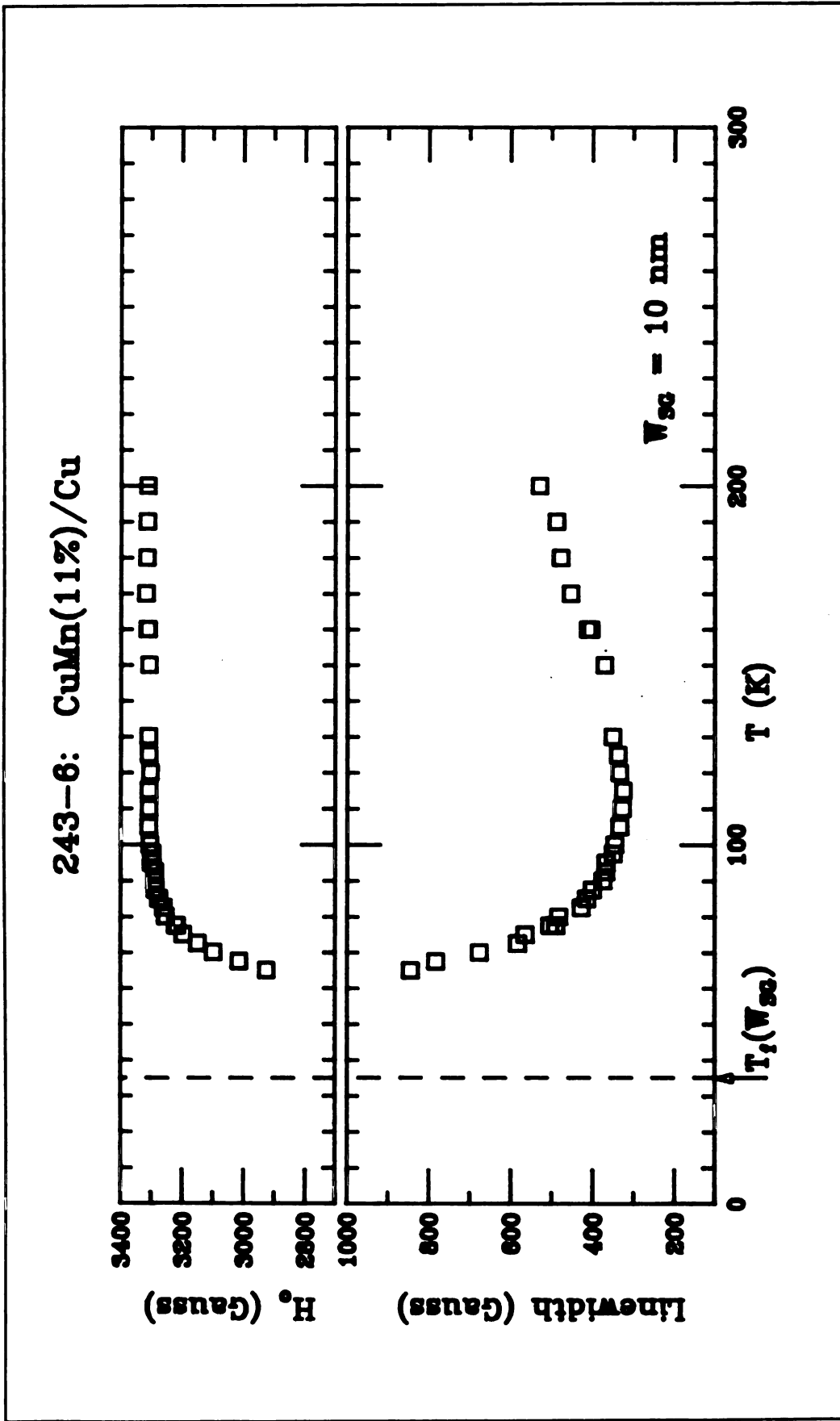
Figure 7-16: $\Delta H(T)$ and $H_0(T)$ for Sample 243-6 - $Cu_{0.89}Mn_{0.11}$ - 10 nm
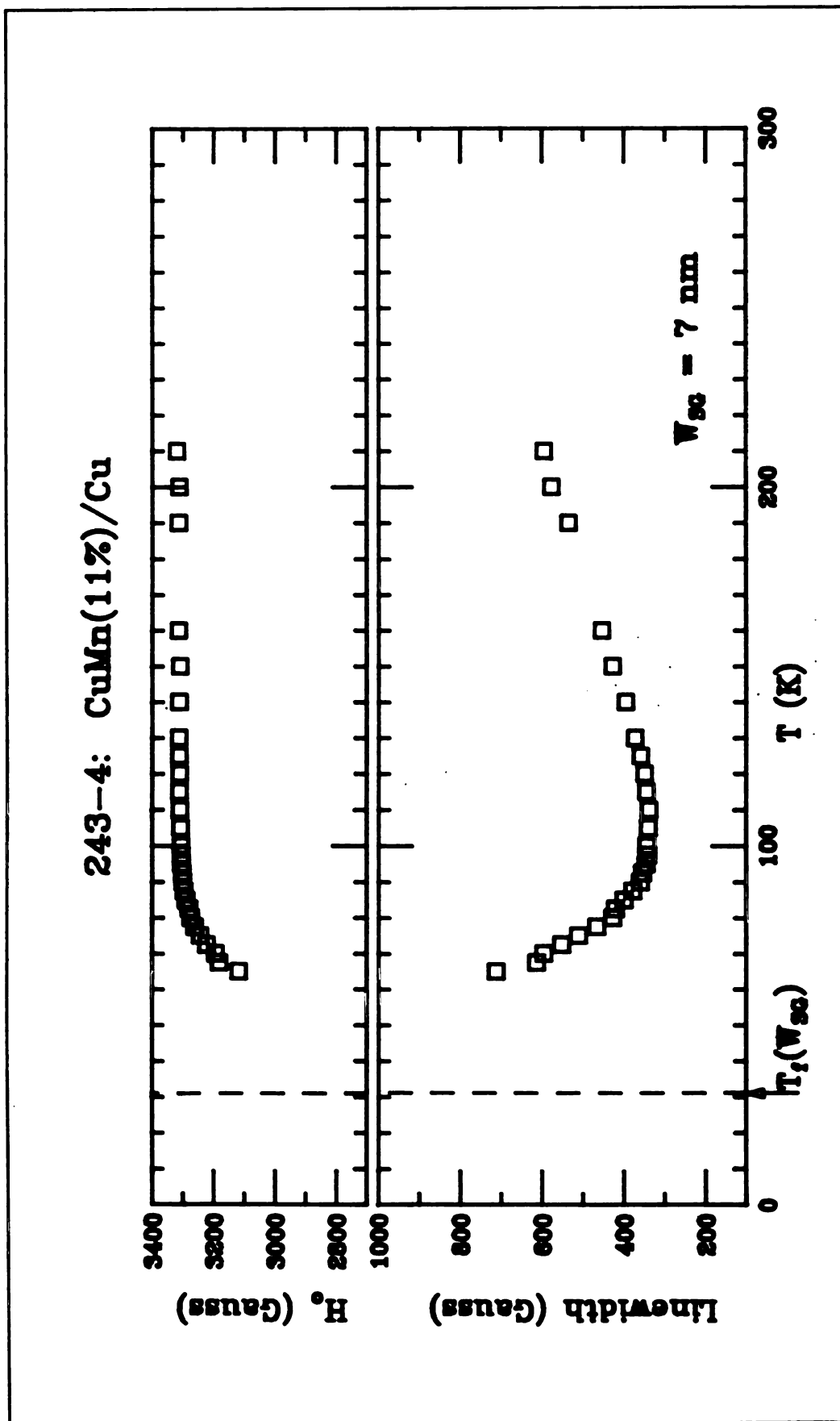
Figure 7-17: $\Delta H(T)$ and $H_0(T)$ for Sample 243-4 - $Cu_{0.89}Mn_{0.11}$ - 7 nm
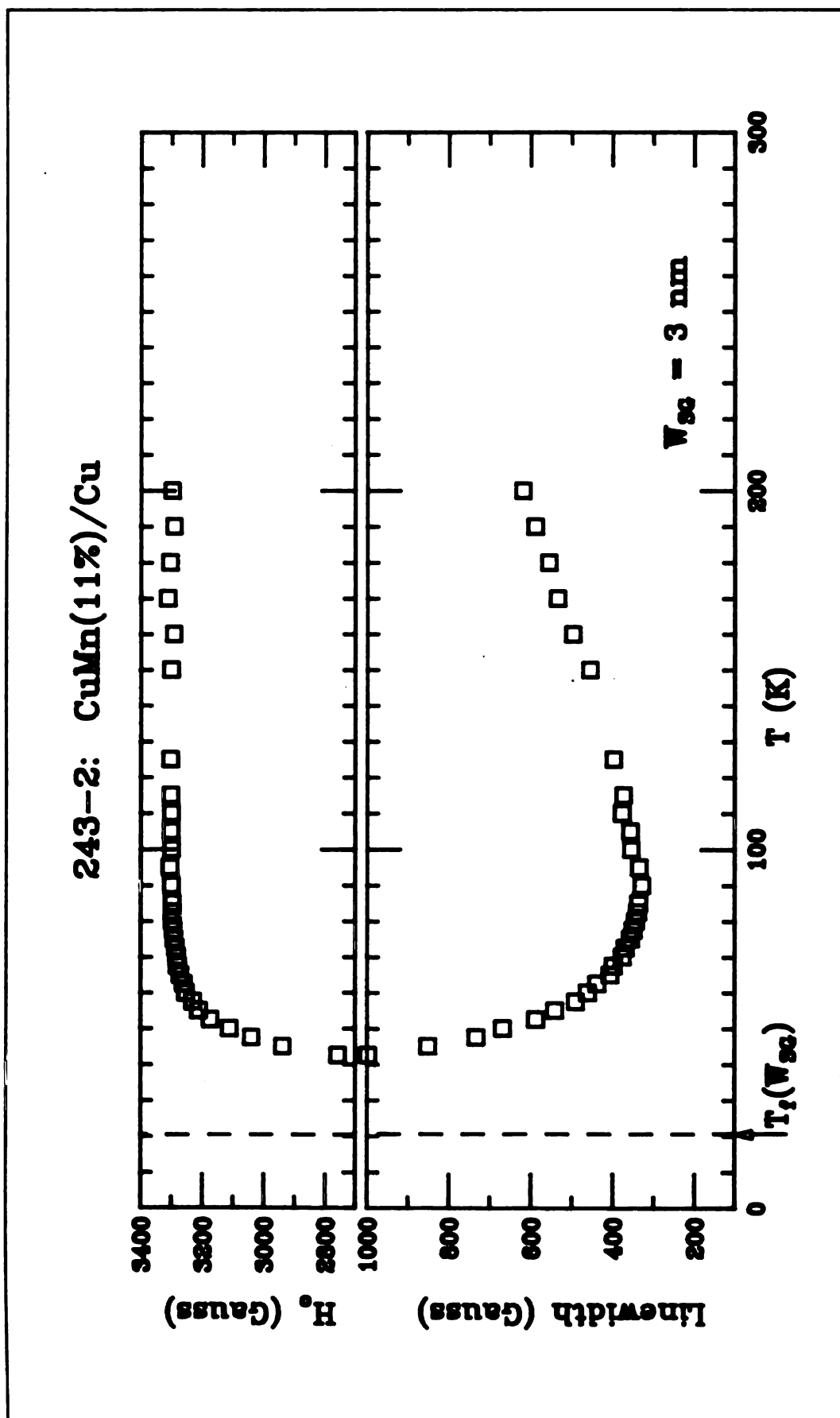
Figure 7-18: $\Delta H(T)$ and $H_0(T)$ for Sample 243-2 - $Cu_{0.89}Mn_{0.11}$ - 3 nm
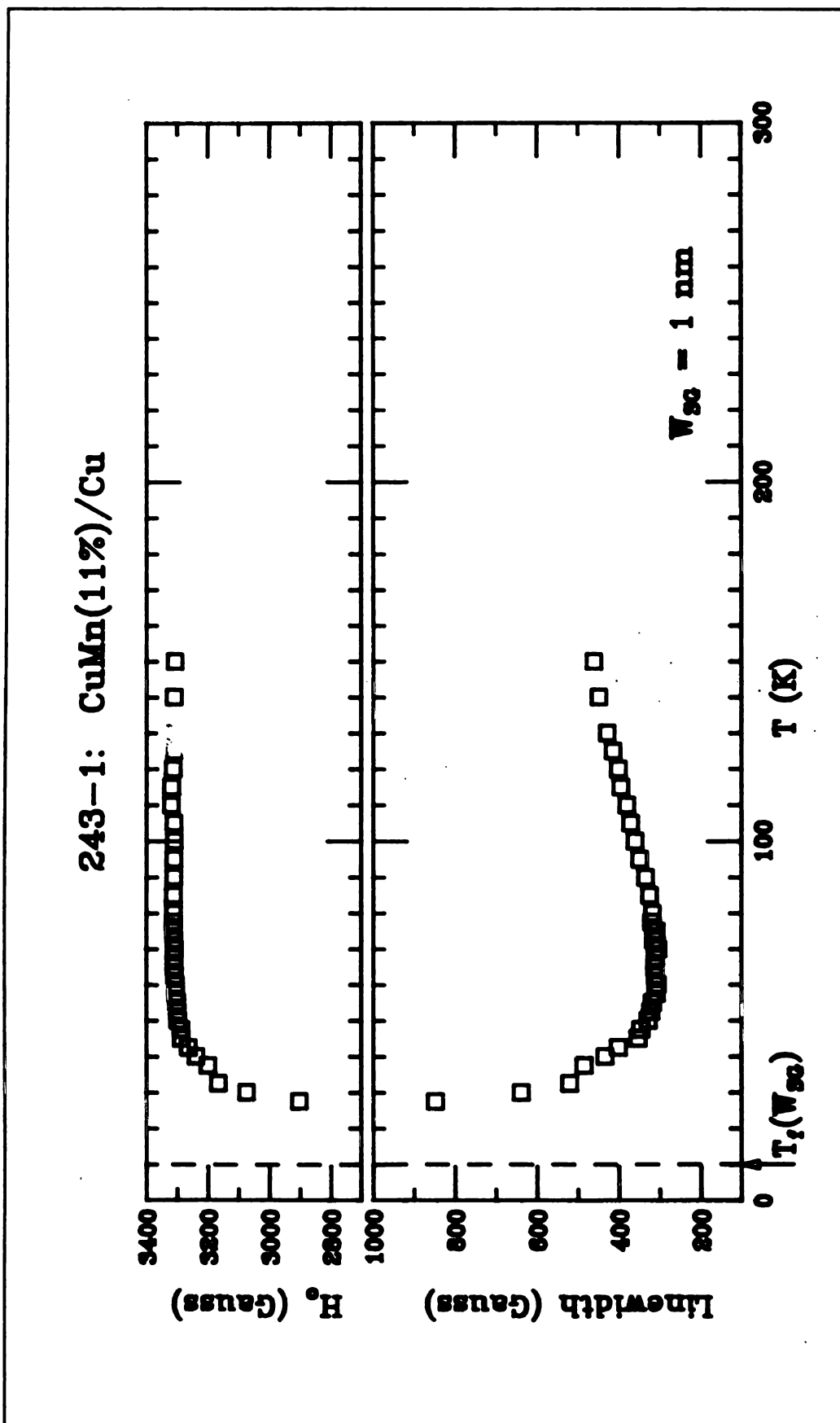
Figure 7-19: $\Delta H(T)$ and $H_0(T)$ for Sample 243-1 - $Cu_{0.89}Mn_{0.11}$ - 1 nm
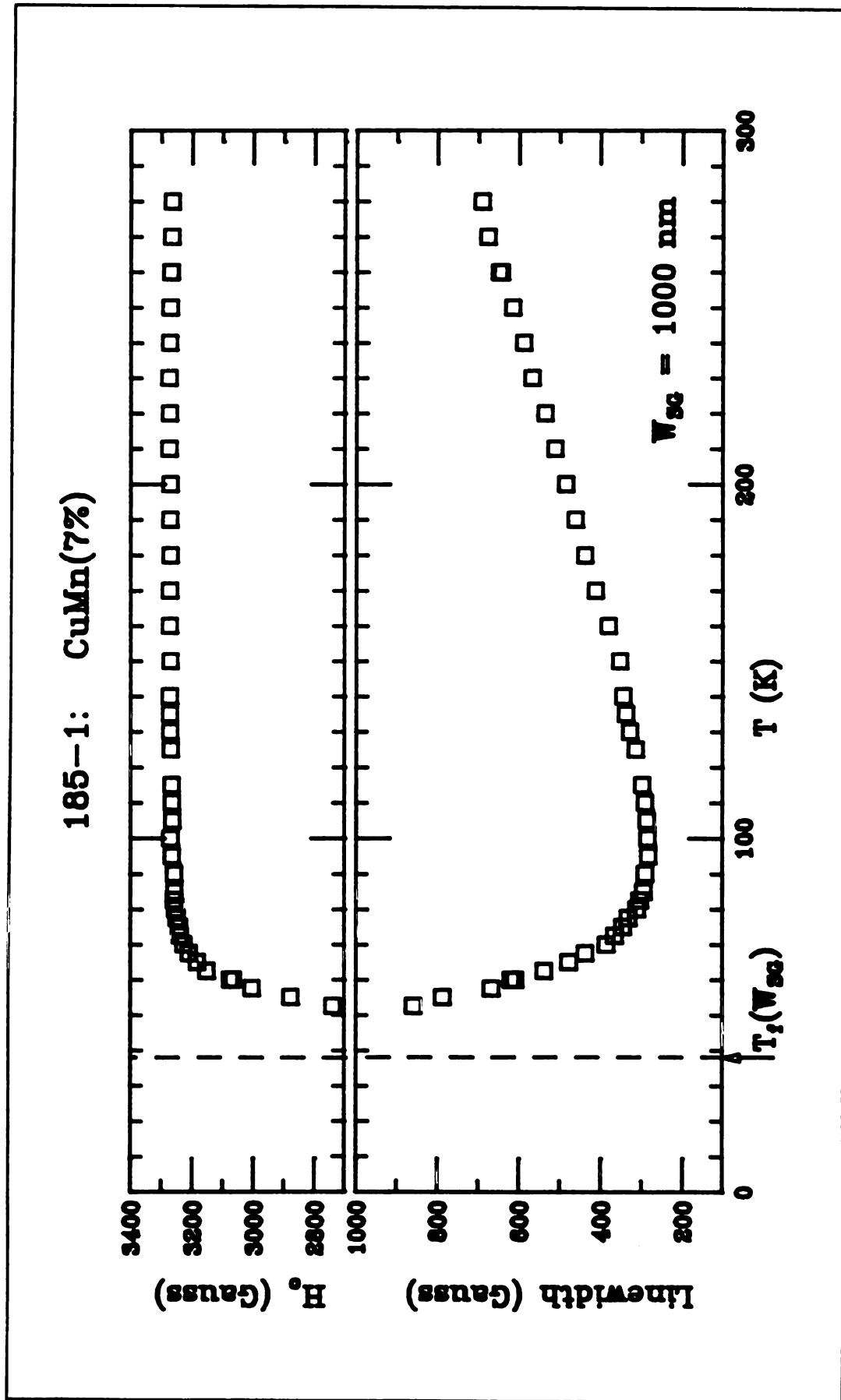
Figure 7-20: $\Delta H(T)$ and $H_0(T)$ for Sample 185-1 - $Cu_{0.93}Mn_{0.07}$ - 1000 nm
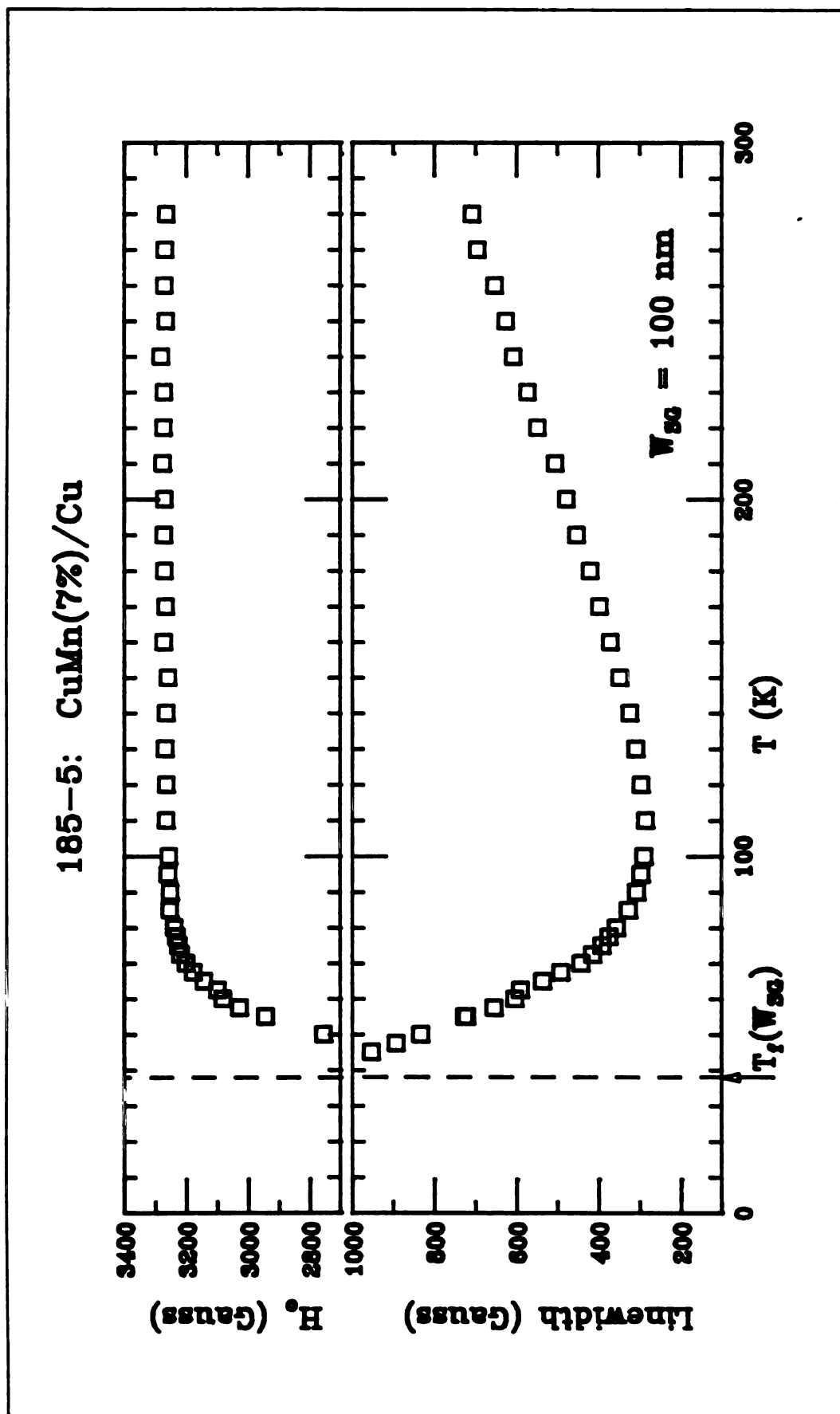
Figure 7-21: $\Delta H(T)$ and $H_0(T)$ for Sample 185-5 - $Cu_{0.93}Mn_{0.07}$ - 100 nm
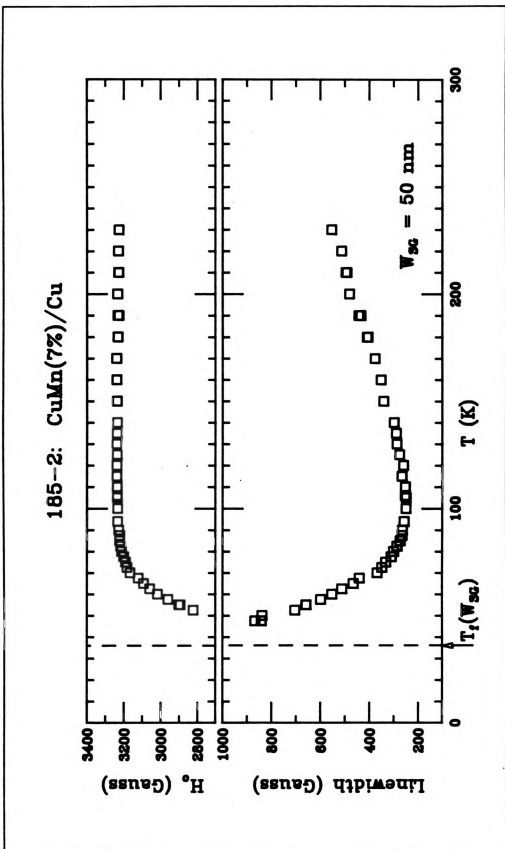
Figure 7-22: $\Delta H(T)$ and $H_0(T)$ for Sample 185-2 - $Cu_{0.93}Mn_{0.07}$ - 50 nm
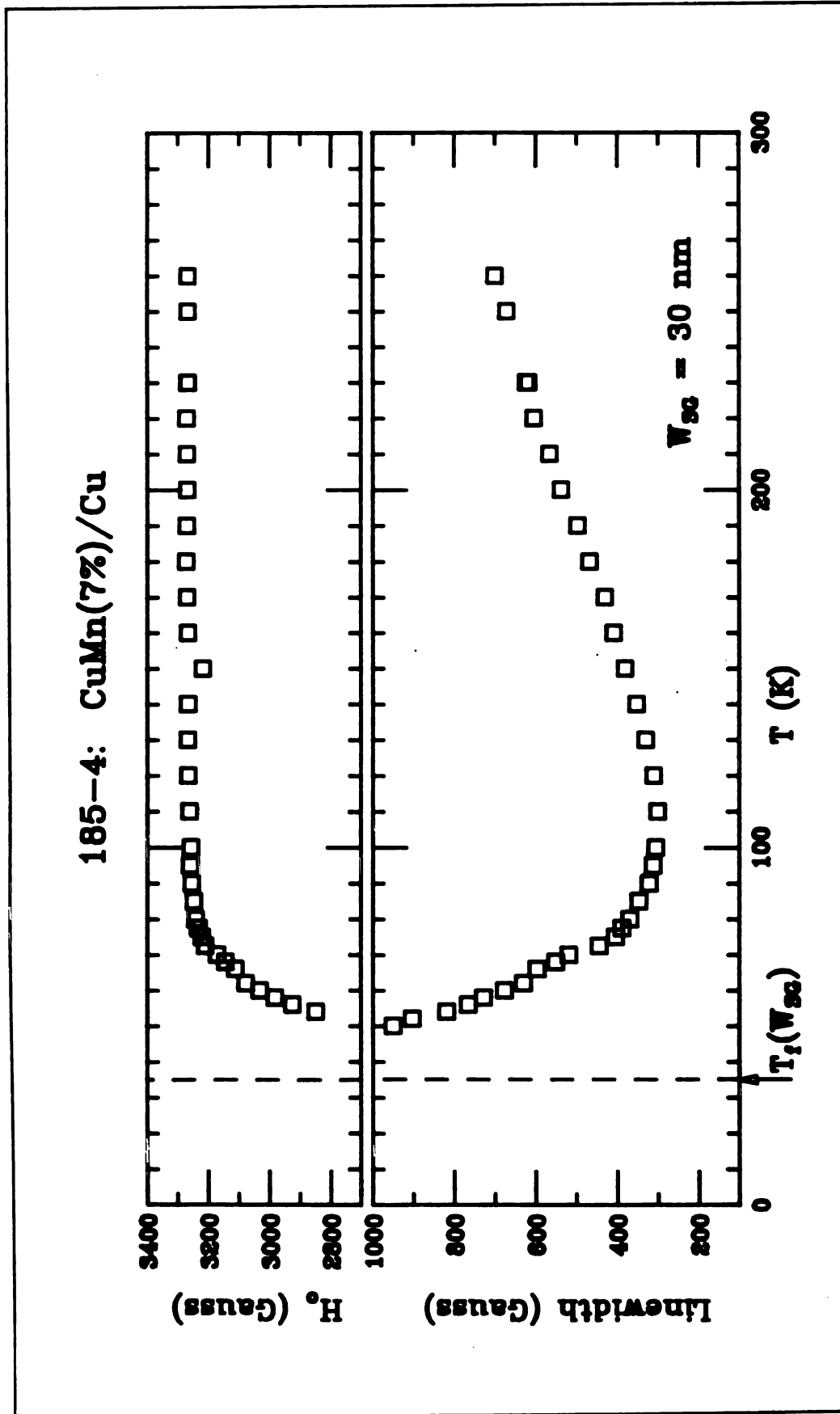
Figure 7-23: $\Delta H(T)$ and $H_0(T)$ for Sample 185-4 - $Cu_{0.93}Mn_{0.07}$ - 30 nm

181
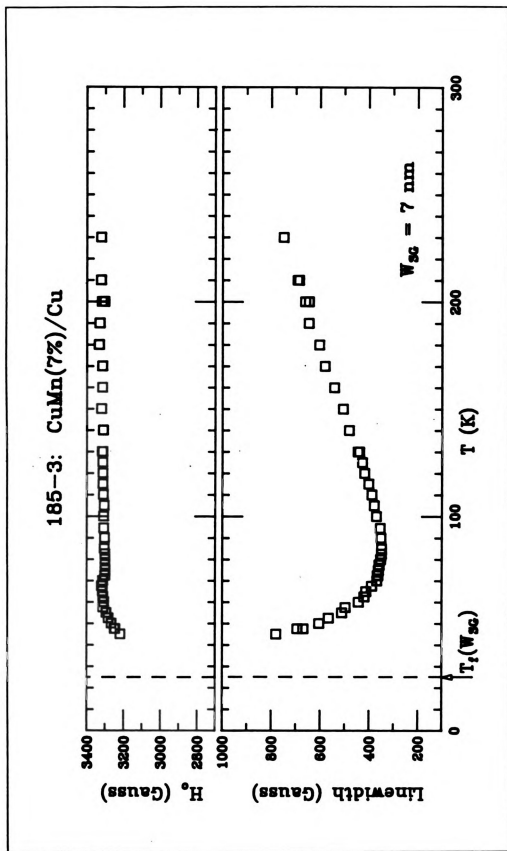
Figure 7-24: $\Delta H(T)$ and $H_0(T)$ for Sample 185-3 - $Cu_{0.93}Mn_{0.07}$ - 7 nm
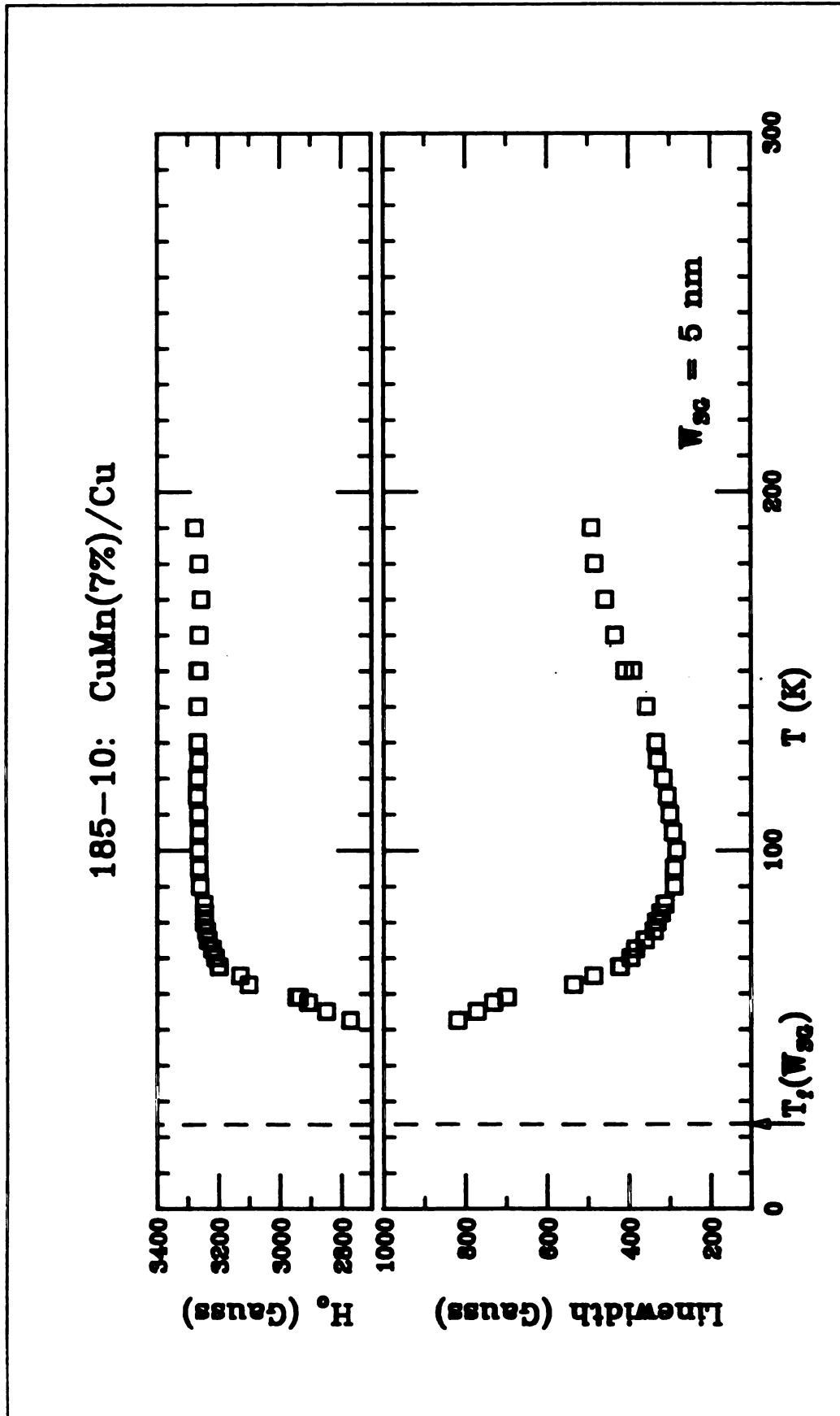
Figure 7-25: $\Delta H(T)$ and $H_0(T)$ for Sample 185-10 - $Cu_{0.93}Mn_{0.07}$ - 5 nm
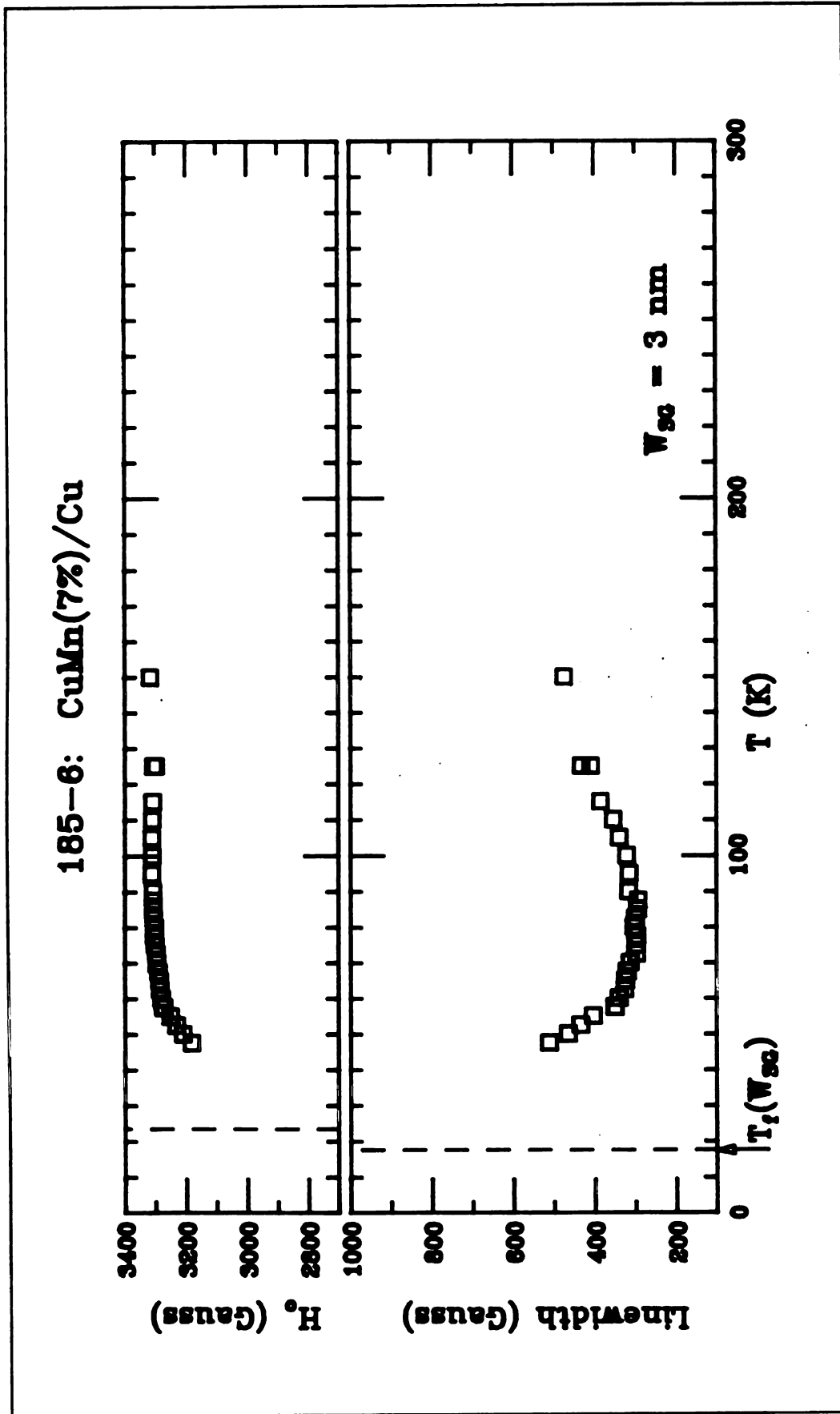
Figure 7-26: $\Delta H(T)$ and $H_0(T)$ for Sample 185-6 - $Cu_{0.93}Mn_{0.07}$ - 3 nm
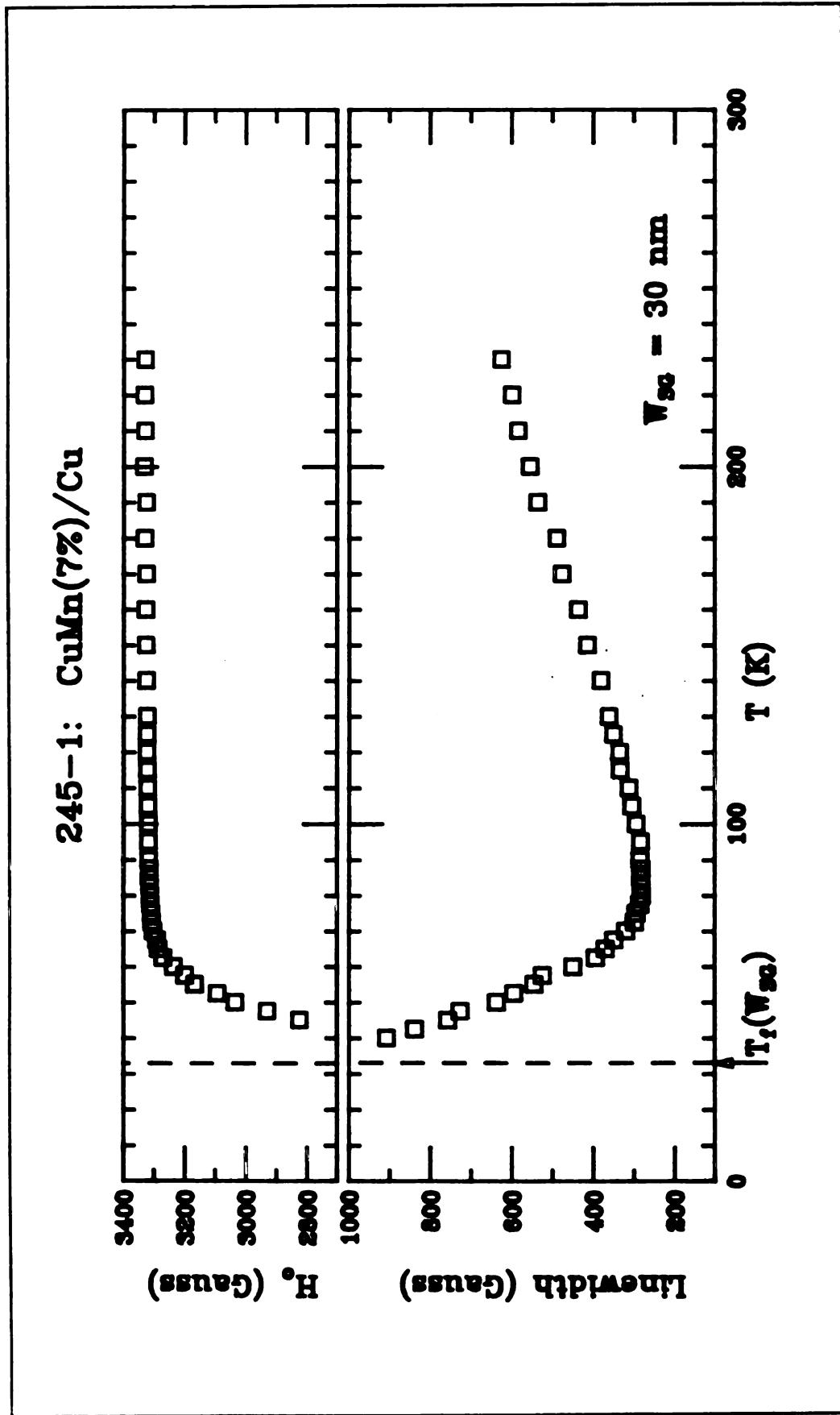
Figure 7-27: $\Delta H(T)$ and $H_0(T)$ for Sample 245-1 - $Cu_{0.93}Mn_{0.07}$ - 30 nm
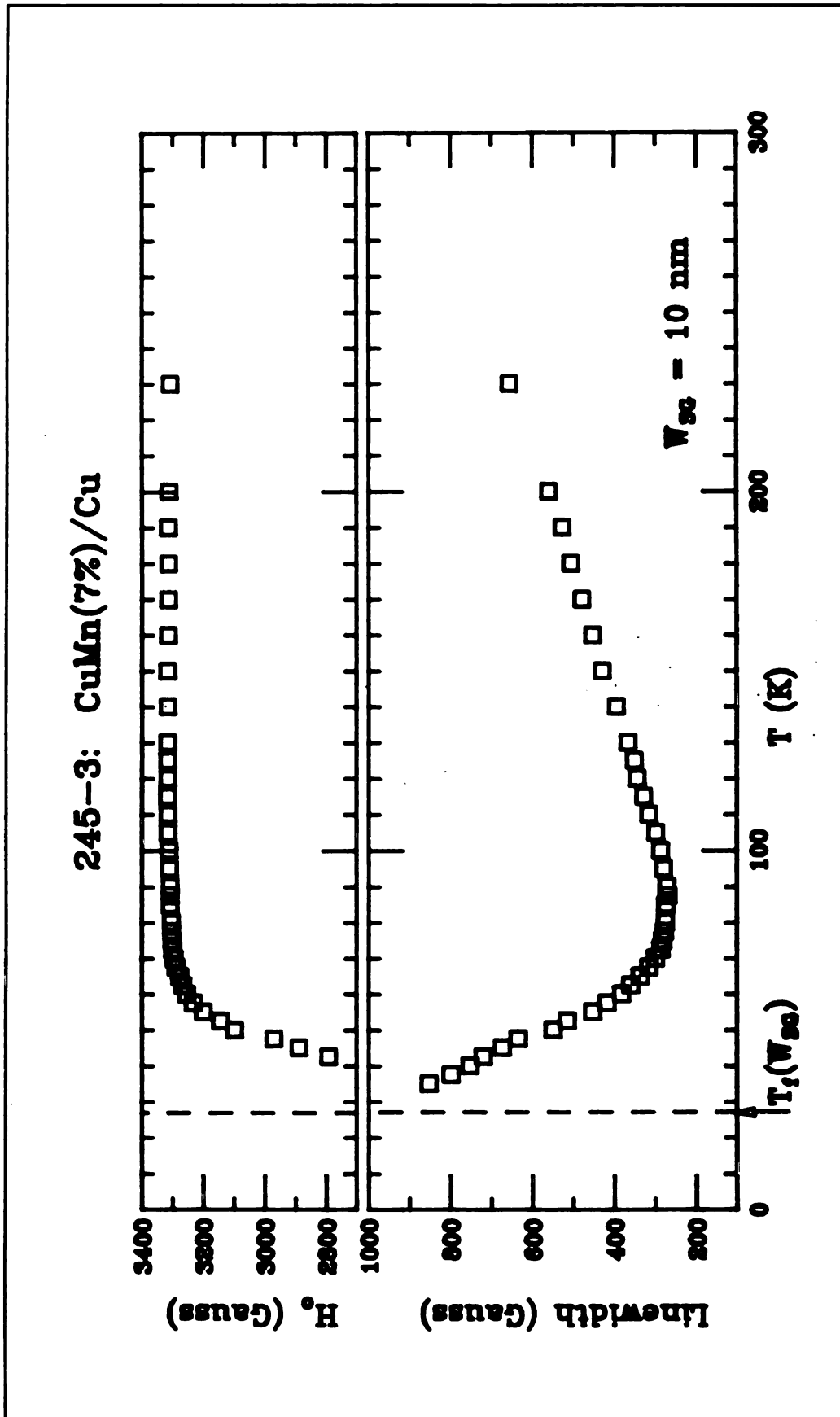
Figure 7-28: $\Delta H(T)$ and $H_0(T)$ for Sample 245-3 - $Cu_{0.93}Mn_{0.07}$ - 10 nm

186
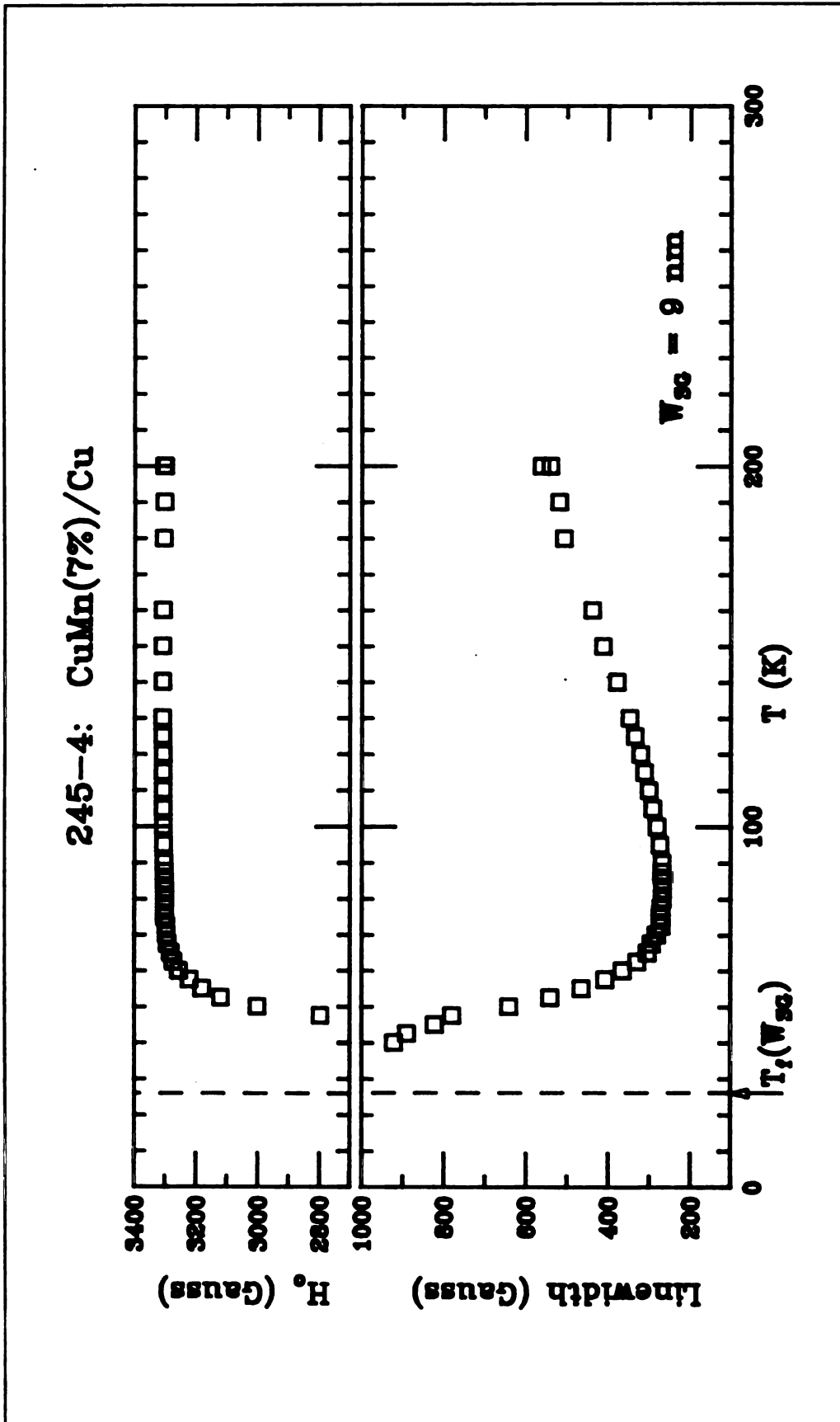
Figure 7-29: $\Delta H(T)$ and $H_0(T)$ for Sample 245-4 - $Cu_{0.93}Mn_{0.07}$ - 9 nm
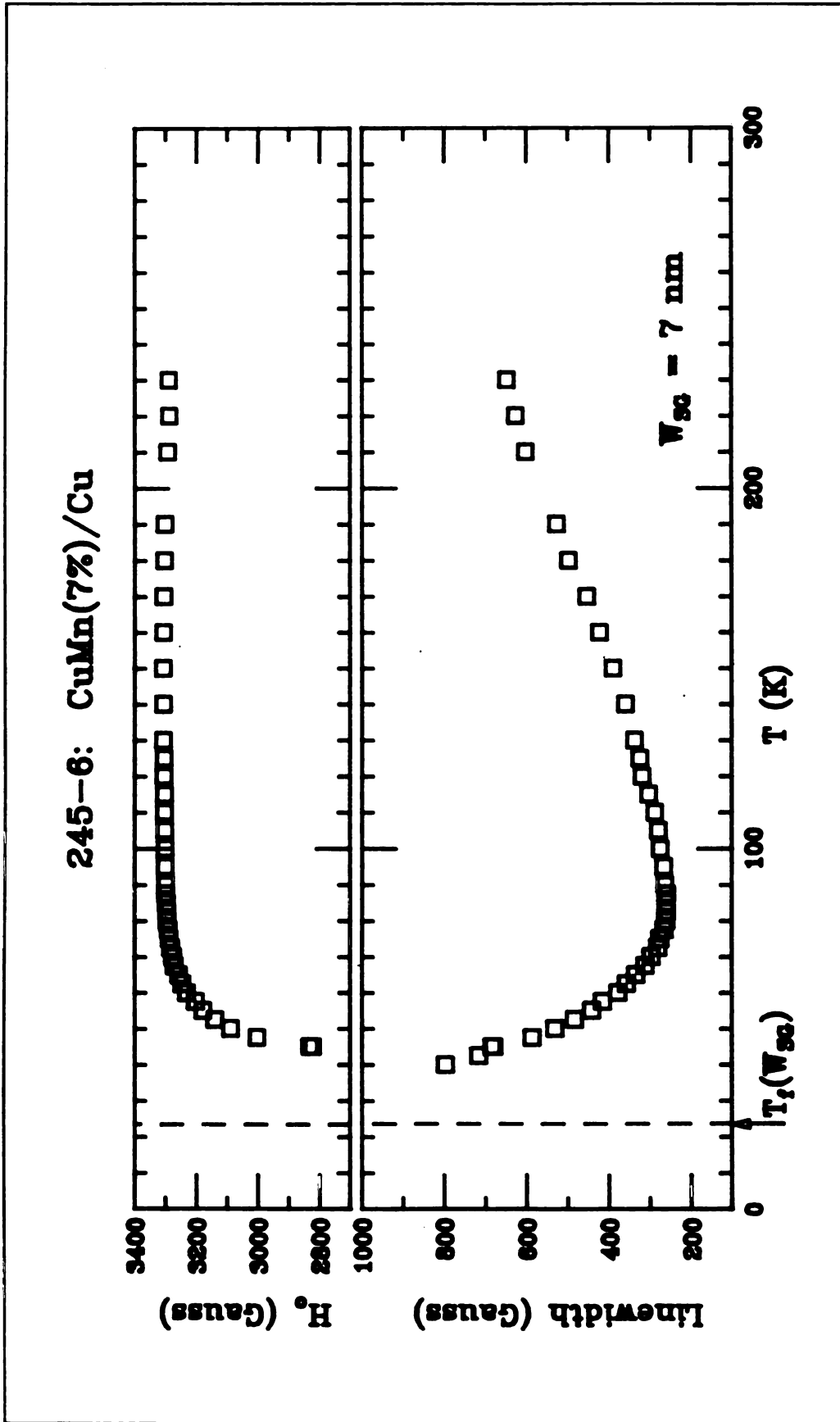
Figure 7-30: $\Delta H(T)$ and $H_0(T)$ for Sample 245-6 - $Cu_{0.93}Mn_{0.07}$ - 7 nm
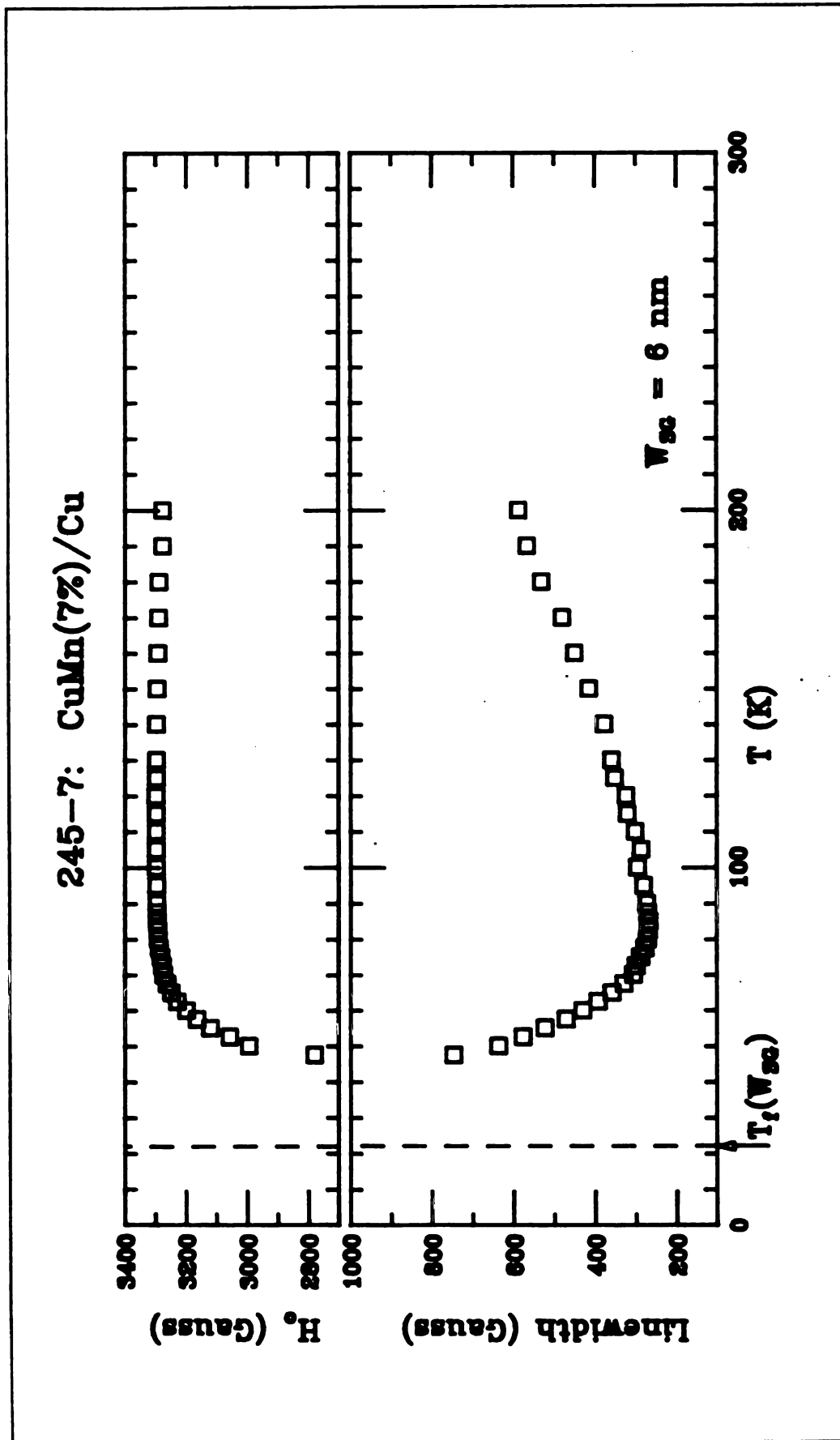
Figure 7-31: $\Delta H(T)$ and $H_0(T)$ for Sample 245-7 - $Cu_{0.93}Mn_{0.07}$ - 6 nm
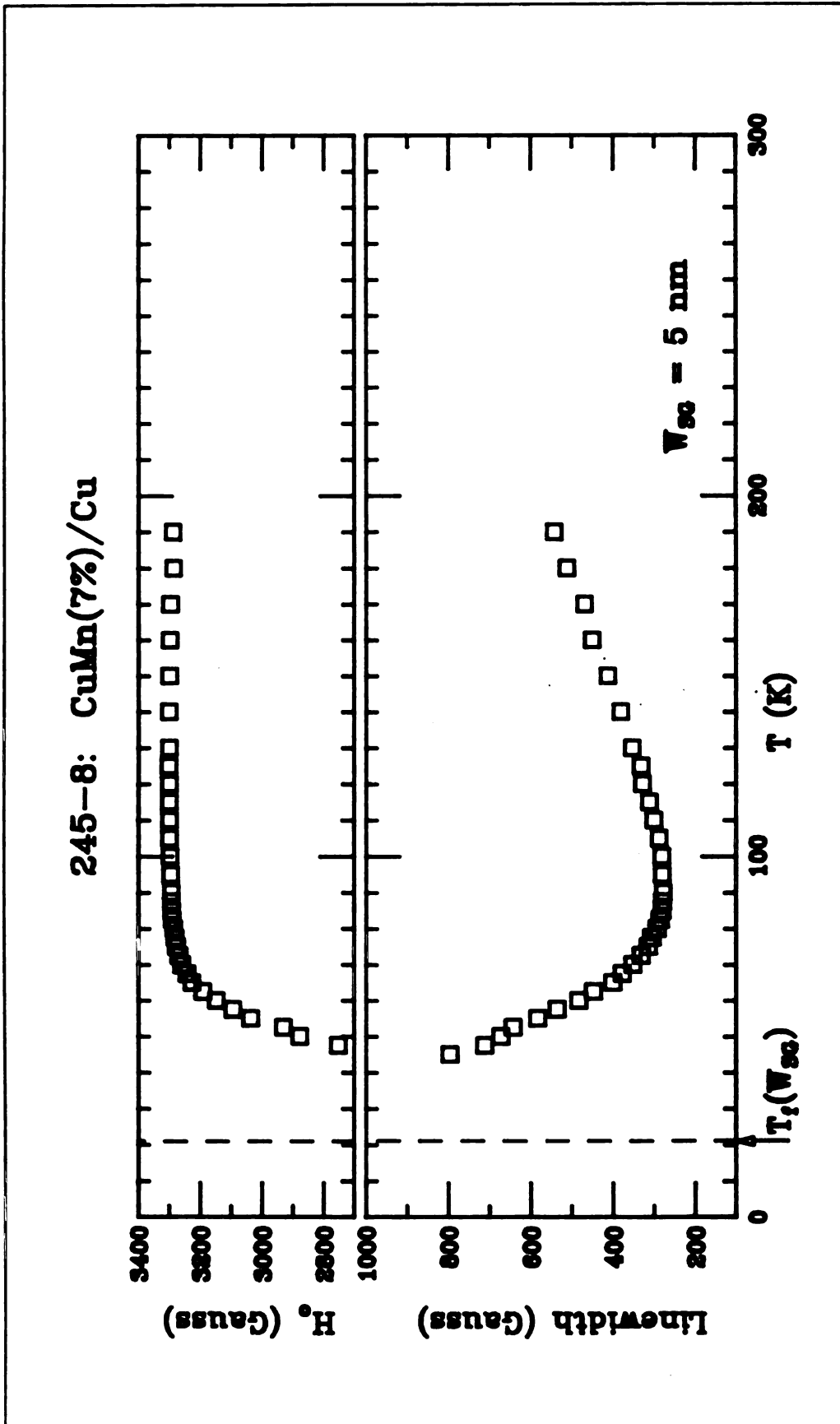
Figure 7-32: $\Delta H(T)$ and $H_0(T)$ for Sample 245-8 - $Cu_{0.93}Mn_{0.07}$ - 5 nm
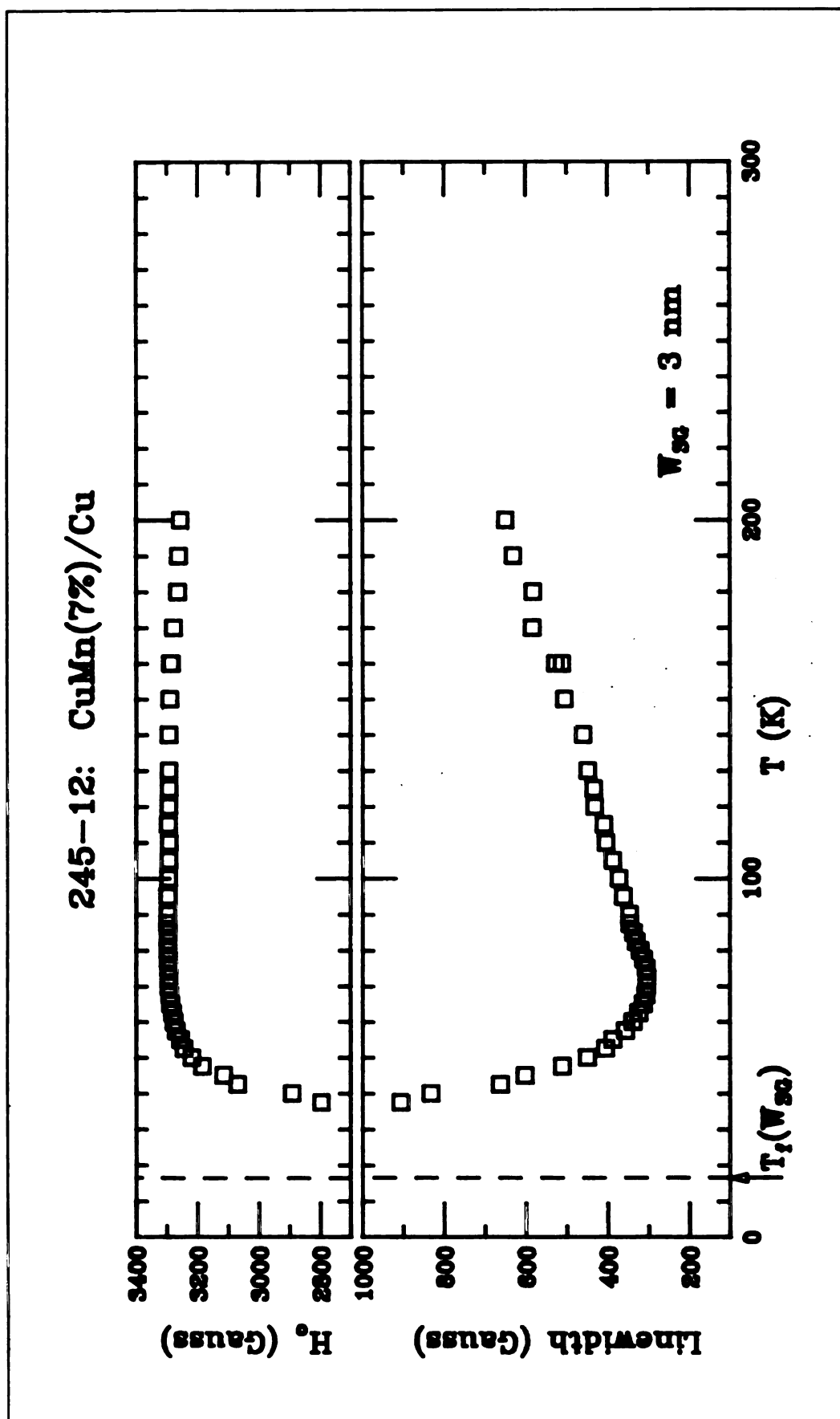
Figure 7-33: ΔH(T) and H_0(T) for Sample 245-12 - $Cu_{0.93}Mn_{0.07}$ - 3 nm

symbols and have been omitted for clarity. In all cases, the same general behavior is observed: the linewidth behaves linearly at high temperatures, reaches a broad minimum and diverges as the freezing temperature is approached.

Qualitative Notes on the Raw Data

As can be seen from the raw data, the same general behavior is seen in samples of all layer thicknesses. The data from sample 185-3 (7 nm) shows anomalous behavior in both the linewidth and the resonance peak position; the minimum linewidth is much larger than the minimum linewidths in the other samples from that run and the resonance peak position as a function of temperature shows a hump not seen in other data. No anomalies in the SQUID measurements were seen.

The lineshift as a function of temperature also exhibits the same qualitative behavior for all layer thicknesses; a g-value $\approx$ 2 is observed over the same region in which the linewidth obeys a linear form. As the linewidth begins to broaden, the position of the line shifts to lower fields. Over the region where the linewidth obeys a power law, the fractional shift in the value of H_0 is only about 5%; the majority of the lineshift occurs below t^*.

Reproducibility

Figure 7-34 shows two different data runs of sample 243-2, a 3 nm $CuMn_{0.89}Mn_{0.11}$ multilayer. The data runs were made about a week apart, and illustrate

the lack of significant run-to run variations. The data illustrated by the squares in Figure 7-34 exhibited a strong baseline, while the data represented by the circles did not, which confirms our ability to extract a reliable value for $\Delta H(T)$ in the presence of the background discussed in Chapter 6.

$\Delta H(T)$ has been compared in samples with data runs taken as much as a year apart, with the no significant changes in the behavior of the linewidth or shift as a function of temperature. No differences in the values of $\Delta H(T)$ or $H_0(T)$ are found in comparing data from ESR samples taken from different parts of the substrate. The primary source of difficulty in making repeated data runs on a given sample is the tendency of the mounted sample to attract dirt due to the presence of the Apiezon grease. Great care was taken in the storage and handling of the samples to minimize contamination. Contamination of the sample is observed as an additional resonance line superposed on the spin glass resonance and is easily identifiable.

Effects Due to the Layered Structure

Figure 7-35 shows data from two samples which were specifically sputtered to test the effect of the interlayers. The data shown in circles is data from a 500 nm $Cu_{0.93}Mn_{0.07}$ film, and the data represented by squares is from a sample with a single 30 nm layer of copper in addition to the 500 nm of CuMn. Agreement between the two sets of data is very good for all temperatures. A study over a larger number of interfaces is difficult due to the trade-off between signal to noise and skin depth constraints.
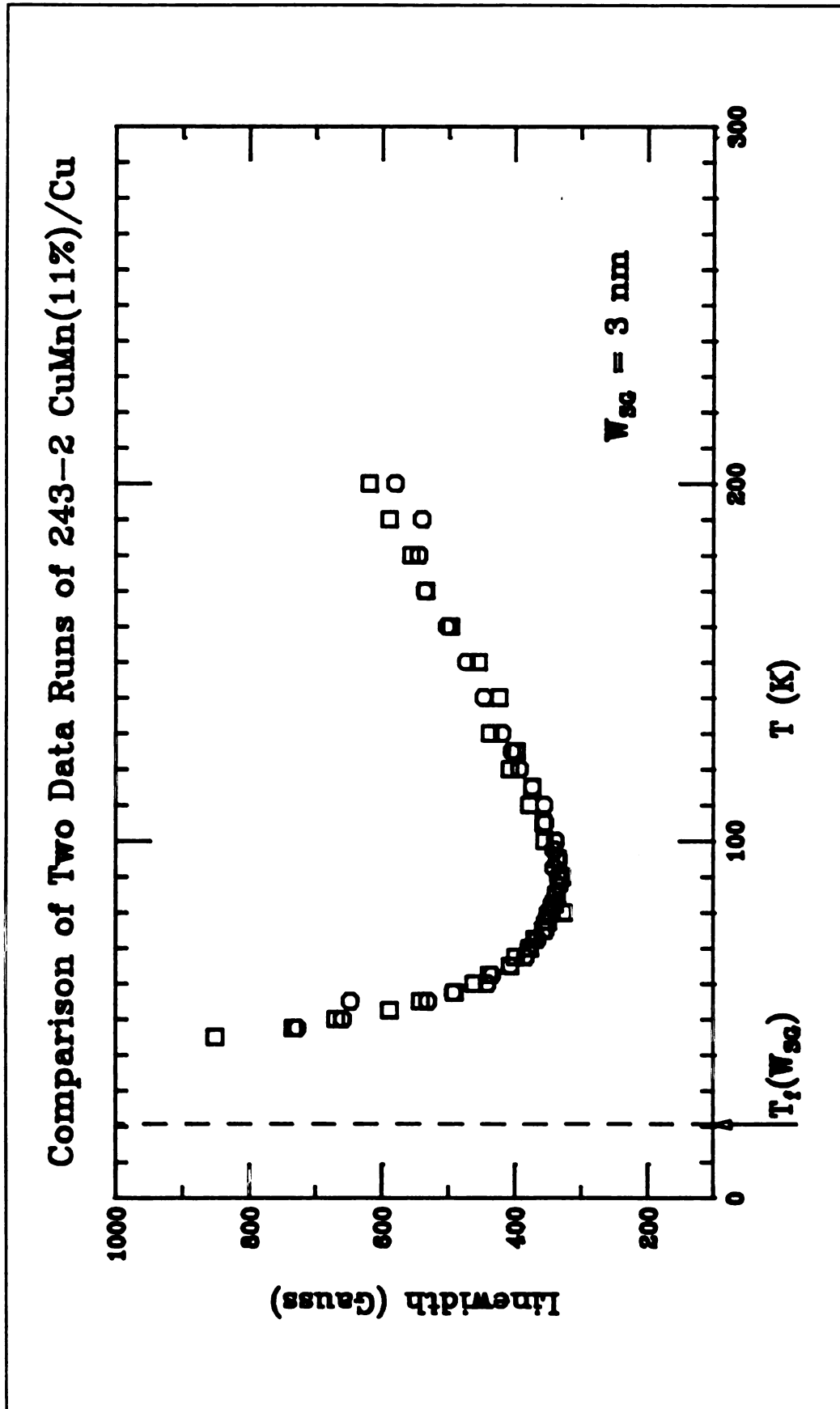
Figure 7-34: *Comparison of Two Separate Data Runs on Sample 243-2 $Cu_{0.89}Mn_{0.11}$*

Dependence of the Position of the Minimum Linewidth on W_{SG}

The position of the minimum linewidth, denoted by T_{min} and the value of the minimum linewidth, $\Delta H(T_{min})$ for Run 243 ($Cu_{0.89}Mn_{0.11}$) are shown in Table 7-9. The position of the minimum, in terms of absolute temperature, gradually shifts as W_{SG} decreases. Viewed in terms of reduced temperature, the change is more dramatic, increasing from 2.5 T_f in the bulk samples to 6.5 T_f in the 1 nm samples.

The minimum linewidth should be a comparison of the strength of the divergent behavior compared to that of the linear behavior. The increased reduced temperature of the minimum linewidth in thinner samples indicates that ordering phenomena become more important compared to the linear behavior at higher reduced temperatures than in samples with large W_{SG}.

Departure From Power Law Behavior

Tables 7-10 through 7-12 tabulate the temperatures at which $\Delta H(T)$ departs from power law behavior as the spin glass layer thickness is reduced. We see from these tables that departure from a power law occurs at higher reduced temperature for smaller W_{SG}. Departures from the power law behavior may be due to 1) the effect of a large field on the nature of the spin glass ordering, 2) regions of the material which, near T_f, are frozen into a spin glass state for times longer than the Larmor period or 3) failure to remain inside the exchange narrowing limit - i.e. the frequency of the exchange is not
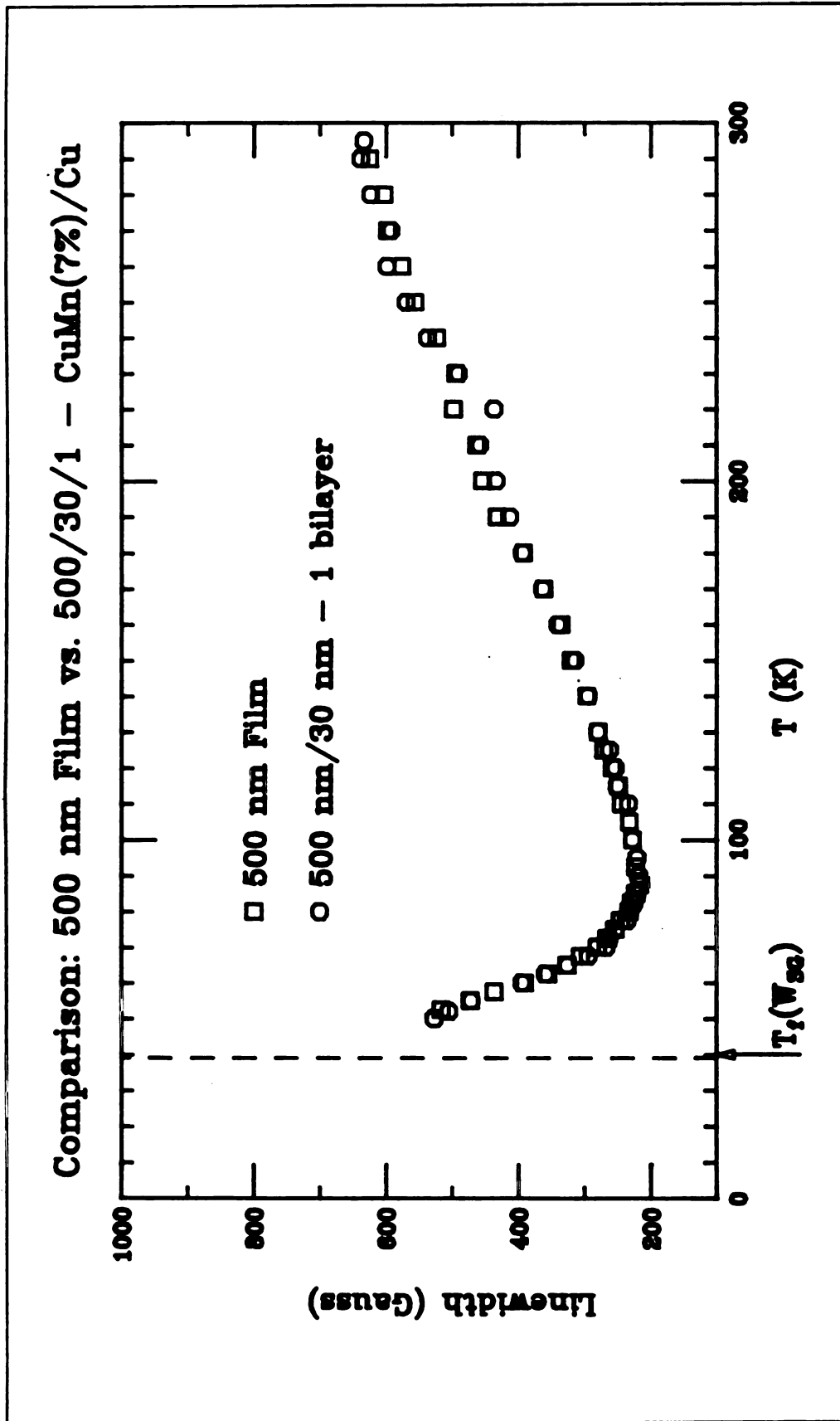
Figure 7-35: *Comparison Between a* $Cu_{0.93}Mn_{0.07}$ *Film with* $W_{SG} = 500$ *nm and a 500/30/1* $Cu_{0.93}Mn_{0.11}/Cu$ *Sample*

Table 7-9: Characteristics of the Minimum Linewidth for Run 243 - $Cu_{0.89}Mn_{0.11}$

Run 243 - $Cu_{0.89}Mn_{0.11}$				
W_{SG} (nm)	T_f (K)	ΔH_{min} (G)	T_{Min} (K)	$T_{Min}/T_f(W_{SG})$
500	47.5	325	115	2.4
100	47.5	338	115	2.4
50	45.0	336	115	2.6
30	42.5	335	115	2.7
10	35.0	329	110	3.1
7	31.0	334	100	3.2
3	20.5	327	90	4.4
1	10.0	316	65	6.5

Table 7-10: Temperature at which $\Delta H(T)$ Departs From a Power Law for Run 243 - $Cu_{0.89}Mn_{0.11}/Cu$

Run 243 - $Cu_{0.89}Mn_{0.11}$			
W_{SG} (nm)	T_f (K)	T^* (K)	t^*
500	47.5	77.5	.63
100	47.5	77.5	.63
50	45.0	75.0	.67
30	42.5	77.5	.83
10	35.0	67.5	.92
7	31.0	70.0	1.35
3	20.5	52.5	1.55
1	10.5	42.5	3.25

Table 7-11: Temperatures at which $\Delta H(T)$ Deviates from a Power Law for Run 185 - $Cu_{0.93}Mn_{0.07}/Cu$

Run 185 - $Cu_{0.93}Mn_{0.07}$			
W (nm)	T_f (K)	T^* (K)	t^*
1000	37.5	60.0	.60
100	38.8	65.0	.68
50	36.0	60.0	.67
30	35.0	68.0	.95
7	25.0	57.5	1.30
5	23.5	62.5	1.66
3	17.5	52.5	2.00

Table 7-12: Temperature at which $\Delta H(T)$ Diverges from a power law for Run 245 - $Cu_{0.93}Mn_{0.07}/Cu$

Run 245 - $Cu_{0.93}Mn_{0.07}$			
W (nm)	T_f (K)	T^* (K)	t^*
30	33.0	57.5	.74
10	27.0	52.5	.94
9	26.0	47.5	.83
7	23.5	55.0	1.34
6	21.0	60.0	1.73
5	20.0	62.5	2.00
3	16.6	50.0	2.00

much greater than the average width of the anisotropy mechanism. Mozurkewich[105], *et. al.*'s study of the effects of increasing the anisotropy by Sb doping showed that there was no dependence of t^* on the Sb doping, as would be expected by the last of these conditions.

The first case would imply that the formation of the spin glass state is being affected by the application of a large field. The importance of field effects on spin glass properties is characterized by the ratio $g\mu_B H/kT_f$, implying that field effects should be less pronounced with smaller T_f's. This would in turn imply that the value of t^* should decrease with decreasing concentration, as is confirmed by the data in Table 7-8. Since samples with smaller W_{SG} have smaller T_fs, t^* should also decrease for decreasing spin glass layer thickness - which is the exact opposite of what is seen.

If formation of clusters is responsible for the deviation from power law behavior, the behavior of t^* with W_{SG} implies that cluster formation must begin at higher temperatures relative to T_f in smaller W_{SG} than in larger W_{SG}.

Fits of $\Delta H(T)$ as a Function of W_{SG}

Tables 7-13 through 7-15 show the values obtained by fitting to Equation 7-4 for runs 243, 185 and 245. Figures 7-36 and 7-37 show representative fits of $\Delta H(T)$ to Equation 7-4 for the smallest W_{SG} (1 nm) and the largest W_{SG} (500 nm) in the 243 $Cu_{0.89}Mn_{0.11}$ run. The appearance of all fits is very similar, so only these two are shown to avoid repetition. In both plots, data points which were not used in the fit (due to the departure from power-law behavior) are shown by solid symbols. Figure 7-38 compares

the theoretical fits for a representative group of spin glass layer thicknesses in the 243 $Cu_{0.89}Mn_{0.11}$. Figures 7-39 and 7-40 show the excess linewidth, $\Delta H^{ex} = \Delta H(T) - (A+BT)$ for representative samples in the 243 and 245 runs. Error bars, which are approximately 10-30 G, have been omitted to increase clarity.

General Behavior of the Fits

We can identify some broad trends as a function of layer thickness. The exponent characterizing the divergence, κ, increases with decreasing layer thickness for samples with $W_{SG} \geq 5$ nm. Below this thickness, the exponents decrease, but still have values greater than the bulk value of $\kappa = 1.5$. Both the residual width, A, and the thermal broadening coefficient, B, tend to increase with decreasing layer thickness. From the data in Table 7-6, the increase in the residual width with decreasing layer thickness might be indicative of a reduced effective concentration. If spreading of the spin glass layer into the interlayer were significant, the sample would have a larger W_{SG}, and a lower concentration; however, the amount of spreading would have to be much larger than the nominal .5-1 nm to explain the magnitudes of the changes seen. The graph of residual width vs. concentration indicates that the $Cu_{0.93}Mn_{0.11}$ 3 nm sample from Run 243 would have to have an effective Mn concentration of 7% to explain the observed value. The concentration study also indicates that decreasing concentration should result in a smaller thermal broadening, and the opposite effect is noted with decreasing W_{SG}. We conclude that the systematic changes in A and B are not due to the spreading of the spin glass

Table 7-13: Fits to $A+BT+CT^{-\kappa}$ for Run 243 - $Cu_{0.89}Mn_{0.11}/Cu$

Run 243 - $Cu_{0.89}Mn_{0.11}$					
W (nm)	T_f (K)	A (G)	B (G/K)	C (G)	κ
500	47.5	-245 ± 13	3.36 ± 0.01	328 ± 13	1.5 ± 0.1
100	47.5	-245 ± 14	3.46 ± 0.02	324 ± 17	1.5 ± 0.1
50	45.0	-236 ± 14	3.40 ± 0.02	366 ± 16	1.5 ± 0.1
30	42.5	-226 ± 14	3.57 ± 0.02	453 ± 16	2.0 ± 0.1
10	35.0	-201 ± 14	3.54 ± 0.02	650 ± 13	2.0 ± 0.1
7	31.0	-183 ± 14	3.70 ± 0.02	890 ± 17	2.2 ± 0.1
3	20.5	-145 ± 15	3.73 ± 0.03	1182 ± 21	1.7 ± 0.1
1	10.5	-88 ± 14	4.18 ± 0.03	2745 ± 63	1.8 ± 0.1

Table 7-14: Fits to A+BT+Ct$^{-\kappa}$ for Run 185 - Cu$_{0.93}$Mn$_{0.07}$/Cu

Run 185 - Cu$_{0.93}$Mn$_{0.07}$					
W (nm)	T$_f$ (K)	A (G)	B (G/K)	C (G)	κ
1000	37.5	-132 ± 32	2.94 ± .04	248 ± 33	1.5 ± 0.1
100	38.8	-151 ± 33	3.00 ± 0.10	280 ± 34	1.5 ± 0.1
50	36.0	-153 ± 33	2.92 ± 0.03	294 ± 35	1.6 ± 0.1
30	35.0	-134 ± 33	3.22 ± 0.02	413 ± 36	2.1 ± 0.1
7	25.0	-34 ± 63	3.45 ± 0.14	566 ± 45	2.1 ± 0.1
5	23.5	-115 ± 33	3.19 ± 0.04	1504 ± 56	2.4 ± 0.2
3	17.5	-82 ± 44	3.62 ± 0.14	1340 ± 31	2.1 ± 0.2

Table 7-15: Fits to $A+BT+Cr^{-\kappa}$ for Run 245 - $Cu_{0.93}Mn_{0.07}/Cu$

Run 245 - $Cu_{0.93}Mn_{0.07}$					
W (nm)	T_f (K)	A (G)	B (G/K)	C (G)	κ
30	33.0	-144 ± 13	3.42 ± 0.02	280 ± 15	1.6 ± 0.1
10	27.0	-127 ± 13	3.40 ± 0.02	423 ± 17	1.7 ± 0.1
9	26.0	-116 ± 13	3.38 ± 0.02	492 ± 16	2.1 ± 0.1
7	23.5	-115 ± 13	3.24 ± 0.03	710 ± 14	2.0 ± 0.1
6	21.0	-105 ± 13	3.42 ± 0.03	1888 ± 46	2.8 ± 0.1
5	20.0	-107 ± 13	3.34 ± 0.03	2868 ± 65	2.8 ± 0.1
3	16.6	-75 ± 13	3.83 ± 0.03	1576 ± 20	2.2 ± 0.1
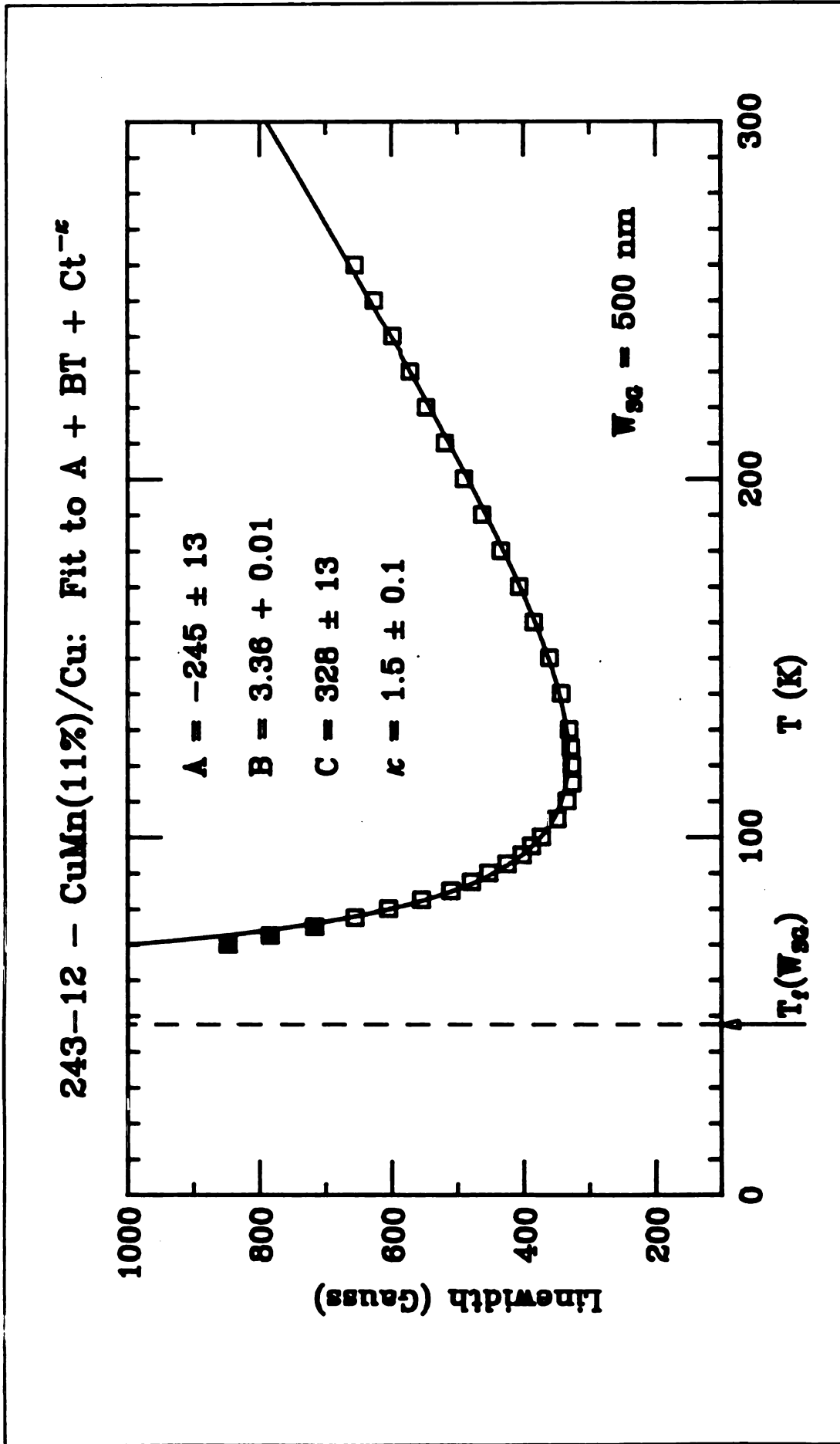
Figure 7-36: *Fit of ΔH(T) for Sample 243-12 - $Cu_{0.89}Mn_{0.11}$ - 500 nm*
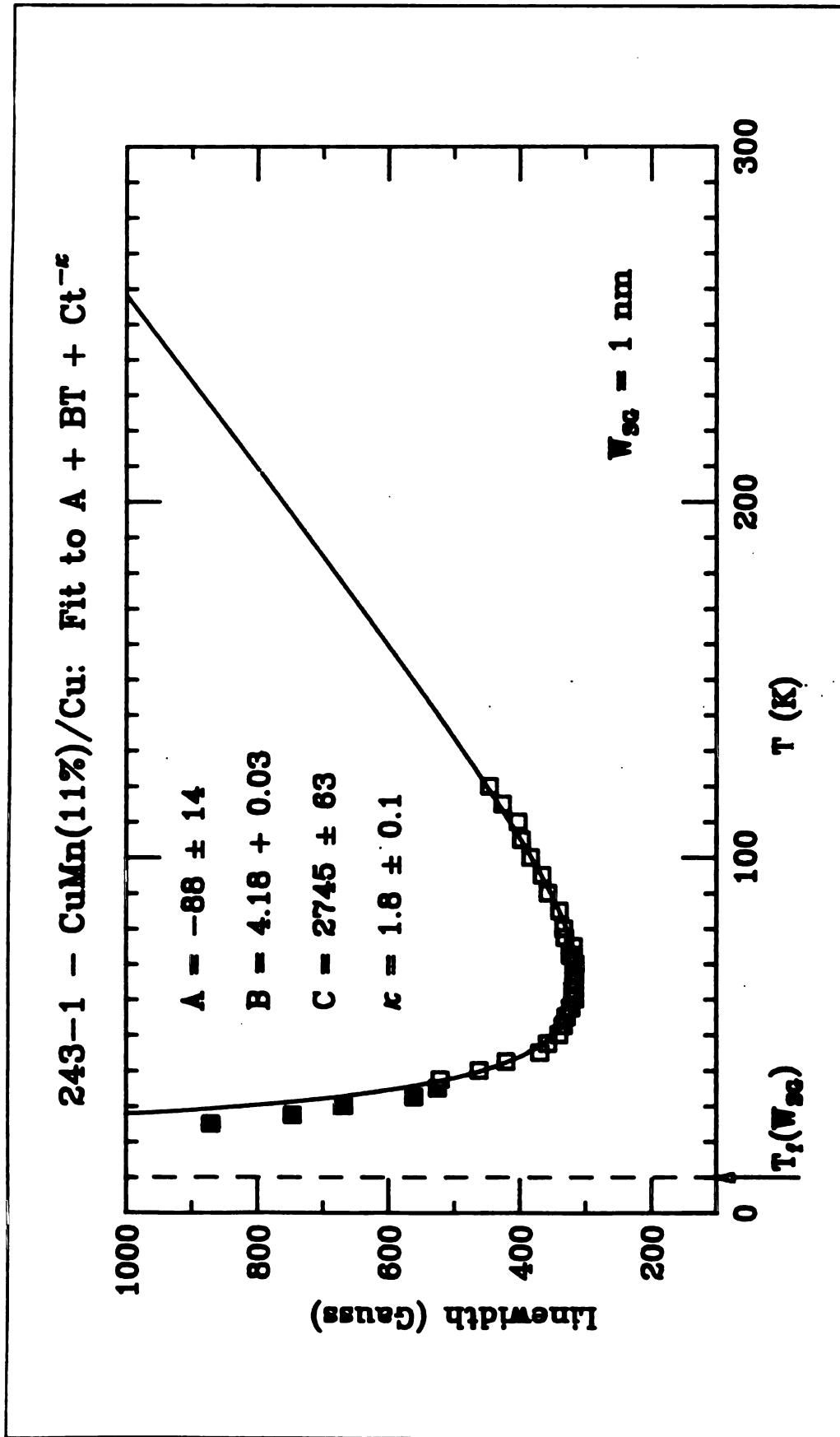
Figure 7-37: *Fit of ΔH(T) for Sample 243-1 - Cu$_{0.89}$Mn$_{0.11}$ - 1 nm*
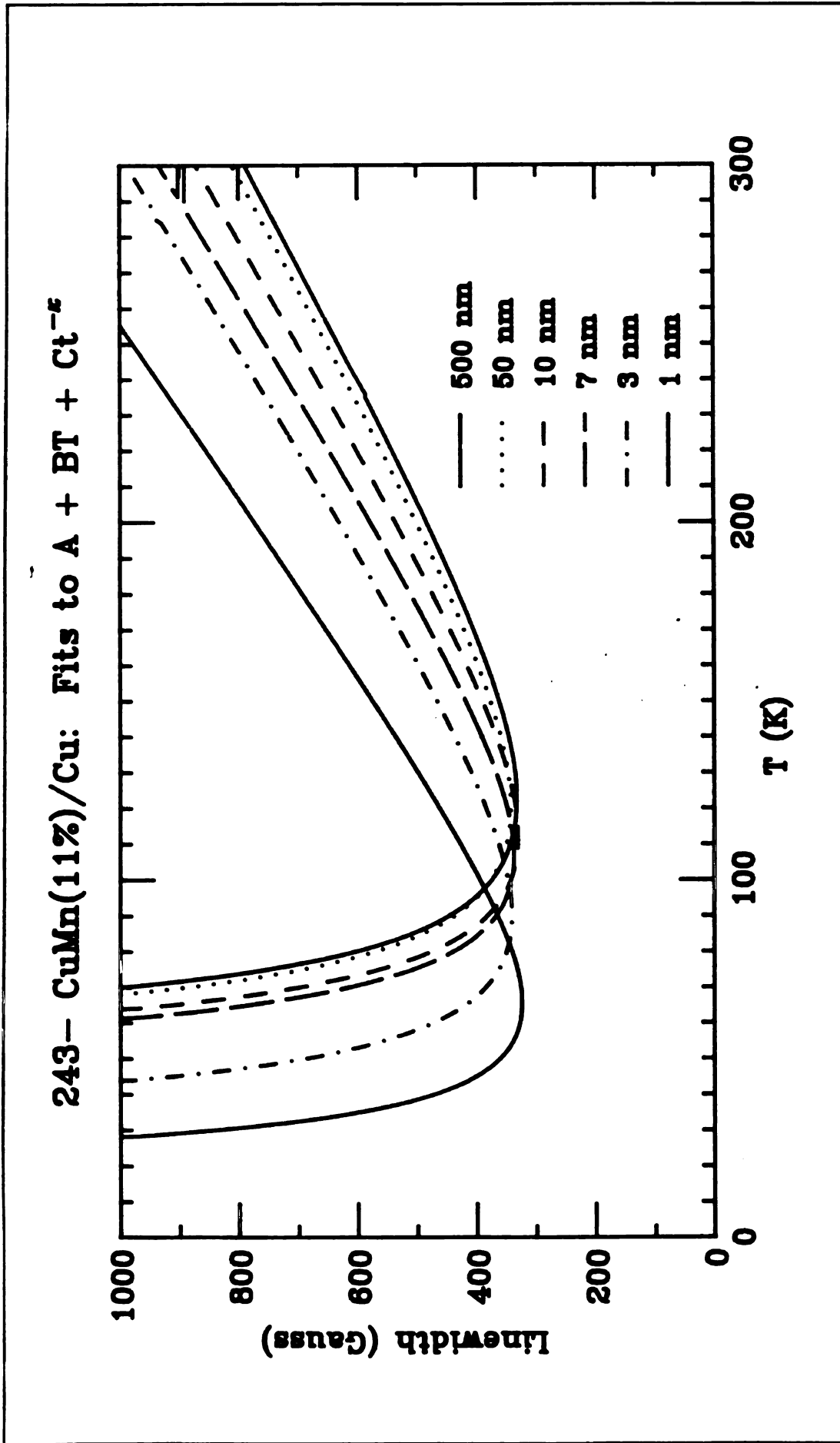
Figure 7-38: *Comparison of $\Delta H(T)$ for the 243 Series - $Cu_{0.89}Mn_{0.11}$*
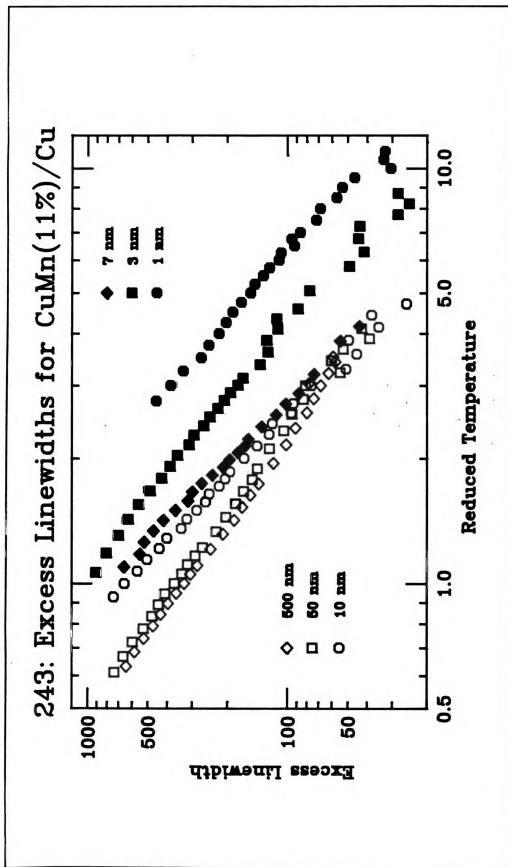
Figure 7-39: *Excess Linewidth, $\Delta H(T)^{ex}$, for the 243 Series - $Cu_{0.89}Mn_{0.11}$*
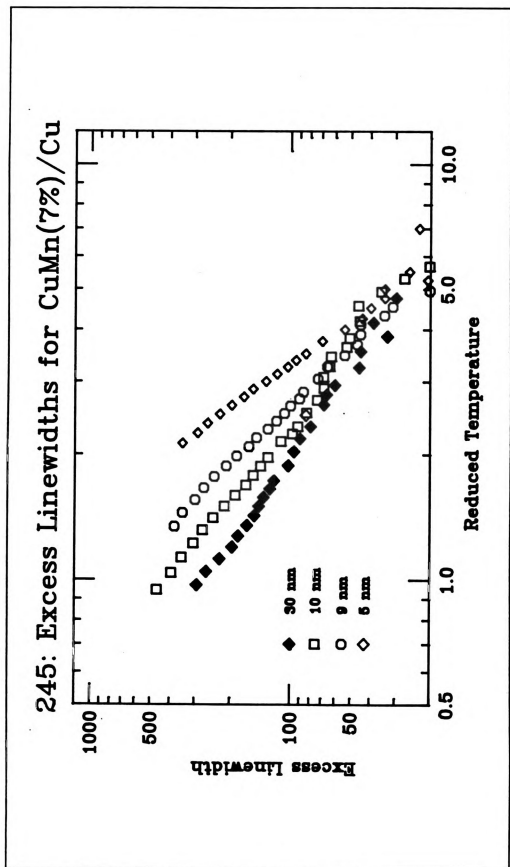
Figure 7-40: Excess Linewidth, $\Delta H(T)^{ex}$, for the 245 Series - $Cu_{0.93}Mn_{0.07}$

layers. The divergence strength, C, also displays a marked increase with decreasing layer thickness.

The larger errors on the 185 run are due to three factors. This data was taken prior to the renovation and fine-tuning of the ESR apparatus. These samples were also fabricated before the substrate cooler was installed, and some of the samples were sputtered as single samples with the substrate centered over the gun, and some were sputtered two at a time, with the midpoint between the two substrates centered over the gun. The susceptibility measurements were somewhat anomalous, with bulk samples sputtered during the same run having T_fs which differed by as much as 3.5 K, (37.5 K to 41.0 K) which is outside the normal estimated errors of $\pm$ 1 K. The difference in T_fs may be caused by changes in the sputtering rate over the course of a sputtering run, differences due to the substrate positions with respect to the gun, or lack of substrate cooling. Target shavings were measured to have a T_f of 38 K. The bulk freezing temperature for this run was taken to be 39 K, which contributed to larger errors on the fits, but allowed a consistent analysis of the run using a single bulk temperature.

INTERPRETATION OF THE MEANING OF T_f IN EQUATION 7-4

As is evident from the preceding chapters (and the opening quote of this chapter) the interpretation of Electron Spin Resonance measurements above T_f, even in bulk spin glasses, is not straightforward. Neither of the two theories discussed (mean field and cluster) has addressed ESR in spin glasses in lower dimensions, and there have been no calculations regarding finite size effects on ESR measurements.

Use of Equation 7-4 in the analysis of multilayered spin glasses raises some questions. The first problem is that our goal - observation of finite size and dimensionality effects - is confused by the presence of $T_f(W_{SG})$ in Equation 7-4. We must therefore determine which of the trends observed in fitting to Equation 7-4 are due to the depression of T_f, and which are indicative of effects on the ESR linewidth. Knowledge of the behavior of $T_f(W_{SG})$ in different field, frequency and dimensionality regimes will contribute to separating these effects.

Zero Temperature (2D) Scaling Forms

The first question is to determine if Equation 7-4, which has been shown to describe the behavior of $\Delta H(T)$ in bulk spin glasses and is consistent with the predictions of both the mean field and the cluster model, is suitable to describe samples with small W_{SG}. The fits described by Tables 7-13 through 7-15 have shown that Equation 7-4 does indeed describe the data for all layer thicknesses for $T > T_f$. Systematic trends as a function of W_{SG} are seen in the parameters, but samples with $W_{SG} \leq 3$ nm do not obey these trends.

Analysis of ac susceptibility measurements of thin multilayers, and of 2D Ising spin glasses, indicate that two dimensional behavior should be characterized by a zero freezing temperature, so that our assumption of a finite T_f in Equation 7-4 results an incorrect form for the divergence. The zero freezing temperature form corresponding to Equation 7-4 is:

$$\Delta H(T) = A + BT + C^* T^{-x} \tag{7-5}$$

where C^* is used to indicate that this coefficient should not be expected to equal the values of C obtained from the fits to finite T_f. Tables 7-16 through 7-18 show the results of fitting to Equation 7-5.

Fitting the samples with $W_{SG} \leq 3$ nm to Equation 7-5 does not substantially change the values of A and B. The value of C^* does not appear to have any obvious relationship to bulk parameters, but does decrease with decreasing layer thickness. The exponents obtained by this fit continue the trend of increasing exponents as the layer thickness decreases.

Figures 7-41 through 7-44 summarize the dependence of the fitting parameters on W_{SG} for run 243. Figures 7-45 through 7-48 and 7-49 through 7-52 show the corresponding information for runs 185 and 245 respectively. In the plots of $A(W_{SG})$ and $\kappa(W_{SG})$, squares indicate parameter values obtained by fitting to a zero temperature transition and circles correspond to fits made with finite values of $T_f(W_{SG})$.

There are two issues to be considered in separating effects on T_f from effects on the ESR linewidth. The first issue is field and frequency effects on T_f, and the second involves the depression of T_f with layer thickness. Thus far, all data has been analyzed in terms of the values of T_f measured at 100 G and a measuring time of 300 seconds. The use of the bulk T_f for all samples will not work; in very thin samples, the linewidth is barely out of the broad minimum at this temperature. We consider these effects in the following sections.

Table 7-16: Fits to $A+BT+C^*T^\kappa$ for Run 243 - $Cu_{0.89}Mn_{0.11}/Cu$

Run 243 - $Cu_{0.89}Mn_{0.11}$					
W (nm)	T_f (K)	A (G)	B (G/K)	C^* (G)	κ
500	47.5	No fit			
100	47.5	No Fit			
50	45.0	No Fit			
30	42.5	No Fit			
10	35.0	No Fit			
7	31.0	-199 ± 14	3.70 ± 0.02	$1.77(\pm.03) \times 10^8$	3.0 ± 0.2
3	20.5	-128 ± 15	3.73 ± 0.03	$1.57(\pm.02) \times 10^7$	2.5 ± 0.2
1	10.5	-76 ± 14	4.18 ± 0.03	$2.57(\pm.06) \times 10^6$	2.4 ± 0.2

Table 7-17: Fits to $A+BT+C^*T^\kappa$ for Run 185 - $Cu_{0.93}Mn_{0.07}/Cu$

Run 185 - $Cu_{0.93}Mn_{0.07}$					
W (nm)	T_f (K)	A (G)	B (G/K)	C^* (G)	κ
1000	37.5	No Fit			
100	38.8	No Fit			
50	36.0	No Fit			
30	35.0	No Fit			
7	25.0	-27 ± 13	3.45 ± 0.14	3.01(±.08) x 10^8	3.4 ± 0.2
5	23.5	-104 ± 13	3.19 ± 0.04	1.90(±.02) x 10^{10}	3.7 ± 0.2
3	17.5	-31 ± 12	3.62 ± 0.14	5.93(±.08) x 10^8	3.7 ± 0.2

Table 7-18: Fits to $A+BT+C^*T^\kappa$ for Run 245 - $Cu_{0.93}Mn_{0.07}/Cu$

Run 245 - $Cu_{0.93}Mn_{0.07}$					
W (nm)	T_f (K)	A (G)	B (G/K)	C^* (G)	κ
30	33.0	No Fit			
10	27.0	No Fit			
9	26.0	No Fit			
7	23.5	No Fit			
6	21.0	-100 $\pm$ 13	3.42 $\pm$ 0.03	6.35($\pm$.16) x 10^9	4.1 $\pm$ 0.2
5	20.0	-101 $\pm$ 13	3.34 $\pm$ 0.03	5.19($\pm$.12) x 10^9	4.0 $\pm$ 0.2
3	16.6	-78 $\pm$ 13	3.83 $\pm$ 0.03	1.24($\pm$.03) x 10^7	2.7 $\pm$ 0.2
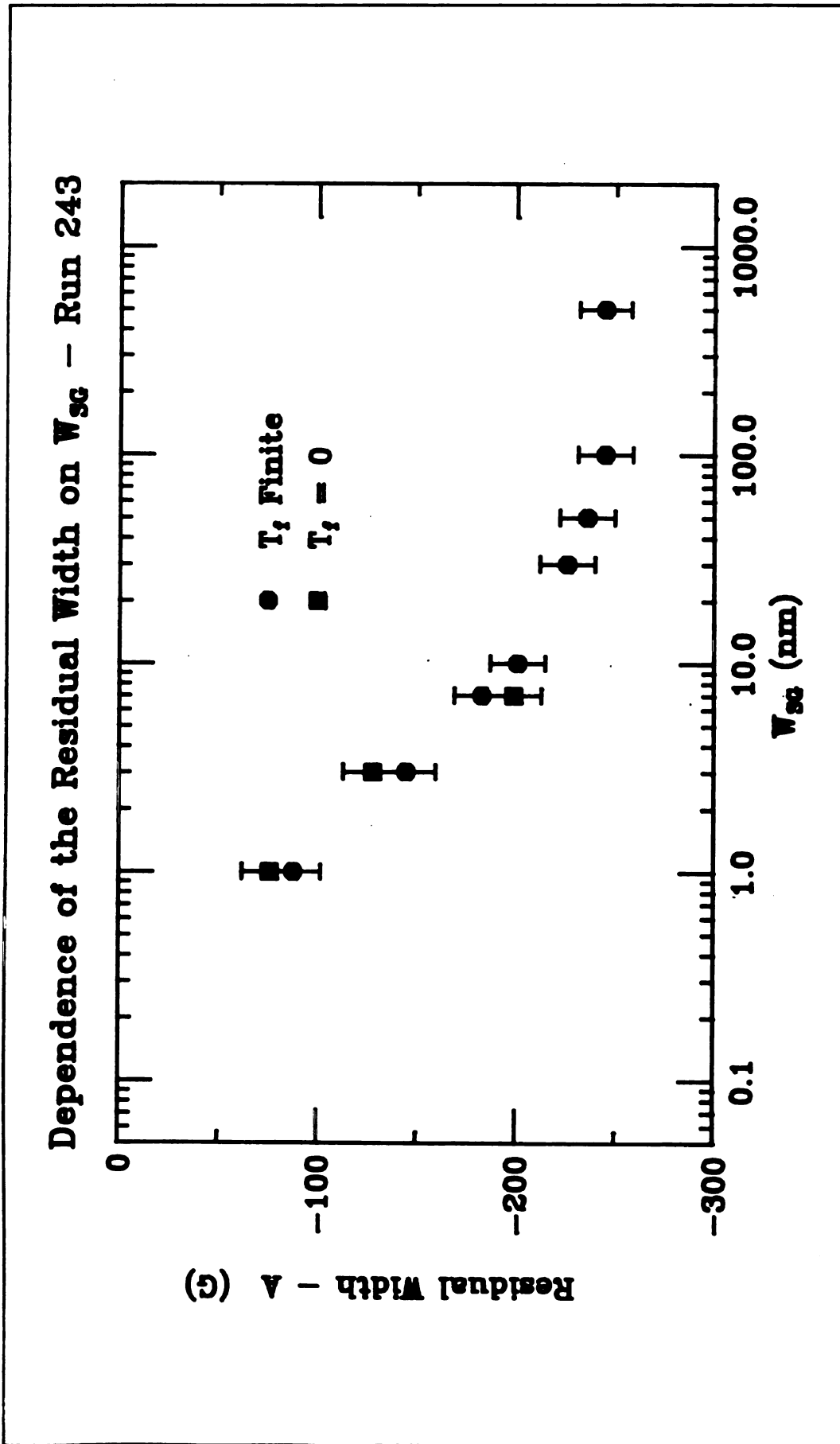
Figure 7-41: *Variation of the Residual Width, A, with W_{SG} for Run 243 - $Cu_{0.89}Mn_{0.11}$*
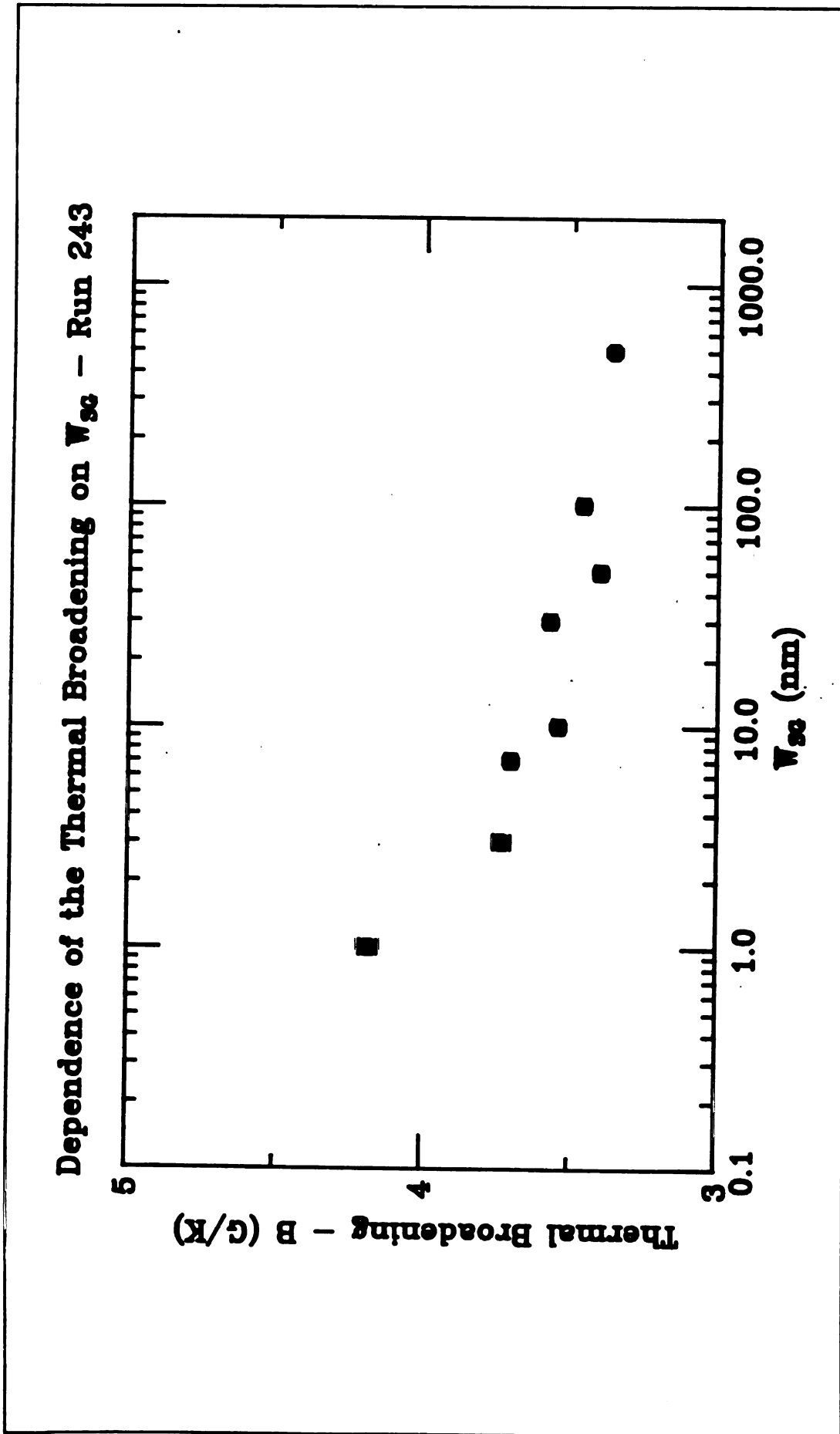
Figure 7-42: *Variation of the Thermal Broadening, B, with W_{SG} for Run 243 - $Cu_{0.89}Mn_{0.11}$*

218
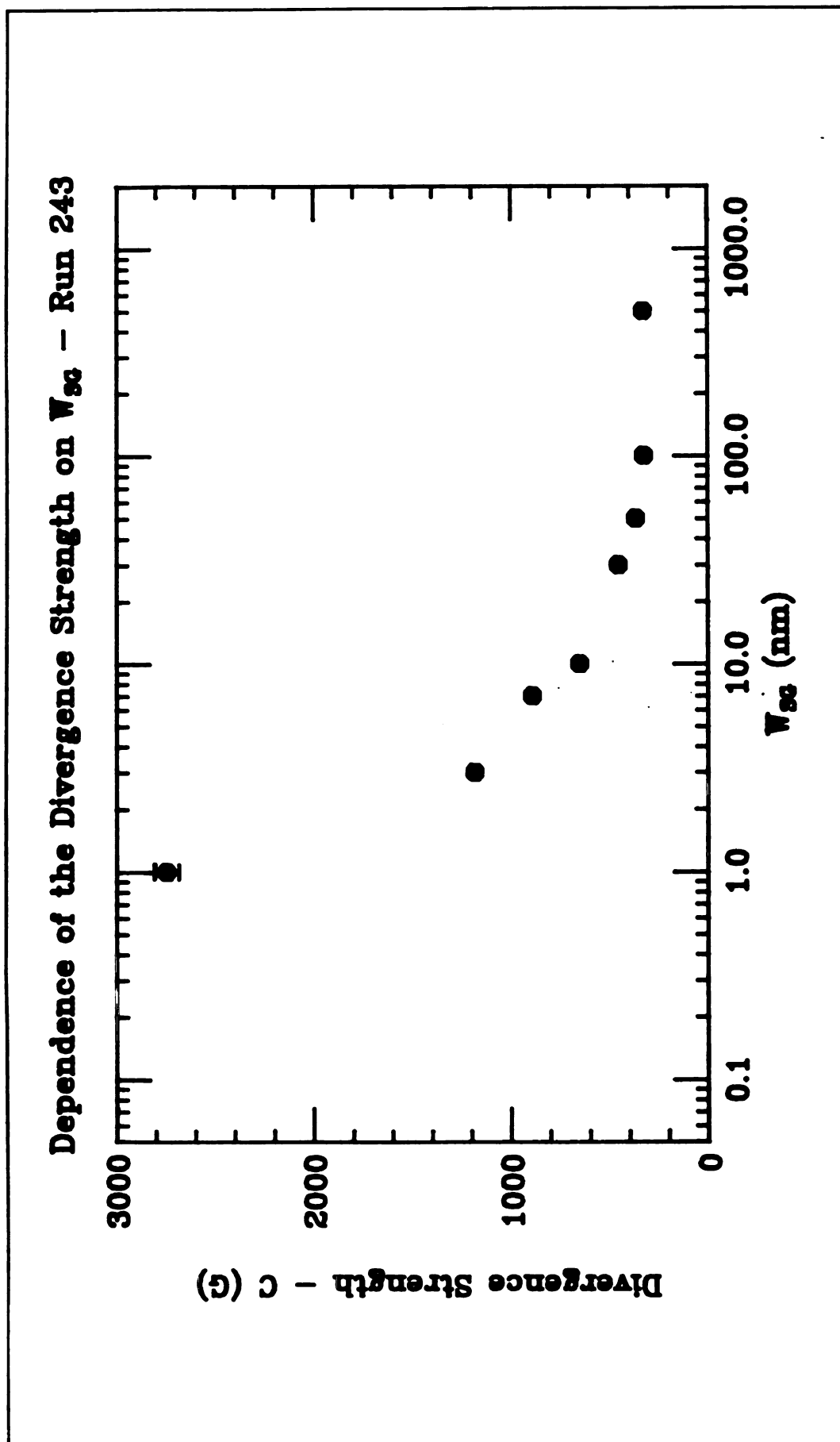
Figure 7-43: *Variation of the Divergence Strength, C, with W_{SG} for Run 243 - $Cu_{0.89}Mn_{0.11}$*
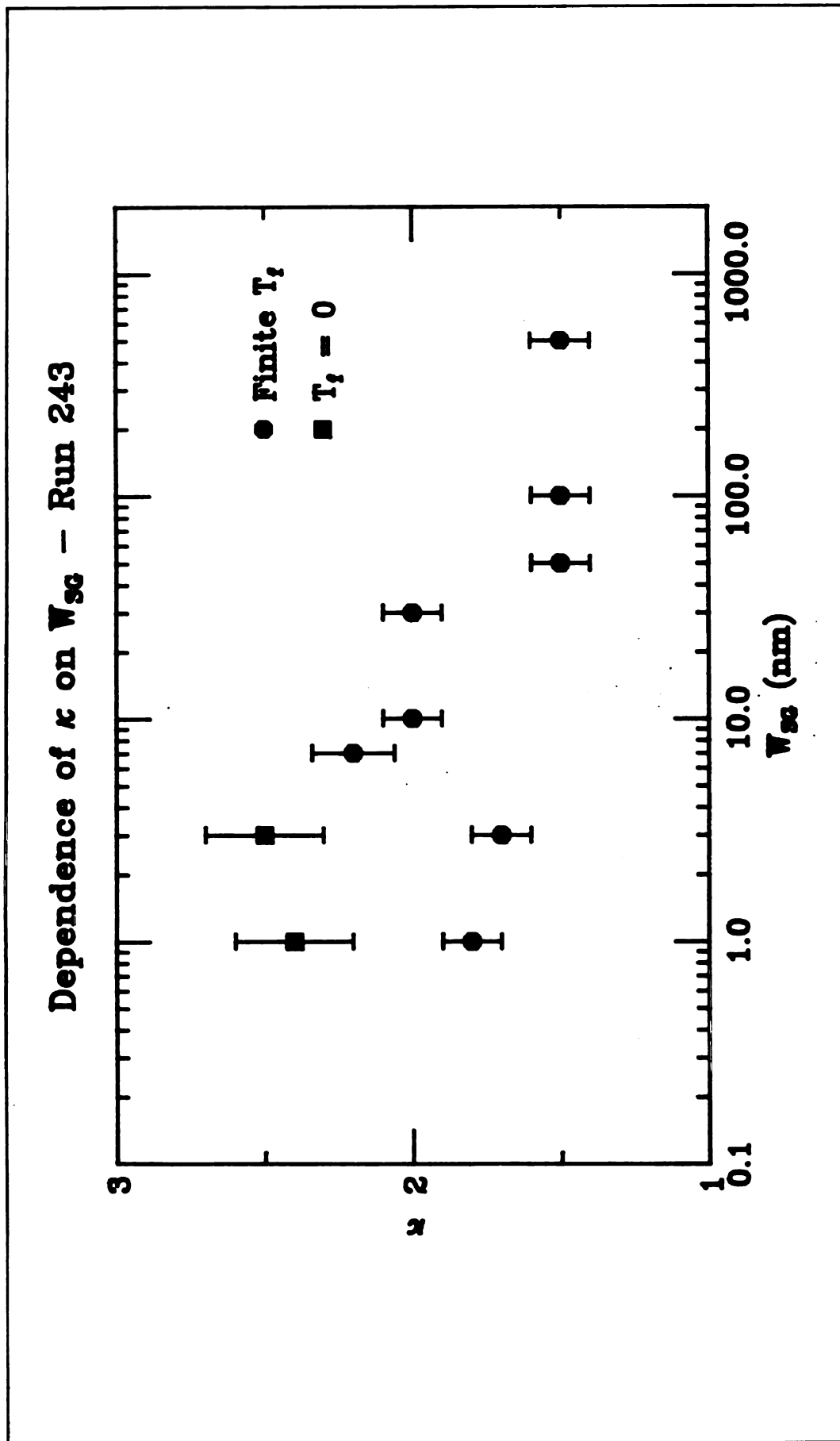
Figure 7-44: *Variation of κ with W_{SG} for run 243 - $Cu_{0.89}Mn_{0.11}$*
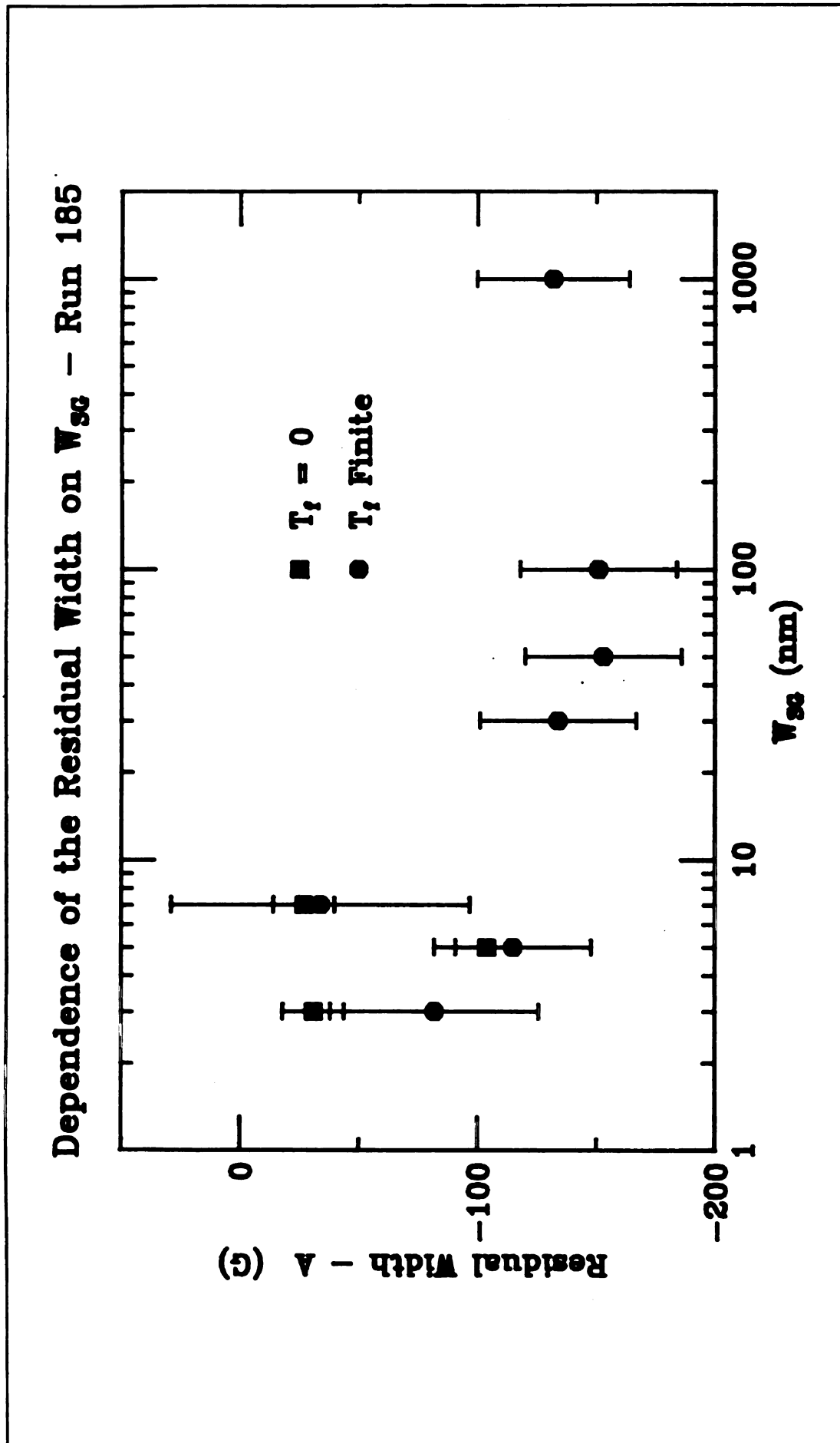
Figure 7-45: *Variation of the Residual Width, A, with W_{SG} for run 185 - $Cu_{0.93}Mn_{0.07}$*
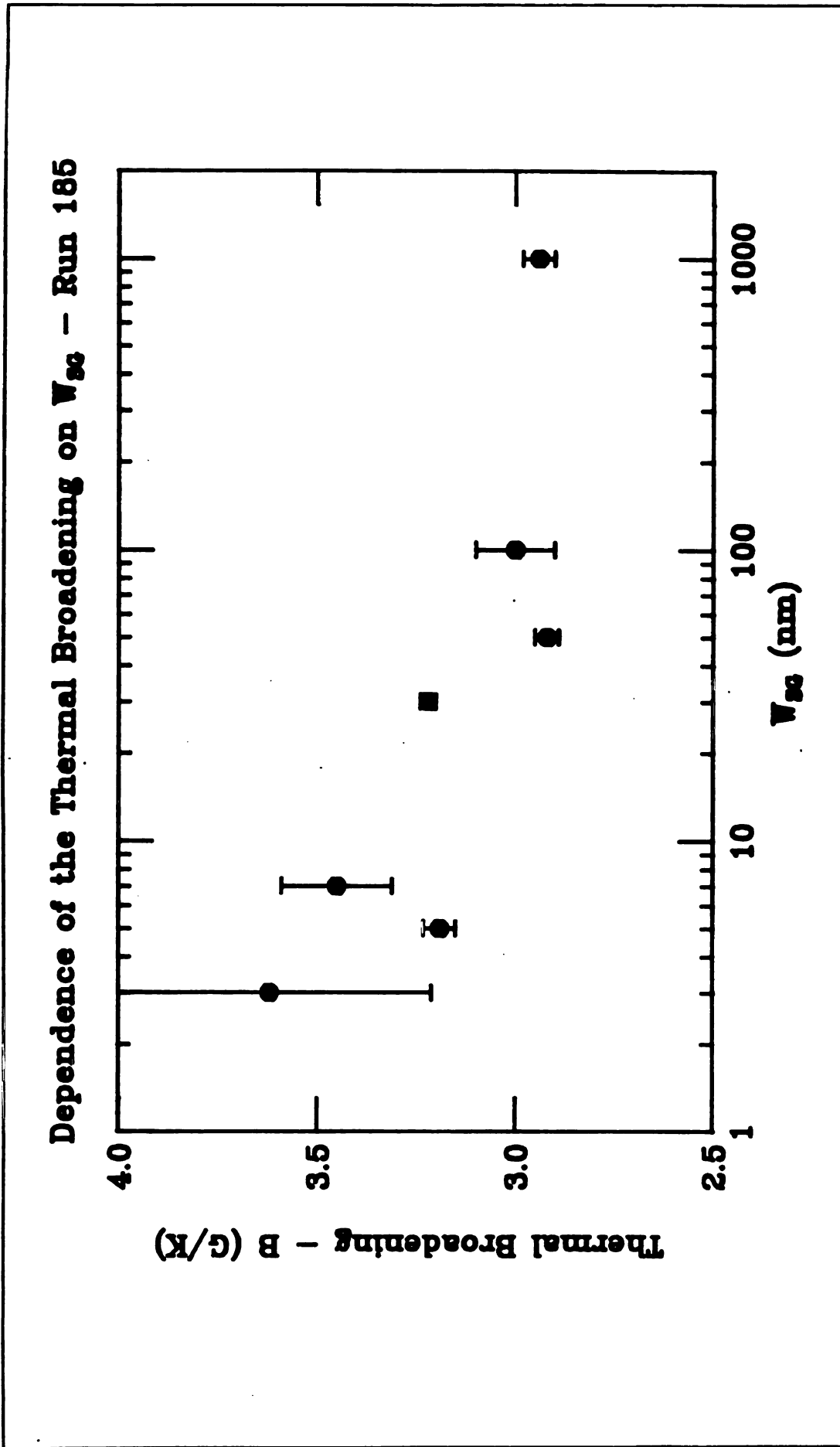
Figure 7-46: *Variation of the Thermal Broadening, B, with W_{SG} for run 185 - $Cu_{0.93}Mn_{0.07}$*
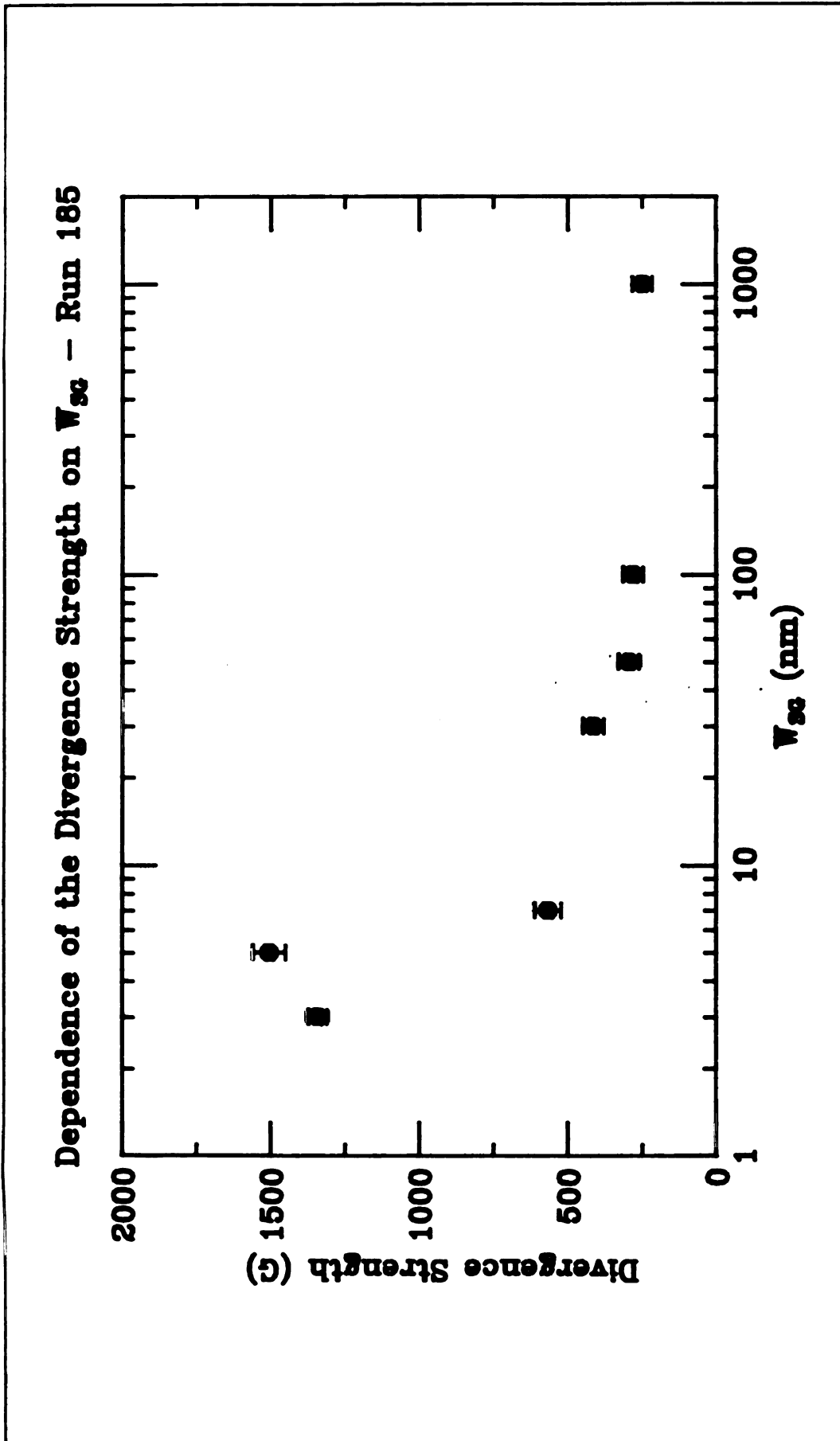
Figure 7-47: *Variation of the Divergence Strength, C, with W_{SG} for run 185 - $Cu_{0.93}Mn_{0.07}$*
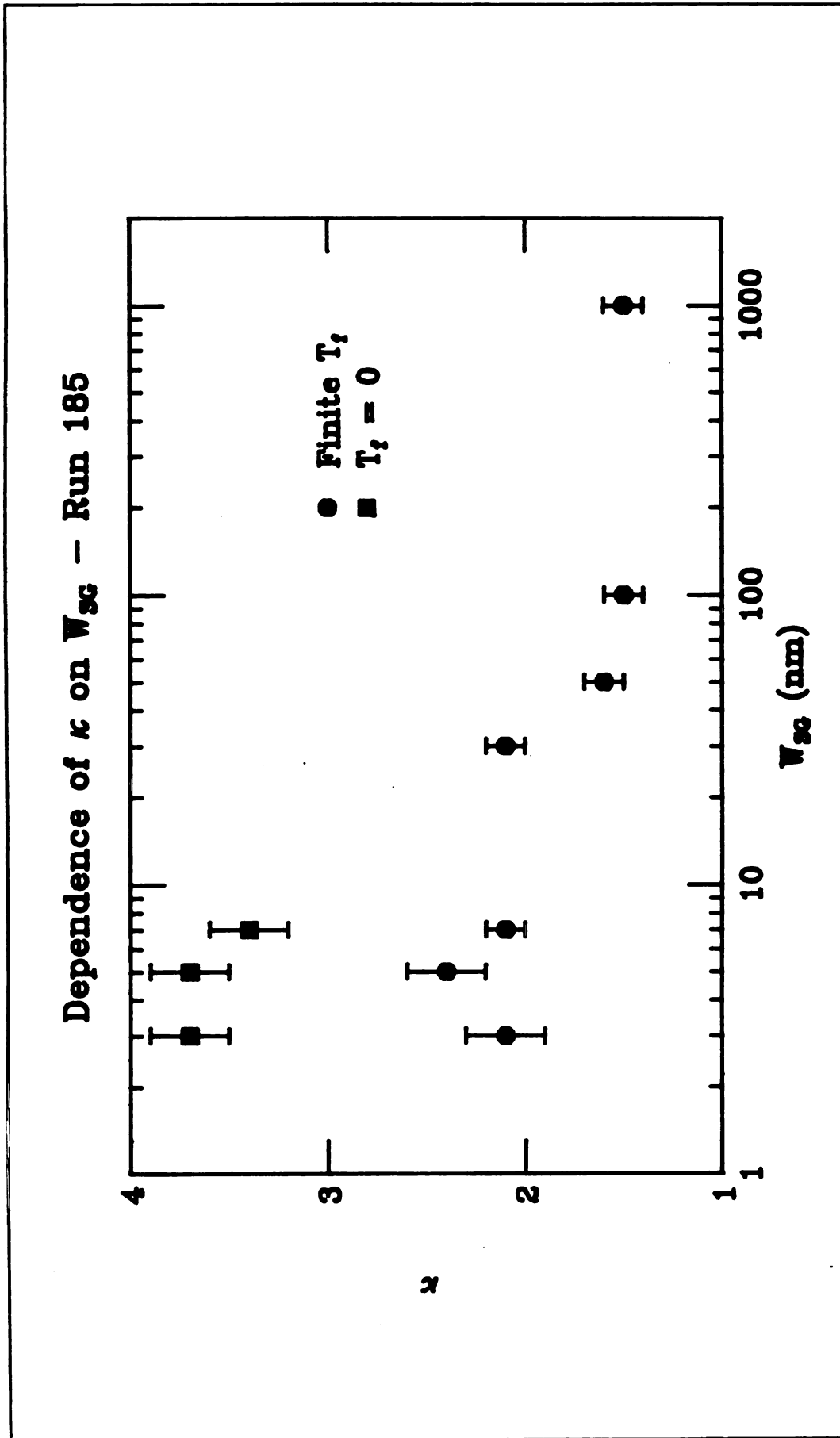
Figure 7-48: *Variation of κ with W_{SG} for run 185 - $Cu_{0.93}Mn_{0.07}$*
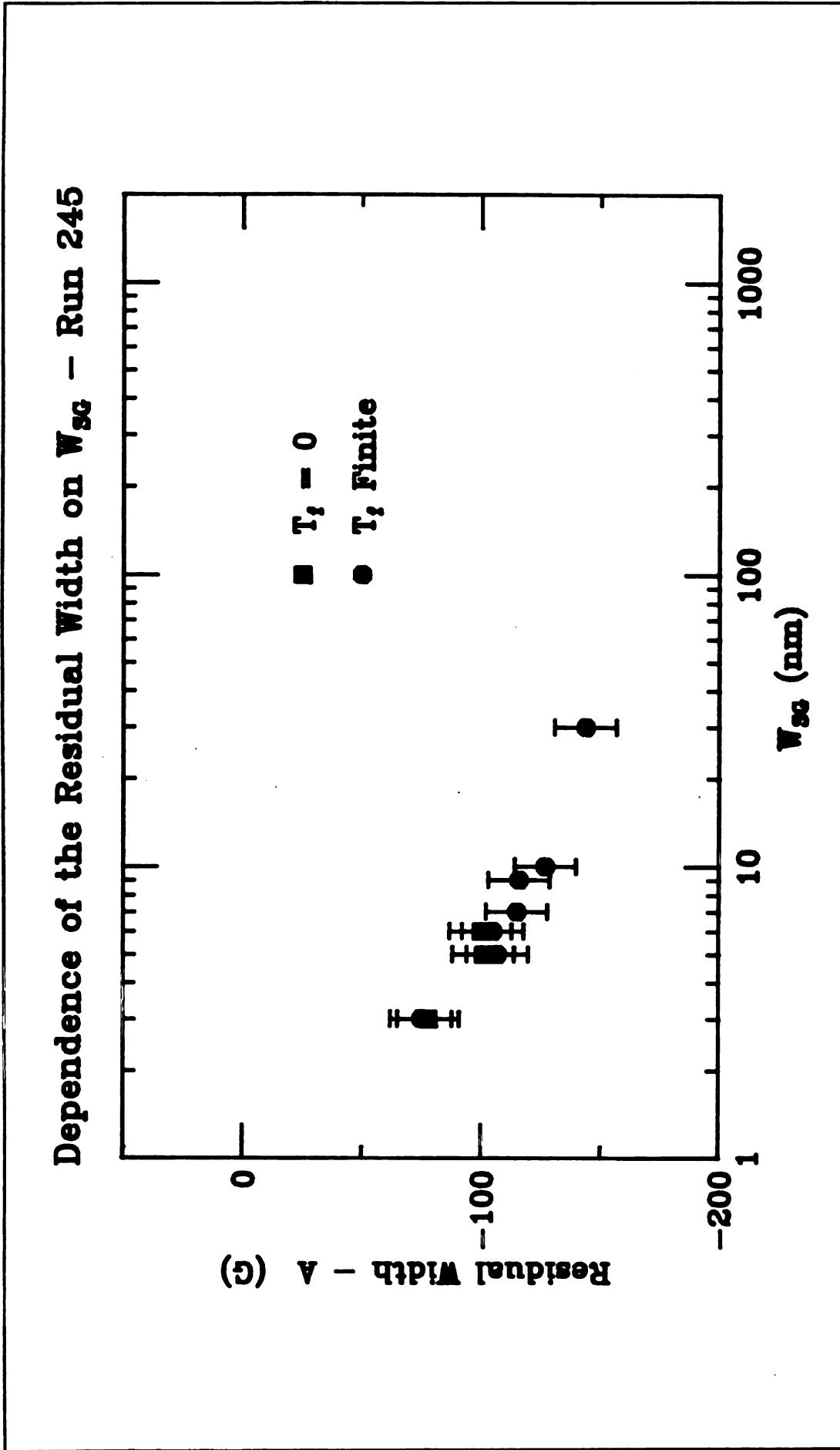
Figure 7-49: *Variation of the Residual Width, A, with W_{SG} for run 245 — $Cu_{0.93}Mn_{0.07}$*
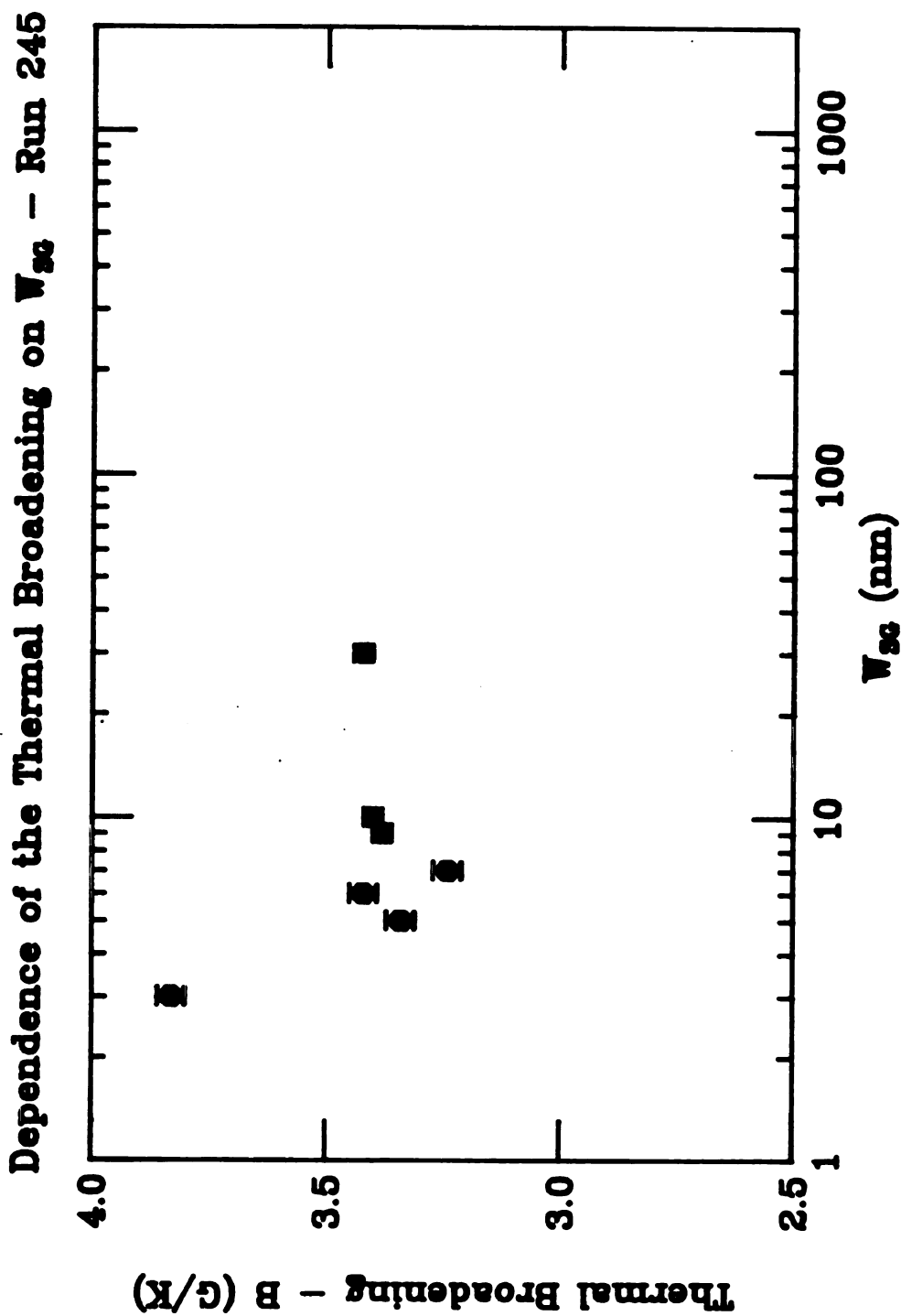
Figure 7-50: *Variation of the Thermal Broadening, B, with W_{SG} for run 245- $Cu_{0.93}Mn_{0.07}$*
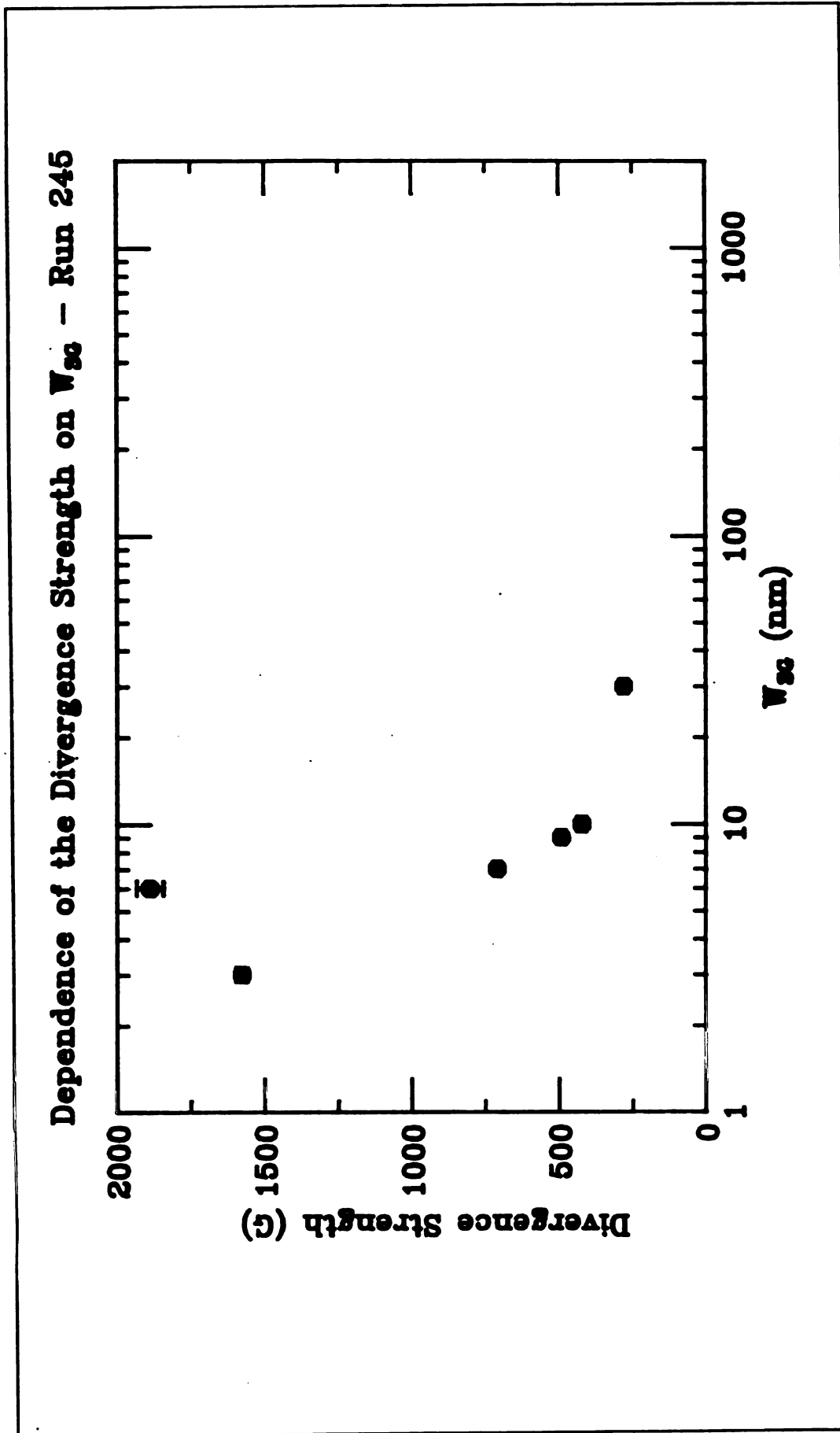
Figure 7-51: *Variation of the Divergence Strength, C, with W_{SG} for run 245 - $Cu_{0.93}Mn_{0.07}$*
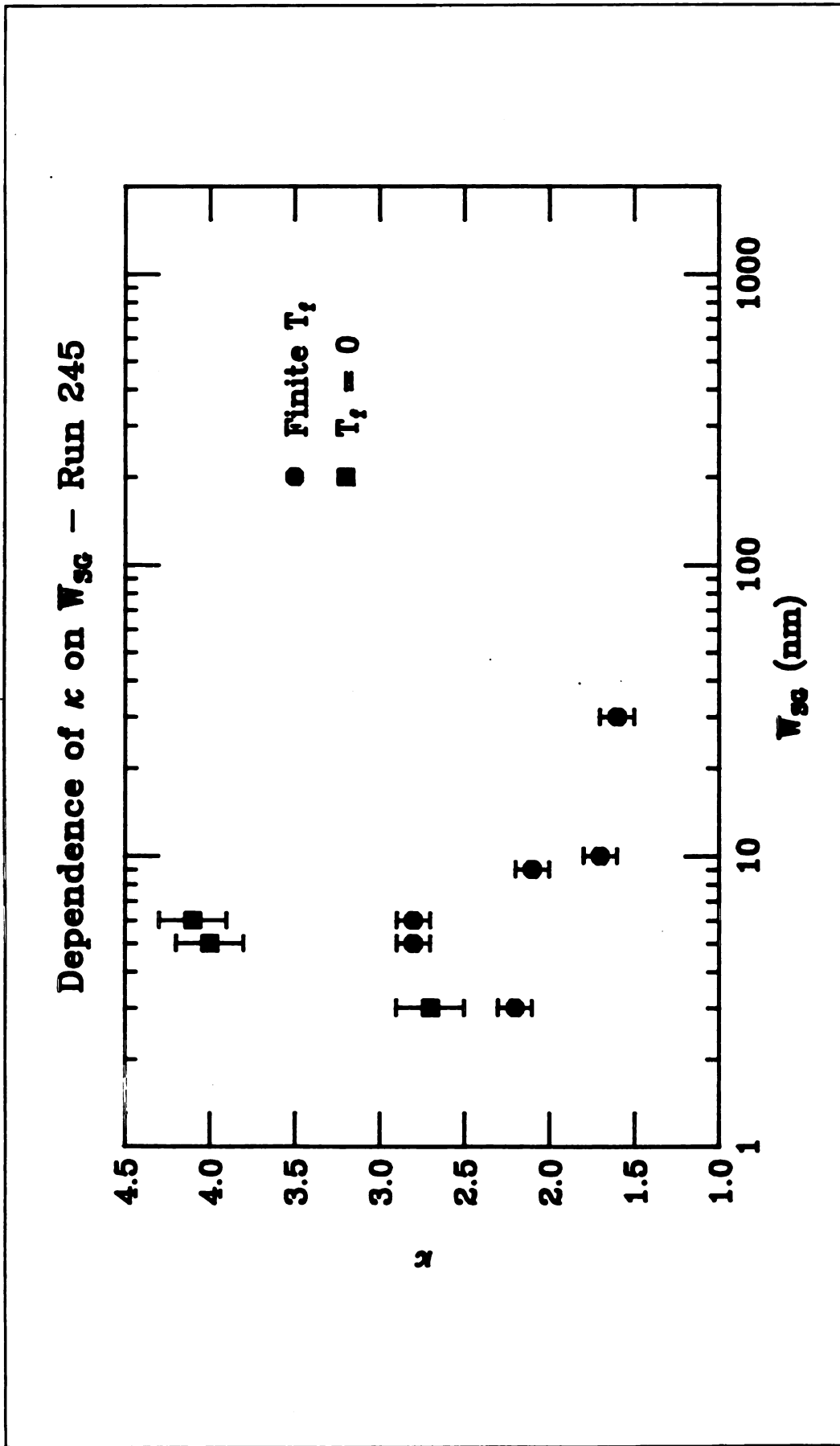
Figure 7-52: *Variation of κ with W_{SG} for run 245 - $Cu_{0.93}Mn_{0.07}$*

Field and Frequency Effects on $T_f(W_{SG})$

In general, the freezing temperature is a function of measuring field, frequency and spin glass layer thickness, so that we must consider $T_f(W_{SG}, H, \omega)$. In ESR measurements, the frequency determines the field used - a frequency of 1 GHz requires a magnetic field of 300 G. For ESR at 9 GHz, a 3300 G field is required. We have seen in Chapter 4 that field and frequency effects have opposite actions on T_f; an increased magnetic field results in a depressed value of T_f, and an increased frequency results in a larger value of T_f. We have also seen that, as the layer thickness is reduced, the form of the frequency dependence changes.

According to the prediction by Fischer[59], and the experimental data by Kenning, et. al.[83], the magnetic field dependence of T_f is different in low fields than in high fields, with the crossover point experimentally found to be between 300 and 500 G in $Cu_{0.93}Mn_{0.07}/Cu$ multilayers for W_{SG} = 2 nm to 500 nm and fields from 2 G to 15000 G. We can use this data to predict the freezing temperature over the range of magnetic fields used in the ESR experiment. Concentration dependence can be taken into account by scaling the freezing temperature like concentration to the 2/3 power.[153]. Table 7-19 summarizes the values predicted for $Cu_{0.89}Mn_{0.11}/Cu$ for the range of fields used in the ESR experiment.

This table shows that the percent change of the value of $T_f(W_{SG}, H)$ from the value measured at 100 G is much greater in the thinner layers than in the thicker layers. For the 1 nm sample, the change from the 'DC' measurement is a 40 to 68 percent depression, while the corresponding change for the 500 nm samples is only 12 to 23

percent. In bulk AgMn, Wu, *et. al.*[107], claim that the freezing temperature is roughly field independent for the magnetic fields used for ESR and assume a single value of T_f for all fields and frequencies in their scaling analysis, in contrast to the predictions of Table 7-19.

The Uppsala group has measured the frequency dependence of the freezing temperature over eight decades from 10^{-4} to 10^4 seconds. Holtzberg, *et. al.*[154] have made a similar measurement on EuSrS from 17 Hz to 2100 Hz, and used a resonant cavity technique to measure T_f at 9 GHz. The EuSrS results indicate that a Fulcher law with a characteristic time of 10^{-13} s describes the data for all frequencies, including 9 GHz.

Assuming this extrapolation to 9 GHz is valid for CuMn, we can use the Uppsala measurements to predict a value of T_f at 9.3 GHz. Figure 7-53 shows the measured values of T_f from the Uppsala data, and the extrapolated T_f at 9.3 GHz. Table 7-20 shows the values of T_f at 9.3 GHz for $Cu_{0.89}Mn_{0.11}$ assuming both a finite T_g and $T_g = 0$. (Recall that T_g is the equilibrium freezing temperature.)

Figure 7-54 shows the ranges of predicted T_f's from the two field/frequency regimes; the circles represent the Uppsala prediction [$T_f(W_{SG}, 10 \text{ G}, 10^{-10} \text{ s})$], the squares represent the magnetic field dependence for the fields used in the ESR experiment [$T_f(W_{SG}, 1000 \text{ G} < H < 6000 \text{ G}, 300 \text{ s})$] and the diamonds represent the values used in the fitting presented here, $T_f(W_{SG}, 100 \text{ G}, 300 \text{ s})$.

Part of the problem in combining these two effects to obtain T_f at conditions appropriate to ESR is that the frequency dependent measurementswere made in the low field regime, which should exhibit Ising-like behavior according to Fischer's predictions,

Table 7-19: Predicted Dependence of T_f on Magnetic Field for $Cu_{0.89}Mn_{0.11}/Cu$

Run 243 - $Cu_{0.89}Mn_{0.11}$				
W_{SG} (K)	$T_f(100\ G)$ (K)	$T_f(1000\ G)$ (K)	$T_f(3300\ G)$ (K)	$T_f(6000\ G)$ (K)
500	47.5	41.7	39.0	36.7
100	47.5	40.4	37.8	35.4
50	45.0	39.8	37.2	34.9
30	42.5	35.3	32.8	30.6
10	35.0	25.8	23.5	21.5
7	31.0	22.7	20.5	18.5
3	20.5	15.3	13.4	11.7
1	10.0	5.9	4.5	3.2
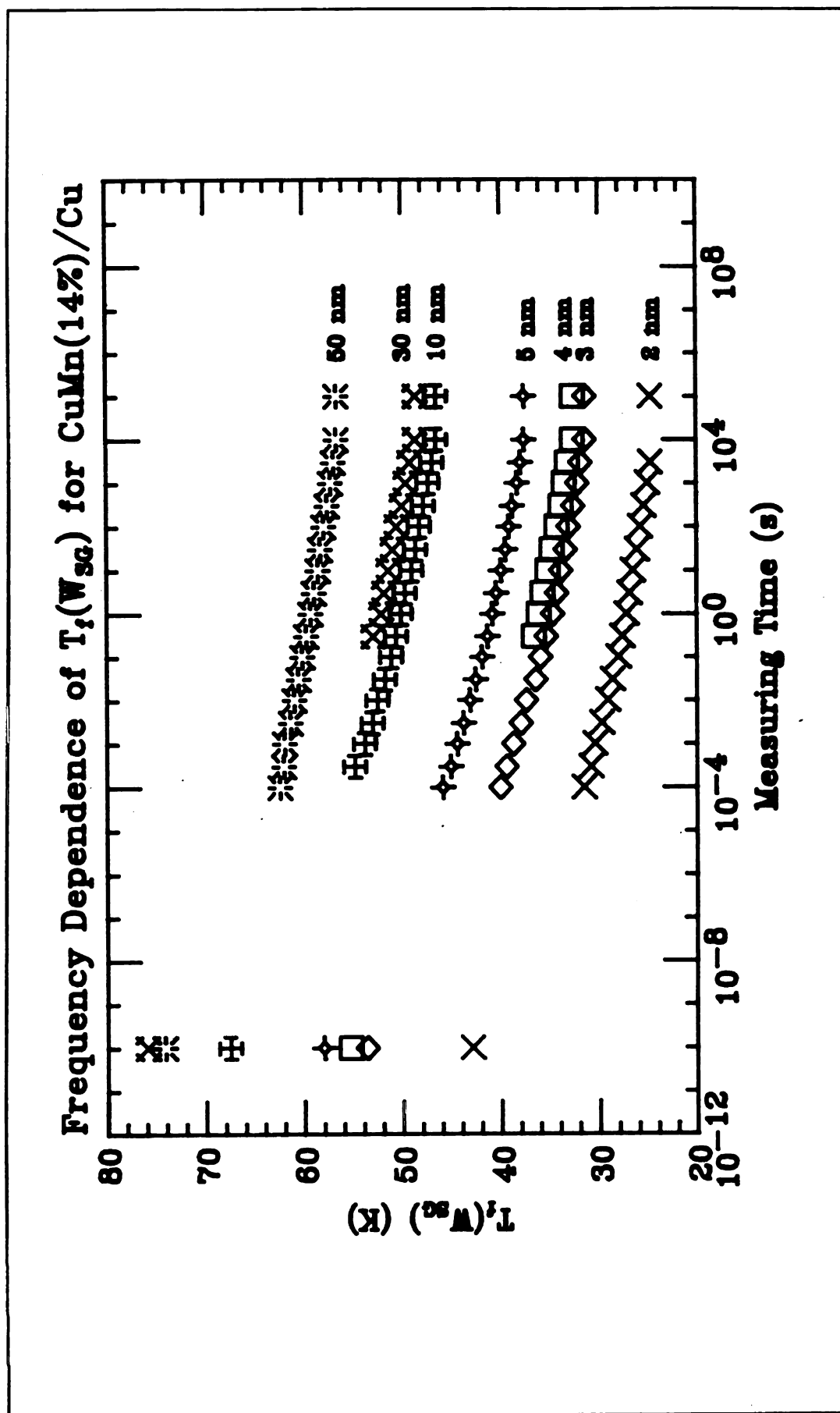
Figure 7-53: *Extrapolation of $T_f(W_{SG})$ at 9.3 GHz for $Cu_{0.89}Mn_{0.11}$.*

Table 7-20: Extrapolation of T_f to 9.3 GHz for $Cu_{0.89}Mn_{0.11}/Cu$

W_{SG} (nm)	T_f(9.3 GHz) (K) T_g = finite	T_f(9.3 GHz) (K) T_g = 0
2	-	42.9
3	-	53.6
4	55.3	54.4
5	58.0	56.6
10	67.5	65.6
20	71.7	68.2
30	75.9	72.4
50	74.1	65.7

while the ESR data is taken well within the Heisenberg-like regime. If we were to use the value of T_f at 9.3 GHz as extrapolated from the Uppsala data in Fischer's prediction for the Heisenberg-like regime, we would substantially overestimate T_f. Use of the values of T_f extrapolated from the Uppsala data with no field correction in Equation 7-4 is incorrect, as the linewidths continue to diverge for temperatures below these values.

Fitting to Equation 7-4 with the value of T_f predicted to apply at 3300 G (roughly the position of the resonance peak center) results in a systematic shift in the parameters A, C and κ. The thermal broadening coefficient remains roughly constant and the trends with decreasing layer thicknesses are unchanged.

The analysis presented in this section leads us to conclude that, at present, we have no better alternative to using the value of T_f from the quasi-static SQUID measurements at 100 G. All of the literature on ESR in bulk spin glasses uses quasi-static measurements of the freezing temperature in analysis of $\Delta H(T)$, which will facilitate comparison between this data and other reports.

Effect of the Depression of T_f on Equation 7-4

The effect of dimensionality and finite size in depressing $T_f(W_{SG})$ in these multilayers has been well documented in Chapter Four. The presence of T_f in Equation 7-4 complicates interpretation of this expression. We must be very careful that the effects of the depression of T_f are separated from possible dimensionality and finite size effects on $\Delta H(T)$. The similarity of the $\Delta H(T)$ curves for all layer thicknesses suggests
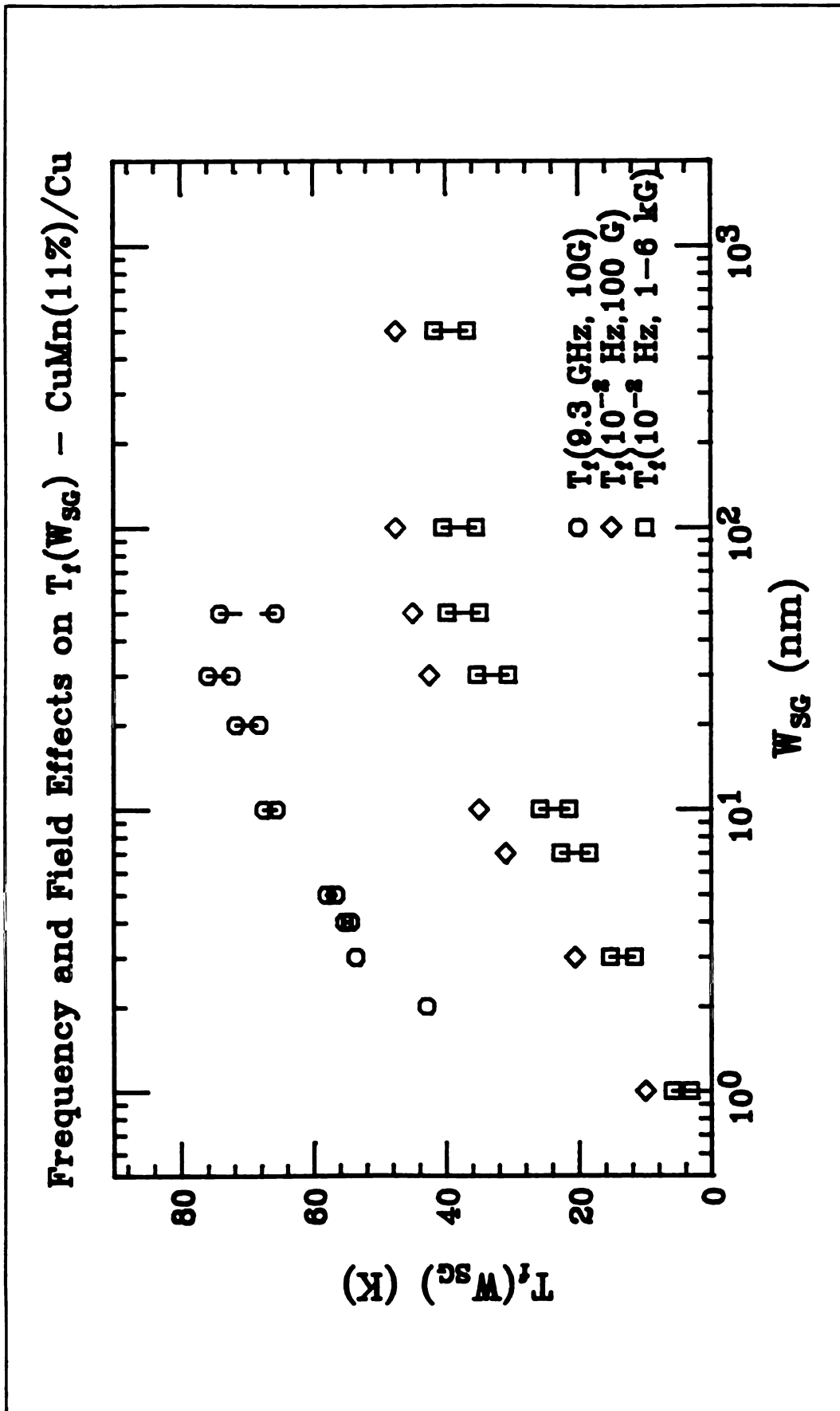
Figure 7-54: *Field and Frequency Effects on $T_f(W_{SG})$ for $Cu_{0.89}Mn_{0.11}$*

that there might be a simple transformation - such as a temperature shift - which will allow us to essentially remove the effects of the depression of T_f.

In general, there exists some function which relates $T_f(W_{SG})$ to the bulk freezing temperature, $T_f(\infty)$. We can look at the specific case of finite size scaling as given by Equation 7-1, although the same analysis is applicable to any general relationship between $T_f(W_{SG})$ and $T_f(\infty)$. We can solve Equation 7-1 for $T_f(W_{SG})$ in terms of $T_f(\infty)$ and plug this result into Equation 7-4. This allows us to write a more general equation which is expressed in terms of a shifted temperature, T'.

$$T' = T + \alpha \ W_{SG}^{-\lambda} \ T_f(\infty) = T + T_f(\infty) - T_f(W_{SG}) \qquad \textbf{7-6}$$

The shift in the temperature scale, T_s, is just the difference between the freezing temperature at W_{SG} and the bulk freezing temperature. Equation 7-4 becomes

$$\Delta H(T') = A' + B \ T' + C' \left(\frac{T' - T_f(\infty)}{T_f(\infty)} \right)^{-\kappa} \qquad \textbf{7-7}$$

where the parameters in Equation 7-7 are related to those in Equation 7-4 by

$$A' = A - B \ \alpha \ W_{SG}^{-\lambda} \ T_f(\infty) = A + B \left(T_f(\infty) - T_f(W_{SG}) \right) \qquad \textbf{7-8}$$

$$C' = C \left(1 - \alpha \ W_{SG}^{-\lambda} \right)^{-\kappa} = C \left(\frac{T_f(W_{SG})}{T_f(\infty)} \right)^{-\kappa} \qquad \textbf{7-9}$$

By using the relationships given by Equations 7-8 and 7-9, we can determine to what extent the trends observed in fitting to the measured $T_f(W_{SG})$ (Equation 7-4) are due to the depression of $T_f W_{SG}$. The values of A and C are predicted to change, but the values of B and κ should remain invariant under this transformation. Tables 7-21 through 7-23 compare the values of A and C under the transformations. Figures 7-55 through 7-60 graphically illustrate the effect of using $T_f(W_{SG})$ in Equation 7-4.

The changes due to this shift are very illustrative, especially in the case of Run 243. The residual width has the same value for all layer thicknesses when fit to Equation 7-7. The divergence strength, C, takes on roughly the same value for all layer thicknesses ≥ 7 nm. Below this thickness, the analysis for Run 243 results in a lower value for the divergence strength. The analysis for run 245 also indicates a departure from systematic behavior at about $W_{SG} = 7$ nm, but the values of C for samples less thanthis thickness are larger than the bulk value. The data for Run 185 indicates a failure between 30 and 7 nm; the quality of the data and the lack of data between these two layer thicknesses makes it difficult to localize where the failure begins. The values of C are on average overestimated, with the exception of the 5 nm sample which has already been identified as behaving anomalously.

Regardless of the model used to predict the depression of the freezing temperature, the temperature shift will always be equal to the difference $T_f(W_{SG})$ and

Table 7-21: Parameters A and C after removal of $T_f(W_{SG})$ dependence of Equation 7-4 for Run 243 - $Cu_{0.89}Mn_{0.11}/Cu$

Run 243 - $Cu_{0.89}Mn_{0.11}$					
W	T_s	Residual Width (G)		Divergence Strength (G)	
(nm)	(K)	A$'$	A	C$'$	C
500	0	-245 ± 13	-245 ± 13	328 ± 13	328 ± 13
100	0	-245 ± 14	-245 ± 14	324 ± 17	324 ± 17
50	2.5	-247 ± 12	-236 ± 14	337 ± 14	366 ± 16
30	5.0	-243 ± 14	-226 ± 14	363 ± 14	453 ± 16
10	12.5	-248 ± 13	-201 ± 14	353 ± 13	650 ± 13
7	16.5	-242 ± 14	-183 ± 14	349 ± 13	890 ± 17
3	27.5	-244 ± 15	-145 ± 15	281 ± 13	1182 ± 21
1	37.5	-246 ± 12	-88 ± 14	166 ± 13	2745 ± 63

Table 7-22: Parameters A and C after removal of $T_f(W_{SG})$ dependence of Equation 7-4 for Run 185 - $Cu_{0.93}Mn_{0.07}/Cu$

Run 185 - $Cu_{0.93}Mn_{0.07}$					
W	T₌	Residual Width (G)		Divergence Strength (G)	
(nm)	(K)	A′	A	C′	C
1000	1.5	-135 ± 32	-132 ± 32	240 ± 33	248 ± 33
100	0.2	-152 ± 33	-151 ± 33	278 ± 34	280 ± 34
50	3.0	-162 ± 33	-153 ± 33	259 ± 34	294 ± 35
30	4.0	-147 ± 33	-134 ± 33	329 ± 35	413 ± 36
7	14.0	-82 ± 63	-34 ± 63	233 ± 46	566 ± 45
5	15.5	-164 ± 33	-115 ± 33	446 ± 38	1504 ± 56
3	21.5	-156 ± 44	-82 ± 44	263 ± 36	1340 ± 31

Table 7-23: Parameters A and C after removal of $T_f(W_{SG})$ dependence of Equation 7-4 for Run 245 - $Cu_{0.93}Mn_{0.07}/Cu$

Run 245 - $Cu_{0.93}Mn_{0.07}$					
W	T_s	Residual Width (G)		Divergence Strength (G)	
nm	K	A′	A	C′	C
30	4.5	-160 ± 13	-144 ± 13	228 ± 14	280 ± 15
10	10.5	-162 ± 15	-127 ± 13	242 ± 14	423 ± 17
9	11.5	-155 ± 13	-116 ± 13	229 ± 13	429 ± 16
7	14.0	-160 ± 13	-115 ± 13	279 ± 15	710 ± 14
6	16.5	-161 ± 13	-105 ± 13	372 ± 19	1888 ± 46
5	17.5	-165 ± 13	-107 ± 13	493 ± 21	2868 ± 65
3	20.9	-155 ± 13	-75 ± 13	262 ± 13	1576 ± 20
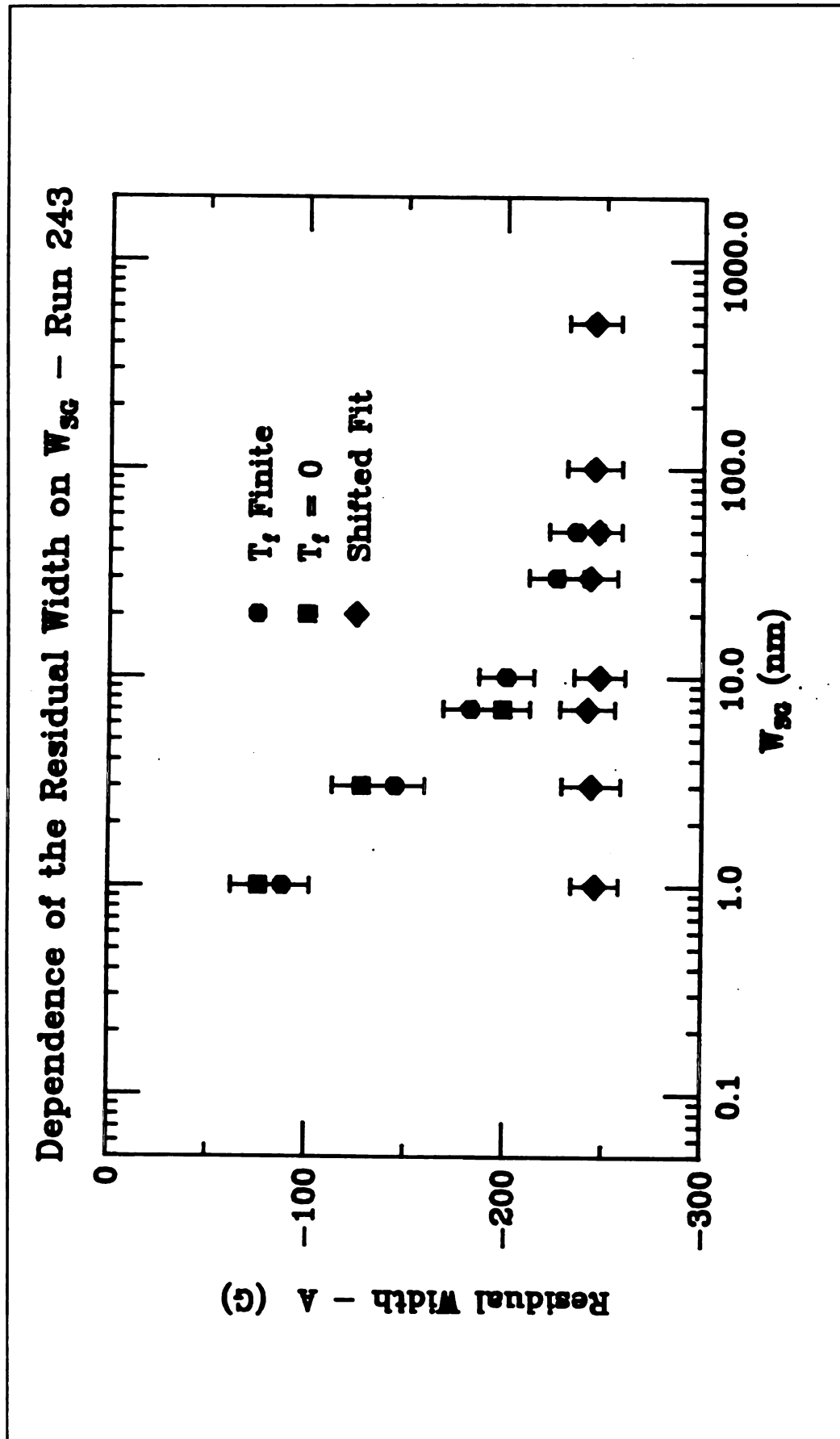
Figure 7-55: *Comparison of the Residual Width from Equation 7-4 and 7-7 for 243 $Cu_{0.89}Mn_{0.11}$*
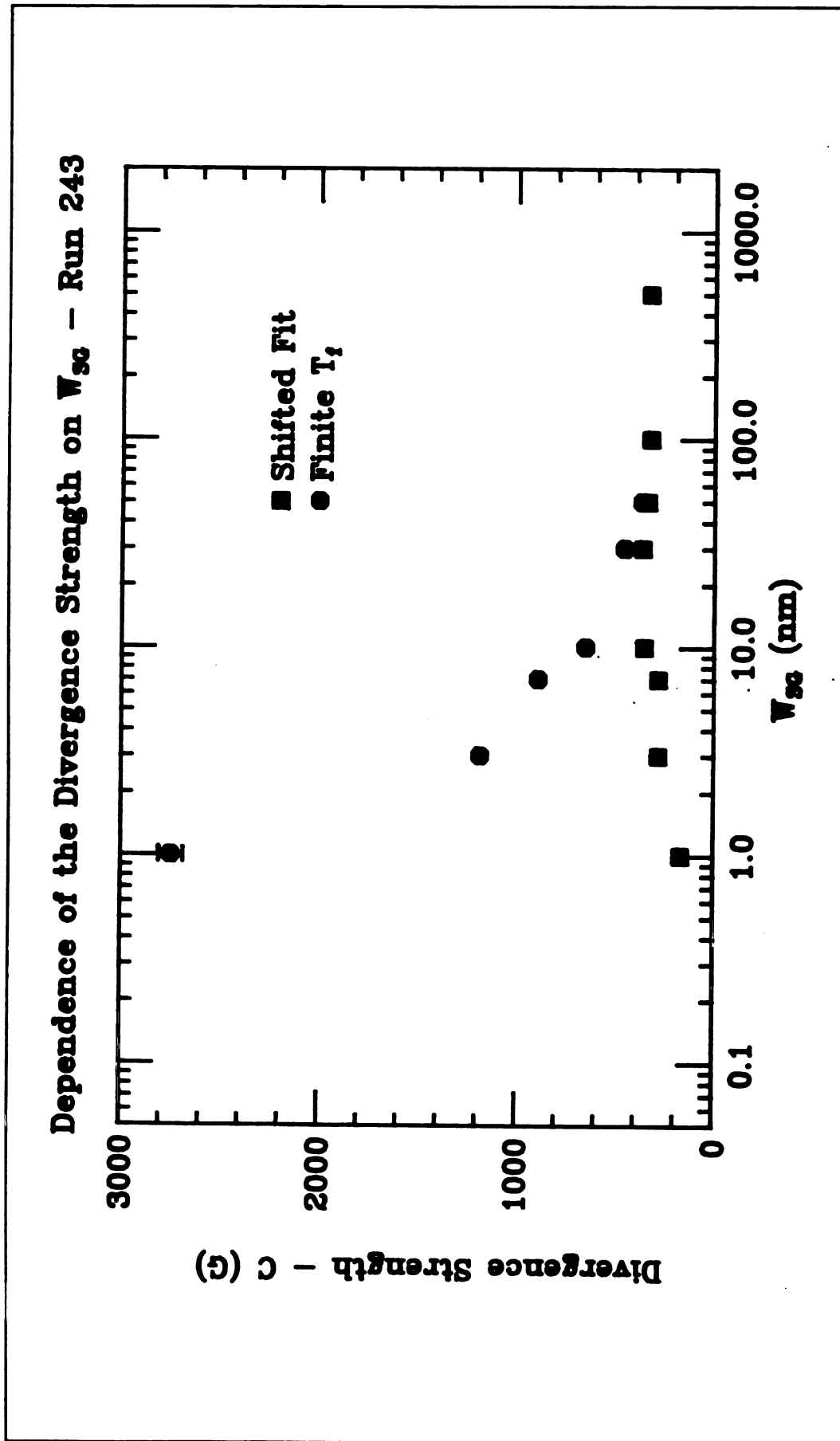
Figure 7-56 *Comparison of Divergence Strength From Equation 7-4 and 7-7 for Run 243 Cu$_{0.89}$Mn$_{0.11}$*
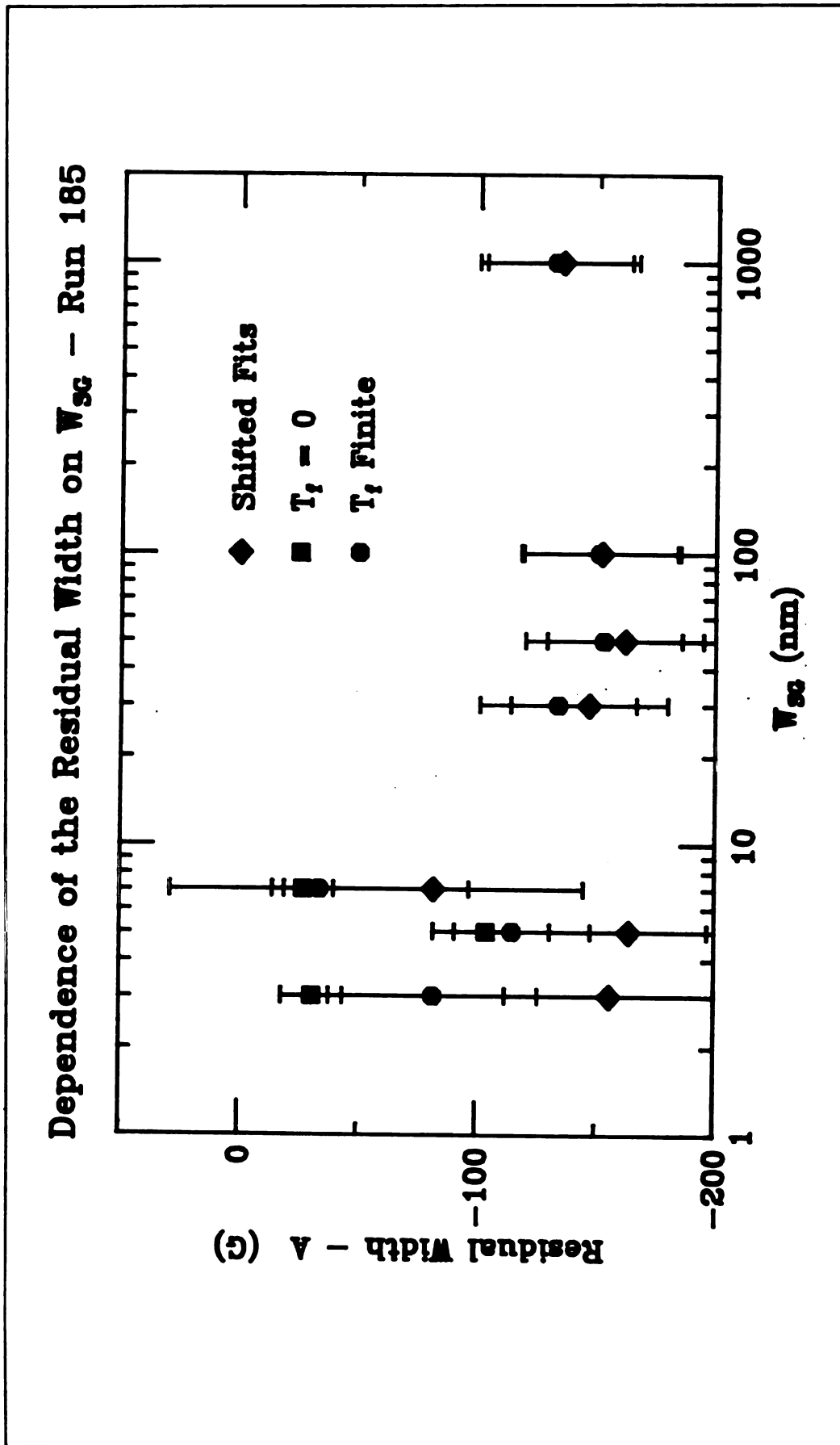
Figure 7-57: *Comparison of the Residual Width from Equations 7-4 and 7-7 for Run 185 - $Cu_{0.93}Mn_{0.07}$*
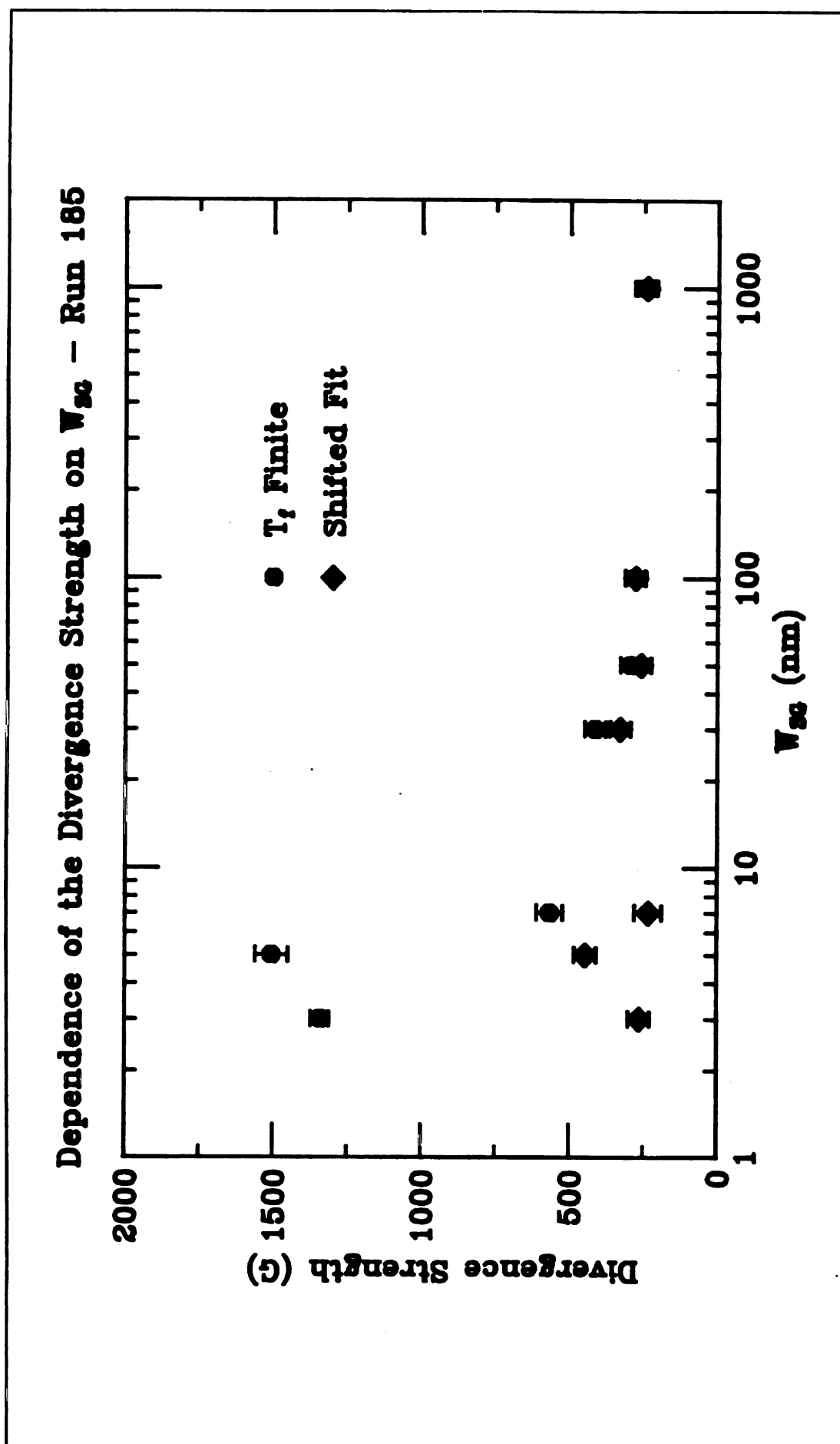
Figure 7-58: *Comparison of the Divergence Strength from Equations 7-4 and 7-7 - Run 185 - $Cu_{0.93}Mn_{0.07}$*
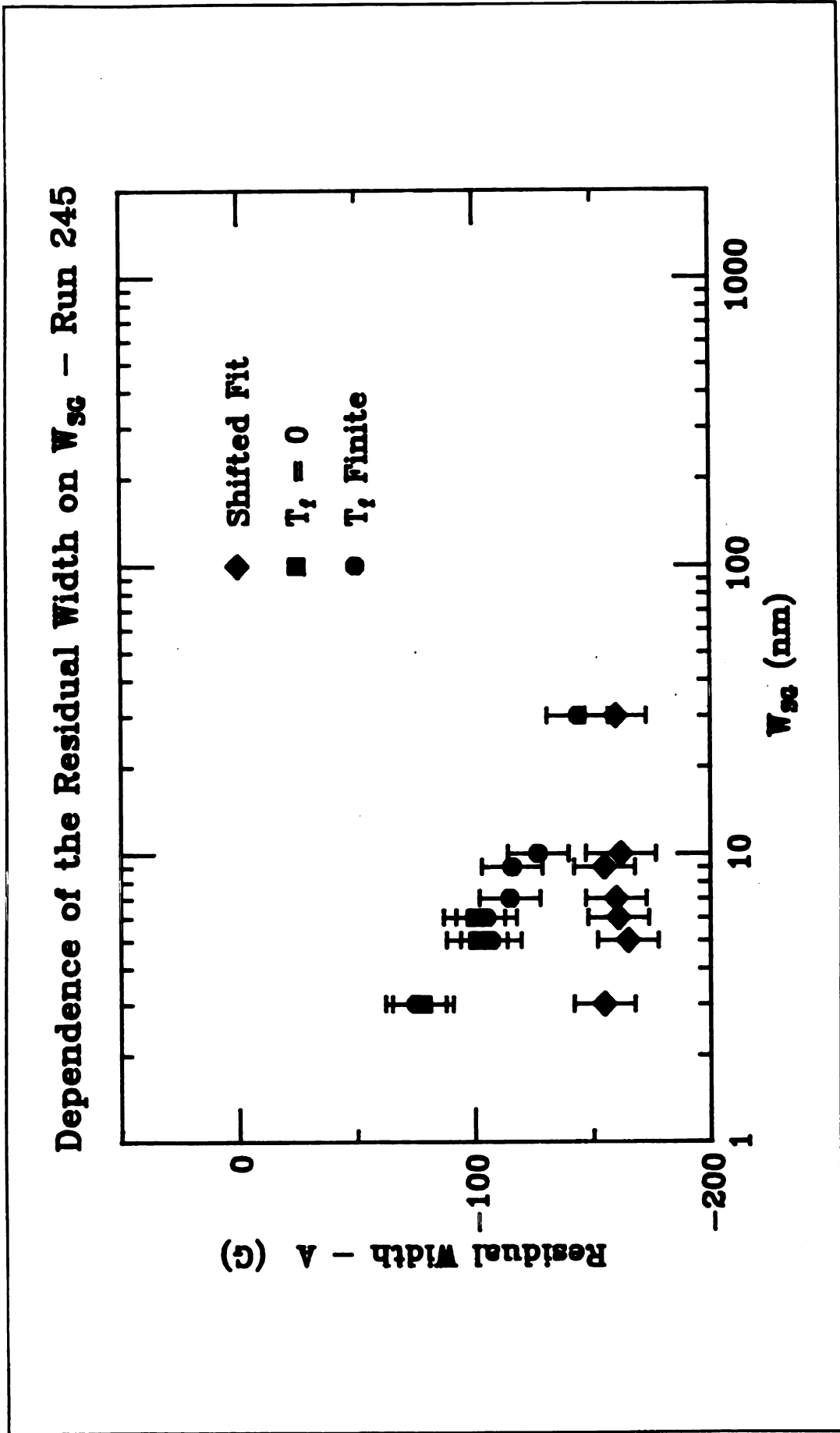
Figure 7-59: *Comparison of Residual Width from Equations 7-4 and 7-7 - Run 245 - $Cu_{0.93}Mn_{0.07}$*
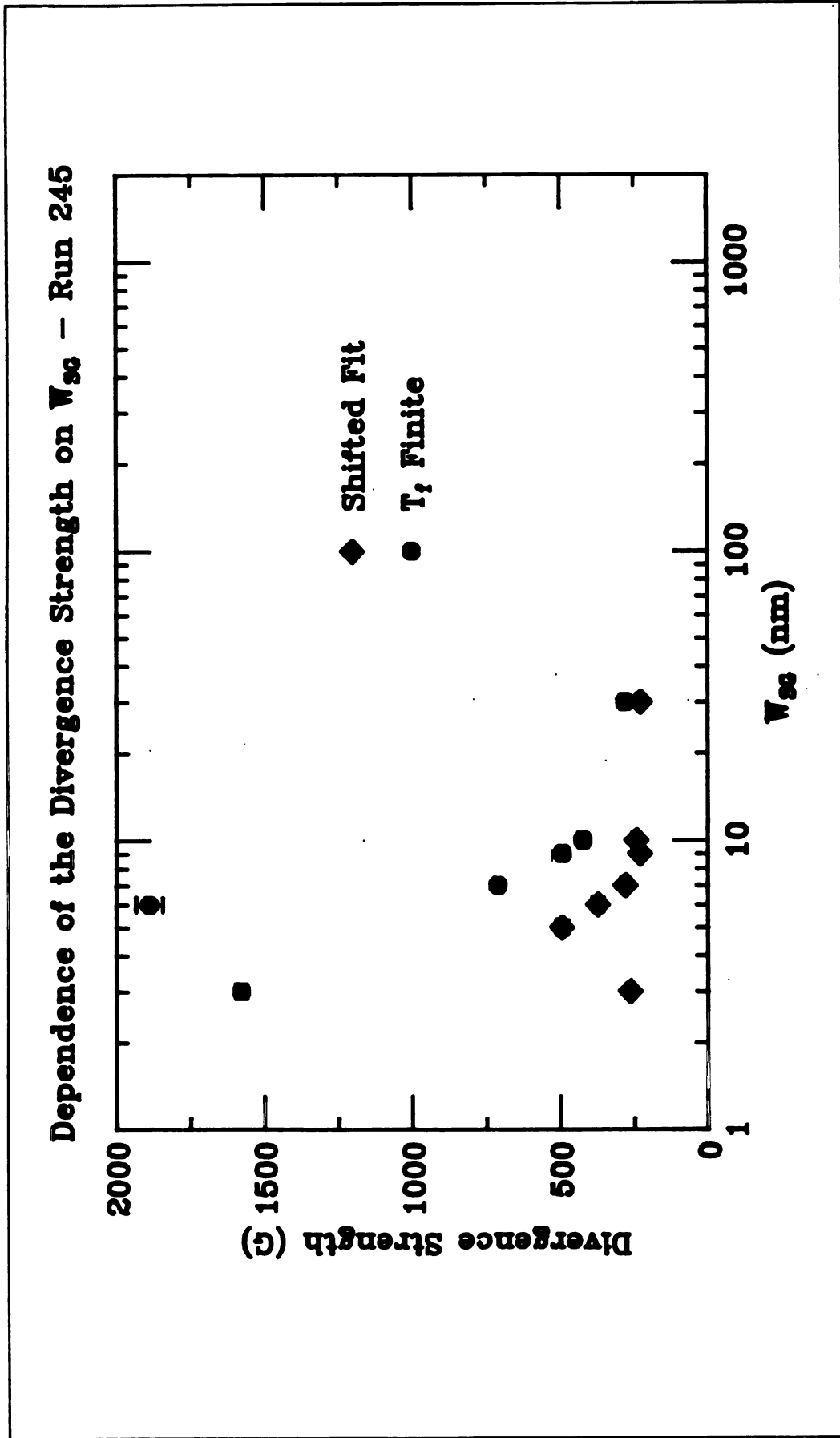
Figure 7-60: *Comparison of Divergence Strengths from Equation 7-4 and 7-7 - Run 245 - $Cu_{0.93}Mn_{0.07}$*

$T_f(\infty)$. A′, which is changed by an additive factor proportional to the magnitude of the shift, will be the same regardless of the function describing the relationship between $T_f(W_{SG})$ and $T_f(\infty)$. The magnitude of C′ will be affected by the form assumed to relate $T_f(W_{SG})$ and $T_f(\infty)$, and the failure of samples with smaller W_{SG} to take on the bulk value of C′ may be due to the failure of finite size scaling in describing this relationship.

A further interesting observation is that the temperature at which deviations from the power law behavior occurs (T*) also becomes relatively constant in the shifted analysis. If T* is shifted by T_s, and the reduced temperature is calculated using $T_f(\infty)$, the resulting values of t* for all layer thicknesses range from .63 to .80 for Run 243 ($Cu_{0.89}Mn_{0.11}$), between 0.60 and 1.0 for Run 185 ($Cu_{0.93}Mn_{0.07}$) and between .65 and 1.1 for Run 245 ($Cu_{0.93}Mn_{0.07}$). *The range of values represent scattered values for the shifted t*, and do not represent systematic trends with decreasing W_{SG}.*

The removal of the dependence of Equation 7-4 on T_f has shown that the systematic changes in the values of the parameters A and C can be attributed to effects on T_f and not to effects on $\Delta H(T)$; however, the value of the exponent, κ, and the Thermal Broadening, B, are not due to the depression of T_f.

COMPARISON WITH THEORY

The two theories developed to explain ESR in spin glasses represent very distinct physical pictures, even though they predict the same functional form of $\Delta H(T)$. This point is exceptionally important; in order to properly interpret these measurements, we must understand what we have measured. The importance of this statement bears a

review of the differences between the pictures before considering the consistency of the data with each.

We would like to look for data which would contradict one or the other of these pictures. Because both pictures predict a power law behavior, but neither model predicts the value of κ, comparing the measured value of κ with theory will not serve to distinguish between the models. We must also consider if, near T_f, the models are consistent with either the general mean field/hierarchical picture or the droplet picture described in Chapter 3.

Comparison with the Mean Field Picture of ESR

In the mean field picture, the ESR resonance is due to critical slowing down as the material approaches the spin glass phase. Physically, this implies that, at high temperatures, the spins are all in the paramagnetic phase and contribute to the resonance. As the temperature is lowered, the relaxation times of the spins begin to diverge, finally going to infinity at T_f, which results in an infinite relaxation time and an infinite width to the resonance line. The ESR resonance thus measures the collective behavior of the spins. Departure from the power law behavior near T_f is attributed to the failure of the exchange narrowing limit near T_f.

The mean field ESR theory is consistent with the mean field picture of spin glasses; this model assumes a phase transition at T_f, and asserts that the transition exists in large (1000 G to 6000 G) magnetic fields. This is inconsistent with the droplet theory, in which a phase transition should not be observed in fields of this magnitude.

The mean field calculations of Levy, Morgan-Pond and Raghavan have been shown[106] to describe low frequency ESR data with accuracy, but fail when applied to high frequency (9 GHz) data. A direct comparison of their analytic expressions with this data is therefore not possible.

One point which seems to have been neglected by proponents of the mean field theory is the relationship of κ to other exponents. If κ is a critical exponent, relationships between κ and other critical exponents should exist. Wu[107] cites calculations which indicate $\kappa = z\nu$, and also $\kappa = z\nu-2\beta$. Appendix B shows that measurements of $z\nu$ vary, even within measurements of metallic spin glasses. Values of $z\nu$ obtained from scaling measurements of the ESR linewidth in metallic spin glasses are between 1 and 3; those obtained from AC susceptibility measurements are in the range 7 to 10. Mean field theory predicts values in the range 2 to 4. Bulk samples are characterized by $\kappa = 1.5$, which corresponds to $z\nu = 1.5$ or $z\nu = 3.5$ from the predictions given above. These values are consistent with other values obtained from ESR scaling, but are different from other measurements of $z\nu$.

If the measurement of the divergence of $\Delta H(T)$ corresponds to the measurement of a phase transition, we would expect to see finite size effects. Finite size effects on the linewidth should manifest themselves by departure from the bulk behavior at a higher temperature, and a rounding of the divergence as the layer thickness decreases. We must be careful to exclude the known effects of the depression of $T_f(W_{SG})$. From the shifted analysis described by Equation 7-7, we find that departure from a power law occurs at approximately the same reduced temperature for all layer thicknesses. In addition, the value of the exponent increases with decreasing layer thickness.

The effect of dimensionality on κ is unclear. One difficulty with numerical comparisons is that departure from the power law behavior occurs at higher reduced temperatures for higher frequencies. The values of κ obtained from our fits would be an underestimate of the actual value if this effect were pronounced. In lieu of measurements at other frequencies, our values can be taken as lower bounds on κ. In analogy with Equation 5-34 and 5-42, the linewidth due to an exchange narrowed broadening should go like $\tau^{1/2}$ in two dimensions. We have no *a priori* reason for assuming that dynamic critical scaling applies in 2D; measurements in multilayers[78] have shown that the Fisher-Huse model is more appropriate.

Comparison with the Correlated Cluster Model

The correlated cluster model as originally presented by Barnes (See Chapter 5) presents a very different picture from the mean field model. At high temperatures, the spins are paramagnetic and all contribute to the resonance. As the temperature is lowered, regions of the sample become correlated, so that when the relaxation time of the correlated clusters becomes very long, these clusters will not contribute to the resonance. *This means that $\Delta H(T)$ is not a measure of spin glass properties, but is actually a measure of the decreasing concentration of uncorrelated (paramagnetic) spins.*

In order to apply the correlated cluster model to multilayered spin glasses, some modifications must be made. Barnes' original model was that the spins are paramagnetic up until the time they become correlated. At that time, he assumes that their relaxation times are longer enough so that they do not contribute to the resonance. Given the broad

spectrum of relaxation times above T_f, this picture seems restrictive, as spins are either paramagnetic and in the resonance, or are correlated and are not in the resonance. The broad spectrum of relaxation times suggests that the resonance line will detect both uncorrelated spins, and spins in clusters which relax with a time faster than the upper limit of detection. Up to now, we have avoided using the word 'droplet' to describe a picture of this sort, but an extension of the Fisher-Huse theory to this regime seems natural.

In the correlated cluster model, the linewidth is not due to the spin glass behavior, and so there is no reason to expect dimensionality or finite size effects. Instead, the effect of decreasing the sample size should manifest itself in how the correlated clusters are formed and grow. As the sample size decreases, the ratio of surface to volume spins increases. Surface spins will be missing nearest and next nearest neighbors, and this could affect the formation and the shape of correlated clusters. Preasymptotic corrections to the RKKY interaction are expected to be important when spins are separated by less than 6 nm in CuMn, and should affect cluster growth and formation which result in a concentration dependence. Chemical clustering in real materials would also contribute to correlated cluster growth.

The fundamental role of anisotropy in ESR above T_f is further emphasized by the fast that those ferro- and antiferro- magnets whose linewidths also diverge in this manner are all anisotropic. Cubic (isotropic) antiferromagnets do not exhibit this behavior. This indicates that anisotropy must play a fundamental role in the growth of correlated clusters. This is especially applicable to highly anisotropic materials (such as $Zn_{13}Mn$; see Chapter 5). In a one dimensional material, ordering occurs within the chain first,

so that we expect clusters to be oblate in nature and oriented along the chain direction. These clusters would contribute to a strongly directional internal broadening field. This indicates that anisotropy may be important to cluster formation and growth.

Relaxation between spins in clusters and the uncorrelated ions will exchange narrow the inhomogeneous broadening due to the internal field distribution, so the behavior of the divergence should be governed by how effectively the clusters and the ions cross-relax relative to the strength of the internal field distribution. The thermal broadening is a measure of the cross relaxation and is dependent upon the amount of short range order. The value of B is inversely proportional to the relaxation time of the electrons to the lattice. As the clusters correlate, their relaxation times to the conduction electrons increase, which should lessen the bottleneck. The weaker bottleneck can not effectively narrow the inhomogeneous broadening and the divergence should be stronger. This is a possible explanation for the behavior of B and κ as a function of decreasing layer thickness.

We would expect that, at some layer thickness, the lack of neighbors would make it harder to form clusters, so that the material would behave in the main as a paramagnet. Awschalom[85] claims from susceptibility measurements of thin CdMnTe multilayers that, when the behavior of a sample is determined by paramagnetic clusters, the dimensionality of the sample is not important.

Summary of the Comparison with Theory

We believe our data to be better explained by the correlated cluster model than by the mean field model. The major difficulty in using Equation 7-4 to analyze $\Delta H(T)$ comes from the presence of a quantity $(T_f(W_{SG}))$ which itself is subject to finite size and dimensionality effects. When the effects of the depression of $T_f(W_{SG})$ are removed from Equation 7-4, as reported in Tables 7-21 through 7-23, we see that the behavior of the residual width and the divergence strength as a function of layer thickness becomes the same as in the bulk. A conceptual explanation of the increase in B and κ in the context of the correlated cluster model has been forwarded.

The lack of correlation between the meaning of ν and other critical exponents, as well as the lack of finite size effects make this behavior difficult to explain within the mean field model. The fact that the values of $z\nu$ obtained from ESR scaling are quite different from the values arrived at from other methods also calls into question the relationship of the ESR linewidth divergence to the spin glass transition.

The question of dimensionality is open, due in part to the fact that our measurements represent a lower bound to the values of κ due to frequency effects. Other measurements on multilayers indicate that we don't expect conventional critical slowing down to describe the data in 2D, so trying to compare the value of κ with other measured or calculated values is futile. The expected characterization of the different dimensions by an exponent which takes on two distinct values is not seen. The value of the exponent is unaffected by the temperature shift analysis, indicating that the increase with decreasing layer thickness cannot be attributed to the depression of T_f.

No mechanisms for the nucleation and growth of clusters have been suggested by Barnes. The proximity of nearest neighbors - especially if the preasymptotic corrections to the RKKY interaction are considered - should be fundamental to ordering. The presence of this behavior in anisotropic ferro- and antiferro- magnets indicates that anisotropy is also important.

INTERPRETATION OF ΔH(T) IN THE CONTEXT OF ACTIVATED CLUSTERS

The primary difference between spin glasses and regular, long-ranged magnets is activated behavior. In a ferromagnet or antiferromagnet, we might expect that the distribution of cluster relaxation times would be very small. In a spin glass, we know that even above T_f there is a broad distribution of relaxation times, so that some fraction of the clusters will be partially frozen but will still contribute to the resonance.

Fisher and Huse predict (Equation 3-30) the relationship between the relaxation time and the reduced temperature near the transition temperature. We can naively appropriate this form, assuming that the linewidth diverges in the same manner as the characteristic relaxation time. We would expect the divergent part of the behavior to obey

$$[\Delta H(T)]^{ex} \sim t^{-\nu_3 z_3} \exp\left[\left(t^{\nu_3} W_{SG}\right)^{\psi_3 + \theta_3 \nu_2 \psi_2}\right] \qquad \text{7-10}$$

which is a modification of Equation 7-4 by an exponential factor. This equation holds when the relaxation time is less than the measuring time, which corresponds to the case

in which the spins can contribute to the resonance. We can gather the exponents to result in a general form.

$$\Delta H(T) = A + BT + C\, t^{-\kappa} \exp(D\, t^{-h})$$

This equation describes data with $W_{SG} \geq 7$ nm consistently but results in lesser quality fits for data ≤ 3 nm. The residual linewidth, A, and the thermal broadening, B, are approximately the same as found by fits of the non-activated expression. The values of C are approximately constant for all $W_{SG} \geq 7$ nm. The correction term, characterized by the values of D and h, was not needed in fitting the samples with $W_{SG} \geq 50$ nm. (The best fit resulted when $D = 0$). The remaining samples are fit with an exponent of approximately $h \approx 1$ and monotonically increasing values of D. The value of κ is 1.5 for all samples. These parameters are summarized in Table 7-24.

The form of Equation 7-11 appropriate to $T_f = 0$ is

$$\Delta H(T) = A'' + BT + C'' \exp(D\, T^{-h}) \qquad \text{7-12}$$

where one must be careful in comparing A'' with the residual widths obtained in the other fits; the high temperature behavior is described by $A'' + BT + C''$, so that the

Table 7-24: Fits of Run 243 - $Cu_{0.8}Mn_{0.11}$ - to Equation 7-11

W (nm)	T_f (K)	A (G)	B (G/K)	C (G)	D	κ	h
			Run 243 - $Cu_{0.89}Mn_{0.11}$				
500	47.5	-257 ± 13	3.36 ± 0.01	356 ± 10	0	1.5	-
100	47.5	-252 ± 17	3.46 ± 0.02	358 ± 17	0	1.5	-
50	45.0	-236 ± 14	3.40 ± 0.02	368 ± 23	0	1.5	-
30	42.5	-249 ± 16	3.57 ± 0.02	356 ± 23	.28 ± .05	1.5	1.2 ± 0.1
10	35.0	-215 ± 18	3.54 ± 0.02	363 ± 36	.63 ± .10	1.5	0.9 ± 0.1
7	31.0	-203 ± 9	3.70 ± 0.02	352 ± 51	.95 ± .17	1.5	0.8 ± 0.1
3	20.5			No Fit			
1	10.5			No Fit			

residual width, A, is actually $A'' + C''$. Samples with $W_{SG} \leq$ can be fit to the zero freezing temperature form, as shown in Table 7-25.

Table 7-25: Fits to $A'' + BT + C''$ exp(D T^{-h}) for Run 243 - $Cu_{0.89}Mn_{0.11}$

W (nm)	T_f (K)	A'' (G)	B (G/K)	C'' (G)	D	h
3	20.5	-182 ± 15	3.73 ± 0.03	15 ± 13	59 ± 4	0.7 ± 0.2
1	10.5	-176 ± 31	4.18 ± 0.03	55 ± 17	59 ± 8	0.9 ± 0.2

The resulting residual linewidths are -167 G for the 3 nm sample and -121 G for the 1 nm sample. We note that the parameter h resulting from the zero temperature fit is the same as the value for the thicker samples with non-zero T_f.

An analysis of the divergence of the linewidth in terms of the relaxation of activated droplets has been shown to consistently describe the data for all layer thicknesses, but at the expense of two additional parameters for which we have no physical feeling. The correction terms become significant for $W_{SG} \leq 30$ nm, and are characterized by an exponent $\approx$ 1 for all layer thicknesses below this limit.

LINESHIFT ANALYSIS

As has been mentioned, the behavior of the lineshift with temperature at 9 GHz does not lend itself to simple quantitative analysis, which is why the majority of this study has focused on the behavior of the linewidth. Over most of the temperature range, the position of the resonance line has a constant value corresponding to g $\approx$ 2. The shift to lower fields is very small over the region in which the power law is obeyed. Equation 5-34 predicts that, in the low frequency limit, the divergence of the lineshift should go like the reduced temperature to a power twice that of the power characterizing the linewidth divergence. The values obtained by fitting the lineshift to

$$(H_0(T) - H_0(\infty)) \sim \left(\frac{T-T_f}{T_f}\right)^{-\Xi} \qquad \text{7-13}$$

are given in Table 7-26 and compared with the values of κ obtained from fitting the linewidth. In making these fits, the same minimum value of t used in making the linewidth fits was used in order to give a direct comparison. Values given in parenthesis for the samples with small W_{SG} represent the values of κ obtained by fitting to a zero T_f. Fits of Equation 7-13 to a $T_f=0$ form resulted in very large errors. The values of $\Xi/2$ are consistently larger than the values of κ, but in the general expected range. Equation 7-13 should strictly hold only for the low frequency limit, so this analysis is mostly to illustrate that there are no drastic changes in the behavior of the lineshift as a function of W_{SG}.

Table 7-26: Fits to $(H(T)-H_0(\infty)) \sim t^{-z}$ for Run 243 - $Cu_{0.89}Mn_{0.11}$

Run 243 - $Cu_{0.89}Mn_{0.11}$				
W (nm)	T_f (K)	H_0 (G)	$\bar{z}$	κ
500	47.5	3319 ± 2	3.6 ± 0.2	1.5
100	47.5	3303 ± 2	3.8 ± 0.4	1.5
50	45.0	3312 ± 2	3.5 ± 0.4	1.5
30	42.5	3318 ± 3	4.5 ± 0.4	2.0
10	35.0	3317 ± 2	4.6 ± 0.4	2.0
7	31.0	3313 ± 3	4.8 ± 0.3	2.2
3	20.5	3304 ± 3	4.2 ± 0.3	1.7 (2.5)
1	10.5	3312 ± 3	5.1 ± 0.7	1.8 (2.4)

SUMMARY

The linewidth and resonance peak position as a function of temperature and spin glass layer thickness have been measured and presented for the multilayered spin glasses $Cu_{0.89}Mn_{0.11}$ and $Cu_{0.93}Mn_{0.07}$ with spin glass layer thicknesses from 1 to 1000 nm. The concentration dependence of bulk spin glasses with Mn concentrations of 4,7,11 and 16% has also been studied. The data has been analyzed in terms of the standard equation (7-4) used to analyze ESR in metallic ferromagnets, antiferromagnets and spin glasses. The relevance of both mean field and correlated cluster interpretations of ESR has been discussed, and the implications of each considered in light of the data presented here. The observation is made that the systematic behavior observed in the residual width and the divergence strength are the result of the depression of $T_f(W_{SG})$ with spin glass layer thickness, as indicated by the shifted temperature analysis. The effects of assuming a finite transition temperature in Equation 7-4 were considered, and samples with W_{SG} $\leq$ 3 nm were found to obey a form of Equation 7-4 with $T_f = 0$.

An alternate fitting form which contains a correction term to take activated behavior into account was proposed, and shown to fit the data for all layer thicknesses consistently, although at the expense of the introduction of two more parameters. The conclusions of this study are presented in Chapter 8.

CHAPTER EIGHT

CONCLUSIONS AND SUGGESTIONS

This chapter summarizes the results of this thesis, and comments on some experiments which have been suggested by this study.

SUMMARY AND CONCLUSIONS

Electron Spin Resonance (ESR) has been shown to be a useful probe of the dynamics of spin glasses above T_f. A straightforward interpretation of ESR results above T_f is difficult owing to the presence of multiple effects (i.e. bottleneck behavior, frequency dependence, etc.), and even confusion as to the origin of the ESR signal in this temperature regime.

The fabrication of multilayered metallic spin glasses with spin glass layer thicknesses, W_{SG}, from 1 nm to 1000 nm has resulted in the observation and analysis of both finite size effects and a crossover behavior from three dimensions to two as W_{SG} is decreased. These effects are observed as a depression of the freezing temperature, $T_f(W_{SG})$. Investigation of the frequency and field dependent behavior of multilayered spin glasses has been limited to susceptibility measurements in the frequency regime from 10^{-4} to 10^4 seconds at low fields, and from 2 G to 55000 G at 10^2 seconds. ESR experiments, which probe a much different part of the field-frequency plane (as shown in Figure 5-3), provide us with a means of testing the behavior of multilayered spin

260

glasses with a different type of measurement. The short time scale of ESR $(10^{-10}$ seconds) opens the door to observation of relaxation phenomena occurring on much shorter time scales than the extended dynamics of the spin glass phase, but still short enough times so that these phenomena cannot be seen by susceptibility measurements.

A large body of experimental evidence, as well as computer simulations, indicates that correlations are evident in spin glasses well above T_f. The two major spin glass theories - the mean field and the droplet models - have by and large neglected this temperature regime, preferring instead to label it as simply 'paramagnetic'. The conclusions drawn from the behavior of the linewidth, $\Delta H(T)$ and the resonance peak position, $H_0(T)$, above T_f depend to a large part on the origin of the resonance. The two theories used in explaining the divergence of these quantities near T_f can be classed as 'mean field' and 'correlated cluster' theories, with both theories predicting a power law divergence, but for different physical reasons. The mean field theory attributes the ESR signal to the divergence of a characteristic relaxation time of the sample as T_f is approached. The temperature dependence of the linewidth is due to an exchange-narrowed anisotropy-broadened line which diverges with the same characteristic exponent as the relaxation time (in 3D).

The correlated cluster model assumes that the dominant activity above T_f is the formation and growth of correlated clusters, composed of moments which interact more strongly with each other than with other moments. We expect that there will be a distribution of relaxation times as a result of a distribution of cluster sizes and correlation strengths. When the relaxation rate of a cluster is sufficiently long, the clusters dominant contribution to the ESR measurement is as a source of random internal magnetic fields.

The broadening of the linewidth as a function of temperature is due to two sources; the random local fields due to the correlated clusters, and a random field due to the DM anisotropy. The latter mechanism is introduced rather ad hoc as a concession to the body of evidence that this anisotropy is indeed fundamental to broadening (cf. Mozurkewich, et. al.[105]). The broadening due to both of these factors is narrowed by cross relaxation between the clusters and uncorrelated spins.

If the mean field theory is correct, and the divergence of the ESR linewidth is indicative of a phase transition, we expect to see finite size and dimensionality effects, as seen in the behavior of T_f in spin glass multilayers. If, as the cluster theory proposes, the ESR linewidth actually measures some intermediate phase between the paramagnetic and the spin glass phases, we expect the effects of reduced sample size will be evident in how the correlated clusters nucleate and grow.

These measurements are the first observation of the Electron Spin Resonance linewidth and lineshift in multilayered metallic spin glasses above T_f. Qualitatively, the same behavior is seen for all layer thicknesses; the linewidth decreases linearly at high temperatures, experiences a broad minimum and diverges as a power law in reduced temperature. The position of the minimum linewidth increases dramatically with reference to the measured freezing temperature as W_{SG} decreases. In bulk samples, the minimum is at about 2.5 T_f; in thinner samples, it moves to as high as 6.5 T_f.

The position of the resonance peak corresponds to a constant value of g $\approx$ 2 for the same temperature range over which the linewidth obeys the linear form. As the linewidth reaches its broad minimum, the position of the resonance peak begins to shift to lower fields. This shift is much more pronounced in the region near T_f where the

power law prediction for the linewidth fails. Analysis of the lineshift is limited to qualitative study, due to the small temperature regime in which a value different than $g = 2$ is seen, and in which the power law behavior holds. The expression used to describe the behavior of the linewidth with temperature in the bulk is given by Equation 7-4. At a reduced temperature t^*, the linewidth departs from this power law, rising less rapidly than predicted.

The concentration dependence of the linewidth in bulk samples of $Cu_{1-x}Mn_x$ ($x = 4,7,11$ and 16 at.%) has been studied. The linewidth of bulk samples diverges with a value of $\kappa = 1.5$ for all concentrations. The residual width, A, and the thermal broadening, B, are found to depend linearly on concentration, with A decreasing with increasing concentration, and B increasing with increasing concentration. The divergence strength, C, is observed to have a sublinear (increasing) dependence on increasing concentration.

We have shown that samples of all layer thicknesses ($1\ nm \leq W_{SG} \leq 1000\ nm$ for concentrations of 7 and 11 at.%) can be fit with the linewidth expression used to fit the bulk, although samples with W_{SG} less than about 3 nm are better fit to an expression corresponding to Equation 7-4, but appropriate to $T_f = 0$. This result is consistent with susceptibility measurements on multilayers with small W_{SG}. The reduced temperature at which departure from power law behavior is observed, t^*, increases with decreasing W_{SG}. Systematic variation of all parameters is seen as a function of layer thickness. The values of the residual linewidth, A, and the thermal broadening coefficient, B, increase with decreasing layer thickness. The divergence strength, C, is also seen to increase dramatically with decreasing layer thickness. Comparison of W_{SG} - dependent data to

concentration dependent data allows us to exclude the possibility of layer spreading as a source of these systematic changes. Considering the case in which samples with $W_{SG} \leq 3$ nm are fit to the zero T_f expression, the value of the exponent, κ, increases with decreasing layer thickness for all layer thicknesses studied. This general behavior is obeyed for both concentrations studied.

In determining if there are finite size effects on $\Delta H(T)$, we must carefully consider the parameterization of Equation 7-4 in terms of $T_f(W_{SG})$; the finite size/dimensionality effects on T_f may be misinterpreted as effects on $\Delta H(T)$. In general, a relationship between $T_f(W_{SG})$ and $T_f(\infty)$ (known to be finite size scaling over some range of W_{SG}) exists. We can use this relationship to remove $T_f(W_{SG})$ from Equation 7-4 so that the reduced temperature is expressed in terms of $T_f(\infty)$ for all layer thicknesses and the data for each W_{SG} is shifted by an amount equal to $T_f(\infty) - T_f(W_{SG})$. This essentially removes the known effects of the depression of T_f from the linewidth measurement. This analysis indicates that A and C are constant for all layer thicknesses ≥ 7 nm. The failure of the assumed form of finite size scaling in representing the dependence of $T_f(W_{SG})$ on $T_f(\infty)$ for samples with $W_{SG} < 7$ nm is responsible for the deviations in the thinner samples. The temperature shift analysis, however, does not affect the value of the exponent, κ, or the thermal broadening. The reduced temperature at which departure from a power law occurs also takes on the same value for all W_{SG} upon shifting and using $T_f(\infty)$ in calculation of t^*. This analysis suggests that finite size effects - which would be expected to appear as a rounding of the divergence, and a departure from bulk behavior at some t^* which should progressively increase with decreasing W_{SG} are not seen in the ESR linewidth. This could be due to the short length

scales which the ESR probes, or it may suggest that the measurement does not correspond to a measurement of the spin glass phase. Our results indicate that no finite size effects are seen in the linewidth; the appearance of these effects is due to the presence of $T_f(W_{SG})$ in Equation 7-4.

We expect dimensionality effects to be characterized by changes in the exponent κ and possible by changes in the ESR lineshape and angular dependence of the linewidth. The ESR lineshape remains Lorentzian for all layer thicknesses to 1 nm in the region where the power law behavior is obeyed. The angular dependence of the lineshape has not been systematically surveyed.

A value of $\kappa = 1.3 - 1.6$ has been widely reported in bulk spin glasses, ferromagnets and antiferromagnets. The only report of κ in two dimensions (in an antiferromagnetic salt) is $\kappa = 2$. Frequency effects in the bulk[107] indicate that values of κ from high frequency measurements (such as the ones reported here) may underestimate κ. In the thinnest samples considered in this study, a value of well over 2 is found. A gradual increase in κ is seen as W_{SG} is reduced, but the data is not sufficient to determine if this change is indicative of a dimensionality crossover, or a result of the changes in cluster growth and nucleation due to the larger surface spin to volume spin ratio.

An added difficulty with the mean field model is in a lack of identification of κ with other critical exponents. Calculations predict that κ should be on the order of $z\nu$; values of $z\nu$ obtained from dynamic scaling are on the order of 1-3, so values of κ in this region are not unreasonable. Most measurements of $z\nu$ in metallic spin glasses using other probes find a value of $z\nu = 7 - 11$, which is very different from the ESR

measurements. This may be a result of an incorrect interpretation of κ as characterizing a critical behavior.

We conclude that the cluster model is more likely to explain the behavior of the ESR linewidth as a function of the spin glass layer thickness than the mean field model. The evidence for correlations above T_f, and the successful description of the stronger correlations below T_f via the Fisher-Huse droplet model suggests that a similar model could describe the phase intermediate to the spin glass and true paramagnetic regimes, and would provide a better theoretical understanding of the nature of the transition at T_f.

As mentioned earlier, the divergent behavior of the linewidth is not unique to spin glasses; however, we expect that the dynamics of the correlated cluster phase will differ from those of long range ordered magnets. If the resonance is due to paramagnetic spins and loosely correlated clusters, we might expect the dynamics of the clusters to obey an activated expression. The behavior of the material can be consistently analyzed across all ranges of W_{SG}, but lack of a theory gives us no feeling for the meanings of the parameters and further interpretation of these results is difficult.

We believe that these ESR measurements are further evidence for the existence of an intermediate phase, with a spectrum of relaxation times which are short enough that they have gone undetected in the longer time susceptibility measurements. This raises the question of the nature of this phase as a function of decreasing sample thickness. The importance of the DM anisotropy to the broadening has been well documented. One possible hypothesis for the increasing value of κ with decreasing layer thickness is the presence of regions of sample which have already condensed into the spin glass phase. These regions would have macroscopic relaxation times and would be sources for the

DM anisotropy, which is known to be most important in the spin glass phase *per se*. We might present a hypothetical phase diagram as shown in Figure 8-1.

For all sample thicknesses, a correlated cluster phase will begin at temperatures in the area of the minimum of the $\Delta H(T)$ curve - about 2-3 T_f. The onset of these correlations is a property of a specific concentration of spin glass and should occur at roughly the same temperature for all layer thicknesses down to some lower limit. At this limit, the nearest and next-nearest neighbor distances between Mn ions will be large enough to be prohibitive to the formation of correlations.

The 'correlated cluster' phase is characterized by a distribution of relaxation times which correspond to those of the weakly correlated clusters and the uncorrelated spins. As the correlations within a cluster grow, the relaxation time of the cluster increases. At some critical value of the correlation strength, the relaxation time of the cluster will become macroscopic and undetectable by the ESR measurement. The cluster is then essentially condensed into the spin glass phase. For a given concentration, this should first happen (for all layer thicknesses) at $T_f(\infty)$, with the caution that an absolute value for the temperature must take into account the field/frequency conditions of the ESR measurement. The question mark in the diagram indicates that, at some layer thickness, the number of neighbors will be so reduced that clusters may be harder to form, which would prevent correlations at higher temperatures.

For samples with $T_f(W_{SG}) < T_f(\infty)$ a phase analogous to the Griffiths phase exists, in which macroscopic portions - but not all - of the sample will be frozen into the spin glass state. This region of gradual freezing continues to $T_f(W_{SG})$, at which point all of the relaxation times are macroscopic. The only reason this Griffith's-like phase could
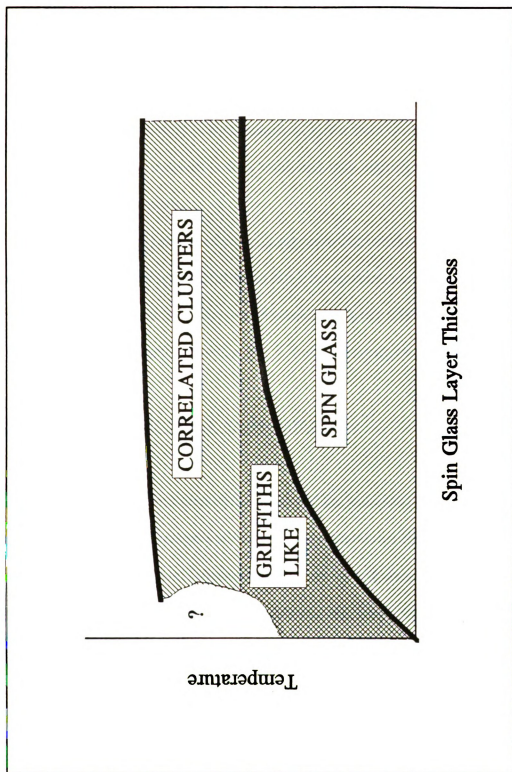
Figure 8-1: *Proposed Temperature - Layer Thickness Phase Diagram for Multilayered Spin Glasses*

be observed in these materials is due to the depression of the spin glass transition temperature via finite size and dimensionality effects. As W_{SG} decreases, the fraction of frozen regions which exist will increase relative to 'free spins'. The length scale over which the critical temperature is significantly different from the bulk critical temperature in ferro- and antiferro- magnets is very small and may entirely preclude observation of this phase in those materials.

The presence of correlated regions suggests that irreversibility effects should be seen above T_f. These effects would be on time scales which are too short to be observed in susceptibility measurements. Irreversible behavior in the ESR linewidth has been seen in these samples, as described in Chapter 6, but not investigated systematically.

SUGGESTIONS FOR FUTURE EXPERIMENTS

The existence of an intermediate phase and the possibility of a Griffiths-like phase suggests a number of experiments which could be important in further defining the nature and dynamics of this phase. Because the nature of research entails both answering questions and knowing which questions to answer, this final section proposes some tests of the existence and the elucidation of the nature of the intermediate phase.

1. We have seen that field and frequency effects influence the value of $T_f(W_{SG})$. The phase diagram shown in Figure 8-1 will be dependent of the values of $T_f(\infty)$ and $T_f(W_{SG})$ at the field and frequency of the measurement. Extension of ac susceptibility measurements to fields on the order of ESR fields would allow an extrapolation of

$T_f(W_{SG},H,\omega)$ which would give an absolute meaning to the parameter values which result from fitting to Equation 7-4.

2. A frequency effect on the divergence has been shown to exist in bulk spin glasses, so that lower frequencies follow the power law behavior to lower reduced temperatures. Measurements of $\Delta H(T)$ at lower frequencies would result in better fits, as a wider range of temperatures can be considered. This would more accurately determine the value of κ. Additionally, the behavior of the resonance peak position with temperature is enhanced at lower frequencies, enabling a more quantitative analysis and comparison with the $\Delta H(T)$ results.

3. As clusters form and 'drop out' of the resonance, the intensity of the ESR line should decrease. The total number of spins is proportional to the area under the ESR resonance peak, and is further proportional to the susceptibility. Careful measurement of the high temperature susceptibility will allow the extraction of the Curie constant and the Weiss temperature for the multilayers. The ESR intensity should deviate from a Curie-Weiss law as more and more spins drop out of the resonance and more slowly relaxing clusters are formed. The reduction in the number of spins could be quantified in this type of analysis, providing information about the growth of clusters, and the temperature at which the correlations are first measurable.

4. The divergent linewidth and resonance peak position is seen in ferromagnets, antiferromagnets and spin glasses. All spin glasses exhibit this behavior, but only some

ferro- and antiferro- magnets. The determining factor in the behavior of $\Delta H(T)$ seems to be anisotropy. This intuitively follows, as anisotropies could influence the shape and dynamics of the cluster, as well as the character of the resulting internal field.

Au and Pt are spin-orbit scatterers in CuMn. Addition of one of these to a series of multilayer films would increase the anisotropy of the film without changing T_f. Mozurkewich, et. al.[105] have studied the behavior of bulk AgMn doped with Sb (which increases the anisotropy and relieves the bottleneck) and found that the exponent governing the divergence increases with increasing anisotropy. Our cluster interpretation would imply that the breaking of the bottleneck increases the effect of the broadening relative to the cross-relaxation. The values of the thermal broadening and the exponent, κ, increase, in agreement with this analysis. This study could shed light on the mechanism governing cluster formation and growth and the relationship between the thermal broadening and the exponent κ.

5) The importance of anisotropy also calls into question the effect of the growth technique on the spin glass character of the material. Comparison with films grown in some other way - such as MBE - would be interesting. Likewise, a similar analysis of a short range spin glass would be of interest.

6) The dilute magnetic semiconductors (like $Cd_{1-x}Mn_xTe$, $Cd_{1-x}Mn_xSe$) are tunable over a wide range of Mn concentration. At low Mn concentration, they are paramagnets, intermediate Mn concentrations result in spin glass behavior, and larger Mn concentrations are antiferromagnetic in nature. By studying a series of these materials

as they change magnetic character, the common (or different) elements of the behavior as T_f (or T_N) is approached can be identified. This would determine if the intermediate state is specific to spin glasses, or if evidence exists in other materials as well. These materials are semiconducting, so the skin depth problem would not limit sample size. Multilayers are routinely fabricated by growth techniques which result in very low strain samples, so data as a function of layer thickness can be taken and compared with susceptibility results.

7) The intermediate phase should exhibit hysteretic effects. A study of these effects would add to understanding of the dynamics of clusters, much as has been done below T_f. The advantage here is that the nature of the hysteretic effects are on relatively short time scales (compared to true spin glass behavior), which are observable via ESR measurements.

One study of MnSe[155] showed distinct hysteretic behavior in the intensity of the linewidth as a function of temperature, and only weak hysteresis in $\Delta H(T)$. MnSe undergoes a structural phase transition as the temperature changes. On cooling, the structure goes from a cubic phase, in which the Mn^+ interact paramagnetically, to a NiAs structure, in which the ions interact antiferromagnetically. The onset of antiferromagnetism is indicated by a decrease in the intensity as the material changes phase. On warming, the signal starts out with low intensity, due to the antiferromagnetic correlations, and the intensity rises rapidly upon the change back to the cubic structure. Some type of hysteretic effects should be seen in the intermediate phase.

8) The observation of the 'Griffith's - like' phase in these samples is possible only because of the large W_{SG} range over which $T_f(W_{SG})$ is different than $T_f(\infty)$. It would interesting to know if a similar range exists for random ferromagnets. More theoretical work has been done on the possibility and characteristics of a Griffiths phase in random ferromagnets, which might shed some additional light on the nature of this phase. We might expect to see two phases; a true Griffiths phase, between $T_c(p=1)$ and $T_c(p)$, where p is the dilution from a pure ferromagnet, and a 'Griffiths like' phase between $T_c(p, \infty)$ and $T_c(p, W)$, where W is the width of the layered random ferromagnet.

9) A systematic search for changes in the lineshape and/or angular dependence could determine if there is a difference in the approach to a three dimensional spin glass vs. the approach to a two dimensional spin glass. A theoretical study of the effect of a distribution of relaxation times on the lineshape could enhance our understanding of the behavior of these materials in the immediate vicinity of T_f.

APPENDIX A

SOLUTION TO THE BLOCH EQUATIONS

The Bloch equations are given by

$$\frac{dM_z}{dt} = -\gamma (\vec{M} \times \vec{H}_{eff})_z + \frac{M_0 - M_z}{T_1} \qquad \text{A-1}$$

$$\frac{dM_{x,y}}{dt} = -\gamma (\vec{M} \times \vec{H}_{eff})_{x,y} - \frac{M_{x,y}}{T_2} \qquad \text{A-2}$$

H_x can be considered to be the real part of a complex field, $H' = 2\,H_1 \cos(\omega t)$, where H_1 is the properly rotating component of H_x. The counter rotating part will have a resonance at $-\omega_o$; when the system is near the resonance for H_1, the other resonance will be far away, so we can neglect the counter-rotating field.

The x component of the magnetization is given by the real part of the complex magnetization, M'_x

$$M_x = \mathbf{R}(M'_x) = \chi\, 2 H_1 e^{i\omega t} \qquad \text{A-3}$$

where the susceptibility, χ, relates the complex magnetization to the complex magnetic field. The susceptibility is now also complex, where

$$\chi = \chi' - \iota \, \chi'' \qquad\qquad \text{A-4}$$

so that

$$\mathbf{R}(M_x') = \chi' 2 H_1 \cos(\omega t) + \chi'' 2 H_1 \sin(\omega t) \qquad\qquad \text{A-5}$$

The Bloch equations are (with the rotating field included)

$$\frac{dM_x}{dt} = \gamma (M_z H_1 \sin\omega t - H_0 M_y) - \frac{M_x}{T_2} \qquad\qquad \text{A-6}$$

$$\frac{dM_y}{dt} = \gamma (H_0 M_x - M_z H_1 \cos\omega t) - \frac{M_y}{T_2} \qquad\qquad \text{A-7}$$

$$\frac{dM_z}{dt} = \gamma (M_y H_1 \cos(\omega t) - M_x H_1 \sin(\omega t)) + \frac{M_0 - M_z}{T_1} \qquad\qquad \text{A-8}$$

We can define the operators $N^{\pm}$;

$$N^{\pm} = e^{\mp \iota \omega t}(M_x \pm \iota M_y) \qquad\qquad \text{A-9}$$

Adding and subtracting Equations A-6 and A-7, we find

$$N^{\pm} = \frac{\gamma H_1 M_z}{\omega_0 - \omega \pm \dfrac{\iota}{T_2}} \qquad\qquad \text{A-10}$$

If we require a steady state solution, $dM_z/dt = 0$, and we find from Equation A-8 that

$$\frac{M_z - M_0}{T_1} = \left(\frac{\gamma H_1}{2\iota}\right)(N^+ - N^-) \qquad \text{A-11}$$

Solving for M_z,

$$M_z = \chi_0 H_0 \left(\frac{1 + T_2^2(\Delta\omega)^2}{1 + T_2^2(\Delta\omega)^2 + \gamma^2 H_1^2 T_1 T_2}\right) \qquad \text{A-12}$$

This is then plugged back into Equations A-9 and A-10 to give

$$M_x = \frac{1}{2}\chi_0 H_0 \gamma_0 T_2 \left(\frac{T_2 \Delta\omega 2H_1\cos(\omega t) + 2H_1\sin(\omega t)}{1 + T_2^2(\Delta\omega)^2 + \gamma^2 H_1^2 T_1 T_2}\right) \qquad \text{A-13}$$

$$M_x = \frac{1}{2}\chi_0 H_0 \gamma_0 T_2 \left(\frac{T_2 \Delta\omega 2H_1\sin(\omega t) - 2H_1\cos(\omega t)}{1 + T_2^2(\Delta\omega)^2 + \gamma^2 H_1^2 T_1 T_2}\right) \qquad \text{A-14}$$

The real and imaginary parts of the susceptibilities are

$$\chi' = \frac{1}{2}\chi_o(\omega_o T_2) \left(\frac{(\omega_o - \omega) T_2}{1 + (\omega - \omega_o)^2 T_2^2 + \gamma^2 H_1^2 T_1 T_2}\right) \qquad \text{A-15}$$

$$\chi'' = \frac{1}{2}\chi_o(\omega_o T_2)\left(\frac{1}{1+(\omega-\omega_o)^2\ T_2^2\ +\ \gamma^2 H_1^2 T_1 T_2}\right) \qquad \text{A-16}$$

when H_1 is small compared to H_0, which is usually satisfied, the last term is the denominator can be ignored. For most nonmetallic samples, the real part of the impedance will depend on χ'', the imaginary part of the susceptibility, so that the average power absorbed is given by

$$P = 2\omega\chi'' H_1^2 \qquad \text{A-17}$$

For metallic samples, the surface impedance, Z, is defined as

$$Z = \frac{4\pi}{c}\left[\frac{\hat{n}\cdot\vec{E}\times\vec{H}^*}{H^2}\right] \qquad \text{A-18}$$

And the power absorbed from the rf field will be given by

$$P_{abs} = \left(\frac{4\pi}{c}\right)^2 |H|^2 Re(Z) \qquad \text{A-19}$$

APPENDIX B

CRITICAL EXPONENTS IN SPIN GLASSES

This appendix summarizes a representative group of measured and calculated exponents, and defines the exponents. The dimensionality is denoted by d. Table B-1 defines some common exponents, and Table B-2 summarizes some important relationships between the exponents. A list of calculated and measured static exponents is given in Table B-3. The dynamic exponent is usually measured from dynamic scaling, so a value of $z\nu$ is found. Some authors distinguish between $z\nu$, which measures the characteristic relaxation time and $z\nu_{ave}$, which is the exponent associated with critical slowing down of the average relaxation time. A value of $z\nu_{ave}$ was cited only if the author identified it as such, and was otherwise assumed to be $z\nu$. These results are tabulated in Table B-4.

Table B-1: Definitions of Some Common Critical Exponents

Exponent and Name		Definition
β	Order Parameter	$q \sim t_\beta$
γ	Susceptibility	$\chi \sim t^\gamma$
α	Specific Heat	$C \sim t^\alpha$
ν	Correlation Length	$\xi \sim t^\nu$
δ	Equation of State	$H \sim M^\delta$
η	Pair Correlation Function ($\Gamma(r)$)	$\Gamma \sim r^{-(d+2+\eta)}$
$\psi\nu$	Fisher-Huse Exponent (2D)	$\tau \sim \exp(T^{-(1+\psi\nu)})$
z	Dynamic Exponent	$\tau \sim \xi^z$

Table B-2: Summary of Relationships Between Critical Exponents

Some Common Relationships Between Critical Exponents	
$\phi = (\gamma + \beta)/2$	
$\gamma = \phi(1-\delta^{-1})$	Widom Scaling Law
$\gamma = \nu(2-\eta)$	Fisher Scaling Law
$2 = \alpha + 2\beta + \gamma$	Rushbrooke Scaling Law

Table B-3: Summary of Static Exponents for Spin Glasses

Ref	Material	δ	ϕ	γ	β	ν	η
	Summary of Theoretical and Experimental Static Critical Exponents						
	Experimentally Obtained Values						
71	CuMn: FSE					1.1-1.6	
77	$CuMn/Al_2O_3$ (6 nm)	7 ± 0.5	6 ± 1	5.1	0.86	3.4	0.5
77	$CuMn/Al_2O_3$ (8 nm)	7.1 ± 0.2	6 ± 1	5.2	0.85	3.4	0.49
77	CuMn bulk	4.4 ± 0.2	3.9	3.0	0.9	1.6 ± 0.2	0.11
11	AgMn bulk	3.3 ± 0.2			0.9 ± 0.2		
13	CuMn bulk	4.0-4.3		3.4 ± 0.4			
13	GdAl bulk	5.9-6.3		3.8 ± 0.5			
78	CuMn/Cu (2nm)			9.3	0	4.6	0
86	$Rb_2Cu_{1-x}Co_xF_4$ -2D			4.4 ± 0.2		2.4 ± 0.3	
106	AgMn		5.0 ± 0.5				
12	CuMn(2%)	1.9 ± 0.1			1		
12	CuMn(.25%)	4.5		3.5			

Summary of Theoretical and Experimental Static Critical Exponents

Ref	Material	δ	ϕ	γ	β	ν	η
12	CuMn(1%)	4.4		3.3	1		
12	CuMnAl(1% Mn)	2.9±0.4					
12	AgMn(10.6%)			1.5±0.5			
12	AgMn	3.1±0.2	3.3±0.2	2.2±0.2	1±0.1		
12	AuFe(1.5%)	2±0.2		1.1±0.2	0.9		
12	GdAl(37%)	5.7±0.2	3.3±0.4	2.7±0.1			
12	$Fe_{10}N_{70}P_{20}$	5.2±0.5		2.3±0.2			
12	$Al_2O_3MnOSiO_2$	3.2	4.5	3.1±0.1	1.4±0.1		
12	$CsNiFeF_6$	3.5	4.2	3±0.5	1.2±0.1		
156	EuSrS(Finite T_f)	2.0±0.2					
156	EuSrS($T_f = 0$)	10.5±2.5					
80	AuFe; Hall Effect				1.6±0.2		
157	$CdCrInS_4$	4.1±0.4	3.1±0.5	2.3±0.4	0.75±.1		
81	CuMn (Low Field)		3.2±0.2	2.2±0.1	1 ± 0.1		
81	CuMn(High Field)	4.5±0.3	4.3±0.5	3.3±0.3	1±0.2		
158	CdMnTe		6	4.8±1	~1	2.3	
159	AgMn				1	1.2	

Ref	Material	δ	ϕ	γ	β	ν	η
				Summary of Theoretical and Experimental Static Critical Exponents			
160	$Al_{78}Mn_{22}$			4.4	0.6		
161	GdAl	5.7±0.2	3.3±0.4	2.7±0.1	0.93±0.04		
162	FeNiPbAl	10±1		3.4±0.1	0.38±0.04		
	Theoretical Calculations and Simulations						
163	2D Ising Model					4.2±0.5	
42	3D Short Range Ising			2.9±0.3	0.5	1.3±0.1	-0.22
164	3D Model	1.4				1.2±0.1	
165	Mean Field	2		1	1	.5	0
58	ϵ Expansion (d=3)	3.2		2.8			
76	2D EA Model	3.5±0.5					
166	3D			3.2	0.5	1.4	-0.28
167	± J Model (2D)			4.1		2.75	
168	± J Model (2D)	2.8		4.54		2.64±0.23	0.28
169	3D Ising Model					3.3±0.6	
170	3D Ising Model					1.8±0.5	
171	2D Ising Model			5.3±0.3			

Table B-4: Values of the Dynamic Exponents for Spin Glasses

	Summary of Dynamic Critical Exponents					
ref	Description	z	$z\nu$	z_{ave}	$z_{ave}\nu$	$\psi\nu$
	Experimentally Obtained Values					
106	AgMn (ESR Scaling)		2.5 ± 0.3			
172	$(Fe_{0.15}N_{0.85})_{75}P_{16}B_6Al_3$		8.2			
86	$Rb_2Cu_{1-x}Co_xF_4$					2.2 ± 0.2
154	EuSrS (Finite T_f)				7.2 ± 0.5	1.6 ± 0.2
74	CuMn sputtered 2 nm film					
74	CuMn sputtered 1000 nm film		9 ± 1			
173	$Fe_{2-x}Ti_{1+x}O_5$ (ESR)		1.4 ± 0.2			
173	$Fe_{2-x}Ti_{1+x}O_5$ (μSR)		1.0 ± 0.2			
156	CdMnTe		13 ± 4			
159	AgMn (ESR Scaling)		3			
157	$CdCrInS_4$		7			
156	EuSrS ($T_f=0$)				8.0 ± 0.5	
	Theoretical Calculations and Simulations					

Summary of Dynamic Critical Exponents

ref	Description	z	zν	z_{ave}	$z_{ave}\nu$	$\psi\nu$
167	2D ± J Model				2.0	
168	2D ± J Model				2.0	
42	3D Short Range Ising	6.1±0.3	7.9±0.1	5.4±0.2	7.2±0.1	
164	3D Monte Carlo	5	6±1		5.6	
164	3D Monte Carlo - $T_f=0$				3.2	
58	Mean Field at H = 0, T→T_f	4	2	2		
171	3D Simulation		9			

BIBLIOGRAPHY

1. K. Binder and A.P. Young, Rev. Mod. Phys. **58**, 4, 801 (1986)

2. V. Cannella and J.A. Mydosh, Phys. Rev. **B 6**, 4220 (1972)

3. C.A.M. Mulder, *et. al.*, Phys. Rev. **B 23**, 1383 (1981)

4. H. Maletta and W. Felsch, Phys. Rev. **B 20**, 1245 (1979)

5. L.E. Wegner and P.H. Keesom, Phys. Rev. **B 11**, 3497 (1975)

6. L.E. Wegner and P.H. Keesom, Phys. Rev. **B 13**, 2845 (1974)

7. P.J. Ford and J.A. Mydosh, Phys. Rev. **B 14**, 2057 (1976)

8. H. Scheyer, *et. al.* J. Magn. Magn. Mat. **4**, 1677 (1977)

9. P. Monod and H. Bouchiat, J. Phys. (Paris) Lett. **43**, 145 (1980)

10. Laurent P. Levy, Phys Rev. **B 33**, 4936 (1988)

11. Laurent P. Levy and Andrew T. Ogielski, Phys. Rev. Lett. **57**, 3288 (1986)

12. H. Bouchiat, J. Phys. (Paris) **47**, 71 (1986)

13. B. Barbara, *et. al.*, Phys. Rev. Lett. **47**, 1852 (1981)

14. L.E. Wenger, in *Proceedings of the Heidelberg Colloquium on Spin Glasses*, ed. J.L. van Hemmen and I. Morgenstern, Lecture Notes in Physics Vol 192, Springer, Berlin (1983)

15. J. Villain, Europhys. Lett. **2**, 871 (1986)

16. D.S. Fisher and D.A. Huse, Phys. Rev. Lett. **56**, 1601 (1986)

17. M. A. Moore and A.J. Bray, J. Phys. **C 18**, L 699 (1985)

18. M.A. Ruderman and C. Kittel, Phys Rev **96**, 99 (1954)

19. K. Yosida, Phys Rev, **106**, 893 (1957)

20. T. Kasura, Prog. Theor. Phys. **16**, 45 (1956)

21. D.C. Mattis, *The Theory of Magnetism I: Statics and Dynamics*, Springer Verlag, Berlin (1988)

22. A.F.J. Morgownik and J. A. Mydosh, Solid State Commun., **47**, 321 (1983)

23. H. Bouchiat and E. Dartyge, J. Physique, **43**, 1699 (1982)

24. Ulf Larsen, Phys. Rev. **B 33**, 4803 (1986)

25. P.M. Levy and Q. Zhang, Phys. Rev. **B 33**, 665 (1986)

26. D.C Vier and S. Shultz, Phys. Rev. Lett. **54**, 150 (1985)

27. L.R. Walker and R.E. Walstead, J. Magn. Magn. Mater. **31-34**, 1289 (1983)

28. J.D. Reger and A.P. Young, Phys. Rev. **B 37**, 10, 5493 (1987)

29. A. Fert, *et. al.*, J. Phys. (Paris) **49**, 1173 (1988)

30. I.E. Dzyaloshinskii, J. Phys. Chem. Solids **4**, 241 (1958)

31. T. Moriya, Phys. Rev. Lett. **4**, 51 (1960)

32. C.P. Slichter, *Principles of Magnetic Resonance*, Springer-Verlag, Berlin, 1990

33. Claude Cohen-Tannoudji, Bernard Diu and Franck Laloë, *Quantum Mechanics, Volume II*, John Wiley and Sons, New York, 1977; pp 1123-1128

34. G.E. Pake, *Paramagnetic Resonance*, W.A. Benjamin, Inc., New York, 1962

35. F. Bloch, W.W. Hansen and M. Packard Phys. Rev., **69**, 127 (1946)

36. H. Eugene Stanley, *Introduction to Phase Transitions and Critical Phenomena*, Oxford University Press, New York, 1971

37. M. Fisher in *Proceedings of the International School of Physics - ,Critical Phenomena*, Academic Press, New York, 1971

38. K. Kawasaki in *Proceedings of the International School of Physics - Critical Phenomena*, Academic Press, New York, 1971

39. Hazime Mori and Kyozi Kawasaki, Prog. Theor. Phys. **27**, 529 (1962)

40. K. Kawasaki, Prog. Theor. Phys. **39**, 285 (1968)

41. A.T. Ogielski, Phys. Rev. **B 32**, 7384 (1985)

42. S.F. Edwards and P.W. Anderson, J. Phys. **F 5**, 965 (1975)

43. D. Sherrington and S. Kirkpatrick, Phys. Rev. Lett. **35**, 1792 (1975)

44. S. Kirkpatrick and D. Sherrington, Phys Rev **B 17**, 4384 (1978)

45. D.J. Thouless, P.W. Anderson and R.G. Palmer, Phil Mag, **35**, 593 (1977)

46. J.R.L. de Almeida and D.J. Thouless, J. Phys. **A 11**, 983 (1978)

47. Marc Mezard, Giogio Parisi, Miguel Angel Virasoro, *Spin Glass Theory and Beyond*, World Scientific, Singapore, 1987

48. G. Parisi, Physics Letters, **73A**, 203 (1979)

49. G. Parisi, J. Phys A: Math. Gen **13** L 115 (1980)

50. M. Mezard, *et. al.*, J. Physique, **45**, 843 (1984)

51. M. Mezard and M.A. Virasoro, J. Physique **46**, 1293 (1985)

52. M. Gabay and G. Toulouse, Phys. Rev. Lett. **47**, 201 (1981)

53. M.A Moore and A.J. Bray, J. Phys. **C 15**, L 301 (1982)

54. A. Fert and P.M. Levy, Phys. Rev. Lett, **44**, 1538 (1980)

55. G. Kotliar and H. Sompolinsky, Phys. Rev. Lett, **53**, 1751 (1984)

56. H. Sompolinsky and Annette Zippelius, Phys. Rev. **B 25**, 6860 (1982)

57. H.J. Sommers and K.H. Fischer, Z. Phys. **B 58**, 125 (1985)

58. K.H. Fischer, Z. Phys **B 55**, 317 (1984)

59. W.L. McMillan, J. Phys. **C 17**, 3179 (1984)

60. W.L. McMillan, Phys. Rev. **B 30**, 475 (1984)

61. A.J. Bray and M. Moore, J. Phys **C 17**, L 463 (1984)

62. A.J. Bray and M.A. Moore, Phys. Rev. Lett. **58**, 371 (1987)

63. D.S. Fisher and D.A. Huse Phys. Rev. **B 36**, 8937 (1987)

64. D.S. Fisher and D.A. Huse, Phys. Rev. **B 38**, 373 (1988)

65. D.S. Fisher and D.A. Huse, Phys. Rev. **B 38**, 386 (1988)

66. Daniel S. Fisher, J. Appl. Phys **61**, 3672 (1987)

67. R.B. Griffiths, Phys. Rev. Lett. **23**, 17 (1969)

68. D. Dhar, in *Stochastic Processes: Formalism and Applications*, ed. S. Agarwal and S. Dattagupta, Springer-Verlag, Berlin, 1983

69. A.J. Bray, Phys. Rev. Lett. **59**, 586 (1988)

70. Mohit Randiera, James P. Sethna and Richard G. Palmer, Phys. Rev. Lett **54**, 1321 (1985)

71. G.G. Kenning, J.M. Slaughter and J.A. Cowen, Phys. Rev. Lett. **59**, 2596 (1987)

72. G.G. Kenning, *et. al.*, Phys. Rev. **B 42,** 2393 (1990)

73. L. Hoines, R. Stubi, R. Loloee, J.A. Cowen, and J. Bass, Phys. Rev. Lett. **66**, 1224 (1991)

74. R. Stubi, J.A. Cowen, D.L. Leslie-Pelecky and J. Bass, Physica B, **165 & 166**, 459 (1990)

75. L. Sandlund *et. al.*, Phys Rev **B 40**, 869 (1989)

76. A.P. Young, Phys. Rev. Lett. **50**, 917 (1985)

77. W. Kinzel and K. Binder, Phys Rev. **B 39**, 1300 (1984)

78. A. Gavrin, *et. al.*, Phys. Rev. Lett **64**, 2438 (1990)

79. J. Mattson, *et. al.*, Preprint for Edinburgh Conference

80. C. Van Haesendonck, *et. al.*, Phys. Rev. Lett, **58**, 1968 (1987)

81. J. Vranken, *et. al.* Physica Scripta, **T 25**, 348 (1989)

82. N. de Courtenay, H. Bouchiat, H. Hurdequint and A. Fert, J. Appl. Phys. **61**, 4097 (1987)

83. I.A. Campbell, N. de Courtenay and A. Fert, J. Phys. (Paris) Lett **45**, L565 (1984)

84. G.G. Kenning, *et. al.* Unpublished

85. K.H. Fischer, Z. Phys. **B 60**, 151 (1985)

86. D.D. Awschalom, *et. al.*, Phys. Rev. Lett. **59**, 1733 (1987)

87. C. Dekker, *et. al.*, Phys Rev. **B 40**, 11243 (1989)

88. A.G. Schins, *et. al.*, Preprint

89. J. Owen, M.F. Brown, W.D. Knight and C. Kittel, Phys. Rev. **102**, 1501 (1956)

90. H. Hasegawa, Prog. Theor. Phys., **27**, 483 (1959)

91. S.E. Barnes, Adv. Phys. **30**, 801 (1981)

92. A.M. Stewart, Austr. J. Phys. **33**, 1049 (1980)

93. H. Mori, in *"Fluctuation, Relaxation and Resonance in Magnetic Systems"*, ed. D. ter Haar, Plenum Press, New York (1961)

94. K. Kawasaki, Prog. Theor. Phys., **39**, 185 (1968)

95. R. Kubo, in *Fluctuation, Relaxation and Resonance in Magnetic Systems*, Ed. D. ter Haar, Plenum Press, New York (1961)

96. R. Kubo and K. Tomita; J. Phys. Soc. Japan **9**, 316 (1954)

97. Alessandro Bencini and Dante Gatteschi, *Electron Paramagnetic Resonance of Exchange Coupled Systems*, Springer-Verlag, Berlin (1990)

98. A.D. Caplin, J.B. Dunlop and R.H. Taylor, J. Phys. Paris, **32**, C16-17 (1971)

99. D. Griffiths, Proc. Phys. Soc. **90**, 707 (1967)

100. M.B. Salamon and R.M. Hermann, Phys Rev. Lett, **41**, 1506 (1978)

101. D.L. Huber, Phys. Rev. **B 6**, 3180 (1972)

102. M.B. Salamon, Solid State Commun. **31**, 781 (1979)

103. M.B. Salamon, J. Magn. and Magn. Mat. **15-18**, 147 (1980)

104. W. Kinzel and K.H. Fischer, Solid State Commun. **23**, (1977)

105. G. Mozurkewich, *et. al.*, Phys. Rev. **B 29**, 278 (1984)

106. P.M. Levy, C. Morgan-Pond, and R. Raghavan, Phys.Rev. Lett, **50**, 1160 (1983)

107. Wei-yu Wu, George Mozurkewich, and R. Orbach, Phys Rev **B 31**, 4557, (1985)

108. K. Baberschke, C. Pappa, H. Mahjour and R. Wendler, J. Magn. Magn. Mat. **54-57**, 179 (1986)

109. H. Mahdjour, C. Pappa, R. Wendler and K. Baberschke, Z. Phys. **B 63**, 351 (1986)

110. M. Zomack *et. al.* Phys. Rev. **B 27**, 4135 (1983)

111. M. Zomack, *et. al.*, Physica **108 B**, 773 (1981)

112. F. Mehran, *et. al.*, Solid State Commun. **52**, 107 (1984)

113. F. Mehran, *et. al.*, Phys. Rev. **B 35**, 5286 (1987)

114. M.A. Continentino, *et. al.*, Z. Phys. **B 72**, 471 (1988)

115. M.K. Hou, M.B. Salamon and T.A.L. Ziman, J. Appl. Phys., **55**, (1984)

116. M.K. Hou, M.B. Salamon and T.A.L. Ziman, Phys. Rev. **B 30**, 5239 (1984)

117. M.J. Park, *et. al*, Phys. Rev. **B 33**, 2070 (1986)

118. M.J. Park, *et. al*, J. Magn. Magn. Mater, **59**, 287 (1986)

119. S.M. Bhagat, *et. al.*, Solid State Commun., **38**, 261 (1981)

120. A.P. Malozemoff and J.P. Jamet, Phys. Rev. Lett **39**, 1293 (1977)

121. D. Fiorani, *et. al.*, Solid State Commun., **41**, 537 (1982)

122. P. Colombet, *et. al.*, J. Magn. Magn. Mat. **51**, 265 (1985)

123. M.C. Aronson, M.B. Salamon, and J.J. Hauser, Phys. Rev. **B 34**, 4645, (1986)

124. N.M.L. Koche, *et. al.*, Solid State Commun., **52**, 781 (1984)

125. R.H. Taylor and B.R. Coles, J. Phys. **F 5**, 121 (1975)

126. A.D. Caplin and J.B. Dunlop, J. Phys **F 3**, 1621 (1973)

127. M.S. Seehra and T.G. Castner Jr., Solid State Commun., **8**, 787 (1970)

128. J.C. Burgiel and M.W.P. Strandberg, J. Phys. Chem. Solids **26**, 865 (1965)

129. N.J. Zimmerman, *et. al.*, Physica, **46**, 204 (1970)

130. L.R. Maxwell and T.R. McGuire, Rev. Mod. Phys. **25**, 279 (1953)

131. J.W. Battles, J. Appl. Phys. **42**, 1286 (1971)

132. Mohindar S. Seehra, J. Appl. Phys. **43**, 1290 (1971)

133. Mohindar S. Seehra, Phys. Rev **B 6**, 3186 (1972)

134. R.E. Dietz, *et. al.*, Phys Rev Lett, **26**, 1186 (1971)

135. T.T.P Cheung, *et. al.*, Phys. Rev **B 17**, 1266 (1978)

136. H.A. Groenedijk, *et. al.*, Physica **106 B**, 47 (1981)

137. R.D. Willet and M. Extine, Phys. Lett. **44A**, 503 (1973)

138. Peter M. Richards and M.B. Salamon, Phys. Rev. **B 9**, 32 (1974)

139. W.M. Walsh, Jr., Phys. Rev. **B 20**, 2645 (1979)

140. D.L. Huber, J. Phys. Chem. Solids, **32**, 2145 (1971)

141. D.L. Huber, Phys. Rev. **B 31**, 4420, (1985)

142. C. Morgan-Pond, Phys. Lett **92 A**, 461 (1982)

143. P.M. Levy and R. Raghavan, J. Magn. Magn. Mat. **54-57**, 181 (1986)

144. Raghu Raghavan and P.M. Levy, J. Appl. Phys. **57**, 3386 (1985)

145. Barnes, S.E., Phys. Rev. **B 30**, 3944 (1984)

146. D.M.S. Bagguley, *et. al.* J. Phys. **F 4**, 594 (1974)

147. Private Communication referred to in reference 106

148. G.G. Kenning, thesis, unpublished, Michigan State University, 1987

149. L.J. Van dePauw, Phillips Res. Rep. **13**, 12 (1958)

150. J. Bass, in *Metals, Electronic Transport Phenomena, Vol 15 a* of the Landolt-Bornstein tables, New Series Group III, Ref 8. p.139

151. Freeman G. Dyson, Phys. Rev. **98**, 349 (1955)

152. George Feher and A.F. Kip, Phys. Rev. **98**, 337 (1955)

153. V. Cannella in *Amorphous Magnetism*, edited by H.O. Hooper and A.M. deGraff), New York, Plenum Press, 1974, p. 237

154. F. Holtzberg, *et. al.*, J. Appl. Phys. **53**, 2229 (1982)

155. S. Chehab, *et. al.*, J. Magn. Magn. Mat. **62**, 312 (1986)

156. N. Bontemps, *et. al.*, Phys. Rev. **B 30**, 6514 (1984)

157. E. Vincent and J. Hammann, J. Phys. C **20**, 2659 (1987)

158. Laurent P. Levy and Paul Bridenbaugh - Preprint

159. H. Mahdjour, *et. al.* Z. Phys. **B 63**, 351 (1986) - ESR scaling

160. F.L.A. Machado, *et. al.* Solid State Commun. **75**, 1 (1990)

161. Malozemoff, *et. al.*, J. Appl. Phys. **53**, 11 (1990) - Susceptibility

162. P. Svedlindh, *et. al.* J. Magn. Magn. Mat. **71**, 22-26, (1987)

163. D. Huse and I. Morgenstern, Phys. Rev. **B 32**, 3032 (1985) - 2D Ising Monte Carlo

164. T. Ogielski and I. Morgenstern, Phys. Rev. Lett **54**, 928 (1985) - 3D model

165. Mean Field Theory Results - See reference 1

166. R.N. Bhatt and A.P. Young, Phy. Rev. Lett. **54**, 924 (1985) 3D model

167. A.P. Young, J. Phys. C **17**, L 517 (1984) 2D $\pm$ J Model

168. W. McMillan, Phys. Rev. **B 28**, 5216 (1983)

169. A.J. Bray and M.A. Moore, Phys. Rev. **B 31**,631, (1985)

170. W. McMillan, Phys. Rev. **B 29**,4026 (1984)

171. R. P. Singh and S. Chakravarty, Phys. Rev. Lett. **57**, 245 (1986)

172. P. Svedlindh, *et. al.* Europhysics. Lett. **3**, 243 (1987)

173. R.L. Lichti, *et. al.*, J. Appl. Phys. **63**, 4351 (1988)